INVESTIGATING NOVEL THERAPEUTIC STRATEGIES IN HIGH GRADE SEROUS OVARIAN CANCER

A thesis submitted to Maynooth University for the degree of

Doctor of Philosophy

By

Jamie Casey, M.Sc., B.Sc.

Department of Biology

Faculty of Science and Engineering

Maynooth University

Maynooth

County Kildare

Ireland

Date: (11/08/2025)

Research Supervisor: Dr Marion Butler

Enterprise Mentor: Dr Frances Drummond

Head of Department: Professor Paul Moynagh

Table of Contents……..Page Number

Table of Contents……..……..ii

Declaration of Authorship…….……..……xviii

Funding Acknowledgement…….…….……xix

Acknowledgements……..…….……..xx

List of Abbreviations…….…..……xxii

Abstract…….…….xxxi

Chapter 1: General Introduction ……..……..……1

Section (1.1): Ovarian Cancer……..……2

(1.1.1) Epidemiology and Clinical Presentation ……..……..……2

(1.1.2) Classification of Epithelial Ovarian Cancer……..……3

(1.1.3) Barriers to Effective Treatment: Metastasis and Resistance…….……...5

Section (1.2): High Grade Serous Ovarian Carcinoma……..……8

(1.2.1) Risk and Prognostic Factors Associated with HGSC……..……8

(1.2.2) Characterisation of HGSC……..……...……9

(1.2.3) Clinical Challenges: Advanced Stage Detection and Chemoresistance…....11

Section (1.3): Interleukin 1 Receptor Associated Kinase 1……..14

(1.3.1) General Overview……..…….14

(1.3.2) IRAK1 Family of Kinases……...….15

(1.3.3) Regulation and Activation of IRAK1……..17

(1.3.4) Signalling Pathways……..……..……18

(1.3.5) Role in Immune system and Autoimmunity…….…….22

Section (1.4): The Role of IRAK1 in Cancer……..……..24

(1.4.1) IRAK1 in Hepatocellular Carcinoma (HCC)……..……..27

(1.4.2) IRAK1 in Melanoma……..……..27

(1.4.3) IRAK1 in Medulloblastoma (MBL)……..……..……28

(1.4.4) IRAK1 in Glioblastoma Multiforme (GBM)……..……..……..28

(1.4.5) IRAK1 in Diffuse Large B Cell Lymphoma (DLBCL)……29

(1.4.6) IRAK1 in Acute Myeloid Leukaemia (AML)……..……30

(1.4.7) IRAK1 in IRAK1 in Breast Cancer (BrCa)……..……..30

(1.4.8) IRAK1 in Myelodysplastic Syndrome…….……..……32

(1.4.9) IRAK1 in Prostate Cancer (PCa)……..…32

(1.4.10) IRAK1 in Nasopharyngeal Carcinoma…….…….…33

(1.4.11) IRAK1 in Pancreatic Cancer (PC)……..…….33

(1.4.12) IRAK1 in Cervical Cancer (CC)……...……...….34

(1.4.13) IRAK1 in Gastric Cancer (GC)…….34

(1.4.14) IRAK1 in Lung Cancer (LC)…….…….35

(1.4.15) IRAK1 in Thyroid Cancer (TC)…….36

(1.4.16) IRAK1 in Ovarian Cancer (OvCa)…….……..36

(1.5) Introduction to The IRA1-JAK2-FLT3 Inhibitor Pacritinib…….….37

(1.5.1) Pacritinib: An IRAK1 Kinase Inhibitor…….……...37

(1.5.2) JAK2 and STAT3 as Therapeutic Targets in Cancer…….41

(1.5.3) FLT3 as a Therapeutic Target in Cancer…….43

(1.6) Introduction to The Human Epidermal Growth Factor Receptor (HER) Family……...46

(1.6.1) The Epidermal Growth Factor Receptor……...49

(1.6.2) Human Epidermal Growth Factor Receptor 2 (HER2)……..50

(1.6.3) Human Epidermal Growth Factor Receptor 3 (HER3)……51

(1.6.4) Human Epidermal Growth Factor Receptor 4 (HER4)……52

(1.7) Introduction to SHP2 and the Allosteric Inhibitor SHP099…….55

(1.7.1) SHP2: General Overview……56

(1.7.1.1) Structure of the Phosphatase SHP2……..56

(1.7.1.2) Conformational Regulation and Activation of SHP2……57

(1.7.1.3) Signalling Pathways……59

(1.7.2) SHP2: Role in Cancer……61

(1.7.2.1) Breast Cancer……...62

(1.7.2.2) Laryngeal Cancer……63

(1.7.2.3) Gallbladder Cancer……..63

(1.7.2.4) Ovarian Cancer……64

(1.7.3) SHP2 in the Tumour Microenvironment……65

(1.7.4) SHP099: A SHP2 Allosteric Inhibitor……66

(1.8) Thesis Aims and Objectives……..69

(1.8.1) Objective 1 – Investigating the role of IRAK1 in OvCa……..69

(1.8.2) Objective 2 – Investigating the role of SHP2 in OvCa……70

(1.8.3) Objective 3 – Evaluating the combination of Pacritinib and SHP099…….70

Chapter 2: Materials and Methods……..…71

Section (2.1): Standard Laboratory Procedures……72

(2.1.1) Good Laboratory Practices……72

(2.1.2) Maintenance of Lentiviral Induced Knockdown……..…72

(2.1.3) Data Management Practices……..……74

Section (2.2): Cell Culture Procedures ……..……75

(2.2.1) Ovarian Cancer Cell Lines……..…75

(2.2.1.1) Human High Grade Serous Carcinoma (HGSC) Cell lines……75

(2.2.1.2) Human Non-HGSC Cell Lines……77

(2.2.1.3) Murine Ovarian Cancer Cell Line……..……77

(2.2.2) Sub Culturing Procedures: Adherent Ovarian Cancer Cell Lines…….……79

Section (2.3): In Vitro Growth Assays……..…..82

(2.3.1) Proliferation Assay (2D Methodology)……..…82

(2.3.1.1) Day 0 – Seeding Plates……82

(2.3.1.2) Day 4 and Day 7 – Counting Cells……..82

(2.3.1.3) Validation of IRAK1 Knockdown……83

(2.3.1.4) Data Analysis and Statistical Significance……83

(2.3.2) Viability Assay – Cell Titre-Glo® 2.0 (2D Methodology) ……84

(2.3.2.1) Day 0 – Seeding Plates……84

(2.3.2.2) Day 1 – Single Agent Treatments……..84

(2.3.2.3) Day 1 – Treating Plates with Drug Combinations……85

(2.3.2.4) Day 4 – Measuring Cell Viability using Cell Titre-Glo® 2.0……..86

(2.3.2.5) Data Analysis and Statistical Significance……86

(2.3.3) Colony Formation Assay……..87

(2.3.3.1) Day 0 – Seeding Plates……87

(2.3.3.2) Day 1 – Treating Cells with Pacritinib……87

(2.3.3.3) Day 14 – Fixing, Staining and Counting Colonies……88

(2.3.3.4) Data Analysis and Statistical Significance……88

(2.3.4) Soft Agar Assay (3D Methodology)……..89

(2.3.4.1) Day 0 – Seeding Plates……89

(2.3.4.2) Day 1 – Treating Cells with Pacritinib and SHP099……..89

(2.3.4.3) Resupplying Complete Media……90

(2.3.4.4) Day 21 – Viability staining, Imaging and Counting Colonies……..90

(2.3.4.5) Data Analysis and Statistical Significance……90

(2.3.5) Matrigel Droplet Migration / Invasion Assay (3D Methodology)……..91

(2.3.5.1) Day 0 – Seeding Plates……91

(2.3.5.2) Day 1 – Replacing Media……..91

(2.3.5.3) Day 7 – Staining cells, Imaging and counting migrated cells……..92

(2.3.5.4) Data Analysis and Statistical Significance……92

(2.3.6) Matrigel Viability Assay (3D Methodology)……..92

(2.3.6.1) Preparation of Poly-HEMA Coated Plates……92

(2.3.6.2) Day 0 – Seeding Plates……93

(2.3.6.3) Day 1 – Treating Plates with Pacritinib and SHP099……...93

(2.3.6.3) Day 1 – Treating Plates with Pacritinib and SHP099 in Combination……94

(2.3.6.4) Day 7 – Measuring Cell Viability using Cell Titre-Glo® 3D Assay……94

(2.3.6.5) Data Analysis and Statistical Significance……95

(2.3.7) Incucyte Spheroid Cell Death Assay (3D Methodology)……...95

(2.3.7.1) Day 0 – Seeding Plates……95

(2.3.7.2) Day 3 – Treating Plates with Pacritinib and SHP099……..96

(2.3.7.3) Data Analysis and Statistical Significance……96

(2.3.8) Happy Cell Media Spheroid Viability Assay (3D Methodology)……..…..97

(2.3.8.1) Day 0 – Seeding Plates……97

(2.3.8.2) Day 1 – Treating Plates with Pacritinib and SHP099……...97

(2.3.8.3) Day 7 – Measuring Cell Viability using Cell Titre-Glo® 3D Assay……97

(2.3.8.4) Combenefit Synergy / Antagonism Data Analysis……..98

Section (2.4): Protein Expression Analysis – Western Blot Analysis……..…100

(2.4.1) General Overview of Western Blot Analysis of Protein Expression……100

(2.4.2) Preparation of Whole Cell Lysates……..…100

(2.4.2.1) Plating Whole Cell Lysates……100

(2.4.2.2) Treating Whole Cell Lysates……101

(2.4.2.3) Harvesting Whole Cell Lysates……101

(2.4.3) Bradford Protein Assay and Whole Cell Lysate Concentration Adjustment……..102

(2.4.3.1) Preparation of Bradford Standards……..102

(2.4.3.2) Standard Curve Preparation……102

(2.4.4) Western Blot Analysis…….……...…..103

(2.4.4.1) Preparation of Polyacrylamide Gels……103

(2.4.4.2) Electrophoresis – Separation of Proteins Based on Size……..103

(2.4.4.3) Electro-Transfer of Proteins to PVDF Membrane……..104

(2.4.4.4) Blocking of PVDF Membranes……104

(2.4.4.5) Primary Antibody incubation and Target Protein Detection……..105

(2.4.4.5) Visualisation of protein expression……..105

(2.4.4.6) Densitometry Analysis and Statistical Significance……..106

Section (2.5): Protein Expression Analysis – Proteomics……113

(2.5.1) Preparation of Whole Cell Lysates for Proteomics…….……...113

(2.5.1.1) Day 0 – Seeding Cells……..……..113

(2.5.1.2) Day 1 – Treating Whole Cell Lysates……..113

(2.5.1.3) Day 2 – Collecting Whole Cell Lysates……114

(2.5.1.4) Determination of Protein Concentration……..114

(2.5.2) Preparation of Whole Cell Lysates for Mass Spectrometry using FASP Methodology……..…114

(2.5.2.1) Day-1……114

(2.5.2.2) Day-2……115

Section (2.6): Protein Expression Analysis – Immunohistochemistry……117

(2.6.1) Breakdown of Tissue Microarray Slides……..……...…117

(2.6.2) IRAK1 Immunohistochemistry……..……..…118

(2.6.2.1) Preparation of Cell Plugs for Optimisation……..….118

(2.6.2.2) Deparaffinisation and Antigen Retrieval……...118

(2.6.2.3) Immunohistochemical Staining of IRAK1……119

(2.6.2.4) Data Analysis……..120

(2.6.3) SHP2 Immunohistochemistry……..120

(2.6.3.1) Preparation of Cell Plugs for Optimisation……..120

(2.6.3.2) Validation of SHP2 Immunohistochemistry using SHP2 Knockdown Cell lines ……..…121

(2.6.3.3) Deparaffinisation of Slides and Antigen Retrieval……..…121

(2.6.3.4) Immunohistochemical Staining using Autostainer Link 48, DAKO…….122

(2.6.3.5) Haematoxylin Counterstaining and coverslip mounting……123

(2.6.3.6) Image Analysis……...123

Section (2.7): Probing Gene Expression Databases……..125

(2.7.1) Probing Gene Expression in OvCa vs Normal Controls using TNMplot……125

(2.7.2) Probing mRNA Expression Correlation with Overall Survival and Progression Free Survival in Ovarian Cancer…….……..…...126

Chapter 3: Evaluating Interleukin-1 Receptor Associated Kinase 1 (IRAK1) as a Potential Therapeutic Target in High Grade Serous Ovarian Cancer…….128

Section (3.1): Introduction…….……..…….129

(3.1.1) Introduction……....129

(3.1.2) Aims and Hypotheses……..130

Section (3.2): Results……..…132

(3.2.1) IRAK1 Knockdown Impairs Growth of Ovarian Cancer Cell Lines in Vitro.……132

(3.2.1.1) Validation of IRAK1 Knockdown in OvCa Cell Lines…….132

(3.2.1.2) IRAK1 Knockdown Results in Significant Reduction in Proliferation of OvCa Cell Lines……132

(3.2.1.3) IRAK1 Knockdown Results in Significant Reduction of Colony Formation and Survival of OvCa Cell Lines in vitro……133

(3.2.1.4) IRAK1 Knockdown Results in Significant Reduction of Spheroid Formation and Anchorage Independent Growth of OvCa Cell Lines in vitro……134

(3.2.1.5) IRAK1 knockdown Results in a Reduction in the Invasion and Migration of OvCa Cell Lines in vitro…….134

(3.2.2) IRAK1 Knockdown Results in Reduced HER4 Expression in Ovarian Cancer Cell Lines.……...141

(3.2.3) Treatment with Pacritinib Impairs Growth of Ovarian Cancer Cell Lines In Vitro.……..……..146

(3.2.3.1) 2D Viability Assay and IC50 Analysis……..146

(3.2.3.2) Treatment with Pacritinib Significantly Reduces Colony Formation of OvCa Cell Lines in vitro……147

(3.2.3.3) Treatment with Pacritinib Significantly Reduces Colony Formation and Anchorage Independent Growth of OvCa Cell Lines in vitro……147

(3.2.3.4) Treatment with Pacritinib Significantly Reduces 3D Viability and Growth of OvCa Cell Lines in vitro……147

(3.2.4) Treatment with Pacritinib Impairs Growth Factor Receptor Signalling and JAK2-STAT3 Signalling in OvCa Cell Lines In Vitro. ……152

(3.2.4.1) Treatment with Pacritinib Reduces the Activation of JAK2 and STAT3 in OvCa Cell Lines in vitro……152

(3.2.4.2) Treatment with Pacritinib Reduces Growth Factor Receptor Activation in OvCa Cell Lines in vitro……153

(3.2.5) Expression Analysis in Serous Ovarian Cancer ……161

(3.2.5.1) STAT3 and IRAK1 Expression and Activation were Profiled in Patient Derived Xenograft Lysates and Parental OvCa Cell Lines……161

(3.2.5.2) HER Family Expression was profiled in PDX and Parental OvCa Cell Lines……161

(3.2.5.3) High IRAK1 mRNA Expression Correlated with Reduced OS in Serous OvCa……162

(3.2.5.4) Immunohistochemical Staining of IRAK1 Shows Increased IRAK1 Expression in HGSC……163

Section (3.3): Discussion……174

(3.3.1) IRAK1 Knockdown and Treatment with Pacritinib Significantly Impairs Growth of Ovarian Cancer Cell Lines……174

(3.3.2) IRAK1 Knockdown and Treatment with Pacritinib Results in Reduced Growth Factor Receptor Activity in Ovarian Cancer Cell Lines……..177

(3.3.3) The Role of JAK2, STAT3 and FLT3 in the Activity of Pacritinib……..…180

(3.3.4) IRAK1 mRNA and Protein is Expressed at Higher Levels in Serous Ovarian Cancer Compared to Normal Controls ……...……182

Section (3.4): Concluding Remarks……..……184

Section (3.5): Future Directions……..……186

Chapter 4: Assessing the Combination of Pacritinib and SHP099 in High Grade Serous Carcinoma……..……188

Section (4.1): Introduction……189

(4.1.1) Introduction……189

(4.1.2) Aims and Hypotheses……..190

Section (4.2) Results……..……191

(4.2.1) SHP2 Expression is Elevated in Cisplatin Resistant PE04 HGSC Cell Line Compared to the Paired Cisplatin Sensitive PE01 HGSC Cell Line……..……191

(4.2.1.1) SHP2 Expression in PDX and Parental HGSC Cell Lines……..191

(4.2.2) SHP2 High Expression Cohort Display Significantly Reduced Overall Survival in Serous Ovarian Cancer…….……194

(4.2.3) SHP2 Protein Expression is Significantly Elevated in High Stage (3 + 4) HGSC Compared to Normal Controls……....198

(4.2.4) Treatment with SHP099 Significantly Reduces the 3D Growth and Viability of HGSC Cell Lines *in Vitro*……...……212

(4.2.5) The Combination of Pacritinib and SHP099 Results in Synergistic Reduction in 3D Viability and Growth of HGSC Cell Lines *in Vitro*…….216

(4.2.5.1) 2D in vitro Growth Assay Models……..216

(4.2.5.2) 3D in Vitro Growth Assay Models……..218

(4.2.6) Proteomics Analysis Identifies Apoptotic Pathways are Impacted Following Treatment of Cisplatin Resistant PE04 HGSC Cell Line with Pacritinib in Combination with SHP099……...……225

(4.2.7) The Combination of Pacritinib and SHP099 Results in Elevated Levels of Cell Death in HGSC Cell Lines Using 3D *in Vitro* Growth Assay Models……..…….241

(4.2.8) The Combination of Pacritinib and SHP099 Results in Elevated Levels of Molecular Markers of Apoptotic Cell Death in HGSC Cell Lines……..……245

(4.2.9) Treatment of Cisplatin Resistant HGSC PE04 Cell Line with SHP099 Results in the Statistically Significant Differential Abundance of 30 Proteins in 3D In Vitro Models……..……..253

(4.2.10) Treatment with Pacritinib and SHP099 in Combination Results in Synergistic Reduction of 3D Growth and Viability of Murine ID8 OvCa Cell Line *in Vitro*……..……267

Section (4.3): Discussion……..……..……273

(4.3.1) SHP2 Represents a Potential Therapeutic Target in High-Grade Serous Carcinoma……..…..……..273

(4.3.2) The Combination of SHP099 and Pacritinib Results in a Synergistic Reduction of 3D Growth and Viability of HGSC Cell Lines *in Vitro*…….277

(4.3.3) The Combination of Pacritinib and SHP099 Results in Elevated Markers of Apoptotic Cell Death in Cisplatin Resistant PE04 HGSC Cell Line *in Vitro*……280

(4.3.4) Treatment with SHP099 Leads to Impacted Nucleotide Metabolism Pathways in Cisplatin Resistant Pe04 HGSC Cell Lines *in Vitro*……..……285

(4.3.4.1) Ribonucleotide Reductase M2 (RRM2)……..288

(4.3.4.2) Thymidine Kinase (TK1)……290

(4.3.4.3) Methylenetetrahydrofolate Dehydrogenase (NADP+ Dependent) 2 (MTHFD2)……..……..291

(4.3.4.4) DEAD-Box Helicase 3, X-Linked (DDX3X)……..……..292

(4.3.5) Treatment with Pacritinib and SHP099 Synergistically Reduces 3D Growth and Viability of Murine OvCa ID8 Cell Line in Vitro ……..……293

Section (4.4): Concluding Remarks……..……..……294

Section (4.5): Future Directions…..……..……...……298

Section (5) Concluding Remarks…..……..……301

Section (6) Posters and Presentations……...305

Section (7) Bibliography……..…...…….……307

Section (8) Supplementary Material……..…..……330

Declaration of Authorship

I hereby declare that I have read and understood the departmental policy on plagiarism. I affirm that this thesis is entirely my own work, except where it has been otherwise acknowledged. All assistance received has been clearly stated. I confirm that this work has not been submitted, either in whole or in part, for any other degree or qualification at this University or any other institute. All sources of information, including published or unpublished work of others, has been appropriately cited and are included in the bibliography.

Name: JAMIE CASEY

Signature: Jamie Casey

Date: 11/08/2025

Funding Acknowledgments

I gratefully acknowledge the support of Research Ireland (Irish Research Council) and Breakthrough Cancer Research, who funded this PhD project through the Enterprise Partnership Scheme. Their contribution was instrumental in enabling this work.

Grant Number: EPSPG/2021/185

Acknowledgments

Completing this thesis marks the culmination of four years of intense research, learning and personal growth. This thesis represents not only the lab work I have done but also the resilience, perseverance and determination it took to see it through. The last four years have shaped the way I think, challenged my limits and deepened my commitment to advancing cancer research. This has been a journey of both discovery and endurance, and I am proud of what this thesis represents – not only a scientific contribution, but also a personal achievement.

I would like to sincerely thank Breakthrough Cancer research for their support throughout my PhD. I am especially grateful to Dr Frances Drummond for her encouragement, thoughtful advice and consistent support. Her guidance provided clarity and direction when it was needed most.

To my friends and fellow PhD students, thank you for the laughs, coffee breaks, support and understanding which made the hardest days easier and the best days even better. Clara, Aaron, Sarah and Courtney - it was an absolute pleasure. I truly don’t know what I would have done without you.

To my amazing girlfriend: I owe you a debt I can never repay. Your support and encouragement were consistent and unwavering. Even in my lowest moments, you lifted me up. I appreciate everything you do for me. From the bottom of my heart, thank you.

To my friends, Michael, Errol, Sean, Liam and Tom. We’ve known each other a long time now and I’m grateful for your friendship throughout the years. Thank you for entertaining the ramblings and ravings about my thesis and PhD journey – Your patience, humour and support have meant a lot.

Finally, and most importantly I would like to dedicate this thesis to my family who have put up with me over the last four years. To my wonderful mother Olivia and my grandmother Bridget you have both been instrumental in the person I am today, and I would not be where I am without you. Cathal, Carmen, Trish, Dec, Siobhan and the newest addition, my godchild Amelia, I appreciate each and every one of you. Thank you for everything you have done for me, for your kindness and for your support. Thank you all for your unwavering encouragement, patience and support. It has meant the world to me. I can say with complete honesty and certainty that I would not have been able to complete this thesis without you all.

List of Abbreviations

ABC DLBCL	Activated B-Cell Like Diffuse Large B-Cell Lymphoma
ABC Transporters	ATP Binding Cassette Transporters
ABCB1	ATP-binding cassette, sub family B (MDR/TAP), member 1
ACACA	Acetyl-Co-A Carboxylase Alpha
AKT	Protein Kinase B
ALKBH5	AlkB homolog 5, RNA demethylase
AML	Acute Myeloid Leukaemia
AP1	Activator Protein 1
APS	Ammonium Persulfate
ATCC	American Type Culture Collection
ATP	Adenosine Triphosphate
BAG6	BAG cochaperone 6
B-ALL	B cell Acute Lymphoblastic Leukaemia
BCL2	B-Cell Leukaemia / Lymphoma 2
BCR	B Cell Receptor
BRAF	B-Raf Proto-Oncogene, Serine/Threonine Kinase
BrCa	Breast Cancer
BRCA1/2	Breast Cancer Gene 1/2
BRIP1	BRCA1 Interacting Protein C-Terminal Helicase 1
BSA	Bovine Serum Albumin
BTIC	Brain Tumour Initiating Cells
BTLA	B- and T- Lymphocyte Attenuator

BZW2	Basic Leucine Zipper and W2 domain containing protein 2
CA125	Cancer Antigen 125
CCNE1	Cyclin E1
CD28	Cluster of Differentiation 28
CNS	Central Nervous System
CO2	Carbon Dioxide
CORO1C	Coronin 1C
COX-2	cyclooxygenase-2
CS	Cell Signalling
CSF-1	Colony Stimulating Factor 1
CTLA4	Cytotoxic T-Lymphocyte Associated Antigen 4
CTNNB1	Catenin Beta 1
DAD1	Defender against cell death 1
DAMP	Damage Associated Molecular Pattern
DC	Dendritic Cells
DCU	Dublin City University
DD	Death Domain
DDX3X	DEAD-box helicase 3, X-linked
DLBCL	Diffuse Large B-Cell Lymphoma
DMEM	Dulbecco's Modified Eagle Medium
DMSO	Dimethyl Sulfoxide
DNA	Deoxyribonucleic Acid
DNAJA3	DNAJ heat shock protein family (Hsp40) member A3
DPBS	Dulbecco's Phosphate Buffered Saline
DTT	1,4-Dithiotritol

ECACC	European Collection of Authenticated Cell Cultures
ECM	Extracellular Matrix
EDTA	Ethylenediamine Tetra-acetic Acid
EGFL6	Epidermal Growth Factor-Like Domain-Containing Protein 6
EGFR	Epidermal Growth Factor Receptor
EIF3C	Eukaryotic Translational Initiation Factor 3 Subunit C
EMT	Epithelial-Mesenchymal Transition
EOC	Epithelial Ovarian Cancer
ER	Oestrogen Receptor
ERK	Extracellular Signal-Regulated Kinase
FAH	Fumarylacetoacetate Hydrolase
FAIR	Findable, Accessible, Interoperable and Reusable
FBS	Foetal Bovine Serum
FDA	Food and Drug Administration
FLT3	FMS-Like Tyrosine Kinase 3
FLT3L	FMS-Like Tyrosine Kinase 3 Ligand
GAB2	GRB2-Associated Binding Protein 2
GBM	Glioblastoma Multiforme
GC	Gastric Cancer
GDP	Guanosine Diphosphate
GEMIN5	Gem (nuclear organelle) associated protein 5
GEO	Gene Expression Omnibus
GFR	Growth Factor Receptor
GPX1	Glutathione Peroxidase 1

GRB2	Growth Factor Receptor-Bound Protein 2
GTP	Guanosine Triphosphate
H2AFV	Histone H2A Variant
H2O2	Hydrogen peroxide
HCC	Hepatocellular Carcinoma
HCl	Hydrochloric Acid
HEC	High Expression Cohort
HER2/3/4	Human Epidermal Growth Factor Receptor 2/3/4
HGSC	High Grade Serous Carcinoma
HRD	Homologous Recombination Repair Deficiency
HRG1β	Neuregulin-1 Beta 1
HRP	Horse Radish Peroxidase
HRR	Homologous Recombination Repair
IACR	International Agency for Research on Cancer
IFN-a	Interferon Alpha
IGF	Insulin-Like Growth Factor
IHC	Immunohistochemistry
IL-1/6	Interleukin-1/6
IL-1R	InterLeukine-1 Receptor
IL-1RAcp	Interleukin-1 Receptor Accessory Protein
IRAK1/2/3/4	Interleukin-1 Receptor Associated Kinase 1/2/3/4
IRF7	Interferon Regulatory Factor 7
ITIM	intracellular immunoreceptor tyrosine-based inhibitory motif
ITISM	immunoreceptor tyrosine-based switch motif
JAK2	Janus Kinase 2
JMML	Juvenile Myelomonocytic Leukaemia

KRAS	Kirsten Rat Sarcoma Viral Oncogene Homolog
LAG3	Lymphocyte Activation Gene 3
LC	Lung Cancer
LEC	Low Expression Cohort
LEPR	Leptin Receptor
LGSC	Low Grade Serous Carcinoma
LPS	Lipopolysaccharide
LSM8	LSM8 homolog, U6 small nuclear RNA associated
LTS	Long Term Survivors
MAT2A	Methionine Adenosyl transferase II, Alpha
MBL	Medulloblastoma
MDS	Myelodysplastic Syndrome
MEK	Methyl Ethyl Ketone
METHFD2	Methylenetetrahydrofolate dehydrogenase (NADP+ dependent) 2
MLH1/3	MutL homolog 1/3
MMP2/9	Matrix Metallopeptidase 2
MRPL15	Mitochondrial ribosomal protein L15
MSH2/6	MutS Homolog 2
MTA2	Metastasis-Associated Protein 2
mTOR	Mechanistic Target of Rapamycin
MyD88	Myeloid Differentiation Primary Response 88
NaCl	Sodium Chloride
NaF	Sodium Floride
NAT	Normal Adjacent Tissue
NaVO3	Sodium Metavanadate
NCa	Nasopharyngeal Carcinoma

NCBI	National Centre for Biotechnology Information
NEMO	NF-kappa-B Essential Modulator
NF-kB	Nuclear Factor Kappa-Light-Chain-Enhancer of Activated B Cells
NLRP3	NLR Family Pyrin Domain Containing 3
NRG1	Neuregulin-1
NSCLC	Non-Small Cell Lung Cancer
NUTF2	Nuclear Transport Factor 2
OS	Overall Survival
OvCa	Ovarian Cancer
PAMP	Pattern Associated Molecular Pattern
PARP	Poly (ADP-ribose) Polymerase
PC	Pancreatic Cancer
PCa	Prostate Cancer
PCBP3	Poly(RC) Binding Protein 3
PD-1	Programmed Cell Death Protein 1
PDAC	Pancreatic Ductal Adenocarcinoma
PDGF	Platelet Derived Growth Factor
PD-L1	Programmed Death Ligand 1
PDX	Patient Derived Xenograft
PFDN5	Prefoldin subunit 5
PFS	Progression Free Survival
PI3KA	Phosphatidylinositol-4,5-bisphosphate 3-kinase catalytic subunit alpha
PMSF	Phenylmethylsulphonyl Fluoride
Poly-Hema	Poly (2-hydroxyethyl methacrylate)
PRPF40A	Pre-mRNA processing factor 40 homolog A

PTEN	Phosphatase and Tensin Homolog Deleted on Chromosome 10
PTP	Protein Tyrosine Phosphatase
PVDF	Polyvinylidene Fluoride
QUB	Queens University Belfast
RAD51C/d	RAD51 homolog C/d
RAF	Raf proto-oncogene serine / threonine protein kinase
RAS	Rat Sarcoma
RLU	Relative Luminescent Units
RNA	Ribonucleic acid
RNF114	Ring finger protein 114
RPM	Rotations Per Minute
RPMI	Roswell Park Memorial Institute Medium
RRM2	Ribonucleotide reductase regulatory subunit M2
RTK	Receptor Tyrosine Kinase
S100A13	S100 calcium binding protein A13
SC	Santa Cruz
SCLC	Small Cell Lung Cancer
SDS	Sodium Dodecylsulfate
SEM	Standard Error around the Mean
SF3B4	Splicing factor 3B subunit 4
SH2	Src Homology 2
SHIP1	Src Homology (SH2) domain-containing inositol polyphosphate 5-phosphatase 1
SHP1/2	Src Homology 2-containing protein tyrosine Phosphatase 1/2

SIRPa	signal regulatory protein alpha
SLE	Systemic Lupus Erythematosus
SNP	Single Nucleotide Polymorphism
SOCS1	Suppressor of Cytokine Signalling 1
SOS	Son of Sevenless
SRPRB	Signal Recognition particle receptor subunit beta
SRSF5	Serine and arginine rich splicing factor 5
STAM	Signal Transducing Adaptor Molecule 1
STAT3/5	Signal Transducer and Activator of Transcription 3
STIC	Serous Tubal Intraepithelial Carcinoma
TAB1/2	TGF-beta activated kinase 1 (MAP3K7) binding protein 1
TAK1	Transforming Growth Factor Beta-activated Kinase 1
TBST	Tris-Buffered Saline + Tween
TCGA	The Cancer Genome Atlas
TCR	T Cell Receptor
TEMED	N'N'N'N'-Tetramethyl ethylenediamine
TFA	Trifluoracetic acid
TGF-a	Transforming Growth Factor Alpha
TGF-β	Transforming Growth Factor Beta
TIC	Tumour Initiating Cells
TIGIT	T-cell Immunoglobulin and ITIM Domain
TIL	Tumour Infiltrating Lymphocytes
TK1	Thymidine Kinase 1
TKI	Tyrosine Kinase Inhibitor

TLR	Toll-Like Receptors
TMA	Tissue Microarray
TMEM33	Transmembrane protein 33
TNBC	Triple Negative Breast Cancer
TRAF6	Tumour Necrosis Factor Receptor-Associated Factor 6
UCD	University College Dublin
UGP2	UDP-glucose pyrophosphorylase
VC	Vehicle Control
VISTA	V-Domain Ig Suppressor of T-cell Activation
WCL	Whole Cell Lysates
WHO	World Health Organisation
WOCC	World Ovarian Cancer Coalition
YAP1	Yes-associated Protein 1
ZAP70	Zeta-chain (TCR) associated protein kinase 70kDa.
ZFPL1	Zinc Finger protein-like 1

Abstract

High Grade Serous Carcinoma (HGSC) accounts for the majority of diagnosis and deaths for patients with Ovarian Cancer (OvCa). HGSC is commonly diagnosed in the advanced stage which is associated with poor prognosis. While patients initially respond quite well to first line therapeutic interventions the majority of initial responders will eventually relapse and develop chemoresistance disease. Second line therapeutic approaches display limited efficacy and the lack of novel druggable target discovery and lack of novel therapeutic strategies in HGSC have contributed to the poor prognosis associated with advanced stage HGSC.

IRAK1 has been shown to represent a novel therapeutic target in several solid cancers and small molecule kinase inhibitors have displayed considerable efficacy in both *in vitro* and *in vivo* models. In this study we have shown that IRAK1 plays important roles in the growth of HGSC cells *in vitro*. IRAK1 knockdown was observed to result in reduced proliferation, colony formation, anchorage independent growth, migration / invasion and HER4 expression. Additionally, the small molecule kinase inhibitor pacritinib was observed to result in reduced colony formation, anchorage independent growth, 3D viability and growth factor receptor activation.

SHP2 has previously been shown to represent a therapeutic target in GAB2 overexpressing OvCa where the allosteric inhibitor SHP099 displayed efficacy *in vitro* and in xenograft models of OvCa. We have shown that higher SHP2 mRNA expression is associated with reduced overall survival in serous OvCa and that SHP2 protein expression is significantly higher in high stage (3+4) HGSC compared to both stage 1 HGSC and normal adjacent tissue. Treatment with SHP099 was observed to display good efficacy in reducing 3D growth and viability of HGSC cells *in vitro* and impair nucleotide metabolism pathways through reducing RRM2 and TK1 expression.

Finally, the combination of pacritinib and SHP099 resulted in a synergistic reduction in 3D growth and viability of HGSC cells *in vitro*. Following combination treatment, we observed synergistic reduction in 3D growth and viability of HGSC cells. Proteomics and Western blot analysis led to the observation that apoptotic cell death is elevated in pacritinib and SHP099 combination treated of OvCa cell lines. These findings indicate the combination of pacritinib and SHP099 may represent a novel therapeutic strategy in HGSC.

Chapter 1

General Introduction

(1.1) Ovarian Cancer

Cancer represents a group of diseases in which the normal cellular mechanisms regulating cell division break down. When this occurs, cancerous cells proliferate uncontrollably and expand beyond their boundaries. Several key features have been aptly described to define and characterise this heterogenous group of diseases which have been termed the hallmarks of cancer. These hallmarks include **i)** sustained proliferative signalling, **ii)** evading growth suppressors, **iii)** activation of invasion and metastasis, **iv)** activation of replicative immortality, **v)** induction of angiogenesis and **vi)** resisting cell death.[1] In an updated review published ten years later **vii)** avoiding immune destruction, **viii)** tumour promoting inflammation, **ix)** genome instability and **x)** deregulation of cellular metabolism were added.[2]

According to the World Health Organization (WHO) cancer is a leading cause of death worldwide and accounted for 10 million (1 in 6) deaths in 2020 alone.[3] Cancer is a disease that poorer countries disproportionately experience higher rates of morbidity and mortality from. While wealthier countries tend to have higher incidence rates (likely attributed to more developed awareness campaigns and increased screenings), low and middle-income countries account for 70% of cancer related deaths.[3]

(1.1.1) Epidemiology and Clinical Presentation

According to the World Ovarian Cancer Coalition (WOCC) and the International Agency for Research on Cancer (IARC), Epithelial Ovarian Cancer (EOC) is the seventh most common cancer among women, accounting for approximately 314,000 cases and 207,000 deaths worldwide in 2020.[45] This makes EOC the most lethal gynaecological malignancy.[6] Projections made in 2020 by

Globocan indicate that the incidence rate of Ovarian Cancer (OvCa) is expected to increase by almost 42% in 2040 while mortality is expected to increase by over 50%.[4] EOC is an age-related disease and is most commonly diagnosed in ageing individuals.[7]

Generally, the clinical symptoms of EOC appear to be non-specific. Patients can present with abdominal bloating, eating difficulties (feeling full quicker), nausea, abdominal distension, change in bowel function, urinary symptoms (changes in urinary or bowel movements), backpain, fatigue and weight loss / gain.[8] This creates considerable challenges with detection and diagnosis of EOC.

Population based screening of EOC has unfortunately proved relatively ineffective with no currently approved strategy. Approximately 75% of EOC patients are diagnosed with advanced stage disease where the cancer has disseminated throughout the peritoneal cavity.[9,10] This is primarily attributed to the asymptomatic nature of EOC as most patients reach the advanced stage by the time they become symptomatic.[11,12] Advanced stage EOC is associated with a poor prognosis and a five-year survival rate of only 29%.[13] Mortality rates have remained relatively unchanged since the 1980's.[12]

(1.1.2) Classification of Epithelial Ovarian Cancer

While only a small fraction of ovarian tumours arise from germ cells or sex chord stromal cells the majority of ovarian tumours arise from transformed epithelial cells and as a result are termed Epithelial Ovarian Cancer (EOC).[14] EOC accounts for between 85% and 95% of all OvCa and has been further divided into several subtypes, based on morphology and tissue architecture which include Serous (70%), Mucinous (3-10%), Endometroid (10%) and Clear Cell Carcinoma (10%).[15] Each of

these subtypes differ in aetiology, pathogenesis, molecular biology, risk factors and prognosis.[16]

Serous EOC can be further divided into High Grade Serous Carcinoma (HGSC) which accounts for 90-96% of serous EOC and Low-Grade Serous Carcinoma (LGSC), which accounts for 4-10% of Serous EOC.[15]

LGSC, clear cell carcinoma and mucinous subtypes represent type I EOC's which are characterised by frequent mutations in oncogenic genes including KRAS, BRAF, PTEN, CTNNB1 and PI3KCA but are commonly wild type p53.[12] HGSC is designated as a Type II EOC which display far more aggressive disease behaviour and are usually widely disseminated at the time of presentation, contributing to poor prognosis.[12] HGSC is also characterised by a high frequency of p53 mutations, the majority of which are missense mutations.[12]

LGSC tend to be slower growing than HGSC and are generally confined to the ovary at diagnosis.[17] LGSC is usually diagnosed at a younger age and associated with a better five and ten-year survival rate.[18] Patients with LGSC receive maximal debulking surgery, lymph node assessment and resection of all viable microscopic residual disease.[18] When confined to the ovaries and pelvis (FIGO stage I-IIa) this treatment is curative in up to 70% of cases.[19] LGSC characteristically display constitutively higher activation of MAPK signalling[17] and higher rates of KRAS and BRAF mutations than HGSC.[18]

The stage of disease is characterised by the extent to which the cancer has spread. For OvCa, stage 1 is confined to one or both ovaries, stage 2 includes spreading to the uterus and bladder, stage 3 includes spreading to the abdomen while stage 4 includes disease spread beyond the peritoneal cavity.[20] Stage 1 accounts for 15-20% of diagnosis and displays a high survival rate of 92.3%[15] and a cure rate as

high as 90% for conventional therapies.[20] The survival rate drops to 29.2% for patients with advanced stage detections.[15]

(1.1.3) Barriers to Effective Treatment: Metastasis and Resistance

Current first line therapeutic approaches in OvCa involve the combination of cytoreductive surgery to remove the tumour bulk followed by platinum-based chemotherapy.[21] This platinum-based chemotherapy which may include bevacizumab.[21] Carboplatin is given for six weeks in combination with paclitaxel following surgery. [22] The goal of this standard of care is to remove as much of the tumour burden as possible and target residual disease with chemotherapy with the goal of giving the best chance for initial remission.

Platinum based chemotherapy can also be given prior to surgical intervention which is referred to as neoadjuvant chemotherapy. This is typically done with the goal of shrinking the tumour in order to enable optimal cytoreductive surgery.

The degree of cytoreduction is a key factor in EOC patient survival. Residual disease less than 1cm is considered to be optimal following surgery as residual disease following surgery is associated with poorer overall survival (OS) rates, progression free survival (PFS) and response to adjuvant chemotherapy.[23]

OvCa differs from a number of other cancers as it primarily disseminates within the peritoneal cavity and tends to be superficially invasive.[24] Passive dissemination involves the passive detachment of OvCa cells from the primary tumour and subsequent migration of these cells through the peritoneal fluid.[20] Alternatively, collective invasion is driven by specialised leader cells allowing for the collective movement of groups of cells as a single unit.[16] Once spread within the peritoneal

cavity, the effectiveness of chemotherapy and debulking surgery is reduced and the five-year survival rate is reduced to just 30% for patients diagnosed in this advanced stage.[20]

Approximately 20% of EOC tumours display initial resistance to platinum-based chemotherapy with the majority of patients responding quite well to first line therapeutic strategies.[25] Despite initial clinical response, recurrence and metastasis will occur in the majority of EOC patients (70%) within the first two years following diagnosis.[26] Previous studies have found chemotherapeutic agents may be promoting metastasis in OvCa.[27] Studies have shown that leader cells involved in collective invasion are enriched following chemotherapy.[16]

Once in the cell the cisplatin becomes hydrolysed and crosslinks with purine bases in DNA which blocks DNA replication and transcription resulting in the cell to promote cell cycle arrest and apoptosis.[28] In addition to this cisplatin is also capable of inducing reactive oxygen species production which can trigger apoptosis independently of triggering DNA damage.[28]

Several mechanisms of chemoresistance have been described in OvCa. Cells may enhance DNA repair or restore DNA-damage response in order to prevent apoptosis caused by cisplatin induced DNA crosslinks or adducts.[29] BRCA1/2 proteins are essential for DNA double strand break repair with approximately 25% of OvCa patients displaying BRCA1/2 mutation and platinum sensitivity.[30] Interestingly reversal mutations to BRCA1/2 wild type has been proposed as a potential mechanism of platinum resistance.[30]

Cancer cells may also prevent apoptosis through the upregulation of anti-apoptotic proteins or suppression of pro-apoptotic proteins.[29] Additionally, cells may reduce the cytotoxicity of chemotherapeutic drugs through reducing intracellular

concentration of chemotherapeutic drugs. Overexpression of efflux pups (such as ABCB1) has been observed to confer this mechanism of resistance. [31]

Cancer cells can also employ detoxification systems for example by upregulating antioxidant enzymes such as glutathione and metallothionein in order to deal with the increased production of reactive oxygen species caused by chemotherapy.[30] Resistance to paclitaxel can additionally occur through altered microtubule structure which effects drug binding.[30]

With the majority of patients displaying either initial resistance to treatment or developing resistance to platinum-based chemotherapy it becomes important to consider the second line therapeutic strategies used to treated OvCa. Maintenance therapies aim to sustain remission. It has been shown that first-line maintenance therapy with PARP inhibitors could improve progression free survival in EOC patients with BRCA mutation or homologous recombination deficiency.[21] Bevacizumab, which targets VEGF, has been approved for used in platinum sensitive recurrent EOC in combination with carboplatin and paclitaxel.[32]

(1.2) – High Grade Serous Ovarian Carcinoma (HGSC)

HGSC accounts for 70% of all EOC at diagnosis.[33] HGSC carries a poor prognosis and less than 35% of patients diagnosed with advanced stage disease survive five years after their diagnosis.[34] HGSC disproportionally accounts for nearly 80% of all advanced stage EOC detections and 70% of all EOC deaths.[15]

(1.2.1) – Risk and Prognostic Factors Associated with HGSC

Like most cancers, several risk factors have been associated with HGSC. For example, obesity has been linked to an increased risk while aspirin and oral contraceptive use has been associated with reduced risk of developing HGSC.[35] Younger age at diagnosis, absence of ascites, low tumour volume, early-stage detection and lower CA125 have all been found to be associated with better prognosis.[36] Several immune related factors have been associated with improved prognosis and long-term survival including the presence of CD103+ and CD3+ TILs and PD-L1 expression.[29]

Ascites (malignant abdominal fluid) frequently develop in patients with advanced stage HGSC and are associated with drug resistance and poor prognosis.[29] Intra-tumour heterogeneity has been shown to be decreased in HGSC following chemotherapy and increased at recurrence.[37] A high level of intra-tumour heterogeneity is associated with shorter first recurrence interval while the loss of heterozygosity is associated with better prognosis.[37]

Patients who survive more than 10 years following diagnosis are termed long-term survivors (LTS) and comprise a heterogenous group of patients both with and without recurrent disease. One retrospective study of HGSC defining LTS as 7 years or greater following diagnosis found that a younger age at diagnosis and lower stage

were both statistically significantly associated with LTS.[38] While other studies have shown that optimal cytoreduction, primary platinum sensitivity[39], low CA125 levels following treatment, increased somatic burden and enrichment of activated CD4+/CD8+ T-cells and effector memory CD4+ T-cells are also associated with LTS.[40]

Short term survival (less than 2 years) associates with lack of BRCA mutation signature, low homologous recombination deficiency score, focal copy number gain of CCNE1 and presence of ESR1-CCDC170 gene fusion.[40]

(1.2.2) – Characterisation of HGSC

Evidence suggests secretory epithelial cells of the fallopian tube are the likely progenitor cells for a substantial proportion of HGSC.[35] HGSC appear to develop from an occult intraepithelial carcinoma in the fimbrial region of the fallopian tube designated serous tubal intraepithelial carcinoma (STIC) and travels to the ovary secondarily.[17]

STIC is characterised by a high frequency of TP53 mutation (over 90%), pleomorphism, hyperchromasia, lack of ciliated cells and high nuclear / cytoplasmic ratio.[17] The shared pattern of TP53 mutation in HGSC and STIC's indicates a shared origin.[41] Proteomics analysis has indicated two potential subtypes of HGSC which arise from fallopian tube epithelium and ovarian surface epithelium.[41]

HGSC are characterised by high grade nuclear atypia with larger hyperchromatic and pleomorphic nuclei and the potential of multinucleation.[12] The nuclear atypia and high mitotic rate which is characteristic of HGSC correlates with a high level of chromosomal instability.[42] HGSC displays a high frequency of p53 mutation (96%).[43] Germline BRCA1/2 mutations are also found in 15-20% of HGCS.[42]

Homologous Recombination Repair (HRR) is a mechanism of DNA repair which fixes DNA strand breaks. Cells with HRR Deficiency (HRD) have a reduced capacity for responding to double strand breaks. Following treatment with platinum-based chemotherapy drugs, HRD results in irreparable DNA damage and ultimately results in apoptosis.[44]

A high proportion of HGSC (approximately 50%) have been shown to display HRD and defects in DNA repair pathways.[35] In HGSC, HRD has been linked to tumorigenesis and sensitivity to platinum-based chemotherapy.[35,44] HRD is often associated with germline, somatic and epigenetic BRCA mutation as well as alterations in other DNA repair genes including RAD51C, RAD51D, BRIP1, MLH1, MSH2, MSH6.[45] Approximately 20% of HGSC patients display germline (17%) and somatic (3%) mutations of BRCA1/2.[46,9]

PARP inhibitors prevent repair of single strand DNA breaks by inhibiting catalytic formation of polymers of ADP-Ribose forming and trapping PARP1 on DNA and inducing double strand breaks.[46] HRD cells have been observed to be sensitive to PARP inhibitors and undergo programmed cell death in response to unrepairable DNA damage.[44]

Studies have shown that the PARP inhibitor Olaparib could significantly increase the PFS of patients with platinum sensitive recurrent HGSC compared to placebo patients.[47] PARP inhibitors are now used as a maintenance therapy in patients with BRCA mutated EOC and have been shown to delay cancer progression, however no improvement in OS was observed.[48]

HGSC, are considered to be immune cold tumours which are characterised by low immune infiltrate and low response to immunotherapies.[49] An immunological subtype of HGSC characterised by increased infiltration of CD8+ and decreased T-regs has been associated with improved therapeutic efficacy.[49] This immunological

subtype has been highlighted as a potential candidate for immunotherapies. PD-L1, which is involved in immune evasion strategies, has previously been observed at higher levels in HGSC.[50]

(1.2.3) Clinical Challenges: Advanced Stage Detection and Chemoresistance

Effective screening remains a current challenge of HGSC. Only 13% of serous EOC's are diagnosed in the earlier stage 1 and stage 2.[12] Early-stage detection displays a 10-year survival of 55% which decreases to 15% for patients presenting at the advanced stage.[12] HGSC diagnosed at the advanced stage is associated with much poorer prognosis compared to early stage.[34] As the majority of HGSC are diagnosed in the advanced stage[15], this represents a major clinical challenge to effective treatment.

It is clear that more effective screening and early detection systems are urgently required to combat this issue. It is possible that biomarker screening may hold promise in this regard by detecting molecular factors associated with the presence of OvCa or HGSC. One study has indicated that glycosite containing peptides of CA125 demonstrated differential expression between tumour and non-tumour samples and could be used for detection of OvCa tumours.[51]

Cisplatin-based chemotherapy was introduced as an adjuvant therapy following surgery in the 1970's for patients with EOC.[12] Cisplatin and carboplatin display similar efficacies but different toxicity profiles[52]. Cisplatin treatment has been associated with several toxicities including hepatotoxicity, ototoxicity, gastro-toxicity, myelosuppression, nephrotoxicity and cardiotoxicity.[28] Carboplatin displays reduced toxicity compared to cisplatin.[53]

Currently the most widely used chemotherapy regimen includes carboplatin and paclitaxel given every three weeks for six cycles.[45] Several second line therapeutic approaches are available to patients including gemcitabine, weekly paclitaxel and bevacizumab, however these have been found to only achieve modest responses in patients.[45]

Cisplatin enters a cell by passive diffusion and facilitated transport before binding to DNA and forming adducts which result in formation of intra-inter-strand cross linking and preventing normal DNA function.[53] This covalent binding of cisplatin to DNA inhibits replication and transcription ultimately resulting in cell cycle arrest and apoptosis.[54] Paclitaxel and docetaxel bind to tubulin polymers (microtubules) stabilising them against depolymerisation, triggering cell cycle arrest and apoptosis.[53]

Cytoreductive surgery is employed in order to remove the bulk of disease which contains poorly oxygenated and non-proliferative cells which have the potential to be resistant to chemotherapy treatment.[53] Smaller tumour volume and higher levels of proliferation following surgery are believed to increase susceptibility of the cancerous cells to chemotherapy.[53]

Following cytoreductive surgery HGSC patients are recommended to undergo adjuvant chemotherapy with approximately 70% of patients initially responding quite well.[12] However, the majority of patients will eventually relapse and experience a cycle of decreasing disease-free periods between treatment remission and relapse with the majority of patients developing recurrent disease within three years.[46]

Unfortunately, 70-80% of these initial responders will relapse and eventually be challenged with chemo-resistant disease which has a poor prognosis and a median progression free survival of 18 months.[55] Follow up treatments are often associated with an increase in adverse events following the development of chemoresistance.[56] Tumours that are resistant to first line chemotherapy

(approximately 15%) tend to have a poor prognosis and a short expected survival of less than twelve months.[45]

Resistance to platinum-based chemotherapy can occur via a complex and dynamic interplay of cellular and molecular mechanisms. One major contributor to resistance is the sequestration of platinum chemotherapy molecules by metallothionein proteins which can reduce the availability of the drug and as a result the toxicity. [53] Tumour cells may also enhance the repair of DNA-platinum adducts [54] or increase their tolerance in order to gain resistance. [53]

The increased expression of ATP binding cassette (ABC) transporters and contribute to reduced drug accumulation in the cytoplasm and reduce toxicity of cisplatin-based chemotherapy in cancer cells.[57] Additionally, resistance may occur due to detoxification via direct binding of glutathione or other thiol-containing molecules to cisplatin making it less effective.[54]

Increased expression or activation of anti-apoptotic proteins and decreased expression of pro-apoptotic proteins has also been observed to confer resistance to platinum-based chemotherapy allowing cells to survive despite the presence of DNA damage.[57] By a similar mechanism the activation of survival signalling pathways such as AKT can promote cell proliferation and inhibit apoptosis.[35]

(1.3) Interleukin 1 Receptor Associated Kinase 1

(1.3.1) General Overview

Kinases and phosphatases both represent actionable molecular targets which, through the use of small molecule inhibitors, can be inhibited to prevent activation or downstream signalling. These enzymes catalyse post-translational modifications through addition (Kinases) or removal (Phosphatases) of phosphate groups to other cellular proteins. Kinases catalyse the transfer of the terminal phosphate group from an adenosine triphosphate (ATP) molecule to a specific amino acid residue on a target protein. This post-translational modification is capable of regulating function, subcellular localisation, degradation and also interaction with other proteins.[58]

The innate immune response represents the rapid and first line defence against infections that is affected via receptors including Toll-Like Receptors (TLRs) and Interleukin-1 Receptors (IL-1R). These receptors mediate the quick detection of pathogens (pattern-associated molecular patterns (PAMP's)) and cell damage (Damage associated molecular patterns DAMP's)).[59] Interleukin-1 Receptor Associated Kinase 1 (IRAK-1) has previously been extensively investigated and characterised for its role in mediating innate immune responses downstream of TLR's and IL-1R.[60] In addition to these important protective functions, IRAK1 has been observed to play key roles in in the growth and progression of several cancer types over recent decades.

(1.3.2) IRAK1 Family of Kinases

The IRAK family of serine / threonine kinases consists of four members, denoted as IRAK1-4, which share up to 30-40% homology[61] and very similar primary structure (Fig. 1.3.1). A Death Domain (DD) is located at the N-terminus of all IRAK family members and is followed by a ProST domain.[62] IRAK1 and IRAK4 both contain Kinase Domains which follow the ProST domain while IRAK2 and IRAK3 contain pseudo-kinase domains instead.[62] IRAK1, IRAK2 and IRAK3 all contain a c-terminus domain which is important for the recruitment and activation of TRAF-6 downstream.[61] All IRAK family members have a tyrosine gatekeeper residue at the centre of the ATP-binding site.[63]

The IRAK1 gene consists of 14 exons which are located on the X-chromosome.[61] The IRAK1 gene encodes a 712 amino acid protein containing an N-terminal DD (a.a. 1-103), central serine-threonine kinase domain (119-522), an activation loop (a.a. 354-388) C-terminal serine-threonine rich region (523-712), putative nuclear location sequence (a.a. 503-508) and a nuclear exit sequence (a.a. 518-526).[64,61]. IRAK1 forms homo/hetero dimers via interactions between DD with Threonine 66 previously being highlighted as an important residue for dimerization.[61]

Analysis of the structure of IRAK1 has previously revealed that C302 is conserved in IRAK4 (C276), however due to conformational differences between these two kinases, the locations of these residues are significantly different.[65] Similarities between IRAK1 and IRAK4 have previously made development of an IRAK1 specific kinase inhibitor difficult. JH-X-119-01 is a chemically synthesised IRAK1 inhibitor that irreversibly binds to C302 of IRAK1 in order to inhibit activation.[66] Due to structural differences between this residue in IRAK1 and IRAK4 the IC50 value for IRAK1 (9.3nM) is much lower compared to IRAK4 (10μM).[66]

IRAK2 is essential in sustaining TLR2 induced expression of genes encoding cytokines despite being dispensable for the activation of the initial signalling cascade.[67] IRAK4 is the only family member lacking a c-terminal domain.[63] IRAK4 is recruited to the Myddosome complex, activated then and causes the phosphorylation and activation of IRAK1 and IRAK2.[68] IRAK4 is required for all MyD88 dependent signalling and has been highlighted as a potential therapeutic target to inhibit aberrant pro-inflammatory responses.[68]

IRAK3 is the only family member that is not ubiquitously expressed and is mainly detected in macrophages in an inducible manner.[61] IRAK3 appears to play a negative role in TLR signalling downstream of Myddosome complexes. cGMP produced via IRAK3 has been observed to modulate NF-κB downstream of TLR4.[69] IRAK3 has been shown to inhibit translational control of pro-inflammatory cytokines via its interaction with IRAK2 and that IRAK3 is required for TLR-7 induced expression of inhibitory molecules (SHIP1, SOCS1, A20, IκBa).[70] In the absence of IRAK1/2, IRAK2 was shown to mediate NF-κB activation downstream of IL-1R.[70]

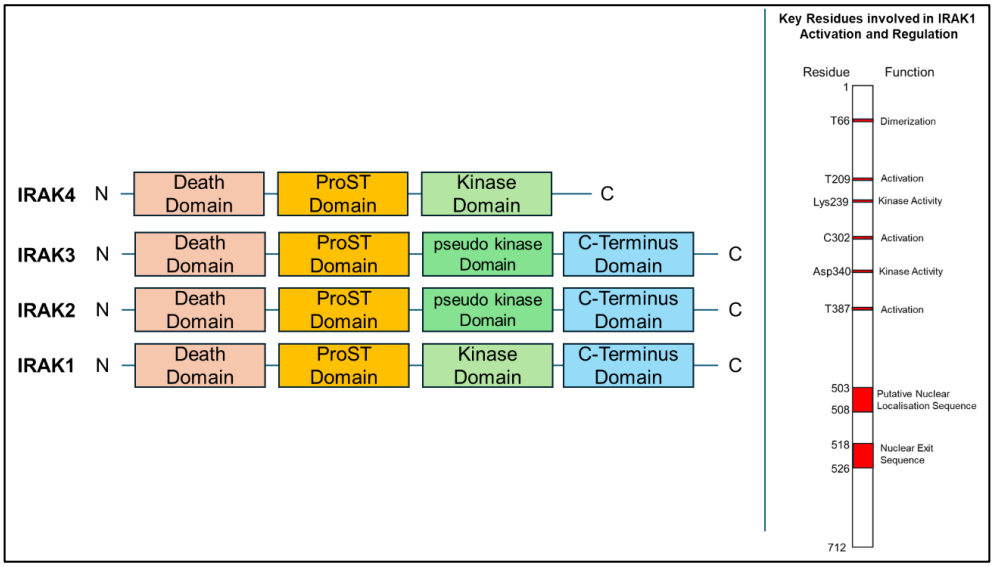

Figure 1.3.1: IRAK1 belongs to a family of threonine / serine kinases. Adapted from the literature.[64,61,65 64,71]

(1.3.3) Regulation and Activation of IRAK1

IRAK1 is subject to a series of post-translational modifications, including phosphorylation and ubiquitination, which are capable of regulating activation and dissociation from the receptor complex and degradation.

IRAK1 is phosphorylated at two key residues, T209 and T387, to regulate activation. It has previously been observed that phosphorylation of IRAK1 at T209 results in a weak activation while the phosphorylation of T387 is required for a more potent activation.[65] The phosphorylation of IRAK1 at T209 and T387 results in dissociation of IRAK1 from the receptor complex and allows for the propagation of downstream signalling.[71]

The third step in IRAK1 activation involves the autophosphorylation of several residues located within the ProST domain.[71] The ProST domain is rich in proline, serine and threonine residues which facilitate the hyperphosphorylation of IRAK1.[63] Two PEST sequences in the ProST domain have been indicated to potentially facilitate the degradation of IRAK1.[63]

IRAK1 is additionally regulated by ubiquitination in which ubiquitin is added to IRAK1 as a post translational modification. Following IL-1 stimulation IRAK1 and TRAF6 acquire Lys63 (K63) linked polyubiquitin chains, which was determined to require enzymatically active TRAF6.[72] Arginine substitution of Lys134 and Lys180 has been shown to impair IL-1R / TLR mediated IRAK1 ubiquitination, NEMO binding and NF-κB activation.[72] In addition to K63 linked polyubiquitination that facilitates the activation of IRAK1, the K48-linked polyubiquitination of IRAK1 targets IRAK1 for degradation.[62]

The residues Lys239 and Asp340 are located within the ATP binding region of IRAK1 and are crucial for the kinase activity of IRAK1.[61] Point mutations at K239S and D340N have been observed to be sufficient to abolish IRAK1 kinase activity.[61]

Interestingly, the overexpression of an IRAK1 kinase dead mutant led to the observation that IRAK1 is not required for NF-κB activation, while degradation of IRAK1 has been shown to require kinase activity and autophosphorylation of IRAK1.[61]

IRAK1 can also be regulated by micro-RNA's. In pancreatic cancer the micro-RNA miR-146 has been shown to downregulate the expression of IRAK1 and TRAF6.[73] Interestingly, it was further observed that miR-146 downregulation of IRAK1 supresses invasion of pancreatic cancer cells.[73]

(1.3.4) Signalling Pathways

IRAK1 has been extensively characterised as acting downstream of Interleukin Receptors including IL-1R, IL-18R and IL-33R and TLR's including TLR2, TLR3, TLR4, TLR7 and TLR9.[61] The TLR family of receptors mediate detection of a wide variety of ligands originating from bacteria, fungi, viruses and parasites (Table 1.3.1). The interleukin-1 receptor family contains ten type I transmembrane proteins which display similar architecture.[74] IL-1R1 and IL-1R2 bind to interleukin-1 ligand while IL-1R3 and IL-1R7 act as accessory proteins.[74] IL-1R2/8/P act as negative regulatory proteins.[74]

Table 1.3.1: Toll-Like Receptor family ligands and sources.[75,76]

Receptor	Ligand	Source
Toll-Like Receptor 1 Toll-Like Receptor 2	Triacyl Lipopeptides Peptidoglycan	Fungi Gram Positive Bacteria
Toll-Like Receptor 2 Toll-Like Receptor 6	Zymosan Diacyl Lipoproteins	Fungi Bacteria
Toll-Like Receptor 3	Poly I:C dsRNA	Viruses
Toll-Like Receptor 4	Lipopolysaccharide	Bacteria
Toll-Like Receptor 5	Flagellin	Bacterial Flagellum
Toll-Like Receptor 7	ssRNA Imidazoquinolinone	Viruses Bacteria
Toll-Like Receptor 9	Unmethylated DNA CpG-DNA Hemozoin	Bacteria Viruses Parasites

Figure 1.3.2 below provides an overview of IRAK1 signalling pathway downstream of TLR and IL-R activation. The binding of TLR's or IL-1R to their respective ligands is sufficient to stimulate the dimerization and activation of these transmembrane receptors.[77] Following this a conformational alteration occurs with these receptors that facilitates the recruitment of Interleukin-1 Receptor Accessory Protein (IL-1RAcp) to Toll- and IL-1R (TIR) domains located on the intracellular domains of these receptors.[78]

Myeloid Differentiation Primary Response 88 (MyD88) is recruited via TIR-to-TIR domain interactions.[77] The death domain of MyD88 then facilitates the recruitment and phosphorylation mediated activation of IRAK4.[59] IRAK4 has been observed to be constitutively active in unstimulated cells while the IL-1 induced autophosphorylation of IRAK4 is initiated by MyD88 induced dimerization of IRAK4 rather than increased catalytic activity of IRAK4.[79] Once activated, IRAK4 then mediates the phosphorylation and activation of IRAK1 and IRAK2.[59] TLR2 and TLR4

both use the TIR adaptor protein Mal in order to recruit MyD88 while TLR3 is capable of signalling independently of MyD88 via TRIF in order to induce activation of IRFs.[63] Studies have shown that pharmacological inhibition of IRAK4 did not impact IL-1 induced activation of IRAK1 which suggests IRAK1 allosteric induced activation of IRAK1 by IRAK4 rather than covalent modification mediated activation.[79]

The Toll-Interacting protein (Tollip) acts as an adaptor protein and forms complexes in the cytosol with unphosphorylated IRAK1. [80] Tollip is recruited to IL-1R with similar kinetics to IRAK1.[80] IRAK1 associated with Tollip is recruited to the death domain of MyD88 where it undergoes phosphorylation at T209 and T387 by IRAK4 and subsequent auto-hyperphosphorylation.[61] Immunoprecipitation (IP) studies have shown that IRAK1 phosphorylation is essential for downstream signalling as it reduces affinity for MyD88 and increases affinity for TRAF6.[80]

Once activated downstream signalling of IRAK1 culminates in the activation of NF-κB[71], c-Jun N-terminal Kinase (JNK)[81] and p38 mitogen activated kinase pathways (MAPK).[82] The binding of TRAF6 to IRAK1 mediates the recruitment of TAK1 and ubiquitin conjugating enzymes UBC13 and UEV1A as well as the TAK1 binding proteins TAB1 and TAB2.[61] Downstream of IL-1 stimulation TRAF-interacting protein with a forkhead-associated domain (TIFA) has been observed to promote NF-κB activation through enhancing association of IRAK1 and TRAF6 through its activity as an adaptor protein.[83] Once activated TAK1 mediates the activation of NF-κB (phosphorylation of IKKa/β) and MAPK (phosphorylation of MAPK 3/4/6) signalling pathways.[61,80]

Following stimulation of TLR4 or the IL-1, IRAK1 has been observed to translocate to the nucleus where it is further involved in the activation of NF-κB dependent transcription.[84] Interestingly following IL-1 stimulation IRAK1 has been observed to bind to STAT3 in the nucleus and direct it to the IL-10 gene promoter.[61]

Previous studies have shown that IRAK1 and IRAK4 are critical in the activation of NLRP3 as the deletion of IRAK1 or IRAK4 in *listeria* monocytes led to defective inflammasome activation.[85]

Downstream of TLR7, IRAK1 has been observed to directly bind to IRF7 and the kinase activity of IRAK1 was found to be critical for IRF7 activation.[86] TLR7 and TLR9 mediated IFN-α production was further observed to be abolished in IRAK1 deficient mice while inflammatory cytokine production remained unimpaired.[86]

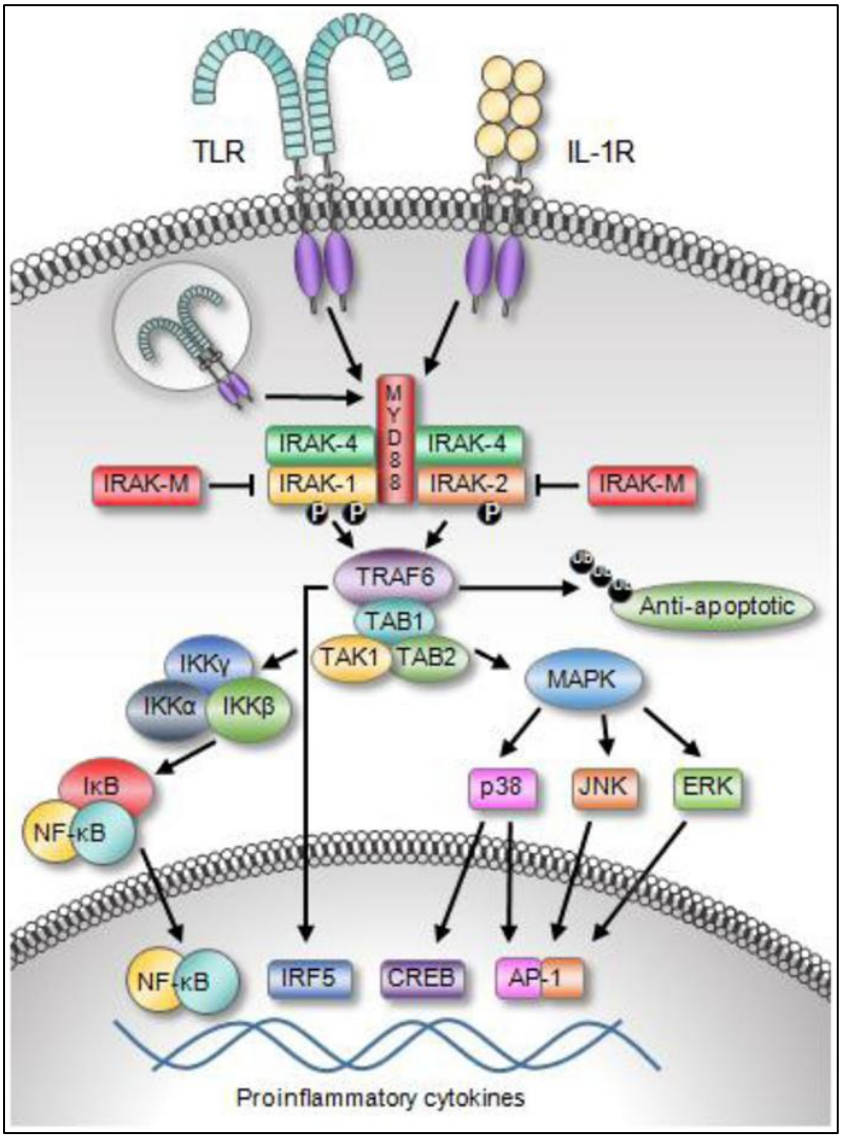

Figure 1.3.2: The activation of TLR and IL-1R mediates the activation of proinflammatory transcription factors via IRAK family signalling. Figure taken from the literature.[71]

(1.3.5) Role in Immune System and Autoimmunity

Due to its intricate role in the innate immune response, it is unsurprising that IRAK1 has a role to play in conditions of immune dysregulation and autoimmune conditions. Pre-term birth is a major cause of both neonatal mortality and morbidity, which is often triggered by chorioamnionitis or intrauterine inflammation with or without infection. As such while pre-term birth is not itself an autoimmune condition it can be driven by immune dysregulation and as such bears mentioning in this section. IRAK1 activation has been observed to be significantly increased in patients with chorioamnionitis compared to controls.[87] It was further observed, using murine models of pre-term birth, that IRAK1 inhibitors could significantly decrease pre-term births and increase live birth rate (dose dependent manner) while IRAK1 knockout mice were observed to be protected from pre-term birth.[87] Finally, IRAK1 was found to induce pre-term birth in murine models via upregulating the expression of COX-2.[87]

IRAK1 has been linked to several autoimmune conditions. Interestingly in the following examples evidence of IRAK1 playing a role comes from genetic association studies. In rheumatoid arthritis it has been shown that the rs1059703 T allele of IRAK1 increases the risk of disease, disease severity and the onset age of disease.[88] Another study has shown that IRAK1 polymorphisms are associated with susceptibility to a rare autoimmune condition called neuromyelitis optica spectrum disorder.[89] Finally a polymorphism in the IRAK1 gene has been associated with systemic sclerosis related pulmonary fibrosis.[90]

Autoimmune hypophysitis is a diseased caused by autoimmune inflammation in the pituitary gland. Studies have shown that IRAK1 is upregulated in the pituitaries of murine models of autoimmune hypophysitis.[91] Furthermore, it was shown that treatment with an IRAK1 specific inhibitor (Rosoxacin) significantly suppressed

murine autoimmune hypophysitis, downregulated cytokine/chemokine production and downregulated class II MHC expression.[91] It was hypothesised by this group that the inhibition of IRAK1 may lead to impaired activation of autoantigen-specific T cells and dampened T cell differentiation / recruitment to the pituitary gland.[91]

Systemic Lupus Erythematosus (SLE) is a chronic autoimmune condition in which the production of self-directed autoantibodies results in chronic inflammation and tissue / organ damage. A combined forward and reverse genetic approach of approximately 5000 subjects identified five single nucleotide polymorphisms (SNP's), spanning the IRAK1 gene, which were associated with both adult and childhood onset SLE.[92] Interestingly, this study further observed that IRAK1 deficiency, in Sle1 and Sle3 models, was sufficient to abrogate IgM/IgG autoantibodies, lymphocyte activation, renal disease and reversed dendritic cell hyperactivity.[92]

Almost a decade later another study found that IRAK1 transcript levels were significantly upregulated in CD4+ T-cells from patients with SLE compared to controls and that IRAK1 expression was positively associated with Th17 / IL-17A in patients.[93] These CD4+ T-cells were found to be more responsive (increased IRAK1 phosphorylation at Thr209) to IL-1b stimulation compared to controls.[93]

Therapeutic targeting of IRAK1 may hold potential benefit for patients. The inhibition of IRAK1 has been shown to repress expression of Th17 markers (retinoic acid receptor-related orphan receptor c, IL-23 and IL-17A) in Th17 polarised CD4+ T cells isolated from SLE patients.[93] Paeoniflorin, which decreases phosphorylation of IRAK1, has been effectively applied to reduce LPS induced activation of NF-κB in macrophages from lupus prone MRL/lpr mice.[94]

(1.4) The Role of IRAK1 in Cancer

As outlined in Section 1.1 and Section 1.2 OvCa and the clinically relevant HGSC subtype require identification and validation of novel therapeutic targets in order to improve treatment for patients. One of the main purposes of this thesis is to evaluate the potential of IRAK1 as a therapeutic target in OvCa and to assess therapeutic strategies targeting IRAK1.

IRAK1 has been well characterised for the role it plays downstream of TLR's and IL-1R where it acts to induce pro-inflammatory gene expression in response to pathogens. In addition to these protective functions IRAK1 has been shown to play important roles in the growth and progression of several cancer types including breast, pancreatic and gastric cancer (Table 1.4.1 and Table 1.4.2).

A pan-cancer analysis of the IRAK family of kinases found that IRAK genes expression showed considerable dysregulated in cancer and correlated to patient survival.[95] It was further observed that these genes correlated with tumour microenvironment, stemness score and immune subtypes in most cases.[95] Another pan-cancer analysis observed that IRAK1 levels are upregulated in more than twenty cancer types compared to normal tissues.[96] Increased IRAK1 expression was associated with poor prognosis with the most frequent DNA alteration being amplification.[96]

Table 1.4.1: IRAK1 has been linked to several aspects of cancer growth and progression in Myelodysplastic Syndrome (MDS), Breast Cancer, Acute Myeloid Leukaemia (AML), Low grade Glioma, Activated B-Cell like (ABC) Diffuse Large B-Cell Lymphoma (DLBCL), Gastric cancer.

Citation	Cancer Subtype	Role of IRAK1 in Cancer Growth
[97]	MDS	IRAK1 overexpressed and hyperactivated. Higher expression of IRAK1 correlates with reduced overall survival.
[98]	Breast Cancer	IRAK1 overexpressed. Knockdown of IRAK1 impaired growth and metastasis in vivo. IRAK1 knockdown impaired paclitaxel induced production of IL-1b, IL-6 and IL-8.
[99]	Breast Cancer	High IRAK1 expression, before and after neoadjuvant chemotherapy associated with shorter survival period. IRAK1 expression was decreased following neoadjuvant chemotherapy.
[100]	Breast Cancer	IRAK1 silencing reduced cell proliferation, invasion and migration.
[101]	Breast Cancer	1q21.3 directed S100A7/8/9-IRAK1 feedback loop promoted tumour sphere growth.
[102]	AML	IRAK1 overexpressed and promotes survival signalling. IRAK1 knockdown reduced leukaemia burden in vivo.
[95].	Low grade Glioma	IRAK1 inhibited cell apoptosis and augment malignancy both in vitro and in vivo.
[103]	ABC DLBCL	MyD88 mutants constitutively activated NF-kB and JAK signalling promoting malignant cell survival. Depletion of MyD88 and IRAK1 led to selective toxicity in vitro.
[104]	Gastric cancer	miR-146a significantly reduced in gastric cancer compared to non-cancerous tissue. miR-146a downregulates EGFR and IRAK1 expression in gastric cancer cells.

Table 1.4.2: IRAK1 has been linked to several aspects of cancer growth and progression in Hepatocellular Carcinoma (HCC), Prostate Cancer (PCa), Pancreatic Cancer Nasopharyngeal Cancer (NPCa), Cervical Cancer, Lung Cancer, and Non-small cell lung cancer (NSCLC).

Citation	Cancer Subtype	Role of IRAK1 in Cancer Growth
[105]	HCC	IRAK1 upregulated. Higher expression correlated with reduced overall survival. IRAK1 knockdown reduced proliferation, invasion, migration, MAPK/NLRP3/IL-1β signalling pathways and EMT in vitro.
[106]	HCC	IRAK1 upregulated. High IRAK1 mRNA and protein expression correlated with advanced stage detection and poor patient survival. IRAK1 regulated the AP1 / ALR1B10 signalling pathway in tumour initiating cells.
[107]	PCa	IRAK1 overexpressed in prostate cancer tissue compared to normal controls.
[73]	Pancreatic Cancer	miR-146 expression was lower compared to normal tissue. miR-146a downregulated EGFR and IRAK1 expression.
[108]	NPCa	IRAK1 knockdown sensitised NPCa cells to paclitaxel treatment in vivo.
[109]	Cervical Cancer	miR-146a promoted cervical cancer cell viability. miR-146a downregulated IRAK1 and TRAF6 expression.
[110]	Lung Cancer	IRAK1 expression significantly increased compared to normal adjacent tissue. Expression of IRAK1 was associated with stage, lymph node metastasis, tumour size and distal metastasis.
[111]	NSCLC	miR-146 downregulated in EGFR TKI resistant NSCLC. miR-146 enhanced sensitivity of EGFR TKI's and downregulated IRAK1 expression.

(1.4.1) IRAK1 in Hepatocellular Carcinoma (HCC)

Liver cancer represents a major global challenge as the third leading cause of cancer death and the eight most frequent cancer.[112] Hepatocellular Carcinoma (HCC) accounts for the majority (80%) of diagnoses and is associated with a poor OS rate and a median survival of only 6-10 months.[112]

IRAK1 is significantly upregulated in HCC.[106] IRAK1 mRNA and protein expression levels were both found to correlate with advanced stage disease and poor patient survival.[106] Another group observed that higher IRAK1 expression was associated with a shorter overall survival.[105]

IRAK1 knockdown in HCC cells inhibits proliferation, invasion and migration which was subsequently attributed to suppression of MAPK / NLRP3 / IL-1b pathway activation *in vitro*.[105] The inhibition of IRAK1 sensitised HCC cells to both doxorubicin and sorafenib *in vivo,* resulting in reduced tumour growth in a xenograft murine model.[106] It was further determined that IRAK1 contributes to the growth of HCC cells by regulating tumour initiating cell traits (self-renewal, tumorigenicity, tumour initiating cell biomarker expression) via the AP-1 / AKR1B10 signalling pathway.[106]

(1.4.2) IRAK1 in Melanoma

Melanoma is the 19th most common cancer worldwide.[113] In 2020 it accounted for 1.7% of new cancer diagnosis (325,000 cases) and approximately 57,000 deaths worldwide.[114] High stage diagnoses (IV) is associated with a poor five-year survival rate of 29.8% compared to stage I and stage II (81.9%) and stage III (68%).[114]

Melanoma cell lines display high levels of IRAK1 (S376) and IRAK4 (T345) constitutive activation.[81] Treatment with the IRAK1/4 inhibitor was observed to increase markers of apoptosis (PARP cleavage and caspase-3 cleavage) in

melanoma cells *in vitro* and augment Apoptosis induced by vinblastine and 5'Fluorouracil (but not cisplatin) in melanoma cell lines *in vitro.*[81]

In murine models (NSG mice subcutaneously injected with melanoma cells) treatment with the IRAK1-4 inhibitor was observed to reduce tumour volume alone and enhance tumour reduction in combination with vinblastine.[81] Interestingly this group also showed that treatment with IRAK1/4 inhibitor led to a reduction in NF-kB activation (p-p65) in melanoma cell lines *in vitro.*[81]

(1.4.3) IRAK1 in Medulloblastoma (MBL)

Medulloblastoma (MBL) is a cancer of the central nervous system (CNS) and is the most common paediatric brain malignancy.[115] MBL accounts for 20% of all CNS neoplasms in children and is the most commonly diagnosed in children aged 1 to 10 years old.[116] The 10-year mortality rate of MBL in children is 34.6%.[116] Aggressive therapeutic strategies with high dose treatment and radiation to CNS results in long term toxicities.[117]

Treatment with IRAK1-JAK2-FLT3 inhibitor pacritinib reduces growth and migration of medulloblastoma cells *in vitro*, increases survival in murine models and synergises both *in vitro* and *in vivo* with a MEK inhibitor (selumetinib).[117]

(1.4.4) IRAK1 in Glioblastoma Multiforme (GBM)

Glioblastoma Multiforme (GBM) is an aggressive malignancy which originates from astrocytic glial cells and accounts for 48.6% of all CNS.[118] GBM is associated with a relatively poor prognosis as the median survival is less than 15 months.[118]

Treatment with pacritinib reduces the viability and sphere forming ability of Brain Tumour Initiating Cells (BTICs) at micromolar concentrations.[119] It was further observed that treatment with pacritinib sensitised resistant BTICs and resulted in increased overall median survival in xenograft models.[119] Interestingly GBM displays frequent mutations in growth factor receptor (GFR) signalling with 88% showing abnormal GFR signalling and 40% EGFR signalling.[120] Treatment with synergises with Afatinib to reduce BTSC growth, sphere forming potential, STAT3 activity and abrogate resistance to EGFR inhibition.[120]

(1.4.5) IRAK1 in Diffuse Large B Cell Lymphoma (DLBCL)

Diffuse Large B-cell Lymphoma (DLBCL) is the most frequently diagnosed (30-40%) non-Hodgkin's lymphoma worldwide.[121] R-CHOP is currently the main therapeutic strategy (consisting of Rituximab, cyclophosphamide, doxorubicin / hydroxydaunorubicin, vincristine / oncovin, prednisone) and results in long-term disease control in 90% patients presenting with limited stage and 60% for patients presenting with advanced stage disease.[122]

Activated B cell-like (ABC) DLBCL displays constitutive NF-κB and JAK kinase signalling which promotes malignant cell survival.[103] It has been observed that MyD88, IRAK1 and IRAK4 are essential for ABC DLBCL survival and that oncogenic mutations in MyD88 are capable of driving NF-κB, JAK kinase and STAT3 signalling through the activation of IRAK1 and IRAK4.[103] Treatment with IRAK1/4 inhibitor was observed to display selective lethality for ABC DLBCL cell lines and resulted in significantly reduced viability *in vitro.*[103]

(1.4.6) IRAK1 in Acute Myeloid Leukaemia (AML)

Acute Myeloid Leukaemia (AML) is the most common acute leukaemia in adults, accounting for approximately 80% of cases.[123] Studies of patients up to 60 years of age have reported the five-year survival rate of AML to lie between 30-35%.[124]

Elevated levels of IRAK1 have been reported in primary AML cells compared to healthy cells.[102] IRAK1 knockdown results in reduced growth of FLT3-wild type and FLT3-ITD (internal tandem duplication mutation) positive cell lines *in vitro* and led to a significant reduction in leukaemia burden in an AML xenograft model.[102] Treatment with pacritinib was further observed to impair the growth of AML cells (to a greater extent than JAK1/2 and FLT3 inhibitors), reduce AML progenitors in vitro and leukaemia burden in an AML xenograft model.[102]

(1.4.7) IRAK1 in Breast Cancer (BrCa)

Breast cancer (BrCa) is one of the most common cancers worldwide and in 2020 it accounted for 11.7% (2.3 million) of all new cancer cases[125] and 685,000 deaths.[126] BrCa can be further divided into molecular subtypes including luminal A, luminal B, Human Epidermal Growth Factor Receptor (HER2)-positive or Triple Negative.[125]

Higher IRAK1 expression prior to and following neoadjuvant chemotherapy has been found to correlate with a shorter survival period.[99] It was additionally shown that IRAK1 is downregulated following neoadjuvant chemotherapy.[99] Another breast cancer study has shown that overexpression of miR-146a or silencing of IRAK1 resulted in impaired cell proliferation, migration and invasion.[100]

Tumour recurrence is a major cause of breast cancer associated mortality. It has been observed that chromosomal copy number amplification at 1q21.3 is enriched in breast cancer tumour initiating cells (TICs).[101] Amplification was enriched in recurrent tumours (70%) compared to primary (10-30%).[101] IRAK1 activation in breast cancer was found to correlate with increased tumour-sphere growth, recurrence and NF-kB signalling.[101] Finally, it was observed that 1q21.3-directed an S100A7/8/9-IRAK1 feedback loop driving tumour sphere growth which could be impaired upon treatment with the IRAK1 inhibitor pacritinib.[101]

Triple negative BrCa (TNBC) are characterised by lack of expression of the oestrogen receptor (ER), progesterone receptor (PR) and HER2.[127] TNBC displays a more aggressive phenotype and more frequent pathologic complete response following neoadjuvant chemotherapy compared to other subtypes of breast cancer.[128] Acquired chemotherapy resistance poses a significant barrier to effective treatment which results in shorter OS compared to other breast cancer subtypes.[98]

IRAK1 is overexpressed in the TNBC subtype.[98] It has further been shown that IRAK1 inhibition could sensitise TNBC cells to paclitaxel treatment and that IRAK1 knockdown impaired TNBC metastasis and growth *in vivo* using a xenograft model.[98] Finally, it was shown that IRAK1 knockdown impaired the production of IL-1b, IL-6 and IL-8 cytokines which were induced by paclitaxel treatment.[98]

Previous studies has shown that HER2 induces a feed-forward loop of IL-1a and IL-6 which stimulates NF-kB and STAT3 pathways for generation and maintenance of breast cancer like stem cells.[129] In HER2-positive breast cancer treatment with an IRAK1 inhibitor was shown to result in a rapid decrease in p65 phosphorylation and NF-kB signalling however no significant impact was observed on cell growth.[129] Interestingly when applied in combination with either CPL or PTX the group observed a synergistically increased induction of cell death in HER2+ breast cancer cells.[129]

Finally, less has been published linking IRAK1 to ER+ breast cancers thank either of the other subtypes. However, one study using the ER+ MCF-7 breast cancer cell line has shown that miR-146a enhances the sensitive of these cells to paclitaxel treatment through the downregulation of IRAK1.[100] It was further shown that silencing of miR-146a and overexpression of IRAK1 was capable of increasing proliferation, invasion and migration in this ER+ cell line.[100]

(1.4.8) IRAK1 in Myelodysplastic Syndrome (MDS)

Myelodysplastic Syndrome (MDS) are a group of disorders (cytopenia's, marrow dysplasia) that arise from a defective hematopoietic stem cell or progenitor cells.[130] Approximately 30% of MDS will develop into aggressive AML.[130]

IRAK1 has been observed to be overexpressed and hyperactivated in MDS with higher IRAK1 expression shown to correlate with reduced OS.[97] Treatment with the IRAK1/4 inhibitor was found to impair expansion, increase apoptosis in MDS clones, inhibit TRAF6 / NF-kB signalling and be selectively detrimental to MDS cells but not normal CD34+ cells.[97] Finally, it was shown using xenograft models that IRAK1 inhibition suppressed MDS *in vivo* and displayed elevated efficacy in MDS clone elimination when applied in combination with BCL2 inhibitors.[97]

(1.4.9) IRAK1 in Prostate Cancer (PCa)

Prostate cancer (PCa) represents the second most common cancer in men accounting for 1,276,106 cases and 358,989 deaths worldwide in 2018.[131] PCa is the highest cause of cancer-associated mortalities in western countries.[132]

In PCa, IRAK1 (mRNA) is significantly enriched in luminal epithelial cells.[107] Interestingly, IRAK1 is significantly overexpressed in PCa compared to normal prostate controls while the expression of IRAK4, MyD88 and TRAF6 were found to display no change.[107]

(1.4.10) IRAK1 in Nasopharyngeal Carcinoma (NCa)

Nasopharyngeal carcinoma (NCa) arises from the epithelial tissue of the nasopharyngeal mucosal lining in the nasopharynx.[133] NCa represents a relatively uncommon cancer accounting for 129,000 new cases (0.7%) worldwide in 2018.[133] NCa displays a high frequency of advanced stage detections with more than 70% of patients being diagnosed at the advanced stage.[134] Advanced stage NCa is associated with a median survival of three years while the 10-year survival for those diagnosed at stage I and stage II is 98% and 60% respectively.[134]

Paclitaxel-resistant NCa cells and relapsed / metastatic clinical samples display increased levels of IRAK1 phosphorylation and constitutive activation of the IRAK1-S100A9 signalling axis.[108] S100A9 was identified to confer resistance to paclitaxel and correlate with poor prognosis in NCa.[108] Treatment with pacritinib results in suppression of S100A9 expression, induce apoptosis and sensitise NCa cells to paclitaxel both *in vitro* and *in vivo.*[108]

(1.4.11) IRAK1 in Pancreatic Cancer (PC)

Pancreatic cancer (PC) accounts for approximately 2% of all cancer cases and 5% of all cancer deaths with pancreatic ductal adenocarcinoma (PDAC) being the most common subtype.[135] PC is associated with a poor prognosis, with a five-year survival rate of 4.2% for all stages of PC.[136]

PC cells have significantly lower expression of miR-146a compared to human pancreatic duct epithelial cell controls.[73] It was further observed that re-expression of miR-146a led to the inhibition of EGFR signalling and inhibition of IRAK1 / NF-kB signalling and MTA2 expression in PC cells.[73] Finally, it was found that miR-146a inhibited PC cell invasion.[73]

(1.4.12) IRAK1 in Cervical Cancer

Cervical Cancer is the fourth most common female specific malignancy and accounted for 569,847 new cases and 311,365 deaths worldwide in 2018.[137] miR-146a, IRAK1 and TRAF6 expression is increased in cervical cancer cell lines compared to a non-tumorigenic control cell line.[109] Transfection of miR-146a has been observed to significantly promote cell growth, decrease apoptosis and reduce IRAK1 and TRAF6 expression in cervical cancer cell lines.[109] Interestingly reduced expression of IRAK1 and TRAF6 using siRNA was observed to promote cell viability in cervical cancer cells.[109] The role of IRAK1 in cervical cancer appears to be protective and may indicate a cancer specific role for IRAK1.

(1.4.13) IRAK1 in Gastric Cancer (GC)

Gastric cancer (GC) accounts for over one million new cases annually and in 2018 it accounted for 784,000 deaths globally.[138] The five-year survival rate for stage IA-IB is between 60 and 80%, while at higher stages this drops considerably with stage III tumours showing a five-year survival rate between 18% and 50%.[139]

In a study of 90 clinical gastric cancer samples observed that miR-146a levels were significantly lower compared to noncancerous tissue controls.[94] It was further

shown that lower miR-146a expression levels were an independent prognostic factor for overall survival and was associated with lymph node metastasis and venous invasion.[104] Finally, it was shown that ectopic expression of miR-146a inhibited migration / invasion and downregulated EGFR and IRAK1 expression in GC cells.[104]

(1.4.14) IRAK1 in Lung Cancer (LC)

Lung cancer is the leading cause of cancer related deaths worldwide.[140] In 2018, LC is estimated to have accounted for 12% of the global cancer burden (2.1 million new cases) and one in five cancer related deaths (1.8 million) worldwide.[141] The five-year survival rate for LC is between 19% and 23% for non-small cell lung cancer (NSCLC) and 6% for small cell lung cancer (SCLC).[141] NSCLC is the most common of these two subtypes and accounts for 80-85% of all LCs.[141]

Immunohistochemical analysis of 365 tumour and 30 normal tissue sections led to the observation that IRAK1 protein expression was significantly increased in LC compared to normal controls.[110] It was further shown that IRAK1 expression was associated with stage of disease, lymph node metastasis, distal metastasis and tumour size.[110]

Treatment of NSCLC cells with pacritinib sensitised cells to erlotinib *in vitro* and reduced AKT, ERK and STAT3 activation.[142] Interestingly another study showed that silencing of IRAK1 enhanced sensitivity of NSCLC to EGFR TKIs.[111] miR-146b-5p was significantly lower in patients with acquired resistance to EGFR TKI treatment and ectopic expression of miR-146b-5p enhanced EGFR TKI induced apoptosis in EGFR TKI resistant cells.[111] miR-146-5p played a role in EGFR TKI sensitivity by targeting the IRAK1-NF-kB signalling axis.[111]

(1.4.15) IRAK1 in Thyroid Cancer

Thyroid cancer represents the ninth most common cancer worldwide with approximately 75% of all cases being diagnosed in women.[143] Anaplastic thyroid cancer is a very aggressive cancer that is associated with poor prognosis and a low median survival of approximately 6 months.[144] Treatment with an IRAK1/4 inhibitor synergised with Lenvatinib to impair proliferation, increase ERK inhibition and induce G2/M cell cycle arrest *in vitro.*[144] Finally, this drug combination enhanced the reduction in tumour volume *in vivo* using a xenograft murine model.[144]

(1.4.16) IRAK1 in Ovarian Cancer (OvCa)

Over recent years, IRAK1 has been shown to play important roles in the growth and progression of several cancers (Table 1.4.1 and Table 1.4.2). IRAK1 has been identified as one of seventeen genes to be differentially expressed (increased) in OvCa compared to normal controls.[134] This study provides an initial link between IRAK1 expression and OvCa, however the role that IRAK1 plays in the growth and progression of OvCa remains unclear.

In a recent study, IRAK1 mRNA expression has been observed to be significantly increased in EOC compared to normal tissue, and carboplatin resistant OvCa compared to sensitive controls.[145] IRAK1 protein levels were elevated in high stage HGSC compared to matched normal fallopian tube tissue.[145] Finally, treatment with an IRAK1 kinase inhibitor (TCS2210) resulted in reduced STAT3 activation, inhibition of EOC cell line growth, increased apoptosis and synergised with cisplatin.[145]

(1.5) Introduction to The IRAK1-JAK2-FLT3 inhibitor Pacritinib

OvCa is the fourth most common female specific cancer worldwide and it accounts for over 300,000 cases and 200,000 cancer related deaths each year.[146] OvCa displays a high incidence (approximately 75%) of advanced stage detection[147] and high frequency (approximately 70% of initial responders) of relapse to first line therapeutic interventions[13]. With a five-year survival rate of only 29% for those diagnosed with advanced stage disease[13], it is clear that novel therapeutic strategies are urgently required in order to improve patient outcomes.

IRAK1 has been shown to promote growth and play important roles in the progression of several cancers typically through hyperactivation or overexpression. These cancers include lymphomas and leukaemia's, along with solid cancers such as pancreatic and triple negative breast cancer .[65, 67, 87, 88, 134] IRAK1 has previously been identified as one of seventeen genes differentially expressed in OvCa compared to normal controls, more specifically IRAK1 was observed to be increased in OvCa.[134] We wanted to investigate the potential of IRAK1 as a novel therapeutic target in HGSC using expression analysis, IRAK1 knockdown and an FDA approved IRAK1 kinase inhibitor (pacritinib) to achieve this.

(1.5.1) Pacritinib: an IRAK1 Kinase Inhibitor

Many studies have shown the potential use of IRAK1 kinase inhibitors in the treatment of various cancers as they have been shown to impair cancer growth both *in vitro* and *in vivo* (Table 1.5.1 and Table 1.5.2). Pacritinib is a commercially available small molecule kinase inhibitor with IC50 values in the nanomolar range that targets Janus Kinase 2 (JAK2) (IC50 = 5nM), FLT3 (IC50 = 14.8nM) and IRAK1 (IC50 =

13.6nM). The kinase profile of pacritinib has previously been outlined and published.[148]

Pacritinib has shown significant efficacy in impairing cancer cell growth both *in vitro* and *in vivo* (Table 3.1 + Table 3.2). In a breast cancer study, amplification of chromosomal region 1q21.3 was found to direct an S100S7/8/9 – IRAK1-positive feedback loop promoting breast cancer tumour sphere growth, which was inhibited following treatment with pacritinib.[101] In nasopharyngeal carcinoma, pacritinib treatment has been shown to resensitise cells to paclitaxel using an acquired resistance model.[108] In medulloblastoma, the treatment of pacritinib impaired cancer cell growth *in vitro,* which was attributed to the inhibition of JAK2 and STAT3.[117] Pacritinib has also been shown to inhibit growth in non-small cell lung carcinoma[142] and reduce leukemic burden in acute myeloid leukaemia (AML) xenograft models[102] To the best of our knowledge, the potential application of pacritinib has not been investigated in OvCa to date.

Pacritinib received FDA approval in February 2022 for the treatment of adults with intermediate / high risk primary / secondary (post-polycythaemia vera or post-essential thrombocythemia) myelofibrosis with a platelet count below $50x10^9$/L.[149] As pacritinib is FDA approved, this gives us a better understanding of the safety profile and tolerance of pacritinib, allowing us to be confident that should this molecule show promising results inhibiting OvCa growth *in vitro* that it may be possible to progress to pre-clinical *in vivo* models and clinical trials with more confidence.

Pacritinib has shown significant efficacy in a number of cancers and has entered phase two clinical trials for colorectal cancer (NCT02277093), prostate cancer (NCT04635059) and relapsed / refractory T cell lymphoproliferative neoplasms (NCT04858256). Additionally, pacritinib has entered a phase 1B/2 clinical trial for the treatment of patients with 1q21.3 amplified solid tumours (NCT04520269). The efficacy observed for pacritinib in these studies has contributed heavily to our

decision to select pacritinib as our IRAK1 kinase inhibitor for the purposes of this study. It is important to appreciate that while pacritinib inhibits IRAK1 kinase activity, it also inhibits JAK2 and FLT3 kinase activity and has been applied in studies to further assess the role and potential of targeting these kinases in cancer.[117,120]

Table 1.5.1: IRAK1 kinase inhibitors have been shown to be effective therapeutic strategies in several subtypes of cancer including Medulloblastoma, Glioblastoma (GBM) Brain tumour stem cells (BTSC's), Breast Cancer, Hepatocellular carcinoma (HCC), Non-small cell lung carcinoma (NSCLC), Melanoma and Nasopharyngeal carcinoma.

Citation	Cancer Subtype	Impact of treatment with IRAK1 inhibitor
[150]	Medulloblastoma	Increased JAK2/STAT3 activation following selumetinib (MEK) treatment. JAK2/STAT3 inhibition using pacritinib impaired tumour growth *in vitro*. Selumetinib plus pacritinib further reduced growth both *in vivo* and *in vitro*.
[151]	GBM BTSC's	Pacritinib impaired BTSC growth and sphere forming capacity *in vitro*. Pacritinib and afatinib were synergistic *in vivo* through inhibition of STAT2 inhibition.
[152]	GBM BTIC's	Pacritinib treatment decreased BTIC viability and sphere forming potential *in vitro*. Pacritinib improved response to TMZ in TMZ resistant BTIC's and improved overall median survival in an aggressive recurrent GBM BTIC xenograft model.
[153]	Breast Cancer	1q21.3 directed S100A7/8/9-IRAK1 feedback loop promotes tumour sphere growth. Treatment with pacritinib reduced tumour sphere growth.
[154],	HCC	Treatment with IRAK1/4 inhibitor sensitised cells to both doxorubicin and sorafenib *in vitro*. Pacritinib plus sorafenib inhibited tumour growth *in vivo*.
[131]	NSCLC	Pacritinib plus Erlotinib synergistically reduced PC-9/ER3 cell growth both *in vitro* and *in vivo*.
[155]	Melanoma	IRAK1/4 inhibitor increased sensitivity to vinvkastine and 5'fluorauraeil but not cisplatin *in vitro*. IRAK1/4 inhibitor resulted in reduced NF-κB activation.
[156]	Nasopharyngeal Carcinoma	Pacritinib resensitised cells to paclitaxel in an acquired resistance model.

Table 1.5.2: IRAK1 kinase inhibitors have shown efficacious inhibition of growth in several subtypes of cancer including Acute Myeloid Leukaemia (AML), Myelodysplastic Syndrome (MDS) and anaplastic thyroid cancer.

Citation	Cancer Subtype	Impact of treatment with IRAK1 inhibitor
[157]	MDS	IRAK1/4 Inhibitor impaired expansion of MDS clones, increased apoptosis, led to the inhibition of TRAF6/NF-κB and suppressed MDS xenograft model. IRAK1 and BCL2 inhibition more effectively eliminated MDS clones.
[158]	AML	Pacritinib impaired growth of AML cells and reduced AML progenitors *in vitro,* reduced leukaemia burden *in vivo* and reduced phosphorylation of IRAK1. AML cells showed increased sensitivity to pacritinib compared to other JAK1/2 or FLT3 inhibitors.
[159]	Anaplastic Thyroid Cancer	IRAK1/4 inhibitor synergistically reduced proliferation when combined with Lenvatinib *in vitro,* reduced tumour volume *in vivo*, reduced ERK activation and increased cell cycle arrest.
[160]	AML	FLT3 inhibition using pacritinib impaired STAT3, MAPK and PI3K signalling and led to reduced primary tumour growth and metastasis using murine models of FLT3-ITD-driven AML.

(1.5.2) JAK2 and STAT3 as Therapeutic Targets in Cancer

In addition to inhibiting the kinase activity of both IRAK1 and FLT3, pacritinib also inhibits the activation and activity of JAK2 and has been used in studies to investigate the potential of targeting JAK2 and STAT3 signalling in several cancers. JAK2 becomes activated in the presence of cytokines such as IL-6 and subsequently mediates the activation of STAT3[161] which plays an important role in regulating cellular processes such as proliferation and differentiation.[162] The activation of the JAK2 and STAT3 signalling pathway has previously been shown to play important roles in several solid cancers including colorectal carcinoma[163], gastric cancer[164], breast

cancer[165], and OvCa.[166] JAK2 has also been shown to represent a potential therapeutic target in colorectal carcinoma[163], gastric cancer[164] and OvCa.[166]

In gastric cancer, the use of the JAK2 inhibitor WP1066 led to the reduced activation of JAK2 – STAT3 induced proliferation and increased apoptosis.[164] It was further observed that treatment with WP1066 led to a significant reduction in tumour volume using a xenograft model of gastric cancer.[164]

The JAK2-STAT3-CyclinD2 signalling pathway has been highlighted as a mechanism for the persistent growth of cancer stem cells following radiotherapy in colorectal cancer.[167] This study further showed that JAK2 transcription was increased following radiotherapy and that targeted knockdown of JAK2 could decrease STAT3 activation and sensitise cells to radiotherapy through enhancing apoptosis. In another colorectal carcinoma study, mesenchymal stromal cell secretion of IL-6 has been shown to contribute to progression via the activation of JAK2-STAT3 signalling pathways.[168] Additionally, cancer associated fibroblasts have been shown to promote TGF-β mediated EMT shift, inhibition of apoptosis and paclitaxel resistance through the expression of IL-6 and activation of JAK2-STAT3 signalling pathways.[165] Finally, inhibition of JAK2-STAT3 signalling has been shown to induce apoptosis in colorectal carcinoma cells.[163]

In ovarian cancer, one study of 341 EOC patients observed nuclear activation of STAT3 in 28% of samples and nuclear activation of JAK2 in 83% of samples.[169] This study further reported that the STAT3 activation positive cohort showed reduced PFS and reduced OS in EOC.[169] Another study showed that STAT3 and JAK2 were significantly more activated in HGSC samples compared to normal tissue and benign tumours.[170] This study further showed that the JAK2 inhibitor AG490 could be used to block mobility, N-cadherin, vimentin, and IL-6 expression while also blocking phosphorylation of STAT3.[170]

AlkB homolog 5, RNA demethylase (ALKBH5) has been shown to be upregulated in cisplatin resistant EOC and the overexpression of ALKBH5-HOXA10 has been observed to activate JAK2/STAT3 signalling in EOC contributing to chemoresistance.[171] It was further shown that the inhibition of JAK2-STAT3, using WP1066, in ALKBH5-HOXA10 overexpressing cells was sufficient to induce cisplatin sensitivity.[171] Similar findings were found in a 2014 study which showed paclitaxel treatment of OvCa cells resulted in cancer stem cell like residual population with activated JAK2-STAT3 signalling.[166] Treatment with a JAK2 inhibitor was found to effectively sensitise these residual cells to paclitaxel treatment.[166]

These four studies examining the JAK2-STAT3 signalling pathway in OvCa provide strong evidence that this pathway plays an important role in OvCa. Furthermore, these studies highlight the potential of targeting JAK2-STAT3 as a therapeutic strategy in OvCa.

(1.5.3) FLT3 as a Therapeutic Target in Cancer

In addition to inhibiting the kinase activity of both IRAK1 and JAK2, pacritinib also inhibits the activity of the FLT3 receptor. The FLT3 ligand (FLT3L) is a growth factor which acts on the FLT3 receptor and is expressed on FLT3+ multipotent progenitor and common lymphoid progenitors in order to activate PI3K and mTOR signalling.[172] Following ligand binding and activation the FLT3 receptor mediates the activation of PI3K, RAS, AKT, STAT5 and ERK1/2 which together contribute to the regulation of cell survival and proliferation.[173]

FLT3L has previously been indicated to activate an antitumour immune response through the activation of dendritic cells.[172] The administration of FLT3L has been observed to result in a delayed appearance of prostate tumours *in vivo* and

resulted in a suppression of metastasis.[174] The use of the JAK2 and FLT3 inhibitor TG02 has been shown to inhibit the proliferation of leukaemia cell lines.[175]

OVCAR-8 cells overexpressing ABCB1 drug efflux transporters provide a model to investigate multidrug resistant cells which was used in the following study. One study using both OVCAR-8 and ABCB1 over expressing OVCAR-8 variant NCI-ADR-RES has shown that midostaurin (FLT3 inhibitor) can resensitise ABCB1 overexpressing cells to chemotherapeutics (including paclitaxel) and induce apoptosis in multidrug resistant cells.[176]

Pancreatic ductal adenocarcinoma (PDAC) represents an aggressive and hard to detect cancer in which FLT3 expression may be a favourable prognostic indicator as the expression of FLT3 and Poly(RC) Binding Protein 3 (PCBP3) have been highlighted as potential biomarkers which are associated with favourable prognosis.[177] A similar finding was observed in breast cancer where FLT3 was observed to be a favourable prognostic indicator.[172] This study observed FLT3 was elevated in breast cancer and associated with menopause, age, stage and histological and molecular subtypes.[172] It was further shown that FLT3 expression correlated with abundance of CD4/CD8+ T cells, myeloid dendritic cells (DC's) and neutrophils which may explain the positive association with prognosis which was observed.[172]

While FLT3 appears to be a positive prognostic indicator in both pancreatic ductal adenocarcinoma and breast cancer the role of FLT3 may be dependent on cancer subtype as studies appear to support a negative role for FLT3 in OvCa. In HGSC patients with metastasis, FLT3, along with Epidermal Growth Factor Receptor (EGFR), Leptin Receptor (LEPR) and activated STAT3, have been found to be upregulated.[178] It was further observed that alternatively activated macrophages (from

healthy donors) were capable of promoting spheroid spreading through the secretion of FLT3L, Leptin and HB-EGF.[178]

(1.6) Introduction to The Human Epidermal Growth Factor Receptor (HER) Family

Receptor Tyrosine Kinases (RTKs) are transmembrane proteins which become activated following the binding of extracellular ligands. RTKs regulate various cellular processes including normal cellular physiology, proliferation, metabolism and differentiation **(Figure 1.6.1)**.[179] The Human Epidermal Growth Factor Receptor (HER) family of RTKs, consists of four members EGFR/HER1, HER2/ErbB2, HER3/ErbB3 and HER4/ErbB4 which play important roles in the regulation of proliferation, survival and migration.[180] HER family members have been extensively characterised to regulate both growth and progression in many types of cancer such as the overexpression of HER2 in HER2 positive breast cancer or activating mutations of EGFR in NSCLC.[181]

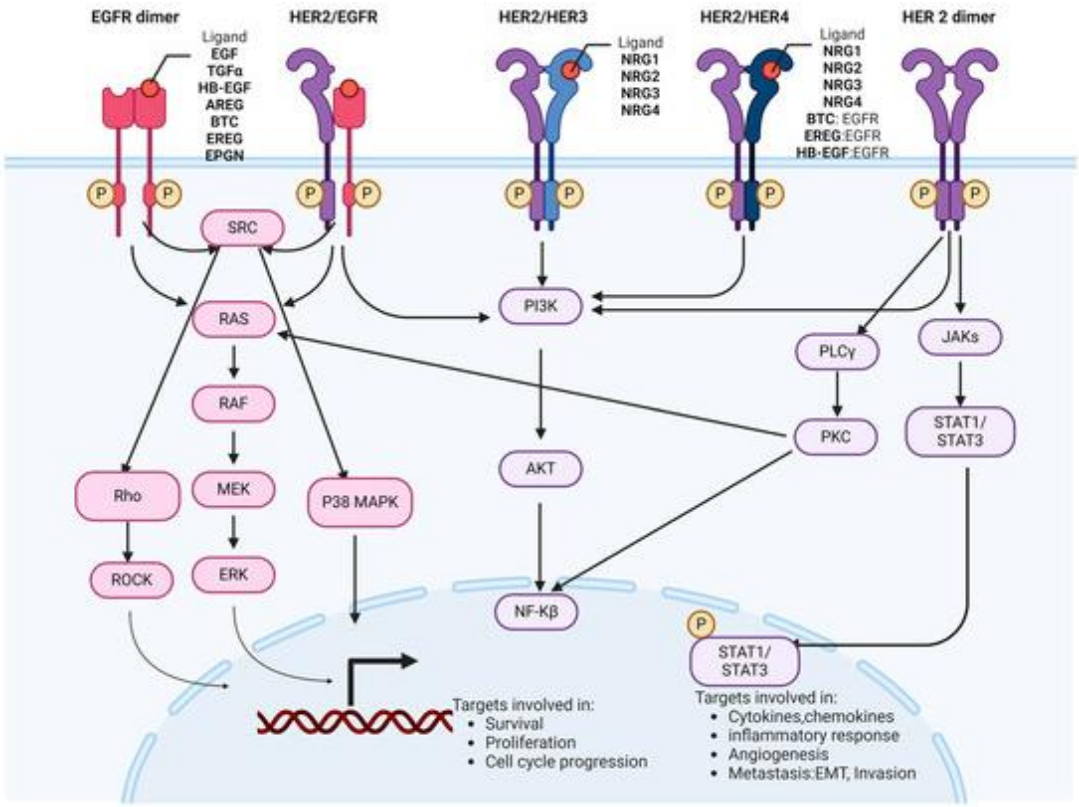

Figure 1.6.1: HER Family receptors regulate various signalling pathways involved in regulation of key physiological processes involved in cancer including survival, proliferation and cell cycle progression. Figure was taken from the literature.[182]

HER family members are activated by growth factors which are capable of promoting the division and migration of normal cells.[183] These growth factors can signal through an autocrine, paracrine or juxtracrine manner in order to mediate the activation of HER receptors.[184] A total of ten known ligands (Table 1.6.1) have been found to be capable of activating HER family members.[185] In addition to roles in normal physiology, growth factors have been identified to play important roles in cancer. For example, increased expression of neuregulin's have been associated with poorer clinical prognosis and has been linked to stemness, invasiveness, proliferation, resistance to apoptosis and angiogenesis in cancer.[186]

In the absence of a ligand, the EGFR, HER3 and HER4 all exist in a tethered and closed conformation which leaves the intracellular dimerization domain

inaccessible for binding.[187] The exception to this is HER2 for which there is no known ligand. HER2 instead remains in an active extended conformation which can form homodimers and heterodimers with other HER family receptors.[180]

Following the binding of a ligand, HER family receptors undergo homodimerization or heterodimerization which enables the phosphorylation of tyrosine residues on the intracellular carboxy terminal domain.[179] This provides a docking site for the recruitment and activation of downstream adaptor signalling molecules.[179] HER3 lacks a tyrosine kinase region and similarly to HER2 requires heterodimerisation to function.[180]

Table 1.6.1: HER family receptors are activated by ten known ligands. [180,187]

HER Family Member	Ligands
EGFR Specific	EGF (Epidermal Growth Factor) TGF-a (Transforming Growth Factor Alpha) Amphiregulin
EGFR and HER4	Betacellulin Heparin-binding EGF-like Growth Factor Epiregulin
HER3 and HER4	Neuregulin 1 Neuregulin 2
HER4	Neuregulin 3 Neuregulin 4

Dimerization interactions between HER family members appear to be both complex and dynamic. EGFR is capable of recruiting HER2, HER3 and HER4 during dimerization.[183] In pancreatic carcinoma and melanoma, HER3 has been identified as the preferred heterodimeric partner for EGFR.[188] Following ligand stimulation and receptor dimerization HER family receptors activate intracellular signalling pathways

including both the RAS-RAF-MEK-ERK and PI3K-AKT signalling pathways which regulate proliferation, differentiation, adhesion, apoptosis and tumorigenesis.[189,190,191,192,193]

HER family receptors have been observed to be broadly expressed in OvCa.[189] Studies of OvCa cell lines have shown that the platinum resistant HGSC PE04 cell line expresses HER4 while the patient-matched platinum sensitive PE01 cell line doesn't express detectable levels of HER4.[194] Analysis of 207 OvCa patient samples including normal ovary (23), borderline (19) and benign (64) led to the observation that protein and median gene expression of HER2, HER3 and HER4 were significantly elevated in OvCa.[189] Protein expression of EGFR was observed to be significantly decreased in OvCa.[189]

Targeted therapies directed against HER family members may hold promise in OvCa. The pan-HER inhibitor Poziotinib has been observed to decrease the proliferation and viability of OvCa stem cells while inducing G1 cell cycle arrest and apoptosis in addition to inhibiting spheroid formation and stemness.[195] This study attributed these findings to reduced WNT, Notch and hedgehog signalling.[195] An important role was shown for HER4 in this study as the inhibition of HER4, using Poziotinib, was found to lead to a reduction in the activation of STAT5, AKT and ERK in HER4 overexpressing OvCa stem cells.[195]

(1.6.1) The Epidermal Growth Factor Receptor

EGFR is a 170kDa transmembrane glycoprotein, consisting of an external ligand binding domain and an intracellular tyrosine kinase domain, which through the activation of MAPK, PI3K and PLCy signalling pathways mediates mitogenic signalling.[196] Phosphorylation of EGFR at residues Y845, Y992, Y1045 and Y1068

are important for receptor stabilisation, degradation and activation of downstream signalling.[197] Phosphorylation at Y1068 has been observed to be particularly important for recruitment of adaptor protein GRB2.[183]

Expression of the EGFR has been reported in 22-75% of ovarian cancers.[196] It was further reported that increased expression of EGFR is associated with poorer OS[196], poor prognosis[197], and the presence of ascites in OvCa.[189]

Targeting EGFR activity using small molecule tyrosine kinase inhibitors (TKI's) has shown significant efficacy in a number of cancers including NSCLC[198] and OvCa.[196,193] Erlotinib received FDA approval in 2004 for treatment of locally progressed or metastatic NSCLC and as a first line therapeutic approach for patients with pancreatic cancer.[198]

While EGFR receptor inhibition has been shown to be an effective treatment in lung cancer the potential of EGFR TKI's in OvCa remains unclear. One study, using a PE04 xenograft model, has shown that the use of ZD1839 (orally active EGFR TKI) could reduce tumour growth *in vivo.*[196] *In vitro* work using OvCa cell lines expressing the EGFR receptor failed to show a reduction in growth following treatment with EGFR inhibitors.[193]

(1.6.2) Human Epidermal Growth Factor Receptor 2 (HER2)

Overexpression, amplification and mutations of HER2 are found in a wide variety of cancers where they are considered to be pathogenic.[199] HER2 overexpression acts in a mitogenic and anti-apoptotic behaviour primarily through the activation of RAS-MAPK and PI3K-AKT signalling pathways.[180] In breast cancer the overexpression of HER2 has been associated with a more aggressive disease attributed to increased proliferation, vessel formation and invasiveness.[200]

HER2 targeted therapies such as the monoclonal antibodies Trastuzumab and Pertuzumab along with TKIs Lapatinib (HER2 and EGFR) and Neratinib (HER2, EGFR and HER4) have all shown considerable efficacy in the treatment of HER2 positive cancers. For example, Trastuzumab in combination with chemotherapy is the first line standard-of-care for the treatment of patients with HER2 positive gastric cancer[199] and Trastuzumab is FDA approved for the treatment of HER2 positive breast cancer.[201]

High expression of HER2 has been observed in 10-40% of OvCa.[202] It was further shown in this study that higher expression of HER2 in OvCa was associated with poorer OS.[202] Similar findings have been observed in another study which found HER2 to be amplified and overexpressed in one third of cancers arising from the breast and ovary.[203] The use of HER2 targeted trastuzumab has shown a low response rate of only 7.3% in OvCa however other targeted therapies may hold more promise as pertuzumab has been shown to inhibit growth in HRG1β and TGFα stimulated PE01, PE04 and PE06 cell lines.[202]

(1.6.3) Human Epidermal Growth Factor Receptor 3 (HER3)

The stimulation of HER3 leads to the activation of PI3K and AKT signalling pathways as well as the activation of the RAS-RAF-MAPK signalling pathway.[187] In cancer, HER3 has shown strong roles in mediating resistance to both EGFR and HER2-targeted therapies with the activation of HER3 associated with resistance to HER2-targeted kinase inhibitors[187], and EGFR inhibitors.[204] HER3 has been linked to resistance to EGFR targeted therapies (colorectal and lung cancer), MEK/RAF inhibitors (melanoma and thyroid cancers) and trastuzumab resistance (breast cancer).[188] Additionally increased HER3 expression in HER2-positive breast cancer has been found to confer resistance to paclitaxel via AKT upregulation of Survivin.[188]

One study has observed HER3 to be detectable in 53% of EOC samples tested.[186] Targeting HER3 in OvCa has shown limited efficacy as seribantumab (HER3 targeted antibody) in combination with paclitaxel failed to show improved PFS in platinum-resistant or refractory OvCa during a phase two clinical trial.[205] This study indicated that patient selection based on HRG expression and low HER2 expression could potentially improve outcomes. In a more recent study, seribantumab has been shown to inhibit activation of downstream signalling and result in the inhibition of NRG1 fusion-dependent tumorigenesis *in vivo* of ovarian patient derived cancer models.[206]

(1.6.4) Human Epidermal Growth Factor Receptor 4 (HER4)

HER4 is a 180kDa RTK which shares extensive extracellular domain homology with HER3 and intracellular domain homology with HER2.[194] Following activation HER4 triggers several downstream signalling pathways including PI3K-AKT, JAK/STAT and RAS/RAF/MEK/ERK.[207] HER4 has been shown to play significant roles in numerous cancers where it appears to be pathogenic in nature including colorectal cancer[208], breast cancer[209] and OvCa.[210]

One colorectal cancer study observed 34% of patients express HER4 with higher expression being associated with both lymph node metastasis and unfavourable clinical outcome in patients.[208] This group further showed that HER4 knockdown inhibited proliferation, increased apoptosis and increased E-cadherin expression while decreasing N-cadherin and vimentin.[208] This led to the conclusion that HER4 promoted the progression of colorectal cancer through epithelial-mesenchymal transition in colorectal cancer.[208]

In OvCa, HER4 has been observed to be detected in 89-95% of serous cystadenocarcinoma.[186] This observation aligns with a 2001 study which detected the extracellular domain of HER4 in 89% of samples and the cytoplasmic domain in 93% of samples.[194] Immunohistochemical staining of 100 serous OvCa samples observed higher expression of HER4 compared to normal tissue controls.[211] Additionally, it was shown that HER4 expression was increased in patients with incomplete responses to platinum treatment compared to those with complete responses.[211] It was further shown that HER4 expression is inversely correlated with OS rates (high = 18 months, intermediate = 22 months, low = 58 months). Finally, a study of 482 serous OvCa samples observed HER4 expression in 90% of samples but could not find any association with any prognostic indicators.[210] To understand this discrepancy in findings we may have to consider the potential importance of alternative spliced cytoplasmic isoforms.

HER4 is capable of undergoing regulated transmembrane proteolysis to release a soluble intracellular domain (mediated by a TNF-α converting enzyme) which is 80kDa in size and is referred to as 4ICD. In breast cancer cytosolic 4ICD expression has been observed to promote apoptosis.[212] Subcellular localisation of the 4ICD has also been shown to correlated with prognostic indicators. In breast cancer nuclear 4ICD inversely correlated with tumour grade while cytosolic 4ICD showed significant positive prognostic value in node-negative breast cancer patients.[209]

The alternatively spliced CYT-1 and CYT-2 appear to also play different roles in OvCa. In OvCa it has been observed that CYT-2 was associated with increased tumour size and presence of ascites while CYT-1 was associated with tumour grade, poor overall survival, proliferation (Ki-67 staining) and abnormal p53 status.[210] The overexpression of CYT-1 *in vitro* was observed to promote anchorage independent growth of OvCa cell lines.[210] It was further observed that CYT-1, and not CYT-2, contained a PI3K binding domain and that the anchorage independent growth of

OVCAR3 cells, stimulated through CYT-1 overexpression, could be blocked through PI3K or HER4 inhibition.[210]

(1.7) Introduction to SHP2 and The Allosteric inhibitor SHP099

High-Grade Serous Carcinoma (HGSC) represents the most clinically relevant subtype of OvCa due to a high incidence of advanced stage detections as well as a high frequency of patients developing chemo-resistant disease. It is clear that novel therapeutic targets and strategies are urgently required for the treatment of this poor prognosis cancer. For this reason we wanted to further investigate a second potential therapeutic target SHP2. We also wanted to assess the efficacy of a SHP2 allosteric inhibitor both alone and in combination with pacritinib.

Drug combinations are very frequently used in treatments. They may be designed to overcome resistance to a given treatment intervention or with the aim of causing synergy and inducing sensitivity of a given drug or treatment or minimise toxicity associated with a treatment. There are several possible outcomes following drug combination. Additive interactions may occur where the benefit of both drugs alone are equal to the total benefit observed from combining both drugs. Alternatively, drug combinations may have synergistic or the inverse antagonistic impacts. Synergy occurs when the total observed benefit exceeds the sum of both individual impacts observed from either drug alone.[213] Antagonism occurs when the combined impact of two drugs is less than the sum of their individual impacts.

Chapter 3 showed a strong role for IRAK1 in serous OvCa and the efficacy of the IRAK1-JAK2-FLT3 inhibitor pacritinib in reducing HGSC cell line growth *in vitro*. Several studies have studied pacritinib combinations and observed increased efficacy across several cancer types. In a P-glycoprotein overexpressing drug-resistant human oral squamous carcinoma cell line, the co-treatment of pacritinib with vincristine re-sensitised cells, and led to reduced viability and upregulation of apoptosis.[214] Pacritinib has shown benefit in combination with selumetinib in

medulloblastoma[117], temozolomide in glioblastoma multiforme[119] and erlotinib in NSCLC.[142] Interestingly in myeloproliferative neoplasms, the combination of a SHP2 inhibitor (RMC-4550) and a JAK2 inhibitor (ruxolitinib) resulted in an enhanced inhibition of growth *in vitro*.[215] These studies provide a rationale for examining efficacy of a novel therapeutic strategy combining pacritinib with SHP2 inhibitors in OvCa.

(1.7.1) SHP2: General Overview

(1.7.1.1) Structure of the phosphatase SHP2

Src Homology 2-containing protein tyrosine phosphatase 2 (SHP2) is a 593 amino acid, non-receptor associated protein tyrosine phosphatase.[216] Structurally, SHP2 contains two N-terminally located Src homology (SH2) domains.[217] The N-terminal of SH2 domain, located between amino acids 2 and 104 is known to play an important role in the activation of SHP2, acting as a conformational switch (Figure 1.7.1).[216] The protein tyrosine phosphatase (PTP) domain of SHP2 is located between residues 221 and 524 and is responsible for carrying out the enzymatic activity of SHP2.[218]

The C-terminal domain of SHP2 is located between amino acid residues 525 and 593[218] and contains tyrosyl phosphorylation sites and a proline rich motif (Fig. 4.1.1).[217] The C-terminal tyrosine residues are phosphorylated following activation of Receptor Tyrosine Kinases (RTK's) and allow for the recruitment of downstream signalling molecules (such as GRB2)[217], serving as docking sites for GRB2/SOS and facilitating the activation of the RAS-RAF-MEK-ERK signalling pathway downstream.[219]

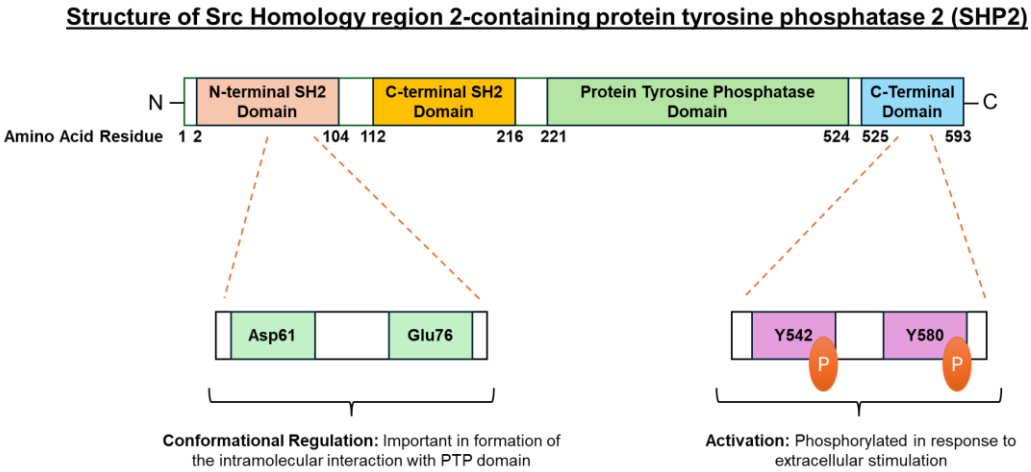

Figure 1.7.1: Structure of the Src Homology Region 2 – Containing Protein Tyrosine Phosphatase (SHP2): SHP2 is a 593 amino acid phosphatase containing two SH2 domains, a protein tyrosine phosphatase domain and a c-terminal domain. This figure was hand generated using the literature available.[216,217,218,220,221,222]

(1.7.1.2) Conformational Regulation and Activation of SHP2

Under basal conditions SHP2 remains inactive which is facilitated through an intramolecular interaction between residues Asp61 and Glu76 of the N-terminal SH2 domain and the PTP domain.[220] The C-terminal SH2 domain, while not directly involved in this interaction, does contribute to binding energy and specificity of this intramolecular interaction.[221] This conformationally closed state prevents access of the catalytic site on SHP2 by any of its substrates.[217]

Following extracellular stimulation such as activation through growth factors or cytokine stimulation, two residues in the C-terminal domain of SHP2 (Y542 and Y580) become phosphorylated.[222] As a result of this phosphorylation, SHP2 undergoes a conformational alteration which results in the relief of autoregulation and activation of SHP2 (Figure 1.7.2).[217] Phosphorylation at Y542 is required in order to release the intramolecular interaction, allowing SHP2 to unfold and become enzymatically active.[222] Interestingly, phosphorylation of SHP2 at Y542 is enhanced

in 3D culture conditions, being attributed to ECM signalling activation.[222] It was further shown that SHP2 inhibitors (SHP099) display increased efficacy against breast cancer cells in 3D growth environments compared to 2D cell culture.[222]

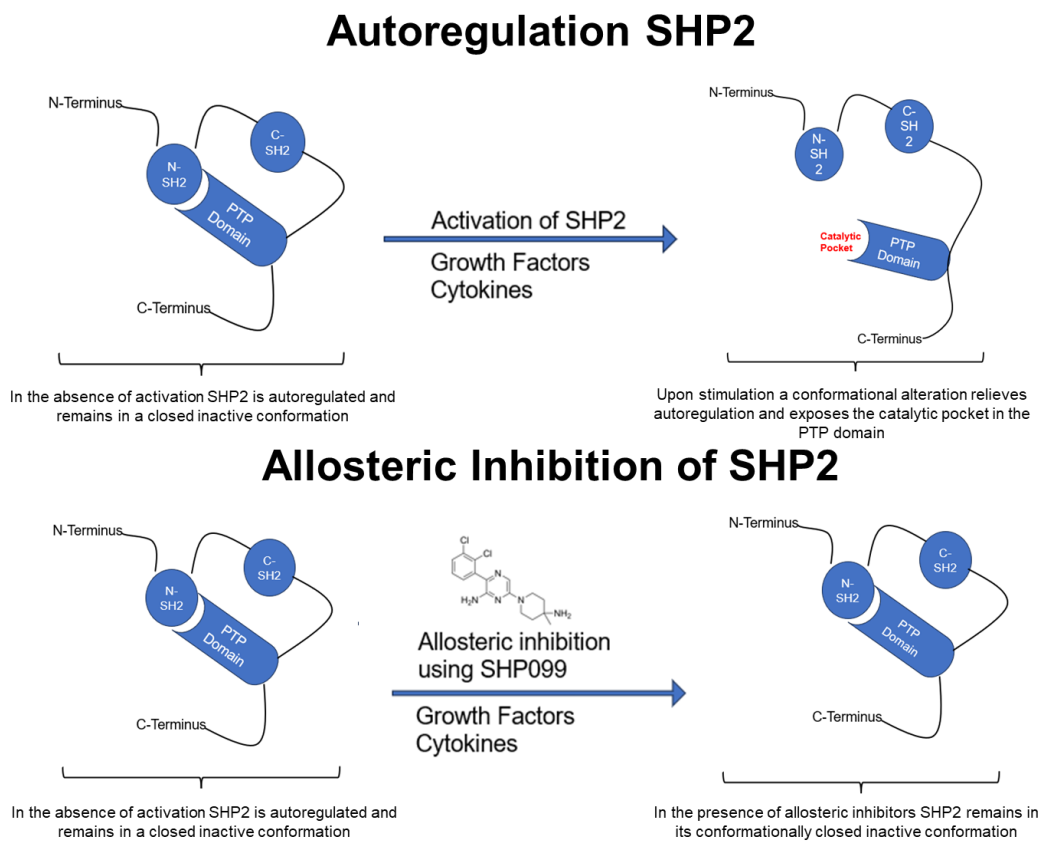

Figure 1.7.2: Diagram outlining the autoregulation of SHP2 and allosteric inhibition using SHP099: SHP2 is present in an inactive conformation under unstimulated conditions. Following stimulation SHP2 becomes conformationally active. This transition from inactive to active states can be prevented by using an allosteric inhibitor. This figure was generated by hand using the literature available.[220, 221, 217]

(1.7.1.3) Signalling Pathways

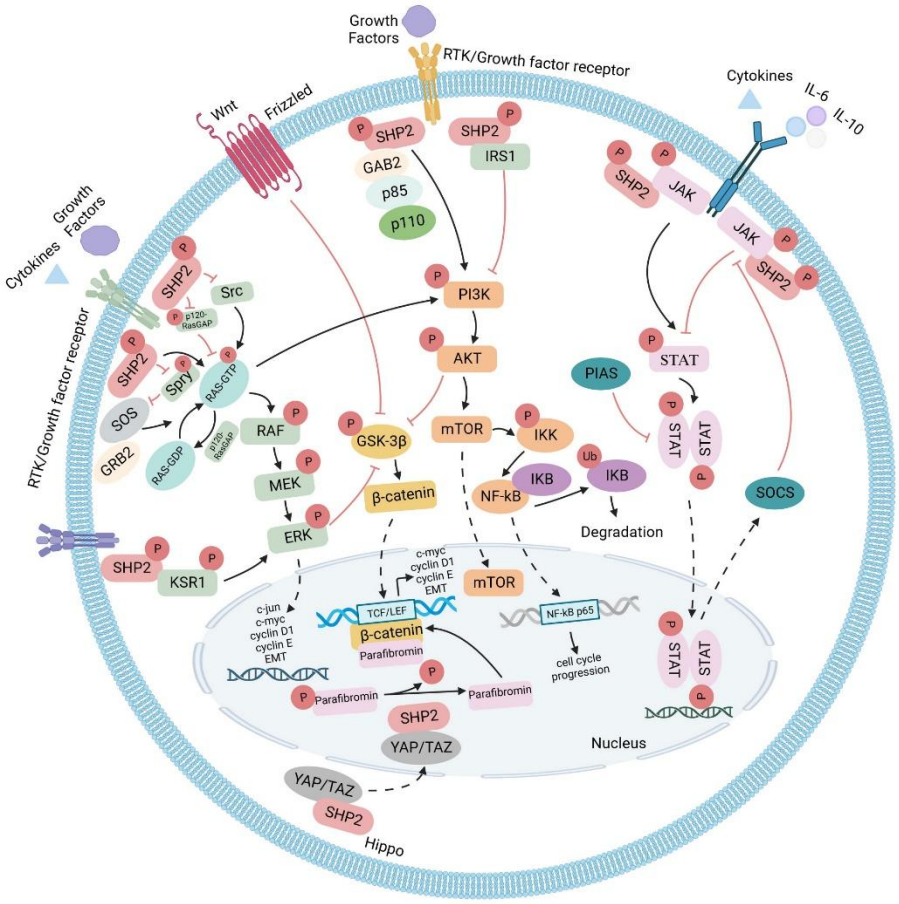

Figure 1.7.3: SHP2 regulates various pathways including RTK's, cytokines and growth factors. Figure was taken from the literature.[223]

SHP2 acts to positively regulate downstream signalling pathways of RTKs, following activation by growth factors, hormones or cytokines (**Figure 1.7.3).** [216] In addition to this, SHP2 acts as a convergent node downstream of multiple immune cell signalling pathways including PD-1.[216] Among other pathways SHP2 is known to regulate JAK-STAT, PI3K-AKT, RAS-ERK and PD-1/PDL-1 signalling pathways.[224, 225, 226, 227]

SHP2 has been observed to play a positive role in the RAS-RAF-MEK-ERK signalling pathway where it promotes the activation of ERK. This signalling pathway is activated downstream of RTK's, TLR's and IL-1R in order to regulate several

important cellular processes including proliferation, differentiation and survival.[228] To give an example of SHP2 in this signalling pathway, EGFR will be used as an example. Following activation and dimerization of the EGFR, Grb2 and SOS are recruited and catalyse the activation of Ras-GDP to Ras-GTP.[229] Once activated Ras-GTP mediates a signalling cascade through Raf, MEK1/2 and finally mediating the activation of ERK1/2.[230]

Ras is constitutively phosphorylated at Tyr32 which in turn inhibits binding of Raf and promotes the hydrolysis of active Ras-GTP into inactive Ras-GDP keeping Ras in an inactive state.[231] SHP2 has been observed to bind to and dephosphorylate Ras at Tyr32, ultimately contributing to the activation of the Ras signalling cascade.[231,225]

The PI3K-AKT pathway is activated downstream of RTK's, TLR's, B cell receptors (BCR's) and T cell receptors (BCR's) and is a major signalling pathway in promoting growth in cancer.[232] PI3K-AKT activation culminates in the activation of several transcription factors which are important in regulating growth and survival.[232]

Activated Ras can also result in the activation of the PI3K-AKT signalling axis which is both pro-growth and pro-survival.[233] A number of studies have highlighted an important role for SHP2 in the PI3K-AKT signalling pathway. Inhibition of SHP2 was shown to reduce platelet derived growth factor (PDGF) and insulin like growth factor (IGF) induced AKT phosphorylation.[234] A similar finding was observed downstream of IGF-1 where SHP2 was observed to be required for AKT activation.[235] Finally, SHP2 knockout was observed to attenuate the activation of the PI3K-AKT-GSK3β activation in breast cancer[236], while SHP2 inhibition using hexachlorophene reduced NSCLC proliferation which was attributed to suppression of both RAS-ERK and PI3K-AKT signalling pathways.[226]

The JAK2/STAT3 signalling pathway plays important roles in several processes including haematopoiesis, tissue repair, inflammation, angiogenesis and apoptosis.[237] Downstream of IL-6, both JAK2 and STAT3 are activated, and it has been observed that SHP2 plays a negative role in this signalling pathway, reducing STAT3 activation through dephosphorylation.[238] This negative role of SHP2 in this pathway has also been observed using an Osteosarcoma model in which SHP2 activation led to the inhibition of JAK2/STAT3 signalling pathway, resulting in the impaired proliferation of cells in this model.[227] These findings could provide a strong rationale for the combination of SHP2 and JAK2/STAT3 inhibition in cancer treatments as a dual action approach to target this signalling pathway. This supported our hypothesis that combination of a SHP2 inhibitor (SHP099) and JAK2/IRAK1/FLT3 inhibitor (pacritinib) may display efficacy in OvCa *in vitro*.

(1.7.2) SHP2: Roles in Cancer

Activating germline mutations of SHP2 has previously been linked to the development of Noonan Syndrome and associated Leukaemias[220] as well as Leopard Syndrome.[217,239] Additionally to this, somatic mutations in SHP2 have been linked to several malignancies such as Juvenile Leukaemia and Juvenile myelomonocytic leukaemia (JMML)[217], with E76K being one of the most common SHP2 activating mutations found in Leukaemia and solid tumours.[221]

Germline and somatic mutations which cause the hyperactivation of SHP2 have been observed in 50% of Noonan Syndrome, 35% of JMML, 10% of myelodysplastic syndromes, 7% of B-cell Acute Lymphoblastic Leukaemia (B-ALL), 4% of Acute Myeloid Leukaemia's (AML) in addition to being observed in several solid tumours including hepatocellular, melanoma and colon cancer.[225] These mutations display gain of function properties which destroy the autoinhibition of SHP2 and lead

to consistent activation or enhanced catalytic activity which in turn drives tumorigenesis, stemness maintenance and invasion.[218]

SHP2 has been observed to play significant roles in the pathology of cancer cells. Activation of the RAS-MAPK and PI3K-AKT signalling pathways play important roles in tumour cell survival, proliferation and differentiation in a number of cancers. SHP2 is a positive regulator of RAS-ERK and PI3K-AKT activation while also negatively regulating the JAK2-STAT3 signalling pathway.[216] SHP2 plays an important role in preventing apoptosis of tumour cells through ERK activation. The suppression of SHP2 has been shown to inhibit growth of leukemic cell clonogenic growth and additionally induce apoptosis.[221]

(1.7.2.1) Breast Cancer

SHP2 immunohistochemical analysis found that 46% of breast cancers were positive for SHP2 protein expression.[240] This study further showed that SHP2 expression is a negative prognostic indicator in breast cancer as it was positively associated with tumour grade, lymph node status and stage of disease with higher SHP2 expression levels associated with significantly worse OS.[240]

SHP2 overexpression in the triple negative breast cancer cell line MDA-MB-231, was shown to accelerate proliferation and increase resistance to cisplatin, while in murine models it was shown to promote mammary tumour growth and enhance tumour angiogenesis.[241] SHP2 inhibition has been shown to block proliferation of metastatic breast cancer cells, delay pulmonary metastatic progression and inhibit growth of drug resistant HER2+ breast cancer cells *in vitro.*[222]

Breast cancer cell lines which express EGFR and HER2 have been reported to require SHP2 for mitogenic cell survival signalling, E-cadherin expression and

sustaining mesenchymal phenotypes.[220] It was further revealed that the inhibition of SHP2 supressed EGF-induced RAS-ERK activation, PI3K-AKT signalling, anchorage independent growth and led to upregulation of E-cadherin.[220]

(1.7.2.2) Laryngeal Cancer

Higher SHP2 expression has been detected in laryngeal cancer compared to other head and neck tumours and its expression was negatively correlated with prognosis and survival rate.[242] This study found that SHP2 overexpression in human laryngeal cancer cell lines promoted growth which was attributed to SHP2 induced activation of the RAS-RAF-MEK-ERK signalling pathway.[242]

(1.7.2.3) Gallbladder cancer

UDP-glucose pyrophosphorylase UGP2 is involved in carbohydrate metabolism. The expression of both SHP2 and UGP2 have been shown to represent negative prognostic indicators.[243] The expression of both proteins was associated with increased expression of vimentin, β-catenin, MMP2/9 and KI-67.[243] This study further showed that in patients with adenocarcinomas and squamous cell / adenosquamous carcinomas, SHP2 and UGP2 expression was associated with increased tumour size, high TNM stage, lymph node metastasis and reduced survival.[243]

(1.7.2.4) Ovarian Cancer

Interestingly several studies have indicated a strong role for SHP2 in OvCa. Using immunohistochemistry analysis, increased SHP2 levels were detected in EOC samples compared to normal ovarian tissue samples.[241] It was further shown that SHP2 expression was associated with clinical stage, histological grade, lymph node metastasis and distant metastasis.[241] Using the EOC cell line A2780 it was found that SHP2 overexpression could enhance cell proliferation, migration/invasion, increase resistance to paclitaxel, increase activation of AKT and promote tumour growth in nude mice.[241]

GAB2 is frequently amplified or overexpressed in HGSC where overexpression of GAB2 is linked to the aberrant activation of the RAS-ERK and PI3K-AKT signalling pathways.[56] Increased GAB2 expression is associated with higher activity of EGDR, RAS and MAPK in primary HGSC.[56] This group further observed a selective sensitivity of GAB2 high OvCa cell lines to SHP2 inhibition which showed synergistic impact with a PI3K inhibitor leading to increased apoptosis and inhibition of AKT and ERK activation together with reduced c-MYC levels.[56]

Stem cell regulatory factor epidermal growth factor-like domain-containing protein 6 (EGFL6) was previously observed to be upregulated in OvCa, primarily HGSC, where it was associated with poor prognosis.[244] EGFL6 has been shown to promote tumour growth and metastasis in ALDH+ OvCa stem cells and, at least in part, this tumour growth was observed to act through SHP2 as silencing of SHP2 resulted in reduced growth of ALDH+ cells in response to EGFL6.[244]

Finally, targeting SHP2 may hold promise in immunotherapies for ovarian cancer. It has been shown that SHP2 depletion in the OVCAR-8 HGSC cell line led to increased immune mediated killing *in vitro.*[245]

(1.7.3) SHP2 in the tumour microenvironment

Immune checkpoint receptors are involved in the process of maintaining self-tolerance, allowing immune cells to determine foreign and dangerous cells in the body. Many cancers will undergo a process of immune evasion, during which they may exploit immune checkpoint pathways to evade immune mediating killing. SHP2 is recruited downstream of a number of immune checkpoint receptors including PD1[246], CTLA4, BTLA, TIGIT, VISTA and LAG3.[216] As a convergent node in the immune cell signalling pathways, SHP2 inhibition represents a promising therapeutic target to enhance immune mediated cancer cell elimination.

SHP2 acts downstream of PD-1 and CTLA4 to supress T cell activation through dephosphorylation of the T-cell receptor, ZAP70 and CD28.[245] The inhibitory receptor PD-1 is expressed by T-cells, B-cells, NK cells, Monocytes and dendritic cells following antigen or cytokine stimulation.[246] Following activation of T cell receptors of intracellular immunoreceptor tyrosine-based inhibitory motif (ITIM) and immunoreceptor tyrosine-based switch motif (ITSM) are phosphorylated on PD-1, by the Src kinase Lck, SHP2 is recruited.[246] SHP2 then contributes to the dephosphorylation and reduction in activation of TCR and CD3 signalling pathways.[246]

Studies have shown that SHP2 may play important roles in the positive regulation of immune suppressive macrophages. The SHP2 inhibitor TNO155 showed inhibition of immune suppressive macrophages which synergised with PD-1 blockade.[247] M2 macrophages are anti-inflammatory in activity. SHP2 is involved in downstream signalling of CSF-1, which promotes macrophage proliferation and polarisation to the M2 phenotype.[245] CSF-1 signalling is essential for T cell suppression by tumour associated macrophages (TAM's).[247] Interestingly, reduced

SHP2 expression in macrophages enhances the TH1-mediated anti-tumour immune microenvironment, contributing to the suppression of melanoma growth.[216]

CD47 is a transmembrane protein which acts as a marker of self and provides a signal against immune mediated killing. It was observed that CD47 is amplified in 5% of OvCa with EOC displaying a higher frequency of expression compared to healthy controls.[248] Following binding of CD47 to signal regulatory protein alpha (SIRPa), SHP2 and SHP1 are recruited and mediate the activation of inhibitory signals for phagocytosis contributing to immune evasion.[248]

(1.7.4) SHP099: A SHP2 allosteric inhibitor

It has previously been noted that phosphatase inhibitors targeting the active site tend to suffer from poor pharmaceutical properties which may impact their clinical application, such as low potency or selectivity, primarily attributed to the presence of conserved polar and charged environments of phosphatase active sites.[225] Alternatively allosteric inhibitors, which rely on basal conformational regulation, can be used to prevent activation and activity of phosphatases. In the case of SHP2, it is possible to use these types of inhibitors to lock SHP2 in its conformationally inactive closed state. SHP2 allosteric inhibitors have shown promising results in the past with TN0155 being one of the first SHP2 allosteric inhibitors to enter into a clinical trial.[225] Since then, other SHP2 allosteric inhibitors including RMC-4630, JAB-3068 and JAB-3312 have followed TN0155 into clinical trials.[249]

TNO155 has entered clinical trials to assess combination with MRTX849 in KRAS (G12C)-mutant advanced solid tumours (NCT04330664), in combination with spartalizumab and ribociclib in patients with advanced tumours (NCT04000529) and with lorlatinib in ALK+ or ROS1+ lung cancer patients (NCT04292119). RMC-4630

has also entered clinical trials for NSCLC (NCT03989115), in combination with sotorasib for KRAS mutant (G12C) NSCLC (NCT05054725) and in combination with LY3214996 in metastatic KRAS mutant cancers (NCT04916236).

SHP099 is a small molecule allosteric inhibitor which inhibits the phosphatase activity of SHP2. It does this through binding to conformationally inactive SHP2 and preventing the transition to a structurally active conformation. SHP099 has been shown to display a high degree of target selectivity for SHP2 as studies have shown it displayed no activity against its closest homolog SHP2 which shares 61% similarity in primary structure.[250]

A search of clinicaltrials.gov does not indicate any ongoing clinical trials using this inhibitor, however SHP099 has been applied in a wide variety of research studies and shown considerable efficacy in several types of cancer both *in vitro* and *in vivo*. It is due to this widespread application and efficacy that we have selected to use this inhibitor for our studies.

In a xenograft model of oesophageal squamous cell carcinoma treatment, with SHP099 led to a significant reduction in tumour volume.[239] A similar finding was observed in NSCLC in which tumour growth was significantly impaired, following treatment with SHP099, in PDX models of KRAS mutant NSCLC.[251] Inhibition of SHP2 activity using SHP099 has shown considerable efficacy in a murine xenograft model of OvCa using IGROV1, an ovarian cancer cell line.[56]

The RAS-RAF-MEK-ERK signalling pathway, which positively regulates proliferation and survival of cancer cells, is one of the most commonly deregulated pathways in cancer with KRAS being one of the most frequently mutated genes in human cancer.[252] SHP2 is known to positively regulate this pathway through promoting GTP loading of RAS.[245] Adaptive resistance to MEK inhibitors result in the induction of RTK's and their ligands and as SHP2 represents a convergent node in

RTK signalling it has been observed that SHP099 in combination with MEK inhibitors resulted in synergistic inhibition of proliferation *in vitro* in multiple cancer cell lines.[252]

SHP099 has shown considerable efficacy in combination with other targeted therapies. SHP099 in combination with B-Raf inhibitors (Vemurafenib) has shown significant efficacy in reducing tumour burden in thyroid and pancreatic cancer models.[253] A study using neuroblastoma xenograft models has shown that SHP099 in combination with RAS pathway inhibitors (Trametinib, vemurafenib and ulixertinib) observed considerable synergy and reversed resistance to SHP2 inhibition in both *in vitro* and *in vivo* models.[254] SHP099 in combination with anti-PD1 led to considerable efficacy in reducing tumour volume in colorectal xenograft models.[255] Finally, SHP099 has shown a synergistic impact with a PI3K inhibitor in a xenograft model of OvCa.[56]

(1.8) Thesis Aims and Objectives

HGSC represents the most lethal subtype of OvCa and is characterised by a high incidence of advanced stage detections and a high frequency of chemoresistant disease. It is clear that novel druggable targets are urgently needed in order to develop improved treatment strategies for these patients.

IRAK1 and SHP2 have emerged in recent years as potential therapeutic targets in several malignancies including OvCa. In addition to this IRAK1 and SHP2 represent actionable targets with small molecule inhibitors available to evaluate the efficacy of inhibiting the activity of these proteins using in vitro models.

While there is strong preliminary evidence in the literature our research aims to further investigate the role of IRAK1 and SHP2 in OvCa and to assess the efficacy of using novel therapeutic strategies to target IRAK1 and SHP2, both alone and in combination. Our research aims to contribute to the identification of novel therapeutic targets and strategies in OvCa. We hypothesise that IRAK1 and SHP2 play a role in the growth and progression of HGSC cells. We further hypothesise that the inhibition of IRAK1 and SHP2 – individually or in combination - will impair OvCa cell growth.

(1.8.1) Aim 1 – Investigating the role of IRAK1 in OvCa

Objective 1. Determine whether IRAK1 knockdown impairs the growth of OvCa cell lines *in vitro*.

Objective 2. Assess the efficacy of Pacritinib, an IRAK1/JAK2/FLT3 inhibitor, on the growth of OvCa cell lines *in vitro*.

Objective 3. Evaluate IRAK1 expression in serous OvCa cells and examine association with prognostic indicators.

(1.8.2) Aim 2 – Investigating the role of SHP2 in OvCa

Objective 4. Examine SHP2 expression in HGSC and assess association with prognostic indicators.

Objective 5. Evaluate the efficacy of the allosteric SHP2 inhibitor SHP099 in HGSC cell lines *in vitro*.

(1.8.3) Aim 3 – Evaluating the combination of Pacritinib and SHP099

Objective 6. Investigate the efficacy of pacritinib and SHP099 in combination on the growth of OvCa cell lines *in vitro*.

Objective 7. Examine the molecular mechanism of action following pacritinib and SHP099 in OvCa cell lines using a proteomics-based approach.

Chapter 2

Materials and Methods

(2.1) Standard Laboratory Procedures

(2.1.1) Good Laboratory Practices

For all procedures outlined below, good laboratory practices were followed. In all cell culture experiments the materials and reagents used were purchased sterile and were individually wrapped. Sterility was maintained throughout using a Class II Biological Safety Cabinet and aseptic technique. All materials, cell lines, reagents and antibodies used are catalogued and provided in tables below. All health and safety regulations were adhered to throughout the course of this project. Personal protective equipment (PPE) including lab coat, nitrile gloves and protective eyewear were always worn while conducting experiments outlined in this chapter.

(2.1.2) Maintenance of Lentiviral Induced Knockdown

Stable knockdown of IRAK1 was performed on OvCa cell lines by Dr Marion Butler and the cell lines were provided at the start of my PhD project. Following manufacturer's instructions, HEK293T cells were transfected with the envelope plasmid pMD2.g (1µg), packaging plasmid psPAX2 (1µg) and IRAK1 shpLKO.1 vector (2µg). Control cells were generated by substitution of IRAK1 shpLKO.1 vector with control short-hairpin RNA (shRNA), a non-targeting shRNA vector. Sequences are provided below and are the same for all cell lines.

Human IRAK1 Sequence (IRAK1sh-1)

CCGGGCCACCGCAGATTATCATCAACTCGAGTTGATGATAATCTGCGGTGGCTT
TTTG

Human IRAK1 Sequence (IRAK1sh-1 for OVCAR3 cell line)

CCGGGCCCGAAGAAAGTGATGAATTCTCGAGAATTCATCACTTTCTTCGGGCTT
TTT

Human IRAK1 Sequence (IRAK1sh-2):

CCGGCCGCTTCTACAAAGTGATGGACTCGAGTCCATCACTTTGTAGAAGCGGTT
TTTG

After 24-, 48- and 72-hours cell culture media was removed and replaced with media containing 30% (v/v) foetal bovine serum (FBS). Lentiviral particle containing media was harvested in media isolated after 48- and 72-hour time points. OvCa cells were then seeded in T75 flasks and transduced with the lentivirus containing medium using hexadimethrine bromide (8μg/ml). Cells were then incubated for twenty-four hours. Finally, cells that were successfully transfected with shRNA constructs were positively selected by addition of puromycin (2μg/ml).

Dr Butler prepared IRAK1 knockdown (IRAK1sh-1 and IRAK1sh-2) and control (Ctrolsh) cell lines using PE01, PE04, OAW42, IGROV1 and OVCAR3 parental cell lines. For all cell lines both knockdown and control cell lines were maintained through the addition of Puromycin as a selective agent. The presence of IRAK1 knockdown was confirmed by preparing whole cell lysates and profiling IRAK1 protein expression using western blot analysis (see procedure below).

(2.1.3) Data Management Practices

Data management throughout this PhD research project followed FAIR (Findable, Accessible, Interoperable and Reusable) practices. Data has been backed up using both Microsoft Teams Cloud platform and an external hard drive. This has ensured integrity of data and enables future long-term storage and preservation of data. Microsoft Teams cloud is a shared platform that has been accessible by my supervisor and this has allowed for increased data visibility and accessibility. Data has been stored in both raw and annotated forms to improve data integrity. Finally, all data has been annotated with key details including experiment ID, experimental type and details, samples and reagents used as well as the researcher ID. All experimental details have been logged using lab-books and experiment ID is sufficient to find both data and experimental details.

(2.2) Cell Culture Procedures

(2.2.1) Ovarian Cancer Cell Lines

Seven human ovarian cancer cell lines and one murine ovarian cancer cell line were used throughout this research project and cover a range of subtypes and chemotherapy status. All ovarian cancer cell lines described below are adherent cell lines and were sub-cultured according to the protocol detailed below. The subtype and chemotherapy resistance / sensitivity status has been summarised in Table 2.1.1 below.

PEA1 and PEA2 cell lines were purchased from the ECACC. OVCAR3 cells were purchased from ATCC. The paired PE01 and PE04 cell lines were kindly provided by Dr Gordon Greville (UCD). OAW42 and IGROV1 cell lines were kindly provided by Dr Neil Conlon (DCU).

Cell line authentication testing and mycoplasma testing was carried out by Eurofins (Germany) for all cell lines used in this work. Stocks of cell lines were saved at low passages in liquid nitrogen and were kept in culture for the different work packages for defined passages numbers.

(2.2.1.1) Human High Grade Serous Carcinoma (HGSC) Cell lines

Five HGSC cell lines were used throughout the following two research chapters in order to investigate the potential of our novel therapeutic strategies. PE01,

PE04, OVCAR3, PEA1 and PEA2 are all derived from patients with the HGSC subtype of ovarian cancer.

PE01 and PE04 are paired cell lines which were isolated from the same patient at different stages of treatment. The morphology of the primary tumour was poorly differentiated serous adenocarcinoma for PE01.[256]

PE01 cells have been defined as 123C3, 123A8 and 92.1 negative while being positive for Vimentin, OC125, CAM5.2, LE61, AUA1, CEA, HMFG1 and CR343 .[256] Interestingly PE04 was shown to display very similar antigen expression profiles to PE01 and was defined as 123C3, CR343, 123A8 and 92.1 negative while being positive for Vimentin, OC125, CAM5.2, LE61, AUA1, CEA, and HMFG1.[256]

PE01 and PE04 cells have also been characterised to display high expression of ERα.[257] It was further shown that both PE01 and PE04 cells were endocrine responsive in 2D and 3D cultures.[257]

PE01 has been used to model chemo sensitive BRCA2 mutant serous ovarian adenocarcinoma while PE04 has been used to model BRCA2 proficient chemoresistance model.[136] Dr Clara Evan's through collaboration in our lab validated the difference in cisplatin sensitivity between PE01 and PE04. Cisplatin IC50 values determined by Dr Evans were 2.82μM+/-0.42μM for PE01 and 15.63μM+/-0.48μM for PE04.

OVCAR3 has been characterised as a HGSC cell line.[258] OVCAR3 was isolated from the malignant ascites of a patient with progressive adenocarcinoma of the ovary following cisplatin-based chemotherapy.[259] In addition to this OVCAR3 has further been characterised as a human ovarian carcinoma cell line expressing both Androgen and Oestrogen receptors.[259]

The PEA1 and PEA2 cell lines are another set of paired cell lines which were isolated from the same patient at different stages of disease. The morphology of the

primary tumour was poorly differentiated adenocarcinoma for PEA1.[256] PEA1 has been used to model cisplatin sensitivity while PEA2 is used to model cisplatin resistance.[260]

Both PEA1 and PEA2 cells have been identified to possess relatively low levels of ER.[261] PEA1 cells have been defined as 123C3 negative while being positive for 123A8, Vimentin, OC125, CAM5.2, LE61, AUA1, CEA, 91.1, HMFG1 and CR343 .[256] While the PEA2 cells were observed to be negative for CR343 and positive for 123C3, 123A8, 92.1, Vimentin, OC125, CAM5.2, LE61, AUA1, CEA and HMFG1.[256]

(2.2.1.2) Human Non-HGSC Cell Lines

OAW42 and IGROV1 were isolated from patients with ovarian cancer. OAW42 has previously been used to model non serous ovarian cancer.[262] While the IGROV1 cell line has been characterised as a hyper mutated ovarian cancer cell line that more closely resembles endometrioid or clear cell ovarian cancer cell lines.[263]

(2.2.1.3) Murine Ovarian Cancer Cell Line

The ID8 DEFb29-VEGF cell line can be used to model ovarian cancer in immunocompetent murine models.[264] This cell line was kindly provided by Dr Niamh Buckley (Queens University Belfast) following an approval request granted to Dr Butler by the group who generated this cell line led by Dr José R. Conejo-Garcia, MD, PhD (Duke School of Medicine, Durham).

Table 2.1.1: Characteristics of human OvCa cell lines used in this work.

Cell Line ID	Histology Subtype	Chemotherapy Resistance status
PE01	High Grade Serous Carcinoma	Sensitive
PE04	High Grade Serous Carcinoma	Resistant
OAW42	Non-Serous	Sensitive
OVCAR3	High Grade Serous Carcinoma	Resistant
IGROV1	Non-Serous	Sensitive
PEA1	High Grade Serous Carcinoma	Sensitive
PEA2	High Grade Serous Carcinoma	Resistant

(2.2.2) Sub culturing Procedures: Adherent Ovarian Cancer Cell Lines

All cell lines were cultured in T75 or T175 flasks in their respective complete medium supplemented with foetal bovine serum (FBS) and incubated at 37˚C and 5% CO_2 until they were ready to be sub cultured. Table 2.2.1 outlines the preparation of complete cell culture media used for each cell line. All reagents required for subculturing of the OvCa cell lines used in these studies are catalogued and provided in Table 2.2.2.

Once confluency had reached approximately 60-80%, cell culture media (Table 2.2.1) was removed and adherent cells were gently washed with prewarmed (37˚C) Dulbecco's Phosphate Buffered Saline (DPBS) (Cat# 10317052). DPBS was then removed and 3ml of 1X or 2X Trypsin-EDTA (Cat# T4714) was added to each flask. Flasks were rocked gently to ensure full coverage of cells with Trypsin-EDTA. Cells were then incubated for five minutes at 5% CO_2 and 37˚C to allow full detachment of cells. Cells were collected by adding a further 7ml of complete media prior to being transferred to a 50ml falcon and pelleted at 1500 rotations per minute (RPM) for five minutes.

Supernatant was then decanted, and the isolated cell pellet was resuspended in 10 ml of complete media until a single cell suspension was obtained. 1 or 2ml of this single cell suspension was returned to a T75 or T175 flask with 10 or 20ml of complete media and incubated at 37˚C for future experiments. The remaining single cell suspension was then used to plate experiments outlined below.

Table 2.2.1: Preparation of complete cell culture media for OvCa cell lines

Cell Line ID	Medium	% FBS	Additives	Trypsin
PE01	RPMI	10	NA	2X
PE04	RPMI	10	NA	2X
OAW42	DMEM	10	NA	2X
OVCAR3	RPMI	20	0.01mg/ml Bovine Serum Insulin	2X
IGROV1	DMEM	10	NA	2X
PEA1	RPMI	10	NA	2X
PEA2	RPMI	10	NA	2X
ID8 DEFb29-VEGF	DMEM	10	NA	1X
Ctrolsh	Cell Line Specific	Cell Line Specific	4µg/ml Puromycin	Cell Line Specific
IRAK1sh-1	Cell Line Specific	Cell Line Specific	4µg/ml Puromycin	Cell Line Specific
IRKA1sh-2	Cell Line Specific	Cell Line Specific	4µg/ml Puromycin	Cell Line Specific

Abbreviations: RPMI = Roswell Park Memorial Institute; DMEM = Dulbecco's Modified Eagle Medium

Table 2.2.2: Tissue Culture Reagents Suppliers and Catalogue Numbers

Reagent	Supplier	Catalogue Number
Puromycin	Invivogen	58-58-2
Trypsin EDTA 10X – 100ml	Sigma	T4714
DMEM	Thermo-Fischer Scientific	41965039
RPMI	Thermo-Fischer Scientific	61870010
Dulbecco's Phosphate Buffered Saline (PBS)	Fischer Scientific	10317052
Virkon	Fischer Scientific	12358667
Foetal Bovine Serum (FBS)	MERCK	F7524-500ML
Bovine Serum Insulin	Sigma	I0516

Abbreviations: DMEM = Dulbecco's Modified Eagle Medium; EDTA = Ethylenediaminetetraacetic acid; RPMI = Roswell Park Memorial Institute; PBS = Dulbecco's Phosphate Buffered Saline

(2.3) *In Vitro* Growth Assays

Reagents used for *in vitro* growth assays were recorded and displayed in Table 2.3.1. All cell lines were cultured using the procedures outlined in section 2.2 above prior to performing *in vitro* growth assays. *In vitro* growth assays used in this section were routinely used in Dr Butlers research lab

(2.3.1) Proliferation Assay (2D Methodology)

(2.3.1.1) Day 0 – Seeding Plates

OvCa cell lines were removed from the tissue culture incubator, trypsinized to detach and resuspended in complete media prior to being counted using a hemacytometer. A cell suspension was then prepared at a concentration of $4x10^4$ cells per ml for PE01, PE04 and OVCAR3 cell lines. Single cell suspensions were prepared at $0.5x10^4$ cells per ml for OAW42 cell lines and $2x10^4$ cells per ml for IGROV1 cell lines.

These single cell suspensions were taken and 1.5ml was added per well to 12 well plates. Three technical replicates were seeded for each condition. Plates were then placed in the tissue culture incubator until cell counts were performed (37˚C + 5% CO_2). Separate 12 well plates were used for day 4 and day 7 cell counts.

(2.3.1.2) Day 4 and Day 7 – Counting Cells

On day 4 and day 7, complete media was gently removed from each well. The adherent cells were then gently washed with 500µl of DPBS (Cat# 10317052) per

well. DPBS (Cat# 10317052) was removed after washing and 400µl of 2X Trypsin-EDTA (Cat# T4714) was added per well and cells were incubated (37˚C + 5% CO_2) for 5-10 minutes to allow for detachment of the adherent cells from the bottom of the well. 600µl of DPBS (Cat# 10317052) was then added per well to bring the final volume to 1ml. Cells were suspended to a single cell mixture. Cell density (cells/ml) was then determined using a haemocytometer allowing for the determination of total cell count.

(2.3.1.3) Validation of IRAK1 knockdown

One extra well was plated for each control and knockdown cell line used for these experiments. Whole cell lysates were prepared using 2X sample buffer. Media was removed from each well and cells were washed with DPBS. 100µl of 2X Sample buffer was then added to each well and cells were placed on the rocker (45 RPM) for 10 minutes. Whole cell lysates were then boiled at 95˚C for 10 minutes. Whole cell lysates were stored at -20˚C. IRAK1 knockdown was validated for each experimental replicate using Western blot analysis.

(2.3.1.4) Data Analysis and Statistical Significance

Graphs were prepared using PRISM. Statistical significance was investigated using a paired student t-test to compare differences observed between Ctrolsh cells and IRAK1sh-1/2. p-values; (*;≤0.05), (**;≤0.01). (***;≤0.001). (****;≤0.0001).

(2.3.2) Viability Assay – Cell Titre-Glo® 2.0 (2D Methodology)

(2.3.2.1) Day 0 – Seeding Plates

On Day 0, OvCa cell lines were trypsinized and counted using a haemocytometer. A cell suspension was then prepared at a concentration of $5x10^4$ cells per ml for PE01, PE04. OVCAR3, OAW42, IGROV1, PEA1 and PEA2 cell lines. 90µl of this single cell suspension was then added per well to a flat bottom 96 well plate and placed in the tissue culture incubator overnight. The next day cells were treated with increasing concentrations of pacritinib (Cat# HY-16379) alone and in combination with the SHP2 phosphatase inhibitor SHP099 (Cat# HY-100388). All treatments were carried out with technical duplicates and 3-4 experimental replicates per cell line.

(2.3.2.2) Day 1 – Single Agent Treatments

On Day 1 treatments were prepared for Pacritinib (Cat# HY-16379) and SHP099 (Cat# HY-100388). Top concentrations 20µM (Pacritinib (Cat# HY-16379)) and 40µM (SHP099 (Cat# HY-100388)) were prepared from working concentrations of these inhibitors. Working concentrations were prepared from stock vials of both inhibitors which were stored at -70˚C. Serial dilutions (1:1 inhibitor to media) were used to prepared lower treatments until the lowest treatment concentration (0.3125µM) was reached.

Pacritinib (Cat# HY-16379) concentrations evaluated include 20µM, 10µM, 5µM, 2.5µM, 1.25µM, 0.625µM and 0.3125µM. SHP099 (Cat# HY-100388)

concentrations evaluated include 40μM, 20μM, 10μM, 5μM, 2.5μM, 1.25μM, 0.625μM and 0.3125μM.

Media was removed from each well to waste. 100μl of final 1X concentration for each treatment was then added per well. Plates were then returned to the tissue culture incubator for a further 72 hours. Vehicle control treatments were prepared using the same volume of vehicle (DMSO (Cat# B10231-100) for Pacritinib or H2O (Cat# 15835408) for SHP099) used for the highest concentration of each inhibitor.

(2.3.2.3) Day 1 – Treating Plates with Drug Combinations

On Day 1 A 2X concentration of pacritinib (Cat# HY-16379) and SHP099 (Cat# HY-100388) were prepared for the top concentrations 5μM (pacritinib) and 10μM (SHP099) from working concentrations of these inhibitors. Serial dilutions (1:1 inhibitor to media) were used to prepare lower treatments until 2X of the lowest treatment concentration 0.3125μM (Pacritinib) and 1.25μM (SHP099) was reached.

Pacritinib (Cat# HY-16379) concentrations evaluated include 5μM, 2.5μM, 1.25μM, 0.625μM and 0.3125μM. SHP099 (Cat# HY-100388) concentrations evaluated include 10μM, 5μM, 2.5μM and 1.25μM.

Media was then removed to waste and 50μl of 2X concentrations were added to each well and diluted to 1X by addition of a further 50μl complete media (Table 2.2.1) or combination drug treatment for a final volume of 100μl per well. Plates were returned to the tissue culture incubator for 72 hours. Vehicle control treatments were prepared using the same volume of vehicle (DMSO (Cat# B10231-100) for Pacritinib or H_2O (Cat# 15835408) for SHP099) used for the highest concentration of each inhibitor.

(2.3.2.4) Day 4 – Measuring Cell Viability using Cell Titre-Glo® 2.0

72 hours after cells were treated with pacritinib (Cat# HY-16379) alone or in combination with SHP099 (Cat# HY-100388) plates were removed from the incubator and 50µl of Cell Titre-Glo® 2.0 reagent (Cat# G924B) was added to each well. Cells were lysed on the cell shaker (500RPM) for 5 minutes and plates were incubated at room temperature for 10 minutes in darkness. Relative Luminescent Units (RLU) were then measured using the CLARIOSTAR (BMG Labtech) plate reader.

(2.3.2.5) Data Analysis and Statistical Significance

Percentage (%) growth was then normalised using vehicle control growth (formula given below). Graphs were prepared using % vehicle control growth and statistical significance was assessed using a paired students t-test comparing each treatment to the respective vehicle control. p-values; (*;≤0.05), (**;≤0.01). (***;≤0.001). (****;≤0.0001).

IC50 Analysis

Fractionated growth (formula given below) was calculated from RLU values and, through the use of Calcusyn software, were used to determine IC50 values. Standard Error of the Mean (SEM) was calculated for each IC50 value (formula given below).

% Vehicle Control Growth = ((Treatment RLU) / (VC RLU)) X 100

Fractionated Growth = ((100%) – (% VC Growth)) / 100

Standard Deviation = (STDEV.s in Excel)

SEM = (standard deviation) / (square root of # of experimental replicates)

Synergy and Antagonism Analysis

Percentage (%) vehicle control growth was determined for each treatment. Dose response matrices were prepared using COMBENEFIT software. The Loewe model was used to assess synergistic or antagonistic drug interactions on viability.

(2.3.3) Colony Formation Assay

(2.3.3.1) Day 0 – Seeding Plates

On Day 0 cells were trypsinized and counted using a haemocytometer. A single cell suspension was then prepared at a concentration of $5x10^4$ cells per ml. Using these single cell suspensions 3000 cells were plated per well (in six-well plates) for PE01, PE04, OVCAR3 and IGROV1 cell lines. For OAW42 cell lines 1000 cells were seeded per well. All conditions were plated in 3ml per well using duplicate technical replicates. Plates were then returned to the tissue culture incubator (37˚C and 5% CO_2) until colonies had reached a sufficient size to be stained and counted. Cells treated with pacritinib were treated 24 hours after plating.

(2.3.3.2) Day 1 – Treating Cells with Pacritinib

24 hours after cells were plated they were treated with 0.5μM, 1μM pacritinib (Cat# HY-16379) or vehicle control. Treatments were prepared in complete media at 11X concentration and diluted to 1X upon addition of 300μl to each well already

containing 3000µl of media. Vehicle control treatments were prepared using the same volume of vehicle (DMSO (Cat# B10231-100) for Pacritinib) used for the highest concentration of pacritinib.

(2.3.3.3) Day 14 – Fixing, staining and Counting Colonies

On Day 14 (or once colonies had reached sufficient size to be stained and counted) plates were removed from the tissue culture incubator and media was removed to Virkon (CAT# 12358667) waste. Cells were washed with ice cold DPBS (CAT# 10317052) and fixed with methanol for 10 minutes prior to staining with 0.5% crystal violet for a further 10 minutes. Images were then captured using a smartphone camera under consistent lighting conditions and the number of colonies per well was counted manually.

(2.3.3.4) Data Analysis and Statistical Significance

Graphs were prepared using PRISM (GraphPad). Statistical significance was assessed using a paired Students t-test comparing IRAK1sh-1/2 colony formation to Ctrolsh colony formation. The impact of pacritinib on colony formation was also assessed using a paired Students t-test comparing pacritinib treated cells to vehicle control (DMSO) treated cells. p-values; (*;≤0.05), (**;≤0.01). (***;≤0.001). (****;≤0.0001).

(2.3.4) Soft Agar Assay (3D Methodology)

(2.3.4.1) Day 0 – Seeding Plates

On day 0 PE01, PE04, OVCAR3 and OAW42 cells were removed from the incubator, trypsinized, resuspended and counted using a hemacytometer. Complete media containing 0.8% low gelling agarose (Cat# 16520-050) was prepared and 500µl was added per well in 24 well plates. This lower agar layer was allowed to cool gradually at room temperature before continuing.

Media containing 0.48% low gelling agarose was used to transfer 6,250 cells to each well. This upper layer was gently pipetted above the lower agarose layer and allowed to cool gradually before plates were placed in the tissue culture incubator (37˚C and 5% CO_2). Cells treated with inhibitors were treated 24 hours after seeding. All conditions were plated in duplicate technical replicates.

Exception: OVCAR3 cell lines were seeded with a lower 0.5% and upper 0.35% low gelling agarose layers.

(2.3.4.2) Day 1 – Treating Cells with Pacritinib and SHP099

24 hours after plating, cells were treated with increasing concentrations of pacritinib (Cat# HY-16379) (0.5µM, 1µM, 2µM and 2.5µM) or SHP099 (Cat# HY-100388) (2.5µM, 5µM and 10µM). Vehicle control treatments were prepared using the same volume of vehicle (DMSO (Cat# B10231-100) for Pacritinib or H_2O (Cat# 15835408) for SHP099) used for the highest concentration pacritinib and SHP099.

(2.3.4.3) Resupplying Complete Media

200µl of complete media was gently resupplied every 3-4 days in order to prevent agar-cell mixture from drying out.

(2.3.4.4) Day 21 – Viability staining, Imaging and Counting Colonies

On day 21 (once cells had formed colonies of sufficient size to be stained and counted) viable cells were stained with Neutral Red Dye (Cat# 24860) (1:100 dilution in DPBS (Cat# 10317052)). Cells were incubated for two hours before being imaged at 4X magnification using an Olympus Microscope in brightfield. Two sets of representative counts of the number of spheroids were taken for each of the two layers of soft agar.

(2.3.4.5) Data Analysis and Statistical Significance

Graphs were prepared using PRISM (GraphPad). Statistical significance was investigated using paired student's t-test comparing IRAK1sh-1/2 to Ctrolsh colony formation. Similarly the impact of pacritinib and SHP099 on colony formation was assessed using a paired students t-test to compare inhibitor treated to vehicle control treated. p-values; (*;≤0.05), (**;≤0.01). (***;≤0.001). (****;≤0.0001).

(2.3.5) Matrigel Droplet Migration / Invasion Assay (3D Methodology)

(2.3.5.1) Day 0 – Seeding Plates

On Day 0 cells were trypsinized and counted using a haemocytometer. A total of $2x10^5$ cells were taken for PE01, PE04, OVCAR3, OAW42 and IGROV1 Control (Ctrolsh) and IRAK1 knockdown (IRAK1sh-1/2) cell lines. Cells were centrifuged for 5 minutes at 1500 RPM. The resulting cell pellet was isolated by removing media before being resuspended in 40µl of Matrigel (Cat# 354230).

10µl droplets were then pipetted directly onto the bottom of a 24 well plate and allowed to solidify at 37˚C for 20 minutes. 2ml of complete media was then gently added to each well. Plates were placed in the tissue culture incubator (37˚C and 5% CO_2). Technical duplicates were plated to ensure consistency with this initial experimental process. On day 7 consistency between duplicates was assessed and a technical singlet was processed for imaging and analysis.

(2.3.5.2) Day 1 – Replacing Media

On Day 1 media was gently removed and replaced with fresh complete media. Plates were then returned to the tissue culture incubator (37˚C and 5% CO_2) until cells were imaged on day 7.

(2.3.5.3) Day 7 – Staining cells, Imaging and counting migrated cells

On day 7, plates were removed from the tissue culture incubator. Media was removed and droplets were washed in 500µl per well of ice cold DPBS (Cat# 10317052). Cells were then fixed and permeabilised in ice cold methanol (Cat# 10675112) for 5-10 minutes. Finally, cells were stained with eosin for 5 minutes and washed with DPBS (Cat# 10317052) until run off was clear. A series of images were taken at 4X magnification (Olympus microscope) and stitched together using a program designed by Dr Bryan Hennelly (Electronic Engineering Department, Maynooth University).

(2.3.5.4) Data Analysis and Statistical Significance

Representative counts were taken of cells which had invaded out of the Matrigel droplet and migrated into the surrounding well. Graphs were prepared using Prism. Statistical significance was assessed using a paired Students t-test comparing control (Ctrolsh) to IRAK1 knockdown (IRAK1sh1/2) cell lines. p-values; (*;≤0.05), (**;≤0.01). (***;≤0.001). (****;≤0.0001).

(2.3.6) Matrigel Viability Assay (3D Methodology)

(2.3.6.1) Preparation of Poly-HEMA Coated Plates

In order to ensure sterility all reagents and plastics required to prepared poly-HEMA (Cat# P3932-10G) coated 96-well plates were only opened in a sterile

biological safety cabinet. 5mg/ml of poly-HEMA (Cat# P3932-10G) was dissolved in 96% molecular grade EtOH prepared with molecular grade water. Poly-HEMA (Cat# P3932-10G) was dissolved by incubation at 50˚C overnight and vortexing well before use. 50µl of This Poly-HEMA solution was then added to each well using a multichannel. Plates were incubated at 30-50˚C until dry. Poly-HEMA coating was repeated an additional time prior to use.

(2.3.6.2) Day 0 – Seeding Plates

Cells were trypsinized, resuspended and counted using a haemocytometer. A single cell suspension of $5x10^4$ cells per ml was prepared in a 2% Matrigel (Cat# 354230) and complete media matrix. 90µl of this single cell suspension was then added to each well of a flat-bottomed poly-HEMA coated 96 well plate. Cells were then placed in the tissue culture incubator overnight (37˚C and 5% CO_2) to allow Matrigel to solidify. Cells were treated with inhibitors the following day.

(2.3.6.3) Day 1 – Treating Plates with Pacritinib and SHP099

Twenty-four hours after seeding cells, plates were treated with pacritinib (Cat# HY-16379) or SHP099 (Cat# HY-100388). 4X treatment concentrations were prepared from working concentrations for pacritinib (1.25µM and 2.5µM) and SHP099 (5µM and 10µM). These treatment concentrations were diluted to 1X concentration upon addition to 90µl already in each well. Each treatment was performed in triplicate technical replicates. Plates were returned to the tissue culture incubator (37˚C and 5% CO_2) until Day 7. Vehicle control treatments were prepared using the same volume of vehicle (DMSO (Cat# B10231-100) for Pacritinib or H_2O (Cat# 15835408) for SHP099) used for the highest concentration of pacritinib.

(2.3.6.3) Day 1 – Treating Plates with Pacritinib and SHP099 in Combination

Twenty-four hours after seeding plates cells were treated with pacritinib (Cat# HY-16379) (1.25μM, 2.5μM and 5μM) and SHP099 (Cat# HY-100388) (2.5μM, 5μM and 10μM) both alone and in combination. 8X treatment concentrations were prepared from working concentrations. These were diluted to 4X (1:1) with 4X vehicle controls (single treatments) or 4X of the other inhibitor (combination treatments). 30μl of these 4X single and combination treatments were then diluted to 1X upon addition to the 90μl already in each well. All treatments were performed in triplicate technical replicates. Plates were returned to the incubator. Vehicle control treatments were prepared using the same volume of vehicle (DMSO (Cat# B10231-100) for Pacritinib or H_2O (Cat# 15835408) for SHP099) used for the highest concentration of each inhibitor.

(2.3.6.4) Day 7 – Measuring Cell Viability using Cell Titre-Glo® 3D Assay

On day-7 plates were removed from the incubator and 50μl of Cell Titre-Glo® 3D reagent (Cat# G9682)was added to each well. Cells were lysed on the cell shaker at 500 RPM for 5 minutes and plates were incubated in the dark at room temperature for 25 minutes. Relative Luminescent Units (RLU) were measured using the CLARIOSTAR (BMG Labtech).

(2.3.6.5) Data Analysis and Statistical Significance

RLU was normalised using vehicle control growth and presented as % vehicle control growth. For single agent treatments graphs were prepared using PRISM (GraphPad). Statistical significance was assessed using paired student's t-test comparing each treatment of Pacritinib and SHP099 to their respective vehicle controls. P-values; (*; ≤0.05), (**; ≤0.01), (***; ≤0.001), (****; ≤0.0001).

COMBENEFIT Synergy / Antagonism Data Analysis

Percentage (%) vehicle control growth was determined for each treatment condition. Dose response and synergy matrices were prepared using COMBENEFIT software. The Loewe model was applied to assess synergistic or antagonistic drug interactions on 3D viability.

(2.3.7) Incucyte Spheroid Cell Death Assay (3D Methodology)

(2.3.7.1) Day 0 – Seeding Plates

A single cell suspension of $5x10^4$ cells per ml was prepared in 1% Matrigel to media matrix. 5000 cells were then transferred (100µl) to each well of a 96 well plate. Greiner Bio-One U bottom CellStar 96-well plates were used for this experiment. These plates have a cell repellent surface which facilitated spheroid formation. Cells were returned to the incubator (37˚C and 5% CO_2) for 72 hours prior to being treated with pacritinib (Cat# HY-16379) and SHP099 (Cat# HY-100388) both alone and in combination.

(2.3.7.2) Day 3 – Treating Plates with Pacritinib and SHP099

72 hours after plating cells were treated with pacritinib (Cat# HY-16379) and SHP099 (Cat# HY-100388) both alone and in combination. 2X treatment concentrations were prepared for pacritinib (2.5μM) and SHP099 (5μM and 10μM) alone and in combination. These treatments were prepared with 2X concentration of Cytotox (1:800 final) (Sartorius-4632) fluorescent dye. Dyes and Inhibitor treatments were diluted to 1X following addition to each well (final volume of 200μl). All treatments were carried out in four technical replicates. Vehicle control treatments were prepared using the same volume of vehicle control (DMSO (Cat# B10231-100) for Pacritinib or H_2O (Cat# 15835408) for SHP099) used for the highest concentration of each inhibitor. Finally, these plates were then transferred to DCU and placed in the Incucyte (Sartorius). Images were captured at 4X magnification every 6 hours for five days. Additionally fluorescent readings were taken every 6 hours for the same duration.

(2.3.7.3) Data Analysis and Statistical Significance

Brightfield and fluorescent readings were provided by Dr Neil Conlon and Luna Stockmann in DCU. These values were then normalised to % vehicle control growth and graphed using PRISM.

(2.3.8) Happy Cell Media Spheroid Viability Assay (3D Methodology)

(2.3.8.1) Day 0 – Seeding Plates

Following subculturing single cell suspensions were prepared from PE01, PE04 and OVCAR3 at $25x10^4$ cells per ml in 0.5X Happy cell media (Cat# VHCK2RPMI). From these single cell suspensions 90µl was added per well in poly-Hema coated flat bottom 96 well plates. Cells were then returned to the tissue culture incubator (37˚C and 5% CO_2).

(2.3.8.2) Day 1 – Treating Plates with Pacritinib and SHP099

24 hours after plating cells were treated with pacritinib (Cat# HY-16379) (1.25µM, 2.5µM and 5µM) and SHP099 (Cat# HY-100388) (2.5µM, 5µM and 10µM) both alone and in combination. Cells were treated with volumes of vehicle control (DMSO (Cat# B10231-100) for Pacritinib or H_2O (Cat# 15835408) for SHP099) equal to the highest concentration of each inhibitor. All treatments were carried out in triplicate technical replicates.

(2.3.8.3) Day 7 – Measuring Cell Viability using Cell Titre-Glo® 3D Assay

On Day 7 cells were treated with 50µl per well of Cell Titre-Glo® 3D (Cat# G9682). Cells were lysed using a plate shaker (500RPM) and after a 25-minute

incubation (in darkness), relative luminescent units were measured using the CLARIOSTAR (BMG Labtech).

(2.3.8.4) COMBENEFIT Synergy / Antagonism Data Analysis

RLU readouts were normalised to percentage (%) Vehicle control growth for each treatment condition. Dose response and synergy matrices were prepared using COMBENEFIT software. The Loewe model was applied to assess synergistic or antagonistic drug interactions on 3D viability.

Table 2.3.1: Growth Assays Reagents Suppliers and Catalogue Numbers

Reagent	Supplier	Catalogue Number
Pacritinib	MedChemExpress	HY-16379
Dimethyl Sulfoxide (DMSO)	Fischer	B10231-100
SHP099	MedChemExpress	HY-100388
H2O (Molecular Grade)	Fisher Scientific Ltd	15835408
Matrigel Basement Membrane Matrix	Corning	354230
Poly (2-hydroxyethyl methacrylate) (Poly-HEMA)	SLS Scientific Laboratory Supplies (Ireland) Ltd	P3932-10G
Happy Cell Media and scale up kit	Medical Supply Co.	VHCK2RPMI
Ultrapure LMP Agarose	Invitrogen	16520-050
Incucyte® Cytotox Red Dye (Sartorius Cat. No. 4632	Satorius	4632
Incucyte® Annexin V Dye for Apoptosis-green	Satorius	4642
Cell Titre Glo 2.0	Promega	G924B
Cell Titre Glo 3D	Promega	G9682
Neutral Red Dye	Sigma	24860
Methanol	Thermo-Fisher Scientific	10675112

(2.4) Protein Expression Analysis – Western Blot Analysis

(2.4.1) General Overview of Western Blot Analysis of Protein Expression

Buffer recipes, reagents and antibody catalogue numbers were recorded and are provided in the Table 2.4.1 to Table 2.4.7. All Western blot data obtained during this research project was retained and organised into a physical rad folder. Electronic copies of these rads were uploaded to Microsoft Teams for long term storage, figure preparation and densitometry analysis. OvCa PDX whole cell lysates were kindly provided by Dr Denis Collins (DCU). Western blot analysis was routinely used in Dr Butlers research lab.

(2.4.2) Preparation of Whole Cell lysates

(2.4.2.1) Plating Whole Cell Lysates

Single cell suspensions were prepared for PE01 ($2.5x10^5$ cells/ml), PE04 ($3x10^5$ cells/ml), OVCAR3 ($1.75x10^5$ cells/ml), OAW42 ($1x10^5$ cells/ml), PEA1 ($2x10^5$ cells/ml), PEA2 ($3x10^5$ cells/ml) and IGROV1 ($1x10^5$ cells/ml). From these single cell suspensions 3ml was plated per well in 6 well plates and incubated (37˚C and 5% CO_2). Cell seeding density was varied between cell lines in order to have confluency at approximately 80% twenty-four hours later when cells were being treated.

(2.4.2.2) Treating Whole Cell Lysates

On the next day, once cells had reached approximately 80% confluency and were treated with pacritinib (Cat# HY-16379) (1μM, 1.5μM, 2μM, 2.5μM) alone and in combination with SHP099 (Cat# HY-100388) (10μM). Treatments were carried out for 24 hours prior to whole cell lysates being harvested.

(2.4.2.3) Harvesting Whole Cell Lysates

Plates were removed from the incubator and media was decanted to the waste. Cells were then washed gently with 1.5ml of ice-cold DPBS (Cat# 10317052) which was subsequently removed to the waste. Between 100μl and 200μl of complete NP-40 lysis buffer (Table 2.4.2) was then added to each well. Plates were then incubated at 4˚C for 40 minutes with constant rocking agitation to facilitate cell lysis. Whole cell lysates were then collected to Eppendorf tubes and centrifuged at 12,000 RPM (4˚C) for 10 minutes. Lysate was carefully collected. Following determination and adjustment of protein concentration (using Bradford protein assay) one third volume of 4X sample buffer was added to each sample and were boiled for 10 minutes at 95˚C. Whole cell lysates were stored at -20˚C.

(2.4.3) Bradford Protein Assay and Whole Cell Lysate Concentration Adjustment

(2.4.3.1) Preparation of Braford standards

Bradford standards were prepared using Bovine Serum Albumin (BSA) (Cat# A7906)in NP-40 lysis buffer (Table 2.4.2). A top standard was prepared at a concentration of 2mg/ml. Using 1 to 1 serial dilutions (with NP-40 lysis buffer) all lower standards were prepared. The range of standard concentrations used include 2mg/ml, 1mg/ml, 0.5mg/ml, 0.25mg/ml, 0.125mg/ml, 0..0625mg/ml and 0.03125mg/ml. NP-40 without BSA was used as a negative (blank) control.

(2.4.3.2) Standard Curve Preparation

5µl of each standard or sample were loaded (in duplicate) in flat bottom 96 well plates. 250µl of Bradford reagent (Cat# B6916)was then added to each well. Plates were incubated at room temperature, in the dark, for 20 minutes. Finally, absorbance was measured at 595nm using the CLARIOSTAR (BMG Labtech) plate reader. Standards were used to prepare a standard curve. The equation of the line from the standard curve was used to determine protein concentration of whole cell lysate samples. Protein concentration was then adjusted using NP-40 lysis buffer to normalise protein concentration within experimental replicates.

(2.4.4) Western Blot Analysis

(2.4.4.1) Preparation of Polyacrylamide Gels

Polyacrylamide gels were prepared using recipes and buffers detailed in the tables below. N'N'N'N'-Tetramethyl ethylenediamine (TEMED) (Cat# T9281) and ammonium persulfate (APS) (Cat# A3676) were added directly prior to pouring gels as these components result in the solidification of polyacrylamide gels. The percentage of polyacrylamide in the resolving gel was altered to improve protein separation based on protein size. For high molecular weight targets 8% was used and for low molecular weight targets a higher percentage (15%) gel was used. A visible protein ladder was included to identify protein separation in kilodaltons (kDa).

Once all reagents were mixed for the resolving gel (Table 2.4.3), the mixture was carefully pipetted into the gel rack and a layer of ethanol careful layered above (using a Pasteur pipette) to ensure that gels set evenly and without air bubbles. After approximately 20 minutes the gels were set, and the ethanol was poured off and dabbed dry with tissue. Gels were washed out gently with H_2O. Finally, the stacking gel (provides a medium for lysates to be loaded) (Table 2.4.4) was pipetted gently on top of the resolving gel and wells formed by inserting a 15-well comb.

(2.4.4.2) Electrophoresis – Separation of Proteins Based on Size

Once gels were prepared, the electrophoresis rig could be assembled and gels completely submerged in running buffer (Table 2.4.2). Between 5µl and 20µl of each lysate was then loaded per well. The addition of an EZ-Run™ pre-stained Rec

protein ladder (Fischer BioReagents Cat# 10638393) allowed for visualisation of protein separation and determination of protein size. Protein migration through the gels was facilitated through the application of an electric current (90 volts for 30 minutes and 120 volts for 2 hours and 15 minutes). Optimal protein separation was adjusted, depending on the size of the target, by adjusting the duration of electrophoresis.

(2.4.4.3) Electro-Transfer of Proteins to PVDF Membrane

Once whole cell lysates had been sufficiently separated based on protein size the gel was isolated and placed on top of a solid PVDF membrane (Cat# 88518), which had previously been activated in methanol and washed with dH_2O. 3 layers of Whatman filter paper (Cat# WHA3030917), soaked in transfer buffer (Table 2.4.2), was place above the gel with another 3 placed below the membrane. This transfer sandwich was then loaded onto an electro-transfer apparatus and an electric current of 0.09 amps per gel was applied for 1 hour in order to transfer protein onto the PVDF membrane (Cat# 88518). This duration was lowered to 35 minutes for low molecular weight proteins.

(2.4.4.4) Blocking of PVDF Membranes

Following electro-transfer PVDF membranes (Cat# 88518) now contained a complex mixture of proteins separated based on size. In order to prevent high levels of background and non-specific signals membranes were blocked in 5% milk (in 1X TBST) for one hour (30 RPM) at room temperature. This step reduces the accessibility of non-specific epitopes to which our primary antibodies would have otherwise bound, allowing specific signals to be more pronounced.

(2.4.4.5) Primary Antibody Incubation and Target Protein Detection

Once blocked, membranes were briefly washed in TBST (Table 2.4.2) before being incubated at 4˚C overnight with primary antibody. Membranes were placed in a 50ml falcon with 7ml of primary antibody. Falcons were placed on a roller to ensure even coverage of the membrane. Primary antibody details were recorded and catalogued and are displayed in the tables 2.4.6 and 2.4.7 below. The next day falcons were brought to room temperature for 2 hours prior to being washed in TBST (Table 2.4.2) 3 times for five minutes each. Membranes were then incubated in secondary antibody for one hour at room temperature. After incubation in horse radish peroxidase (HRP) linked secondary antibody, membranes were washed for a final three times in 1X TBST (Table 2.4.2) for five minutes each.

(2.4.4.5) Visualisation of Protein Expression

Membranes were incubated in Luminata (low expression targets) or ECL mix (A+B solutions mixed in a 1:1 ratio – Detail listed in appendix). Luminescence, relative to protein abundance, was then captured using autoradiography films. Exposure duration was varied depending on abundance of the target protein, typically ranging from 5 minutes to 40 minutes. Autoradiography film (Cat# sc-201697) was developed in a dark room using X-RAY developer (Cat# RGD) and fixed using X-RAY fixer (Cat# RGF).

(2.4.4.6) Densitometry Analysis and Statistical significance

Optical density was determined for each band using Image J software. Protein expression was normalised using loading controls. Beta actin and Tubulin were used as loading controls during this research project. Tubulin expression tended to be lower and allowed for easier interpretation of results while Beta actin provided an additional reliable control. Where possible statistical significance was investigated using paired students t-test. P-values; (*; ≤0.05), (**; ≤0.01), (***; ≤0.001), (****; ≤0.0001).

Table 2.4.1: Western Blot Reagents Suppliers, and Catalogue Numbers

Reagent	Supplier	Catalogue Number
Ammonium Persulfate (APS)	Sigma Life Science	A3678
Sucrose Minimum 99.5%	Sigma Life Science	S9378
Tween 20	Sigma Aldrich	P1379
Glycine	Thermo-Fischer Scientific	11464894
Tris-Base	Fischer Scientific	10376743
N,N,N',N' -Tetramethyl ethylenediamine (TEMED)	Sigma	T9281
2-Marcaptoethanol	Sigma Aldrich	M6350
Ultra-Pure Protogel	National Diagnostics	Order# 5C890
Sodium Dodecylsulfate (SDS)	Thermo-Fischer Scientifics	28312
Sodium Chloride (NaCl)	Fisher Scientific Ltd	10216410
Immobilon Forte Western HRP substrate	Millipore	WBLUF0500
p-Coumaric Acid	Sigma Aldrich	C9008
Luminol	Fluka AppliChem	09253 (A2185,0005)
Phenylmethanesulfonyl PMSF	Thermo-Fischer Scientific	36978
Hydrogen Peroxide (30%)	VWR	23622.298
Bromophenol Blue	Fischer	BP114-25
Bovine Serum Albumin	Sigma	A7906
1,4-Dithiotreitol (DTT)	Roche	10-197-777-001
Phos-STOP	MERCK life science limited	4906837001
Complete Tablets Mini Protease inhibitor cocktail tablets	Roche	5892970001
X-Ray Developer	SLS Scientific Laboratory Supplies (Ireland) Ltd	RGD
X-Ray Fixer	SLS Scientific Laboratory Supplies (Ireland) Ltd	RGF
NP-40 (IGAPAL)	Sigma Aldrich	I3021
BRADFORD Reagent	Sigma Aldrich	B6916
EZ RunTM Protein Ladder	Fischer Scientific Ltd.	10638393
PVDF Membrane	Thermo-Fischer Scientific	88518
Methanol	Sigma	N4638
Autoradiography Film – Ultra-Cruz	Santa Cruz	SC-201697
Whatman Paper	MERCK	WHA3030917

Table 2.4.2: Recipes for Western Blot Buffers: Outlined in the table below are the recipes for various buffers used during Western blot analysis.

Buffer	Recipe
NP-40 Lysis Buffer	50mM Tris Hydrochloric Acid (HCl) (pH 7.5) 150mM Sodium Chloride (NaCl) 0.5% NP-40 50mM Sodium Fluoride (NaF) Diluted to desired volume with dH2O
NP-40 Lysis Buffer additives (added fresh prior to WCL Preparation)	Protease inhibitor (1 tablet to 10ml) Phosphatase inhibitor tablet (1 tablet to 10ml) 1mM Sodium Orthovanadate (NaVO3) 1mM Beta-Glycerophosphate 1mMPhenylmethylsulphonyl Fluoride (PMSF) 1mM Dithiothreitol (DTT)
4X Sample Buffer	0.25M 4X Laemmli Upper Tris Buffer 6% Sodium Dodecyl Sulphate (SDS) 40% Sucrose 0.04% Bromophenol Blue Diluted to 20ml with dH2O 5ml Beta-Marcaptoethanol
4X Laemmli Lower Tris Buffer	0.4% Sodium Dodecyl Sulphate (SDS) 1.5M Tris Base pH 8.8
4X Laemmli Upper Tris Buffer	0.5M Tris Base 0.4% Sodium Dodecyl Sulphate (SDS) Ph 6.8
10X Running Buffer	1% Sodium Dodecyl Sulphate (SDS) 0.25 Tris Base 1.92M Glycine pH 8.3 Diluted to 1X Running buffer with dH20 before use
10X Tris-Buffered Saline (TBS)	pH 7.5 0.5M Tris-HCl 1.5M Sodium Chloride (NaCl) Diluted to 1X TBST (0.1% Tween) before use
Transfer Buffer	20% (v/v) Methanol 25mM Tris Base 0.2M Glycine

Table 2.4.3: Preparation of Resolving Gel for Western Blot. 10% Resolving (Lower) polyacrylamide gels were prepared to the below specifications and used to run the Western blot analysis. Each recipe is sufficient for 4 gels.

% Acrylamide	8%	10%	12%	15%
29:1 Polyacrylamide Bis	6.67	8.35	8.35	12.5
dH20	12.1	10.5	8.75	6.25
4X Lower Tris Buffer	6.25	6.25	6.25	6.25
TEMED	14ul	14ul	14ul	14ul
10% APS	130ul	130ul	130ul	130ul
TOTAL Volume	25ml	25ml	25ml	25ml

Abbreviations: APS = Ammonium persulfate; TEMED = N,N,N,N'-Tetramethyl ethylenediamine.

Table 2.4.4: Preparation of Stacking Gel for Western Blot. 5% Stacking (Upper) polyacrylamide gels were prepared to the below specifications and used to run Western blots analysis. Each recipe is sufficient for 4 gels.

% Acrylamide	5%
29:1 Polyacrylamide Bis	1.7ml
dH_20	5.8ml
4X Upper Tris Buffer	2.5ml
TEMED	20ul
10% APS	40ul
TOTAL Volume	10.06ml

Abbreviations: APS = Ammonium persulfate; TEMED = N,N,N,N'-Tetramethyl ethylenediamine.

Table 2.4.5 ECL Mix: recipe for ECL Mix Used in Western Blot Analysis of lysate samples described above. Solutions A and B were mixed in a 1:1 reaction prior to use.

Reagent	Solution A	Solution B
Tris Hydrochloric acid (HCl)	100mM	100mM
Luminol	2.5mM	NA
p-Coumaric Acid	400uM	NA
Hydrogen peroxide (H_2O_2)	NA	1:1640 (v/v) 30% H2O2
Diluted to final volume with dH_2O	10ml	10ml

Table 2.4.6: Catalogue of antibodies used for Western blot analysis A.

ANTIBODY NAME	kDa	SOURCE AND CAT NO	Isotype	DILUTION TO USE	BSA OR MILK (5%)
Anti-Mouse	NA	CS-7076		1:2000	Milk
Anti Rabbit	NA	CS-7074		1:2000	Milk
Tubulin	55kDa	CS-3873T	Mouse	1:2000	Milk
Beta-Actin	43kDa	Sigma	Mouse	1:2000	Milk
STAT3	79, 86	SC-8019	Mouse	1:1000	BSA
Phospho STAT3 (Y705)	79, 86	CS-9145	Rabbit	1:500	BSA
IRAK1	80	Santa Cruz 5266	Mouse	1:1000	BSA
IRAK1	78-105	CS-4504 (D51G7)	Rabbit	1:1000	BSA
Phospho IRAK1	90-105 Detects 80kda band	CS-12756	Rabbit	1:500	BSA
JAK2	125 kDa	CS-3230	Rabbit	1:1000	BSA
p-JAK2 (Tyr211)	125	CS-3774	Rabbit	1:1000	BSA
HER4	180	CS-4795T	Rabbit	1:1000	BSA
p-HER4 (Tyr1284) **Also detects EGFR(1173)**	180	CS-4757	Rabbit	1:1000 1:500 works better.	**BSA**
HER3	185	CS-12708 (D22C5)	Rabbit	1:1000	BSA
p-HER3 Y1289	185	CS-2842	Rabbit	1:1000	BSA
HER2	185	CS-4290	Rabbit	1:1000	
p-HER2 (Tyr1221/1222)	185	CS-2243	Rabbit	1:1000	
EGFR	175	CS-4267 (D38B1)	Rabbit	1:1000	BSA
p-EGFR (Tyr1068)	175	CS-3777 (D7A5)	Rabbit	1:1000	BSA

Table 2.4.7: Catalogue of antibodies used for Western blot analysis B.

ANTIBODY NAME	kDa	SOURCE AND CAT NO	Isotype	DILUTION TO USE	BSA OR MILK (5%)
Caspase-3	35, 19, 17	CS-14220	Rabbit	1:1000	BSA
Cleaved Caspase-3	19, 17	CS-9664	Rabbit	1:1000	Milk
PARP	116, 89	CS-9542	Rabbit	1:1000	Milk
Cleaved PARP	89	CS-5625	Rabbit	1:1000	BSA
ERK	44, 42	CS-137F5	Rabbit	1:1000	BSA
p-ERK	44. 42	CS-9101	Rabbit	1:1000	BSA
SHP2	68	SC-7384	Mouse	1:1000	Milk

(2.5) Protein Expression Analysis – Proteomics

(2.5.1) Preparation of Whole Cell Lysates for Proteomics

(2.5.1.1) Day 0 – Seeding Cells

Proteomics analysis was carried out under the guidance and supervision of Dr Paul Dowling. Single cell suspensions were prepared at $2.5x10^5$ cells per ml in 0.5X Happy Cell ASM RPMI 3D cell culture media (Vale Life Sciences Cat# VHCK2RPMI) from the HGSC PE04 cell line. From this single cell suspension, 1ml was added to each well in poly-HEMA coated 24 well plates. Cells were then returned to the tissue culture incubator (37˚C and 5% CO_2). Poly-HEMA coated plates were prepared using the same protocol outlined for Matrigel 3D growth assay in section 2.3.6.

(2.5.1.2) Day 1 – Treating Whole Cell Lysates

Twenty-four hours after seeding, cells were treated with 2.5μM Pacritinib (Cat# HY-16379), 10μM SHP099 (Cat# HY100388), the combination of 10μM SHP099 and 2.5μM Pacritinib or vehicle control. Treatments were carried out in four technical replicates. Cells were returned to the tissue culture incubator for twenty-four hours prior to harvesting whole cell lysates.

(2.5.1.3) Day 2 – Collecting Whole Cell Lysates

Cells were de-suspended using the Happy Cell Inactivation Solution (Vale Life Sciences Cat# VHCK2RPMI) (12.5µl per ml) for 60 minutes prior to harvesting whole cell lysates. Cells were transferred to an Eppendorf tube, centrifuged at 1500 RPM for five minutes (room temperature). Supernatant was then discarded, and cells were washed with PBS prior to being centrifuged again at 1500 RPM for five minutes (room temperature). Supernatant was discarded and cells were resuspended in 150µl of complete NP-40 lysis buffer (Table 2.4.2). Samples were incubated, with constant agitation, for thirty-five minutes at 4˚C. Samples were finally centrifuged at 12,000 RPM for 10 minutes and lysate was collected to a fresh Eppendorf tube.

(2.5.1.4) Determination of Protein Concentration

Protein concentration was determined using Pierce 660nm Protein Assay, following the manufacturers protocols.

(2.5.2) Preparation of Whole Cell Lysates for Mass Spectrometry using FASP Methodology.

(2.5.2.1) Day-1

The filter unit was assembled by placing a filter into the spin column / collection tube. 200µl of 8M UA (Urea in 100mM Tris HCl (pH 8.5)) and 15ug of protein worth of whole cell lysates were added to each. Samples were centrifuged at 14,000 RPM for fifteen minutes. A further 200ul of UA was added to each filter and samples were

centrifuged again for fifteen minutes at 14,000 RPM. Flow through was then decanted and the filter reattached. 100µl of 10nM DTT solution was the added to each filter. Samples were mixed at 600 RPM (Thermo-mixer) for one minute at room temperature before being incubated without mixing, in the dark, for twenty to thirty minutes.

After this incubation samples were centrifuged at 14,000 RPM for ten minutes before adding 100µl of IAA and mixing again at 600 RPM for one minute. Samples were incubated in the dark for a further thirty minutes prior to being centrifuged at 14,000 RPM for ten minutes. 100µl of UA was added to each filter unit and the samples centrifuged at 14,000g for fifteen minutes. This step was repeated one more time. 100µl of 50nM ABC to each filter unit and samples were centrifuged at 14,000g for ten minutes. This step was repeated one more time.

50µl of 0.05% ProteaseMax with Trypsin (enzyme to protein ratio of 1:50) was added and mixed at 600 RPM for one minute. Samples were then placed in a humidity chamber and incubated at 37˚C for eighteen hours to allow trypsin to digest protein.

(2.5.2.2) Day-2

Following the eighteen-hour protein digest, filters were transferred to fresh collection tubes and centrifuged at 14,000 RPM for ten minutes. 30µl of ABC was then added to each filter and samples were mixed at 600 RPM for one minute prior to centrifuging at 14,000g for ten minutes. Filters were discarded and 36µl was taken to a fresh Eppendorf tube. 4µl of TFA mass spec buffer was added to each Eppendorf tube. Samples were centrifuged for ten seconds, vortexed for five seconds and 20µl of each sample was then transferred to mass spec vials ensuring there were no air bubbles. 4µl was then loaded into the mass spec for each sample.

Data Analysis

Raw mass spectrometry files were transformed into formats compatible with PERSEUS using MaxQuant. PERSEUS was used to analysis data. Background was removed and data was filtered based on valid values (detected in at least three replicates of one group). Binary comparisons were performed for each group and PCA plots, volcano plots and heatmaps were generated using PERSEUS. Statistically significant proteins were identified as having a p-value less than 0.05. Differentially abundant proteins were defined as having a fold change greater than 1.5.

(2.6) Protein Expression Analysis – Immunohistochemistry

Immunohistochemistry staining kits and reagents were recorded and are displayed in Table 2.6.2.

(2.6.1) Breakdown of Tissue Microarray Slides

Paraffin-embedded ovarian cancer tissue microarrays were purchased from US Biomax. OV802B and OV809B contained a combined 160 tissue cores from patients with ovarian cancer. These slides also included normal adjacent tissue (NAT) cores as controls. Breakdown of high-grade serous carcinoma (HGSC) cores broken down by stages is outlined in the Table 2.6.1. SHP2 immunohistochemistry optimisation, validation and TMA staining were all carried out in collaboration with Professor William Gallaghers group in UCD.

Table 2.6.1: Breakdown of High-Grade Serous Carcinoma (HGSC) and normal adjacent tissue (NAT) cores in OV802B and OV809B TMAs.

Slide	OV802B	OV809B	Total
# NAT	10	8	18
# HGSC	32	54	86
# Stage 1 HGSC	14	8	22
# Stage 2 HGSC	11	13	24
# Stage 3 HGSC	11	30	41
# Stage 4 HGSC	0	3	3

Abbreviations: NAT = Normal Adjacent Tissue; HGSC = High Grade Serous Carcinoma.

(2.6.2) IRAK1 Immunohistochemistry

(2.6.2.1) Preparation of Cell plugs for optimisation

Paraffin embedded cell plugs were prepared for use in the optimisation of cell staining. Control and IRAK1 knockdown cells were seeded in T175 flasks until they were 80% confluent at which point cells were trypsinized, washed and collected by centrifugation at 1500 RPM for five minutes. Cells were washed in 10ml of ice-cold PBS (Cat# 10317052) before being fixed in 10ml of 10% formalin overnight. Cells were centrifuged at 1500 RPM for five minutes and formalin was disposed of. Pellets were washed in PBS (Cat# 10317052) and fixed cells were collected through centrifugation at 1500 RPM for five minutes. Cell pellets were resuspended in 0.4% agarose (400µl) and moulded into a plug using the lid of an Eppendorf tube prior to being placed in a tissue processor cassette. Submerged in increasing concentrations of ethanol for one hour each (80%, 95%, 100%) and finally xylene for one hour prior to being submerged in paraffin wax for at least one hour. Once solidified slices were cut using the microtome at a thickness of five microns and mounted onto slides.

(2.6.2.2) Deparaffinisation and Antigen Retrieval

Slides were prebaked for two hours at 60˚C. Paraffin was removed through submerging slides in decreasing xylene first (two five minute washed) followed by decreasing concentrations of ethanol (100%, 95% and 0%). Two washes were performed (ten minutes each) for each concentration of ethanol. Antigen was retrieved at via incubation at 95˚C in citrate buffer (pH 6) for ten minutes. Slides were

then allowed to gradually cool to room temperature for thirty minutes before continuing to immunohistochemical staining of IRAK1.

(2.6.2.3) Immunohistochemical staining of IRAK1

Immunohistochemical staining was carried out using R&D IHC kit (CTS002). The steps involved in the use of this kit are detailed as follows. Endogenous peroxidases were blocked for five minutes using peroxidase blocking reagent. Slides were washed for a further five minutes in washing buffer (1X TBS). Cells were permeabilised using 0.2% Triton for ten minutes and washed for five minutes.

Nonspecific staining was blocked using Serum Blocking reagent G (15 minutes), Avidin Blocking reagent (15 minutes) and Biotin Blocking reagent (15 minutes). In between each blocking reagent slides were drained and dabbed dry. Slides were then stained with 600µl of primary Santa Cruz IRAK1 targeted antibody (sc-5288) at 1:50 dilution. Slides were placed in a sealed lunch box with damp tissue and incubated overnight at 4˚C.

The following morning slides were washed three times (15 minutes each) with washing buffer, incubated in secondary antibody for one hour and washed a further three times (15 minutes each) in washing buffer. Slides were then incubated in HSS-HRP for thirty minutes before being washed three more times (two minutes each). DAB chromogen was then added for ten minutes and slides were washed for another five minutes in washing buffer. Coverslips were mounted using HISTOMOUNT mounting media (HS-103) and representative brightfield images were taken of each tissue core at 20X magnification (Olympus Microscope).

(2.6.2.4) Data Analysis

IRAK1 protein expression was determined via immunostaining, and the intensity of staining was quantified using Image J software. For each core representative regions of interest were identified and densitometric measurements were taken. To enable comparisons across samples these raw intensity readings were normalised to Z-scores which provides a standardized metric which accounts for variation in the baseline intensity. Graphs were prepared using PRISM. Statistical significance between groups was investigated using unpaired Students t-test. P-values; (*;≤0.05), (**;≤0.01), (***;≤0.001), (****;≤0.0001).

(2.6.3) SHP2 Immunohistochemistry

Reagents used for SHP2 immunohistochemistry have been recorded and catalogued. These reagents are included In the Table 2.6.2.

(2.6.3.1) Preparation of Cell plugs for optimisation

SHP2 control (CTsh) and SHP2 knockdown (SHP2sh-1/2) human microglial cell lines (CHME3) were provided by Dr Marion Butler. These cells were routinely used for previous post-doctoral studies in Dr Butlers lab. SHP2 expression and knockdown was confirmed by western blot analysis.

paraffin embedded cell pellets were prepared using these cells by facilities available in UCD. Control and knockdown cells were seeded in T175 flasks until they were 80% confluent at which point cells were trypsinized, washed and collected by centrifugation at 1500 RPM for five minutes. Cells were washed in 10ml of ice-cold PBS (Cat# 10317052) before being fixed in 10ml of 10% Formalin overnight. Cells

were centrifuged at 1500 RPM for five minutes and formalin was disposed of. Pellets were washed in PBS (Cat# 10317052) and fixed cells were collected through centrifugation at 1500 RPM for five minutes. These fixed cells were then provided to UCD facilities for the preparation of paraffin embedded cell plugs.

(2.6.3.2) Validation of SHP2 Immunohistochemistry using SHP2 knockdown Cell Lines

Cell plugs generated from SHP2 control (SHP2 expressing) and knockdown (SHP2 deficient) cell lines were used to validate immunohistochemical staining procedures. Knockdown was confirmed using Western blotting. Two antibodies were initially tested one from Cell Signalling (cs-3397) and Santa Cruz (sc-7384). At high concentrations of 1:50 dilution the Cell Signalling antibody resulted in minimal IHC staining and was not further evaluated.

Increasing dilutions were evaluated for sc-7384. It was confirmed that higher dilutions of this antibody showed lower levels of background staining. The final stage of validation involved evaluating staining in full face tissue section (HUCAT311) using sc-7384. Background staining was confirmed to be optimal by a clinician in collaboration with Professor William Gallaghers group (UCD) before we progressed to staining OV809B and OV802B Tissue microarray slides.

(2.6.3.3) Deparaffinisation of Slides and Antigen Retrieval

Slides were prebaked at 60˚C for two hours prior to deparaffinisation. Slides were then completely submerged in decreasing concentrations of ethanol (100%,

90%, 80%, 0%) for three minutes each. Antigens were the retrieved at 95˚C, for fifteen minutes, at pH9 using DAKO PT Link.

(2.6.3.4) Immunohistochemical staining using Autostainer Link 48, DAKO

All steps in this section were carried out at room temperature. Staining was carried out using an immunostainer. Endogenous peroxidases were blocked using DAKO peroxidase blocking reagent for ten minutes. Slides were then washed three times for three minutes in washing buffer (0.05% Tween in PBS) prior to being incubated in UV blocking reagent (Cat# TA-060-UB) for ten minutes. Following a further three washes in washing buffer slides were incubated in SHP2 primary antibody (sc-7384) at a 1:250 dilution in DAKO antibody diluent (Cat# DM830), for thirty minutes. After another three washes slides were incubated with mouse linker for thirty minutes. Slides were washed three more times in washing buffer prior to being incubated in horse radish peroxidase (Cat# SM802) for twenty minutes. Finally, slides were washed another three times before being incubated in DAB chromogen (DM827 + SM803) for five minutes.

No antibody controls (NAC) were used as a negative control throughout the validation experiments. In each case these slides were treated the same except no antibody was added to the DAKO antibody diluent.

Sc-7384 is directed against SHP2 has been described by the manufacturer Santa Cruz as being recommended for use in both western blot analysis and immunohistochemistry. SC-7384 has been used in published work to investigate the expression of SHP2 in a study on colorectal cancer.[265]

(2.6.3.5) Haematoxylin counterstaining and coverslip mounting

Slides were counterstained with haematoxylin (Cat# SK203) for five minutes prior to being washed in deionised H_2O for three minutes. DPX mounting solution was then used to mount coverslips.

(2.6.3.6) Image Analysis

Slides were scanned using Aperio® AT2 – Leica Biosystems. Images were analysed using QuPath image analysis software. Positive cell detection was optimised by adjusting threshold parameters. This was repeated to assess cellular, cytoplasmic and nuclear staining of SHP2 in both tissue microarrays. Graphs were prepared using PRISM. Statistical significance between groups was investigated using unpaired Students t-test. P-values; (*;≤0.05), (**;≤0.01), (***;≤0.001), (****;≤0.0001).

Table 2.6.2: Immunohistochemistry Reagents, Suppliers and Catalogue Numbers

Reagent	Catalogue Number
R&D Immunohistochemistry Kit	CTS002
DAKO PT Link and pH 9 Buffer	DM828
Endogenous peroxidase block	SM801
Ultra vision protein block Thermo	TA-060-UB
DAKO antibody diluent	(DM830)
mouse linker	(DAKO-GV821)
HRP	(SM802)
DAB chromogen	(DM827 + SM803)
Haematoxylin	(SK203)
DPX histology mountant	(06522).
Santa Cruz SHP2	(SC-7384)
Cell Signalling SHP2	cs-3397
Cell Signalling IRAK1	sc-5288

(2.7) Probing Gene Expression Databases

(2.7.1) Probing Gene Expression in OvCa vs Normal Controls using TNMplot

TNMplot database contains 56,938 unique samples collected from GEO, GTex, TCGA and TARGET databases. Gene expression analysis was performed for OvCa datasets, and all graphs were generated using the TNMplot interface. The gene chip dataset included mRNA expression analysis in ovarian tumour (744), metastatic (44) and normal controls. The RNA sequencing dataset included gene expression analysis in Ovarian Serous Cystadenocarcinoma (374) and normal controls (133).

As recommended by the TNMplot database, the following reference for TNMplot.com was included:

Please kindly cite our paper: A. Bartha, B. Gyorffy, TNMplot.com: A Web Tool for the Comparison of Gene Expression in Normal, Tumour and Metastatic Tissues Int. J. Mol. Sci. 2021, 22(5), 2622.

(2.7.2) Probing mRNA Expression Correlation with Overall Survival and Progression Free Survival in Ovarian Cancer

KM Plotter uses gene chip datasets. We probed for association between targets of interest and OS. Where possible the JetSet best probe set was selected for each target. The JetSet used for each target is recorded in Table 2.7.1 below. For each target, auto select best cut off was confirmed and outlier arrays were excluded from analysis.

As recommended by the KM Plotter database, the following reference for TNMplot.com was included:

Please kindly cite our paper: Gyorffy B: Discovery and ranking of the most robust prognostic biomarkers in serous ovarian cancer, Geroscience, 2023, doi: 10.1007/s11357-023-00742-4.

Table 2.7.1: Target ID and the Affy ID for each target examined.

Target ID	JETSET (Affy ID)
IRAK1	201587_s_at
PTPN11 (SHP2)	212610_at
H2AV	202487_s_at
STAM1	203544_s_at
GPX1	200736_s_at
COR1C	222409_at
ZFPL1	209428_s_at
SF3B4	209044_x_at
PFD5	210908_s_at
RN114	211678_s_at
DDX3X	201210_at
METK2	200768_s_at
5MP1	217809_at
DNJA3	205963_s_at
SRPRB	227737_at
TMM33	225492_at
RM15	218027_at
RIR2	201890_at
BAG6	210208_x_at
EIF3C	NA
PR40A	226687_at
KITH	202338_at
ACACA	212186_at
GEM15	225712_at
MTDC	201761_at
LSM8	228529_at
DAD1	200046_at
SRSF5	NA
MLH3	204838_s_at
FAAA	202862_at
NTF2	228379_at
S10AD	202598_at

Chapter 3:

Evaluating Interleukin-1 Receptor Associated Kinase 1 (IRAK1) as a Potential Therapeutic Target in High Grade Serous Ovarian Cancer

(3.1.1) Introduction

As outlined in Chapter 1 OvCa is the 7th most common cancer among women and the most lethal gynaecological malignancy worldwide.[45] Approximately 75% of OvCa patients are diagnosed in the advanced stage[9,10] which is associated with poor prognosis and a five-year survival rate of only 29%.[13] Current first line therapeutic interventions include surgical removal of the tumour and treatment with cisplatin based chemotherapy.[21] While 20% of patients exhibit initial resistance to platinum based chemotherapy the majority of patients will respond quite well to this treatment.[25] Unfortunately 70% of these initial responders will display recurrence and metastasis within the first two years following diagnosis.[26]

It is clear that both advanced stage detection and frequence of chemoresistance are two considerable barriers to the effective treatment of OvCa patients. Novel therapeutic strategies and targets are urgently required in order to improve outcomes for patients diagnosed with advanced stage OvCa or chemo-resistant OvCa. In this chapter we will outline how IRAK1 may represent a novel therapeutic target in OvCa and that treatment with the IRAK1-JAK2-FLT3 inhibitor pacritinib may represent a novel therapeutic strategy targeting IRAK1 in OvCa.

IRAK1 is a serine/threonine kinase which has been characterised extensively for the role it plays downstream of TLR's and IL-1R in order to mediate innate immune responses to pathogens.[61] Interestingly several studies, outline in Table 1.4.1 and 1.4.2, have shown that IRAK1 plays in the growth and progression of several types of cancer. In OvCa IRAK1 has been found to be increased compared to normal controls.[134] We wanted to further investigate the role IRAK1 plays in a series of OvCa cell lines to evaluate further its potential as a novel therapeutic target.

Pacritinib is a commercially available small molecule kinase inhibitor which targets IRAK1, JAK2 and FLT3. Several studies, detailed in Table 1.5.1 and Table

1.5.2 have shown pacritinib significantly impairs various cancer types in both *in vitro* and *in vivo* models. Pacritinib has also received FDA approval for treatment of patients with myelofibrosis[149] and has entered clinical trials for the treatment of patients with colorectal cancer (NCT02277093), prostate cancer (NCT04635059) and relapsed / refractory T cell lymphoproliferative neoplasms (NCT04858256)**.** For this reason, we wanted to evaluate using *in vitro* growth assays if pacritinib could represent a novel therapeutic strategy in OvCa which targets IRAK1 in addition to JAK2 and FLT3.

(3.1.2) Aims and Hypotheses

OvCa represents a poor prognosis cancer displaying a high frequency of chemoresistance and a high incidence of advanced stage detection. In the absence of effective second line therapeutic interventions the identification and validation of novel druggable targets are urgently required to provide further options for the treatment of patients with OvCa.

Over the past decade IRAK1 has been proposed as a novel druggable target in several cancers and has shown promise as a therapeutic target. Pacritinib has received FDA approval for treatment of patients with myelofibrosis and has entered clinical trials for the treatment of other cancers including prostate cancer. IRAK1 has previously been shown to be one of seventeen genes differentially regulated (increased) in OvCa [266]. This study provided a link between IRAK1 and OvCa but left several questions unanswered as to the exact role that IRAK1 plays in the growth and progression of OvCa and the potential application of using the IRAK1 kinase inhibitor pacritinib to target OvCa.

The aim of this study is to determine whether IRAK1 plays a role in the growth of OvCa cel lines representing HGSC using the following specific objectives.

Specific Objectives:

1. Determine whether IRAK1 knockdown impacts the growth of OvCa cell lines in vitro.
2. Determine whether treatment with pacritinib impairs growth of OvCa cell lines in vitro.
3. Determine whether IRAK1 is expressed in high levels in serous OvCa and examine whether the expression of IRAK1 negatively correlates with prognostic indicators.

(3.2) Results

(3.2.1) IRAK1 Knockdown Impairs Growth of Ovarian Cancer Cell Lines *in Vitro*.

(3.2.1.1) Validation of IRAK1 knockdown in OvCa cell lines

We first generated stable knockdown of IRAK1, using two independent shRNA's, targeting IRAK1, through a lentiviral approach in the HGSC cell lines PE01, PE04, and OVCAR3 and in the low grade serous OAW42 and non-serous IGROV1 OvCa cell lines (Section 2.1.2).

Relative IRAK1 protein expression was quantified using Western blot analysis (Section 2.4) and normalised using the house keeping proteins β-actin or tubulin as loading controls. We first began by validating IRAK1 knockdown. IRAK1 protein expression is significantly reduced following knockdown of IRAK1 in all five cell lines (Fig. 3.1.1 and Fig. 3.1.2). These cell lines were then used to further evaluate the role of IRAK1 in the growth of OvCa cell lines *in vitro* by comparing IRAK1 expressing control cells to IRAK1 deficient cells.

(3.2.1.2) IRAK1 knockdown results in significant reduction in proliferation of OvCa cell lines

Next we investigated the role of IRAK1 in OvCa by evaluating if IRAK1 knockdown had an impact on proliferation. Control (Ctrolsh) and IRAK1 knockdown

(IRAK1sh-1/2) cell lines were seeded at the same density and cell counts were taken four days and seven days after seeding. The increase in cell number between seeding and counting was then used as a quantitative measurement of proliferation *in vitro*. (Section 2.3.1)

The confluency of IRAK1sh-1 and IRAK1sh-2 is lower than the Ctrolsh for PE01, PE04, OAW42, OVCAR3 and IGROV1 cell lines on both day 4 and day 7 after seeding (Supp. 3.1.1). Quantitative cell counts taken on day 4 and day 7 confirm this visual assessment and show reduced proliferative ability of all five OvCa cell lines following knockdown of IRAK1 (Fig. 3.1.1). These observations indicate IRAK1 knockdown leads to reduced proliferation in OvCa cells.

(3.2.1.3) IRAK1 knockdown results in significant reduction of colony formation and survival of OvCa cell lines *in vitro*

We next aimed to assess the role of IRAK1 in 2D survival and colony formation in OvCa cell lines using IRAK1 knockdown (Section 2.3.3). Ctrolsh and IRAK1sh-1/2 cells were seeded at the same density and 10-21 days later (depending on cell line) colonies were counted as a measure of colony forming ability. Representative images show IRAK1sh-1 and IRAK1sh-2 form colonies less frequently than their Ctrolsh counterparts for all cell lines (Fig. 3.2.1). Visually it also appears that these colonies are smaller than their control counterparts, though we did not have the means to provide a quantitative measurement of this. IRAK1 knockdown led to significantly reduced colony formation in HGSC cell lines PE01, PE04 and OVCAR3 in addition to OAW42 and IGROV1 OvCa cell lines (Fig. 3.2.1). These findings further support IRAK1 plays a positive role in the growth of OvCa cells *in vitro*.

(3.2.1.4) IRAK1 knockdown results in significant reduction of spheroid formation and anchorage independent growth of OvCa cell lines *in vitro*

3D *in vitro growth* assay models provide methodologies (Section 2.3.4) to assess cancer cell growth *in vitro* which more accurately represent how cancer grows *in vivo*. Cancer cell line spheroids growing in 3D more closely resemble the complex 3D structure of tumours *in vivo*. A key feature of cancer growth is the ability of transformed cells to divide and grow without being attached to a solid structure or matrix. This is referred to as anchorage independent growth. In order to assess the role of IRAK1 in anchorage independent growth we seeded single cells in low percentage agarose and assessed spheroid formation following IRAK1 knockdown.

Visually, IRAK1sh-1 and IRAK1sh-2 cells form smaller spheroids at a lower frequency than their IRAK1 expressing counterpart control cells (Fig. 3.3.1). Quantitative measurements were taken by counting the number of spheroids formed in each well. These counts provide a measure of anchorage independent growth. IRAK1 knockdown cell lines displayed significantly reduced anchorage independent growth and spheroid formation in PE01, PE04, OVCAR3, OAW42 and IGROV1 cell lines (Fig. 3.3.1). These findings further support the hypothesis that IRAK1 plays a positive role in the growth of OvCa cells.

(3.2.1.5) IRAK1 knockdown results in a reduction in the invasion and migration of OvCa cell lines i*n vitro*

Both migration and invasion in OvCa are complex processes. Advanced HGSC is widely disseminated and associated with additional complications to treatment. In order to model invasion and passive dissemination, characteristics of

OvCa metastasis, we employed a Matrigel droplet assay (Section 2.3.5) in which a single droplet of Matrigel containing $5x10^4$ OvCa cells was adhered to the bottom of a twenty-four well plate. This Matrigel droplet was then submerged in complete cell culture media (containing FBS) in order to stimulate invasion of cells out of the Matrigel droplet. The number of cells outside of the Matrigel droplet after day 7 was used as a quantitative measurement of invasion and migration.

On day-7 images were taken at 4X magnification and stitched together with the use of a programme designed by Dr Bryan Hennelly (Engineering Department, Maynooth University) (Section 2.3.5). IRAK1sh-1 and IRAK1sh-2 PE01, OAW42, OVCAR3 and IGROV1 cell lines show fewer cells invading and migrating out of the Matrigel droplet and into the well surrounding the droplet (Fig 3.4.1). PE04 Ctrolsh and IRAK1sh-1/2 cells did not invade or migrate into the surrounding well. OAW42 and IGROV1 cells show a very high level of migration and invasion compared to HGSC PE01 and OVCAR3 cell lines. The number of cells migrated out of the Matrigel droplet were counted and graphed. PE01, OVCAR3, OAW42 and IGROV1 IRAK1 knockdown cells display significantly reduced migration and invasion compared to control cells (Fig. 3.4.1). These findings provide further support that IRAK1 plays a positive role in the growth of OvCa cells.

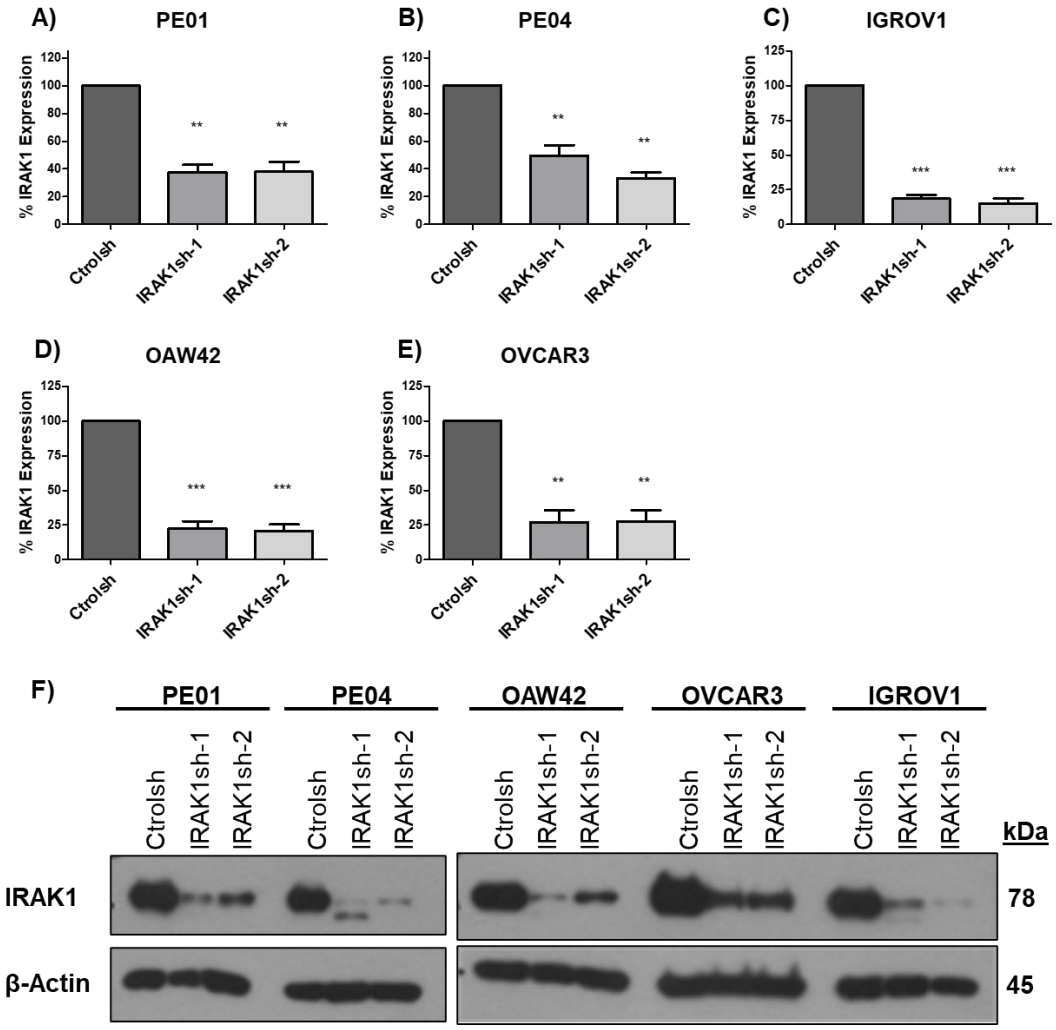

Figure 3.1.1: Confirmation of IRAK1 knockdown in OvCa cell lines by Western blot analysis using Image J densitometry. Whole cell lysates were prepared on day 7 to match the above proliferation assay, from **A)** PE01, **B)** PE04, **C)** OAW42, **D)** OVCAR3 and **E)** IGROV1, control (Ctrolsh) and IRAK1 knockdown (IRAK1sh-1/2) cell lines. Optical density was measured using image-J and normalised using β-actin expression as a loading control. Statistical significance was assessed (PRISM) using a paired students t-test comparing control to IRAK1 knockdown cells. P-values; (**;≤0.01) and (***;≤0.001). **F)** On day-7 whole cell lysates were prepared from Ctrolsh and IRAK1sh-1/2 cells and IRAK1 expression was assessed using Western blot analysis to confirm IRAK1 knockdown.

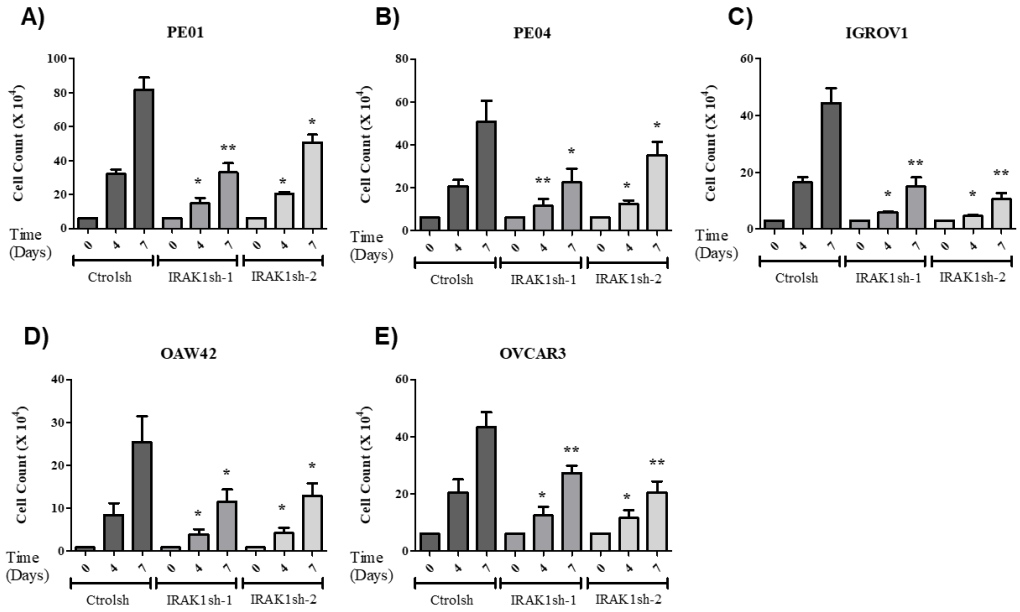

Figure 3.1.2: Stable knockdown of IRAK1 significantly inhibits the proliferation of Ovarian Cancer cell lines. **A)** PE01, **B)** PE04, **C)** IGROV1, **D)** OAW42 and **E)** OVCAR3 IRAK1 knockdown cells display significantly reduced proliferation at both four days and seven days following seeding. Results are representative of greater than or equal to three independent experimental replicates. Statistical significance was investigated using a paired student's t test comparing control (Ctrolsh) to IRAK1 knockdown cell lines (IRAK1sh-1/2), p-values; (*; ≤0.05), (**; ≤0.01).

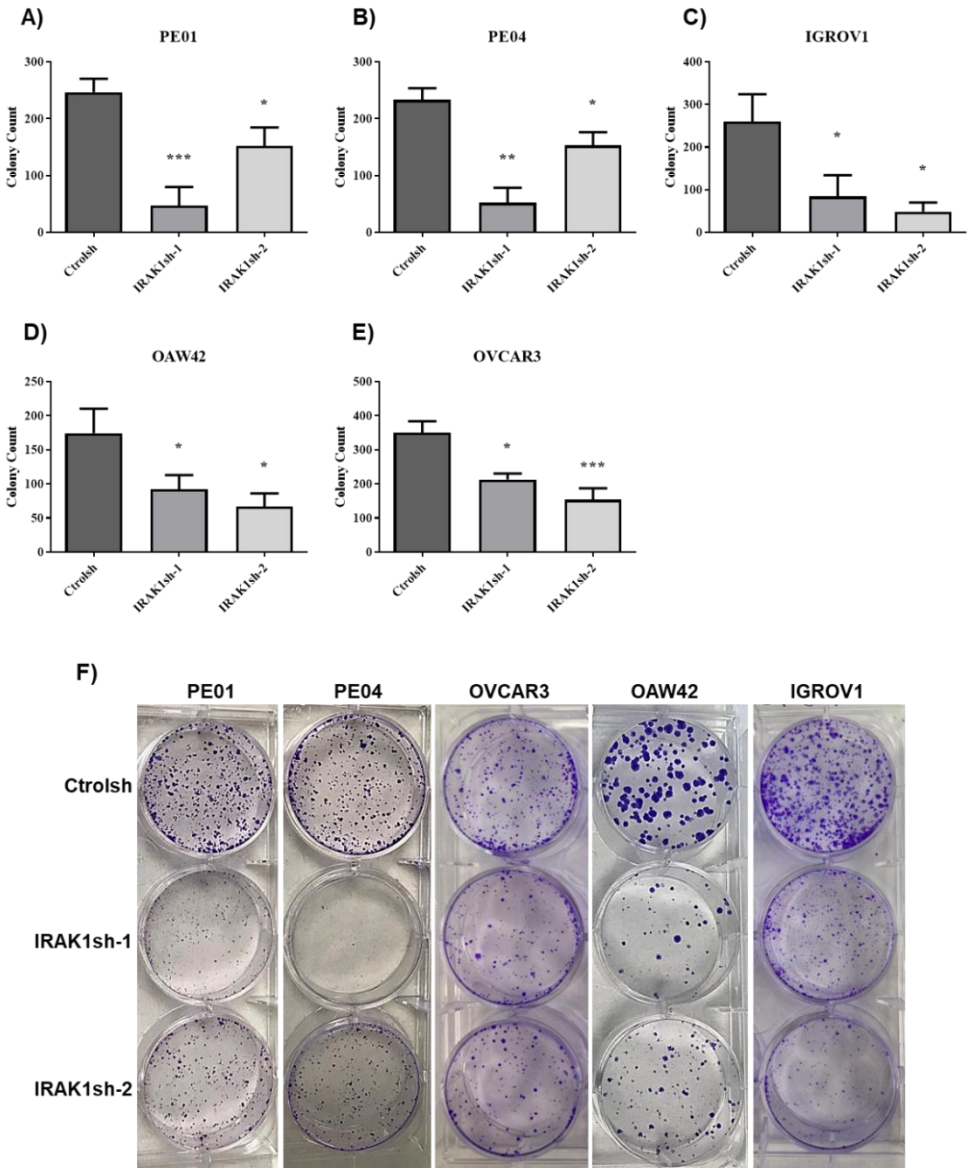

Figure 3.2.1: Stable knockdown of IRAK1 significantly reduces colony formation. **A)** PE01, **B)** PE04, **C)** IGROV1 **D)** OAW42 and **E)** OVCAR3 knockdown cells all display significantly reduced colony formation compared to control cells. Statistical significance was investigated using paired students t-test comparing Ctrolsh cells to IRAK1sh cells, p-values (*;≤0.05), (**;≤0.01), (***;≤0.001). Results are representative of greater than or equal to four experimental replicates. **F)** Representative images are displayed for the colony formation observed. Data was contributed by Dr Devlin Wall-Coughlan for PE01, OAW42 and PE04 and by Jamie Casey for PE04, OVCAR3 and IGROV1.

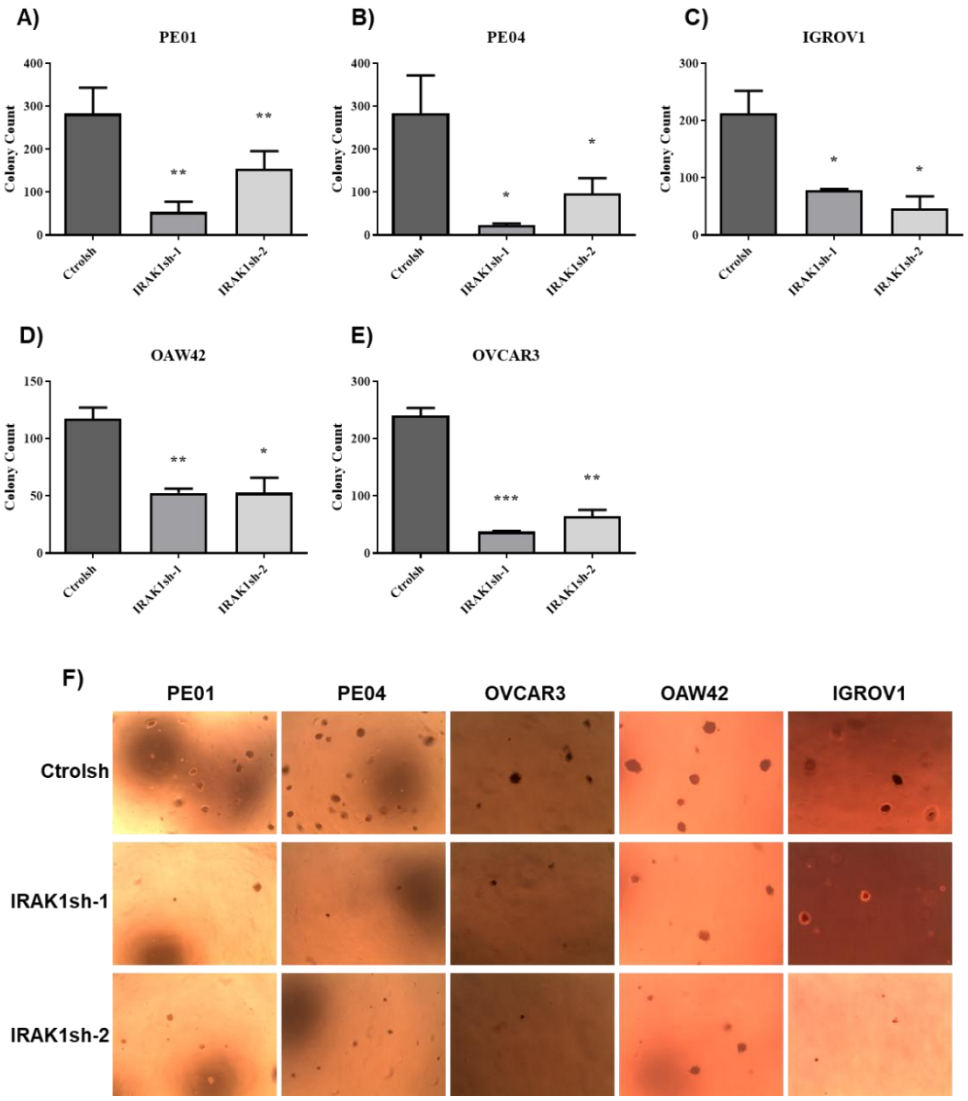

Figure 3.3.1: Ovarian Cancer cell lines show reduced anchorage independent growth following IRAK1 knockdown. **A)** PE01, **B)** PE01, **C)** IGROV1, **D)** OAW42 and **E)** OVCAR3 IRAK1 knockdown cells all display significantly reduced anchorage independent growth compared to control cells. **F)** Representative images were captured at 4X Magnification. Statistical significance was carried out using a paired students t-test comparing Ctrolsh cells to IRAK1sh cells. P-values (*;≤0.05), (**;≤0.01), (***;≤0.001). Results are representative of greater than or equal to four independent experimental replicates. Data was contributed by Dr Devlin Wall-Coughlan for PE01, OAW42 and PE04 with Data being contributed by Jamie Casey for all five cell lines.

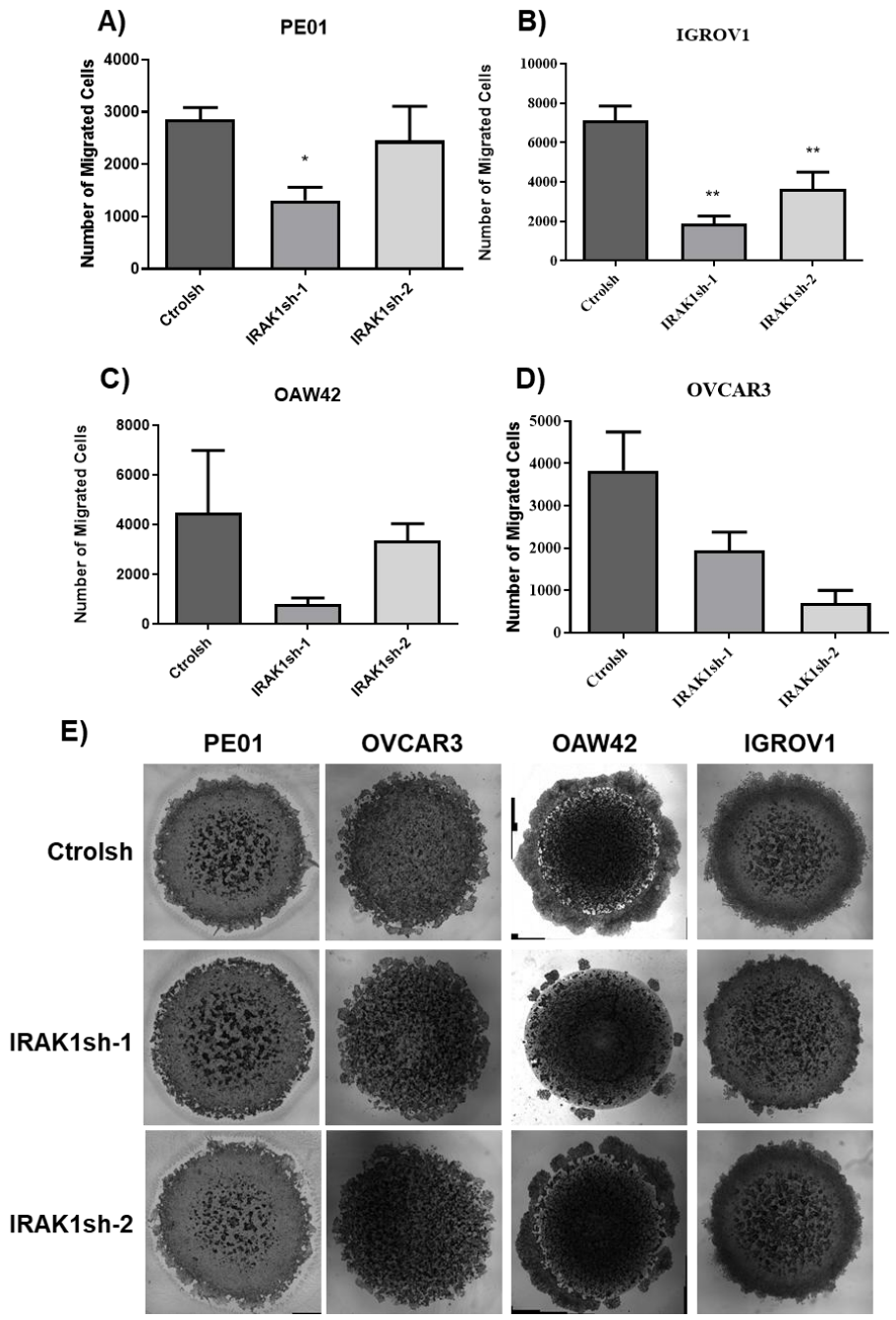

Figure 3.4.1: IRAK1 knockdown reduces the invasion and migration of ovarian cancer cell lines as assessed by Matrigel Drop assay. A) PE01 **C)** OAW42 and **D)** OVCAR3 IRAK1 knockdown cells display reduced migration / invasion while **B)** IGROV1 IRAK1 knockdown cells display significantly reduced migration and invasion. **E)** Representative images were captured. Results are representative of greater than or equal to three independent experimental replicates. Statistical significance was investigated using a paired students t-test comparing Ctrolsh cells to IRAK1 knockdown. P-values; (*;≤0.05), (**;≤0.01).

(3.2.2) IRAK1 Knockdown Results in Reduced HER4 Expression in Ovarian Cancer Cell lines.

IRAK1 knockdown led to a significant reduction in 2D proliferation, colony formation, migration / invasion, colony formation and anchorage independent growth in PE01, PE04, OVCAR3, OAW42 and IGROV1 cell lines (Section 3.2.1). This series of experiments provides a strong indication that IRAK1 plays a key role in the growth of OvCa cell lines *in vitro*. Furthermore, these studies may indicate that IRAK1 represents a potential therapeutic target in OvCa. We next wanted to investigate the molecular mechanisms through which IRAK1 knockdown impairs growth in these cell lines.

We profiled HER family protein expression in PE01, PE04, OVCAR3 and OAW42 cells using Western blot analysis. No significant decrease in EGFR, HER2 or HER3 was observed in any cell line following IRAK1 knockdown (Fig. 3.5.3, Supp. 3.2.1). However, in HER4 expressing cell lines (PE04, OVCAR3 and OAW42) showed a significant reduction in HER4 expression following IRAK1 knockdown (Fig. 3.5.1, 3.5.2). Finally, HER4 80kDa ICD, which was more challenging to detect due to lower expression, was observed to be reduced in PE04 IRAK1sh-1/2 cells (n=2) (Fig. 3.5.3, Supp. 3.3.1).

While reduced HER4 may represent one potential mechanism through which IRAK1 knockdown impairs growth in PE04, OAW42 and OVCAR3 cell lines we must remain open to a number of other possibilities. The PE01 HGSC cell line showed reduced growth following IRAK1 knockdown and does not display detectable levels of HER4 by Western blot analysis. This potentially indicates that a common mechanism of action between all four cell lines still remains to be observed following IRAK1 knockdown.

It is unclear if this reduction of HER4 expression contributes to the reduced proliferation, colony formation, migration/invasion and anchorage independent growth observed in section (3.2.1). Further experiments are required in order to investigate whether reduced HER4 expression is causative of the reduced growth observed.

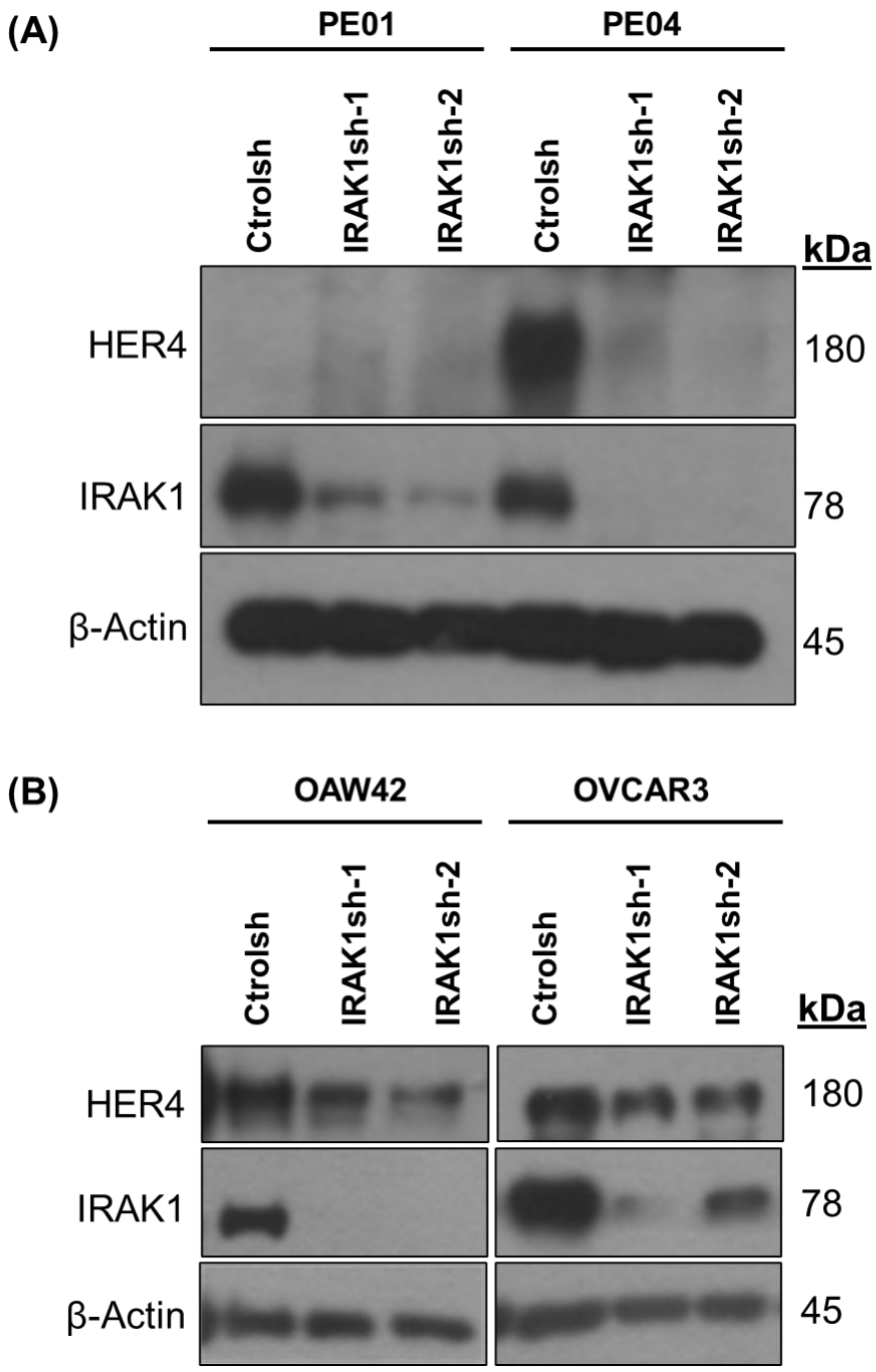

Figure 3.5.1: The knockdown of IRAK1 results in reduced expression of Full-Length (180kDa) HER4 levels in HER4 expressing OvCa Cell lines. HER4 expressing **A)** PE04, **B)** OAW42 and **C)** OVCAR3 display significantly reduced expression of HER4 following IRAK1 knockdown (IRAK1sh-1/2) compared to control cells (Ctrolsh). B-actin was used as a loading control. Western blots shown are representative of greater than or equal to four independent experimental replicates.

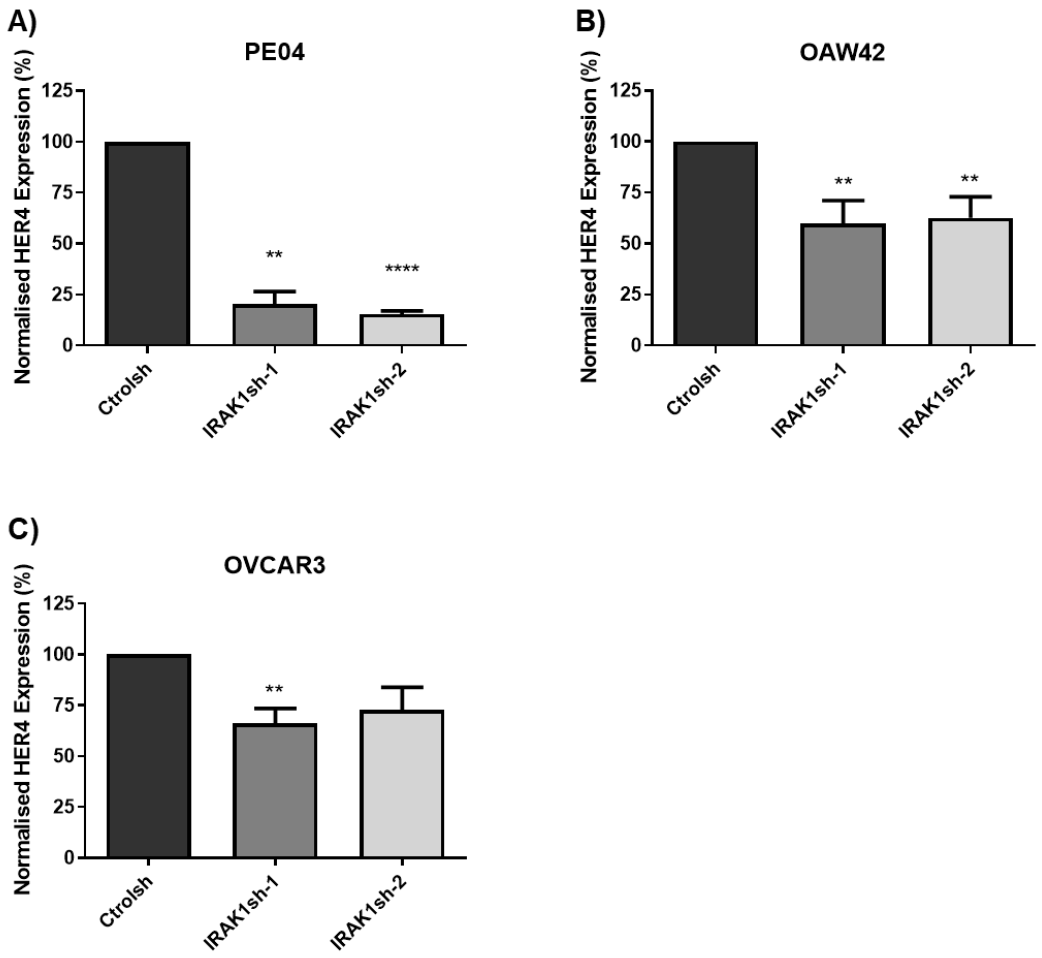

Figure 3.5.2: HER4 expression is significantly reduced in OvCa cell lines following IRAK1 knockdown. A) PE04 and B) OAW42 IRAK1 knockdown cells display significantly reduced HER4 compared to control cells. C) OVCAR3 cells display a significant reduction in HER4 for one knockdown cell line and a numerically reduced level of HER4 in the second knockdown cell line. Statistical significance was investigated using a paired students t-test comparing HER4 expression in Ctrolsh to IRAK1sh. p-values; (*;≤0.05), (**;≤0.01), (***;≤0.001), (****;≤0.0001). Data was contributed by Dr Marion Butler.

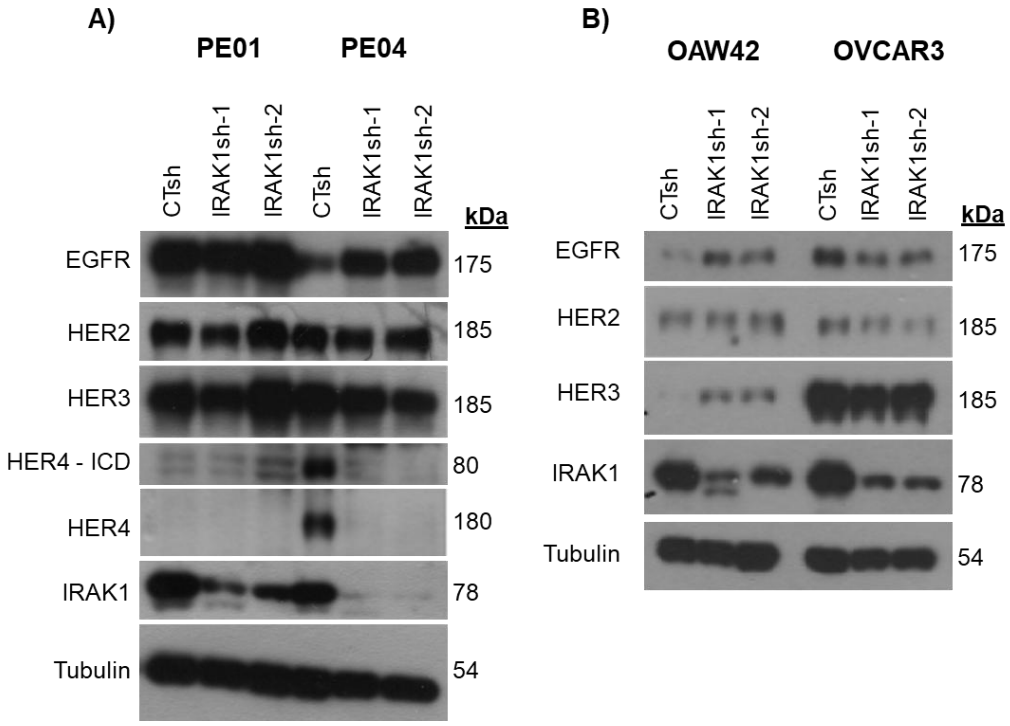

Figure 3.5.3: The knockdown of IRAK1 results reduced 80kDa HER4 ICD in PE04 cells. A) HER4 and HER4 80kDa ICD are reduced in PE04 IRAK1 knockdown cells. A-B) EGFR, HER2 and HER3 display no significant difference in expression following IRAK1 knockdown in PE01, PE04, OAW42 or OVCAR3 cell lines. Whole cell lysates were prepared from control (Ctrolsh) and IRAK1 Knockdown (IRAK1sh-1/2) ovarian cancer cell lines. Western blots shown are representative of greater than or equal to three independent experimental replicates with the exception of **A)** HER4 ICD (n=2), p-HER2 (n=2) **B)** HER3 (n=2).

(3.2.3) Treatment with Pacritinib Impairs Growth of Ovarian Cancer Cell Lines *In Vitro*.

The IRAK1 kinase inhibitor selected for this work was pacritinib. This small molecule inhibitor has previously received FDA approval for use in myelofibrosis and has entered phase two clinical trials for certain cancers including prostate cancer. This makes pacritinib a particularly attractive candidate for this study as both safety and efficacy have previously been shown. It is important to note that while pacritinib inhibits IRAK1 kinase activity it also inhibits the activity of JAK2 and FLT3 which does complicate its use in mechanistic studies to understand the role IRAK1 kinase inhibition plays in OvCa growth.

(3.2.3.1) 2D Viability Assay and IC50 Analysis

We began by assessing the 2D viability of OvCa cell lines treated with increasing concentration of Pacritinib (Fig. 3.6.1). Pacritinib was observed to potently impair 2D viability, in a dose dependent manner, of all PE01, PE04, OVCAR3, OAW42, PEA1 and PEA2 OvCa cell lines at concentrations less than 3μM. IC50 values were determined for each cell line (Table 3.2.1). Pacritinib displays low IC50 values below 3μM for all OvCa cell lines evaluated. These findings support the hypothesis that pacritinib may provide a novel therapeutic strategy in OvCa.

(3.2.3.2) Treatment with pacritinib significantly reduces colony formation of OvCa cell lines *in vitro*

Following treatment with low micromolar concentrations (0.5μM or 1μM) of pacritinib we observed a significant reduction in colony formation of PE01, PE04, OVCAR3 and OAW42 cell lines (Supp. 3.4.1), in a dose dependent manner. These findings support the hypothesis that pacritinib may provide a novel therapeutic strategy in OvCa.

(3.2.3.3) Treatment with pacritinib significantly reduces colony formation and anchorage independent growth of OvCa cell lines *in vitro*

Treatment with Pacritinib resulted in a significant reduction of colony formation and anchorage independent growth in PE01, PE04, OVACR3 and OAW42 cell lines (Fig. 3.7.1), in a dose dependent manner. These findings support the hypothesis that pacritinib may provide a novel therapeutic strategy in OvCa.

(3.2.3.4) Treatment with pacritinib significantly reduces 3D viability and growth of OvCa cell lines *in vitro*:

OvCa cells were seeded in 2% Matrigel matrix and treated with Pacritinib (1.25μM and 2.5μM) or vehicle control. Treatment with Pacritinib resulted in a dose dependent significant reduction in 3D viability of PE01, PE04 and OVCAR3 cell lines (Fig. 3.8.1). These findings support the hypothesis that pacritinib may provide a novel therapeutic strategy in OvCa.

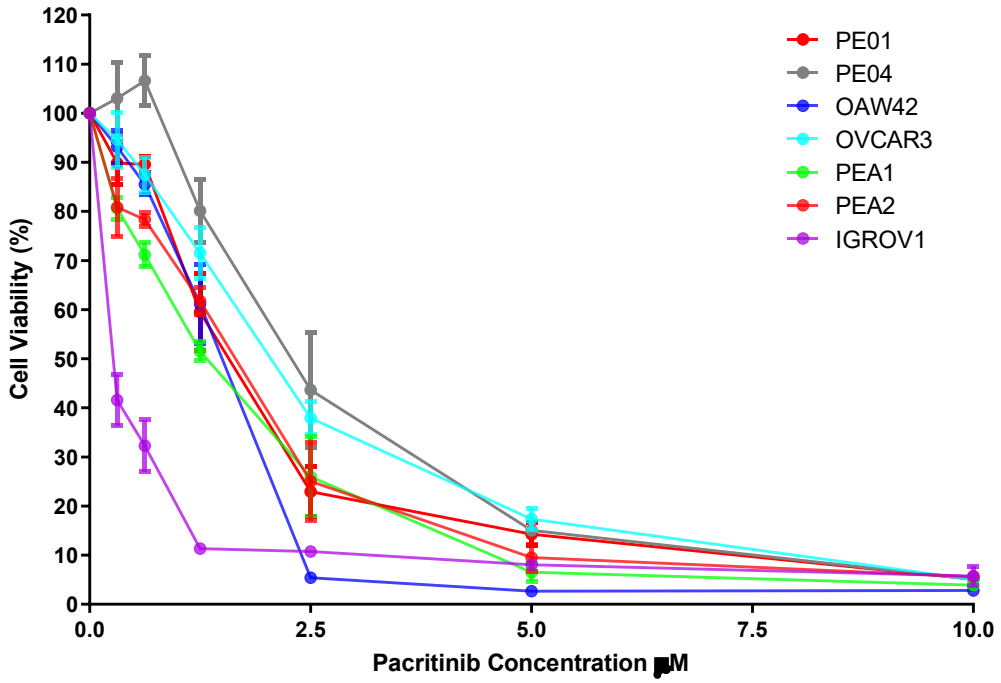

Figure 3.6.1: Treating a selection of ovarian cancer cell lines with increasing concentrations of IRAK1-JAK2-FLT3 inhibitor (Pacritinib) results in a significant dose dependent decrease in cell viability. Treatment with Pacritinib resulted in a dose dependent decrease in viability in high grade serous OvCa (HGSC) cell lines PE01, PE04, OVCAR3, PEA1 and PEA2 and displayed a similar profile in the non-HGSC cell lines tested OAW42 and IGROV1. Results are representative of 3 independent experimental replicates.

Table 3.2.1: IC50 Values, of IRAK1, JAK2 and FLT3 inhibitor (pacritinib) observed for a Selection of Ovarian Cancer Cell Lines. IC50 values were calculated using Calcusyn software using the 2D viability data shown in Figure 3.6.1.

Cell Line	Subtype	Compound	IC_{50} (μM) ± SEM
PE01	High Grade Serous Ovarian cancer	Pacritinib	1.61 μM ± 0.06 μM
PE04	High Grade Serous Ovarian cancer	Pacritinib	2.67 μM ± 0.06 μM
OVCAR3	High Grade Serous Ovarian cancer	Pacritinib	1.9 μM ± 0.27 μM
PEA1	High Grade Serous Ovarian cancer	Pacritinib	0.97 μM ± 0.10898 μM
PEA2	High Grade Serous Ovarian cancer	Pacritinib	1.26 μM ± 0.22 μM
OAW42	Low Grade Serous Ovarian cancer	Pacritinib	1.21 μM ± 0.03 μM
ID8 Defb29 VEGF	Murine Ovarian Cancer Cell Line	Pacritinib	2.39 μM ±0.35753 μM

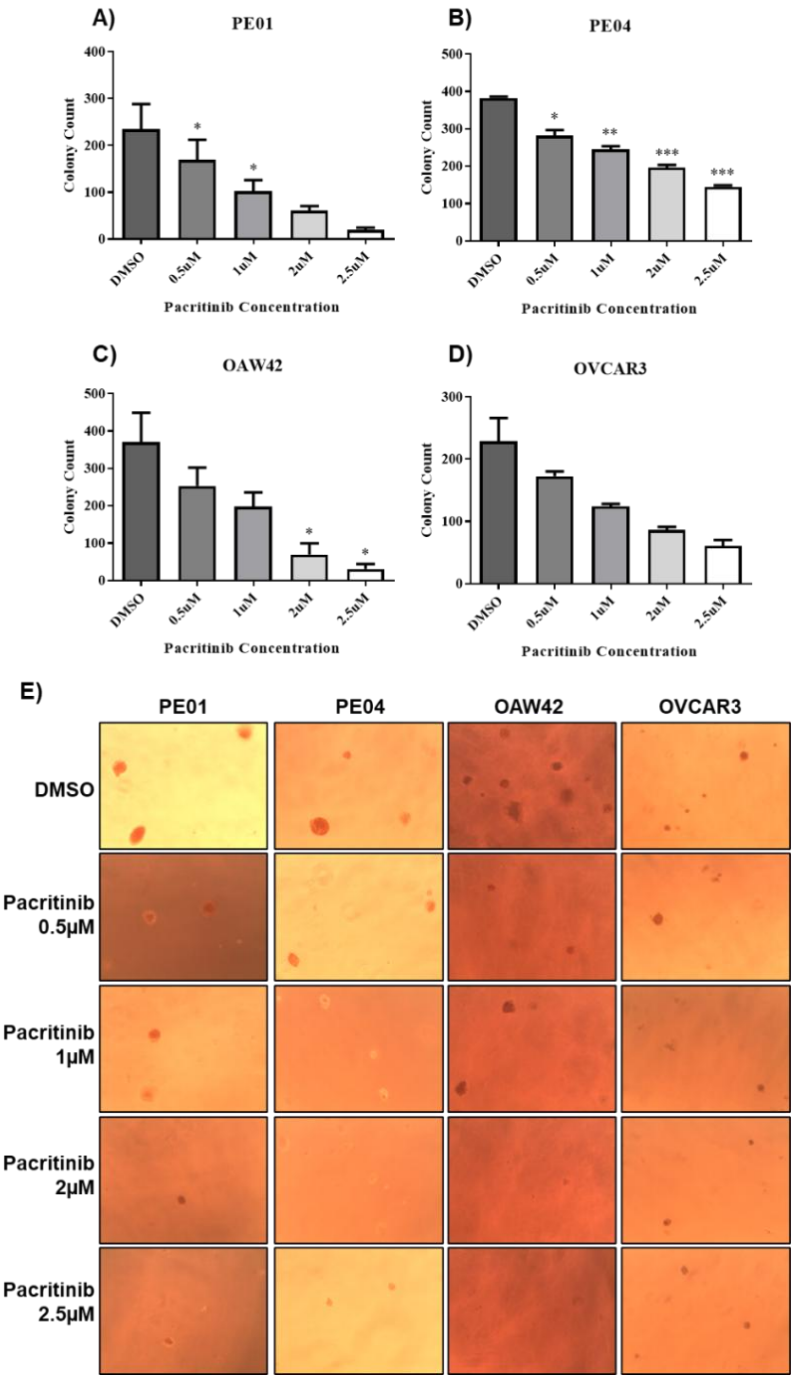

Figure 3.7.1: Pacritinib significantly reduces anchorage independent growth of OvCa cell lines. Treatment with pacritinib resulted in reduced anchorage independent growth in **A)** PE01**, B)** PE04**, C)** OAW42 and **D)** OVCAR3. This reduction is significant at all concentrations in PE04, at 0.5μM 1μM in PE01 and at 2μM, 2.5μM in OAW42. **E)** Representative Images were captured at 4X magnification and representative counts were taken of the number of colonies per well. Statistical significance was assessed using a paired students t-test. P-values; (*;≤0.05), (**;≤0.01), (***;≤0.001). Results are representative of greater than or equal to three independent experimental replicates.

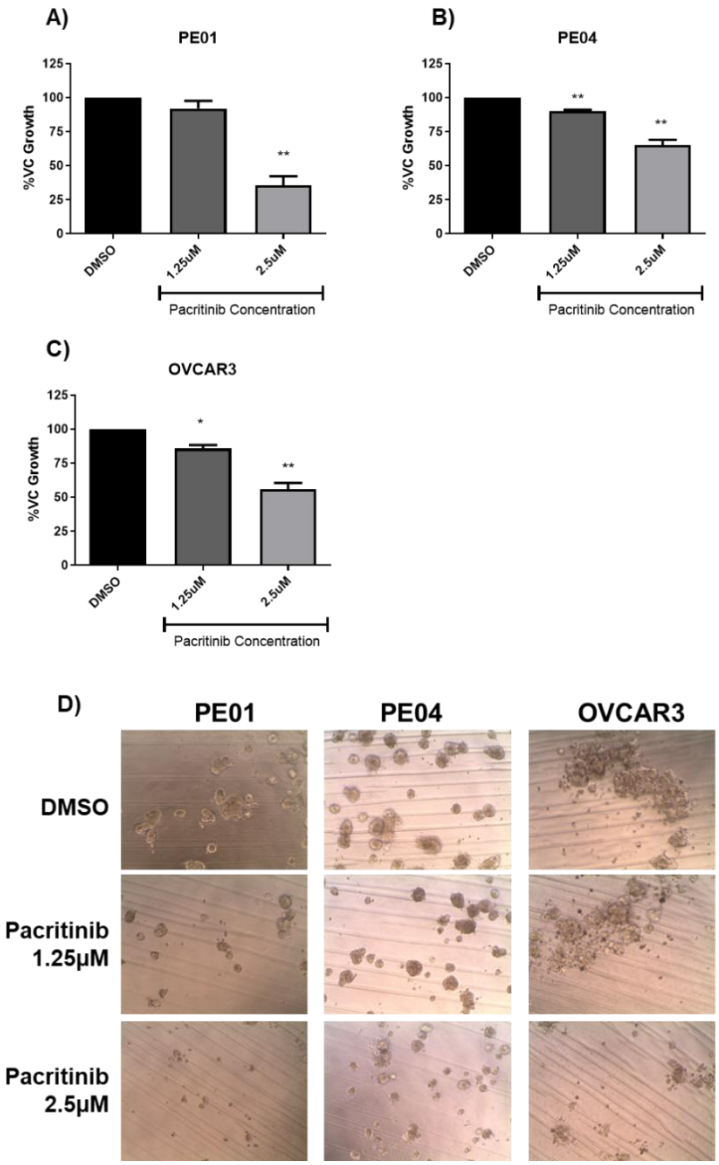

Figure 3.8.1: Pacritinib significantly reduces the 3D viability of ovarian cancer cell lines. **A)** PE01, **B)** PE04 and **C)** OVCAR3 display significantly reduced 3D viability following treatment with 2.5μM pacritinib while **B)** PE04 and **C)** OVCAR3 display significantly reduced 3D viability following treatment with 2.5μM pacritinib. Statistical significance was assessed using students paired t-test. P-value; (*;≤0.05), (**;≤0.01). Results are representative of four independent experimental replicates. **D)** Representative images were captured on day-7 at 4X magnification.

(3.2.4) Treatment with Pacritinib Impairs Growth Factor Receptor Signalling and JAK2-STAT3 Signalling in OvCa Cell Lines *In Vitro*.

Whole cell lysates were prepared from PE01, PE04, OVCAR3 and OAW42 cells treated with 1μM, 1.5μM, 2μM of Pacritinib or vehicle control for twenty-four hours. Using Western blot analysis (Section 2.4), we profiled protein expression in these lysates in order to investigate the molecular mechanisms which may be contributing to the reduced growth observed in OvCa cell lines treated with Pacritinib *in vitro*.

Unfortunately, Cell Signalling phospho-IRAK1 antibody CS-12756 was discontinued during this project. It would be important moving forward with this project for the validation of IRAK1 inhibition following treatment with pacritinib to be confirmed using western blot analysis. This could be achieved through validation of phospho-IRAK1 targeted antibody from another supplier and examining expression levels using western blot analysis.

(3.2.4.1) Treatment with pacritinib reduces the activation of JAK2 and STAT3 in OvCa cell lines *in vitro*

In addition to inhibiting IRAK1 kinase activity pacritinib also acts as a kinase inhibitor of JAK2. Following treatment with low micromolar concentrations of pacritinib that we observed reduced JAK2 in PE01, PE04 and OAW42 cells (Fig. 3.9.1, 3.9.2). We also observed significantly reduced phosphorylation of JAK2 at (Tyr211) in PE01, PE04 and OAW42 (Fig. 3.9.1, 3.9.2). Treatment with pacritinib resulted in a numerical reduction in activation of JAK2 in OVCAR3 which was not significant. In addition to

this, we observed decreased phosphorylation of STAT3 (Y705) in PE01, PE04 and OAW42 (Fig. 3.9.1, 3.9.2). At the concentrations evaluated the activation of STAT3 does not appear to be reduced in the OVCAR3 cell line following treatment with pacritinib.

Here we observe that, at the concentrations tested, pacritinib treatment did not result in a significant reduction in STAT3 activation in OVCAR3 cell line. This may indicate that STAT3 inhibition may be cell line dependent or concentration dependent. Further experiments are required to determine which of these may be the case. The concentration range assessed in these Western blots cover the concentrations that resulted in impaired colony formation and anchorage independent growth of OVCAR3. This may indicate that reduced STAT3 activation does not fully explain the reduced growth observed in OVCAR3.

(3.2.4.2) Treatment with pacritinib reduces growth factor receptor activation in OvCa cell lines in vitro

In Section 3.2.2 we observed IRAK1 knockdown resulted in a reduction of HER4 expression in PE04, OAW42 and OVCAR4 cell lines which express this growth factor receptor. As a follow up to this, we wanted to assess if growth factor receptor signalling was impacted following treatment with pacritinib. Following treatment with pacritinib, we observed considerable reduction in growth factor receptor activation / phosphorylation in PE01 and PE04 cells (Fig. 3.10.1, 3.10.3) as well as in OAW42 and OVCAR3 cells (Fig. 3.10.2, 3.10.3)

Total protein expression of HER family members was not impacted in any cell line (Fig. 3.10.1, 3.10.2, 3.10.4). The HGSC PE01 cell line displayed reduced activation of EGFR (Tyr1068) following treatment with pacritinib. Interestingly the

paired cisplatin resistant PE04 cell line showed reduced activation of EGFR (Tyr1068), HER3 (n=2) (Y1289) and HER4 (Tyr1284). The HGSC OVCAR3 cell line showed reduced activation of EGFR (Tyr1068), HER3 (n=2) (Y1289) and HER4 (Tyr1284) while the OAW42 OvCa cell line displayed reduced EGFR (Tyr1068) and HER4 (Tyr1284) following treatment with pacritinib.

In section 3.2.2 we showed IRAK1 knockdown led to a significant reduction in total HER4 expression in PE04, OAW42 and OVCAR3 cell lines. It is therefore interesting that downstream of treatment with pacritinib we observed impaired HER4 activation in PE04, OAW42 and OVCAR3 cell lines. Due to observing considerable reductions in growth in these cell lines following both IRAK1 knockdown and treatment with pacritinib, these findings may indicate that HER4 plays a considerable role in the growth of these OvCa cell lines.

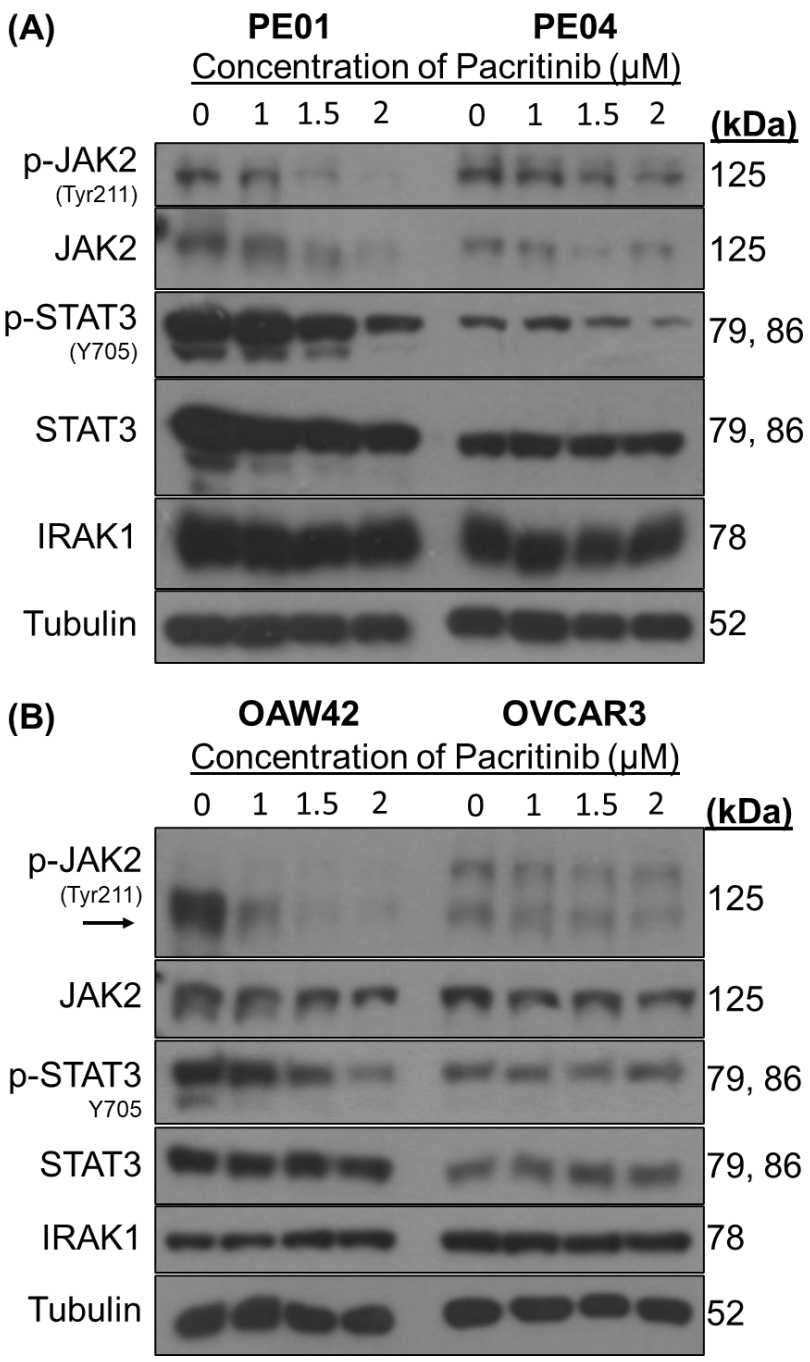

Figure 3.9.1: Pacritinib reduces the activation of JAK2 and STAT3 in Ovarian Cancer cell lines: Treatment with pacritinib resulted in reduced activation of JAK2 in **A-B)** PE01, PE04, OAW42 and OVCAR3 cells. Treatment with pacritinib resulted in reduced STAT3 activation in PE01, PE04 and OAW42 cells. Western Blots shown are representative of three independent experimental replicates.

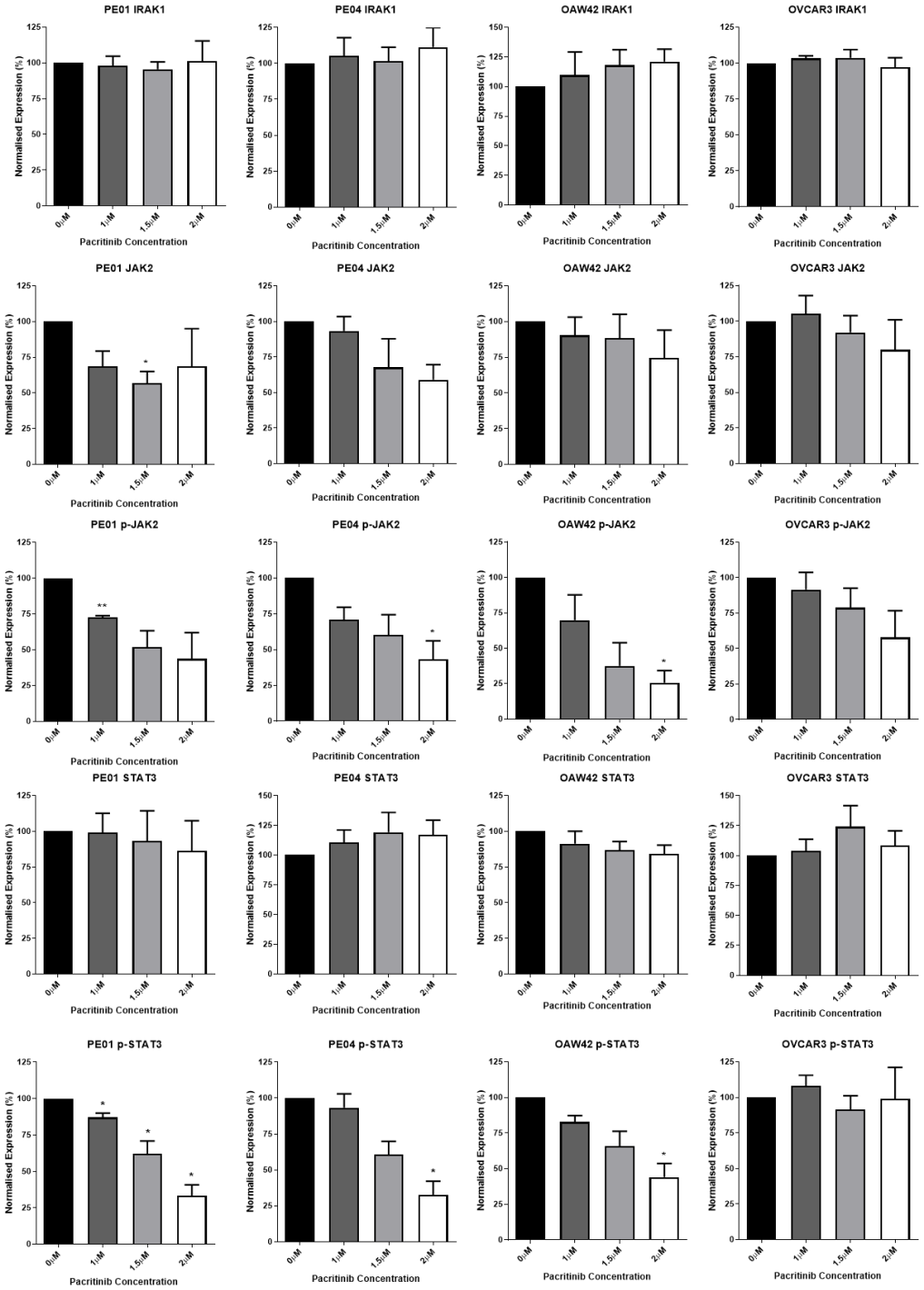

Figure 3.9.2: Treatment with Pacritinib results in reduced activation of the JAK2-STAT3 signalling pathway in ovarian cancer cell lines. Treatment with pacritinib resulted in reduced activation of JAK2 in **A-B)** PE01, PE04, OAW42 and OVCAR3 cells. Treatment with pacritinib resulted in reduced STAT3 activation in PE01, PE04 and OAW42 cells.. Statistical significance was assessed using paired students t-test comparing expression following treatment to expression in vehicle control. p-values; (*;≤0.05), (**;≤0.01), (***;≤0.001), (****;≤0.0001).

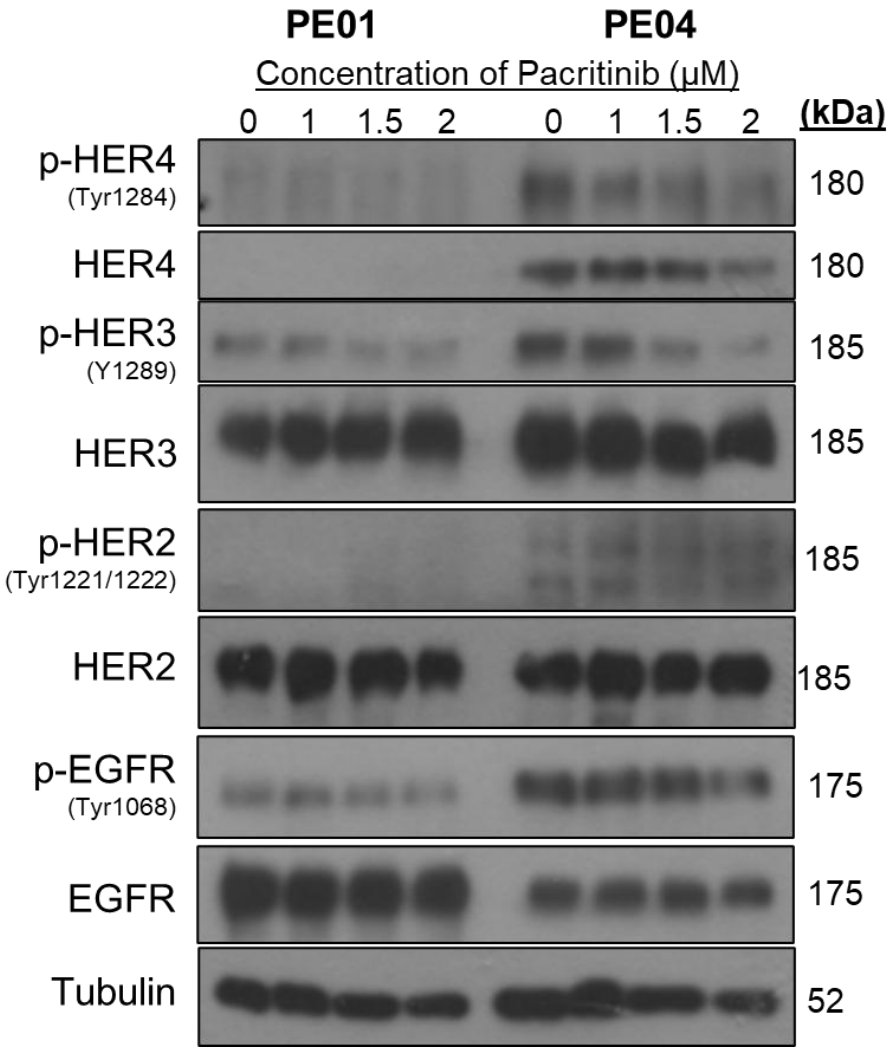

Figure 3.10.1: Pacritinib reduces growth factor receptor activation in PE01 and PE04 Ovarian Cancer cell lines. Treatment with Pacritinib resulted in reduced activation of EGFR in PE01 and reduced activation EGFR, HER3 and HER4 in PE04 cells. Results are representative of three independent experimental replicates for each cell line, with the exception of p-HER3 and HER3 which are representative of N=2.

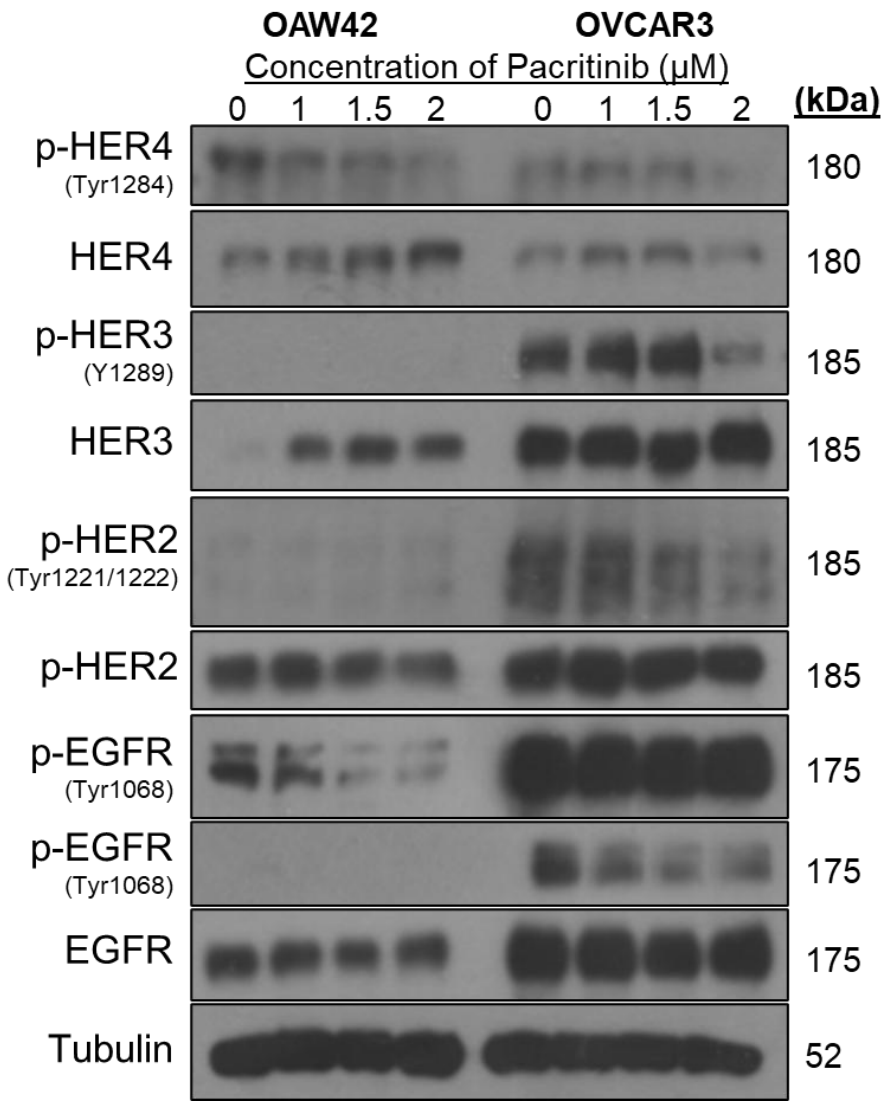

Figure 3.10.2: Pacritinib reduces growth factor receptor activation in OAW42 and OVCAR3 Ovarian Cancer cell lines. Treatment with pacritinib resulted in reduced activation of EGFR and HER4 in both OAW42 and OVCAR3 cells. Results are representative of three independent experimental replicates for each cell line, with the exception of p-HER3 and HER3 which are representative of N=2.

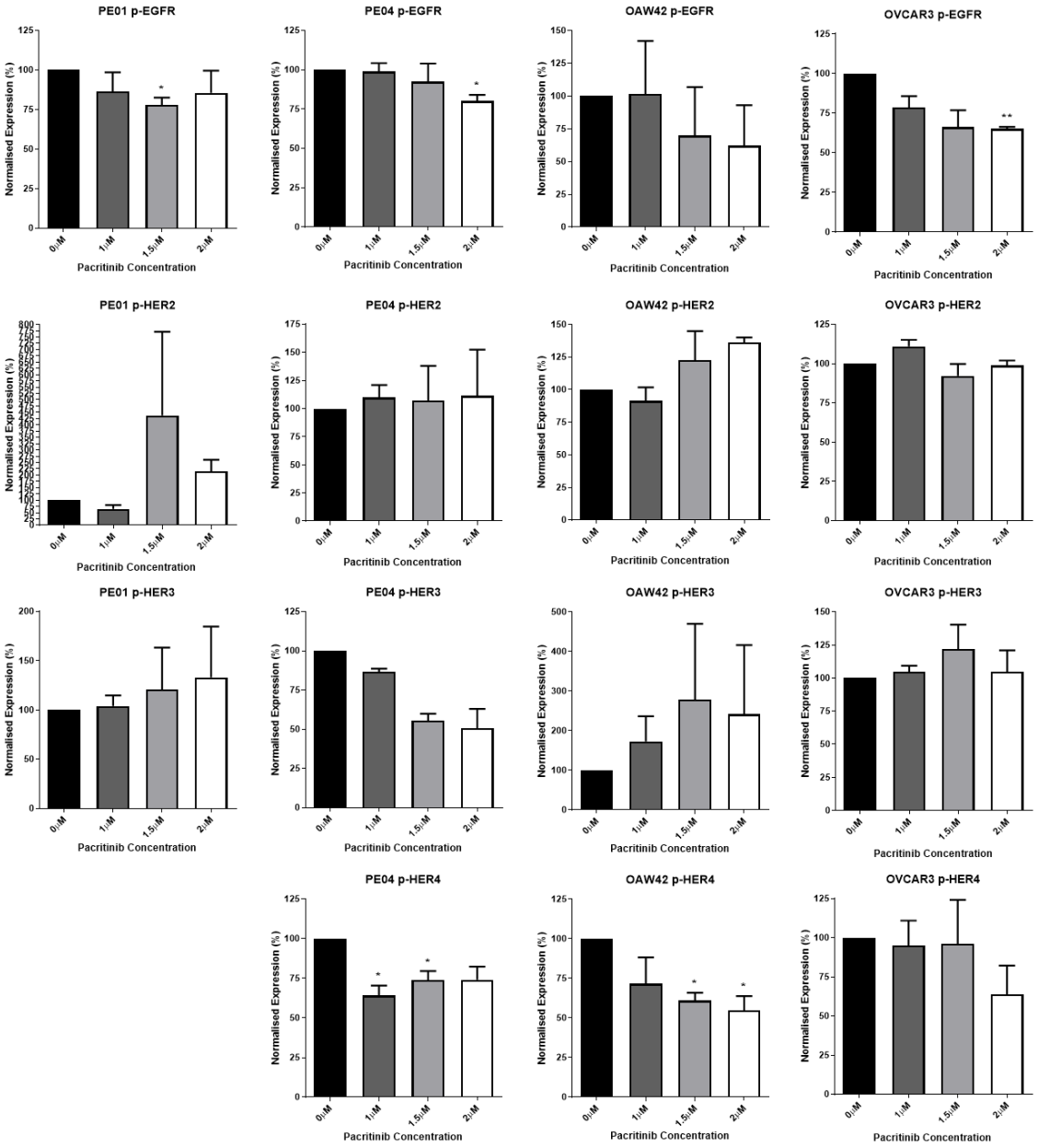

Figure 3.10.3: Treatment with Pacritinib results in reduced activation of HER family members in ovarian cancer cell lines. Treatment with pacritinib resulted I reduced activation of EGFR PE01, PE04, OAW42 and OVCAR3 cells as well as a reduction in activation of HER4 in PE04, OAW42 and OVCAR3 cells. Results shown are representative of three independent experimental replicates per cell line. Statistical significance was assessed using paired students t-test comparing expression following treatment to expression in vehicle control. p-values; (*;≤0.05), (**;≤0.01).

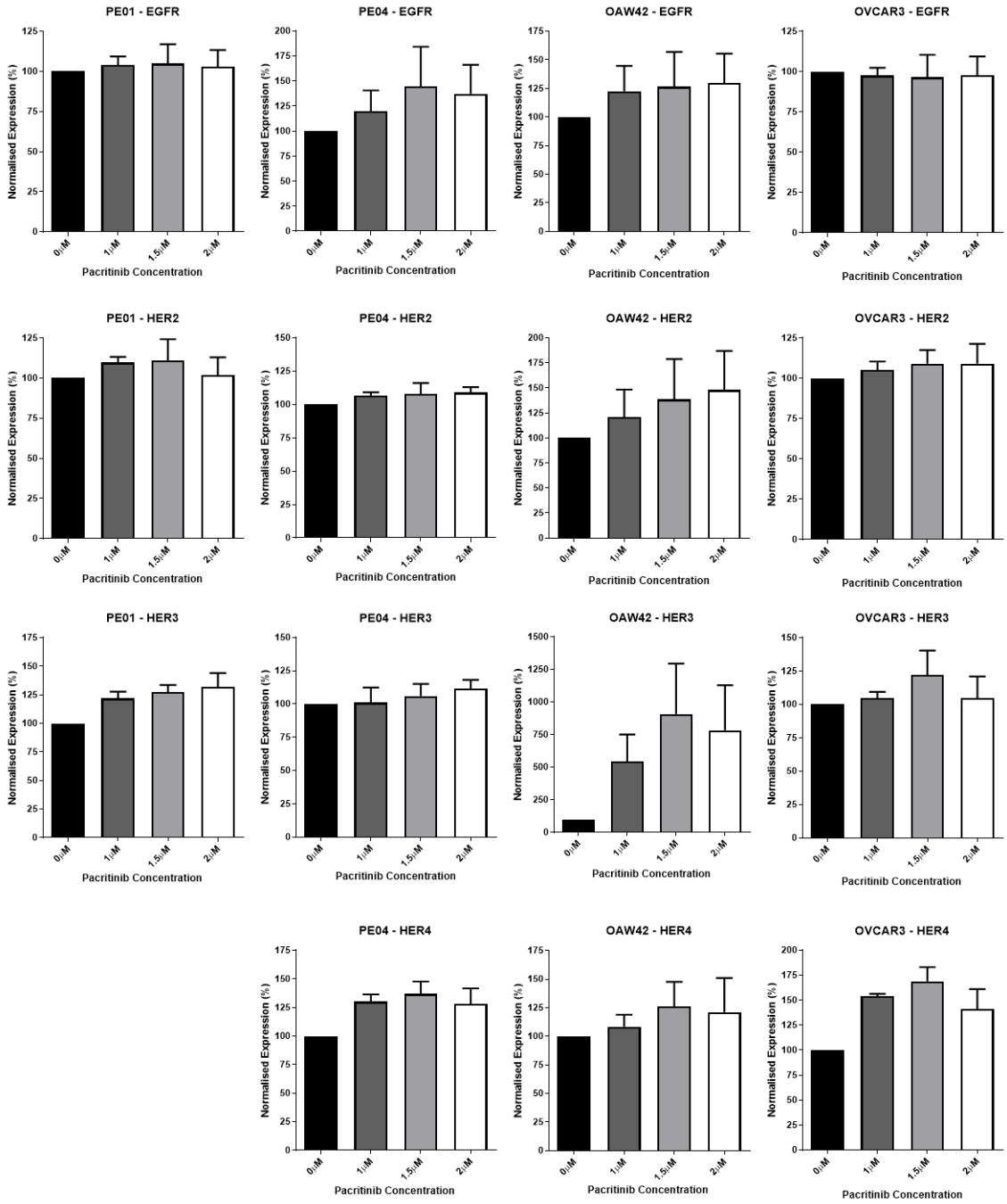

Figure 3.10.4: Treatment with Pacritinib does not reduce HER family levels in ovarian cancer cell lines. No significant difference was observed in HER family levels following treatment with pacritinib in PE01, PE04, OAW42 or OVCAR3 cells. Results shown are representative of three independent experimental replicates per cell line.

(3.2.5) Expression Analysis in Serous Ovarian Cancer

(3.2.5.1) STAT3 and IRAK1 expression and activation were profiled in patient derived xenograft lysates and parental OvCa cell lines

Patient Derived Xenograft (PDX) whole cell lysates were provided by Dr Denis Collins (DCU) and were used to profile the expression of STAT3 and IRAK1 along with their activation (Fig. 3.11.1, 3.11.2). High levels of IRAK1 and STAT3 expression were observed in most PDX samples. In all PDX whole cell lysates IRAK1 was observed to be hyperactivated by probing with p-IRAK1 (T209) targeted antibody. Interestingly PE04 shows numerically lower expression and activation of STAT3 compared to the paired PE01 cell line. In Section 3.2.4.1 we showed treatment with pacritinib impairs STAT3 activation in both PE01 and PE04 cells and results in significant reduced growth (Section 3.2.3) regardless of the difference in basal STAT3 activation.

(3.2.5.2) HER Family expression was profiled in PDX and parental OvCa cell lines

HER family protein expression was profiled using western blot analysis (Section 2.4) in OvCa PDX whole cell lysates and parental OvCa cell lines (Fig. 3.11.3, 3.11.4). HER4 and EGFR were observed to be expressed by the majority of PDX samples while HER3 and HER2 are expressed by three PDX samples each. PE04 and OVCAR3 both express all four HER family members while PE01 does not express detectable levels of HER4 and the OAW42 cell line does not express

detectable levels of HER3. These findings of HER4 expression in the PE01 and PE04 cell lines has previously been reported.[194]

mRNA expression analysis in serous OvCa

TNMplot is a publicly available database which was probed for the mRNA expression of several key targets in serous OvCa and normal controls using the RNA sequencing dataset (Section 2.7). This analysis shows that both IRAK1 and FLT3 mRNA expression are significantly increased in Serous OvCa compared to normal controls (Fig. 3.12.1). It is important to note here that FLT3 gene expression is very low in both serous OvCa and normal controls (Fig. 3.12.1). JAK2 gene expression is significantly decreased in serous OvCa compared to normal controls (Fig. 3.12.1).

We additionally examined mRNA expression of HER family members in serous OvCa and normal controls using TNMplot database (Fig 3.12.2). Gene expression shows that HER2, HER3 and HER4 are all significantly increased in serous OvCa compared to normal control while EGFR is significantly decreased in serous OvCa compared to normal controls. These findings indicate HER family members may play a prominent role in the progression of OvCa.

(3.2.5.3) High IRAK1 mRNA expression correlated with reduced OS in serous OvCa

The publicly available KM Plotter database was probed (Section 2.7) for IRAK1 mRNA expression (201587_s_at) using the JetSet best probe set, with outlier arrays excluded (Fig. 3.13.1). IRAK1 high mRNA expression was found to be a negative prognostic indicator in serous OvCa. The IRAK1 high mRNA expression cohort shows significantly reduced OS in serous OvCa and high stage (3+4) serous OvCa when compared to the IRAK1 low mRNA expression cohort.

(3.2.5.4) Immunohistochemical staining of IRAK1 shows increased IRAK1 expression in HGSC

We next wanted to assess the protein expression of IRAK1 in HGSC OvCa. In order to achieve this, we used immunohistochemistry (Section 2.6). IRAK1 protein expression was observed to be significantly higher in HGSC samples compared to normal adjacent tissue (Fig. 3.14.1). Additionally, IRAK1 protein expression was observed to be significantly higher in high-stage (3 + 4) HGSC (Fig. 3.14.2). This immunohistochemical work involved a collaboration with a histopathologist and IHC slides were assessed independently by his group. This led to the conclusion that background staining should be further optimised in order to confirm the findings of this work.

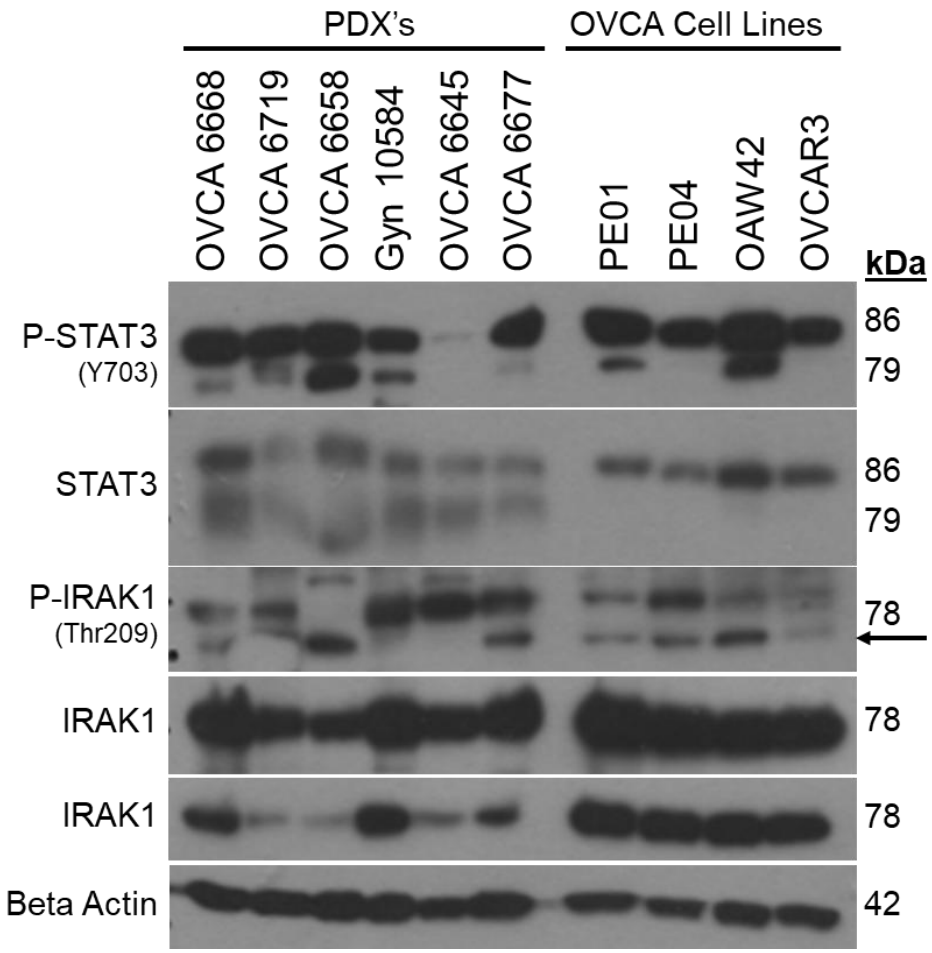

Figure 3.11.1: Expression of IRAK1 and STAT3 was profiled in Ovarian Cancer PDX and OvCa cell lines *in vitro*. A panel of six PDX samples display expression of IRAK1 and STAT3. STAT3 expression and activation was observed to be lower in cisplatin resistant PE04 compared to paired cisplatin sensitive PE01 cells. p-IRAK1 was achieved for N=1 while IRAK1, STAT3 and p-STAT3 were achieved for three independent experimental replicates.

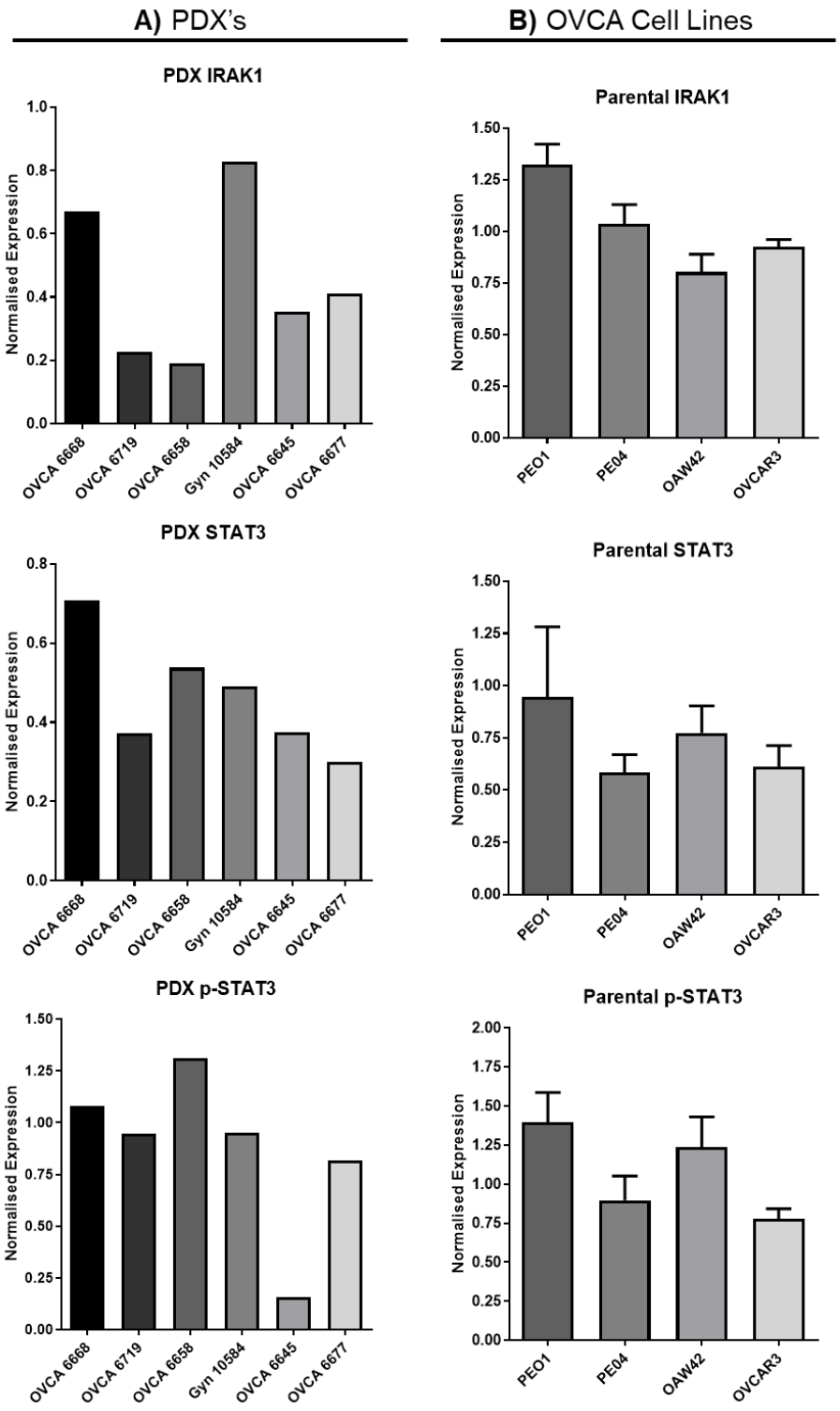

Figure 3.11.2: IRAK1, STAT3 and p-STAT3 were profiled in both PDX and parental OvCa cell lines. A panel of six PDX samples display expression of IRAK1 and STAT3. STAT3 expression and activation was observed to be lower in cisplatin resistant PE04 compared to paired cisplatin sensitive PE01 cells. Results are representative N=1 for **A)** PDX targets and representative of three independent experimental replicates for **B)** ovarian cancer cell line targets.

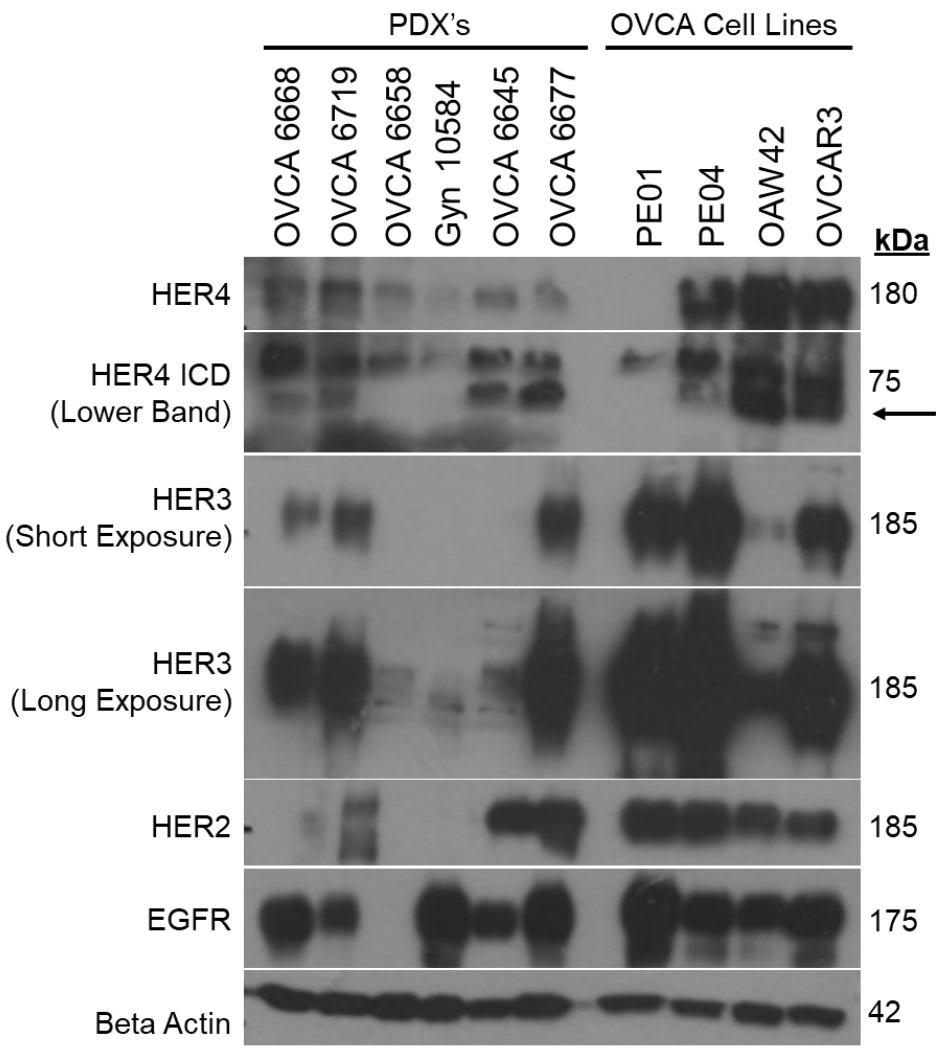

Figure 3.11.3: Expression of HER Family members was profiled in OvCa PDX and OvCa cell lines in vitro. A panel of six PDX samples display varying expression of HER family receptors EGFR, HER2, HER3 and HER4. For PDX samples each target is representative of N=1. For each Ovarian Cancer cell line western blots are representative of three independent experimental replicates.

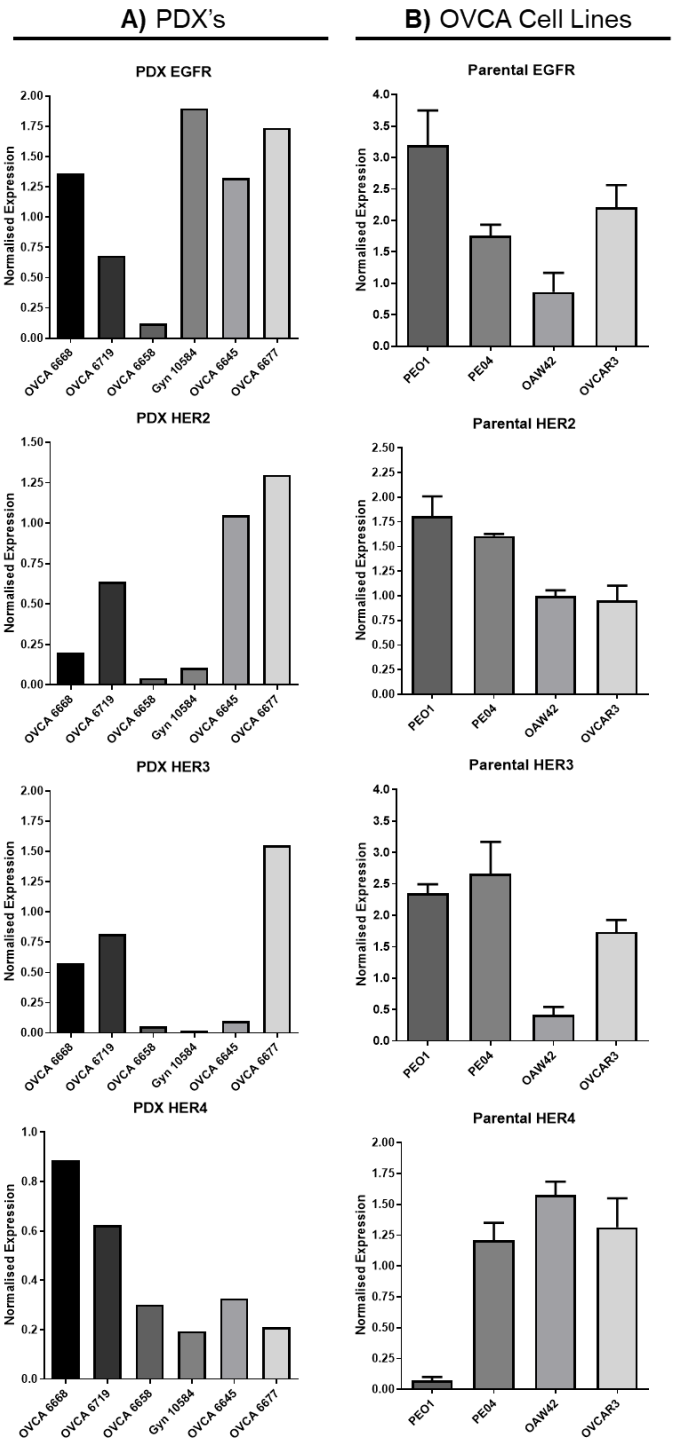

Figure 3.12.4: HER Family members were profiled in both ovarian cancer PDX and parental OvCa cell lines in vitro using western blot analysis. A panel of six PDX samples display varying expression of HER family receptors EGFR, HER2, HER3 and HER4. A) PDX results are representative of N=1. B) Parental ovarian cancer cell line results are representative of three independent experimental replicates.

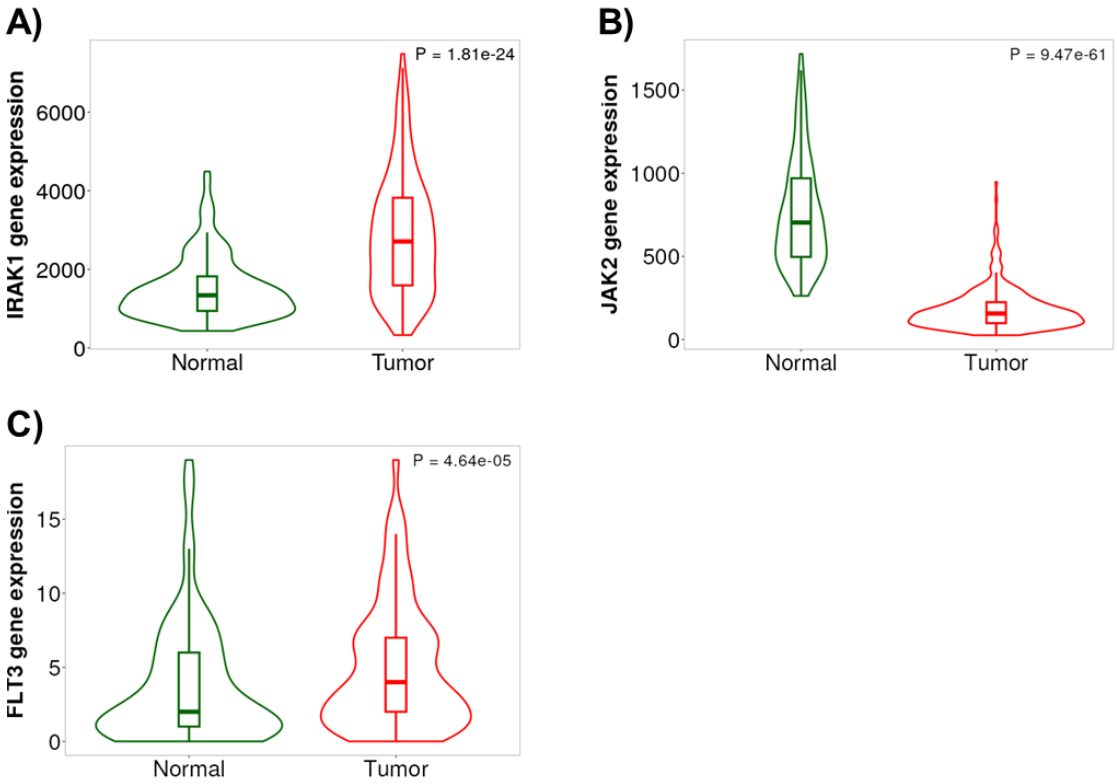

Figure 3.12.1: IRAK1 gene expression is significantly higher in serous OvCa samples compared to normal control. Gene expression for **A)** IRAK1, **B)**, JAK2 and **C)** FLT3 was visualised using the TNMplot database. Serous Ovarian Tumour Samples (374) show significantly increased expression in **A)** IRAK1 and significant decrease in **B)** JAK2 compared to normal controls (133). Gene expression of **C)** FLT3 is very low in both normal and serous ovarian cancer samples.[267]

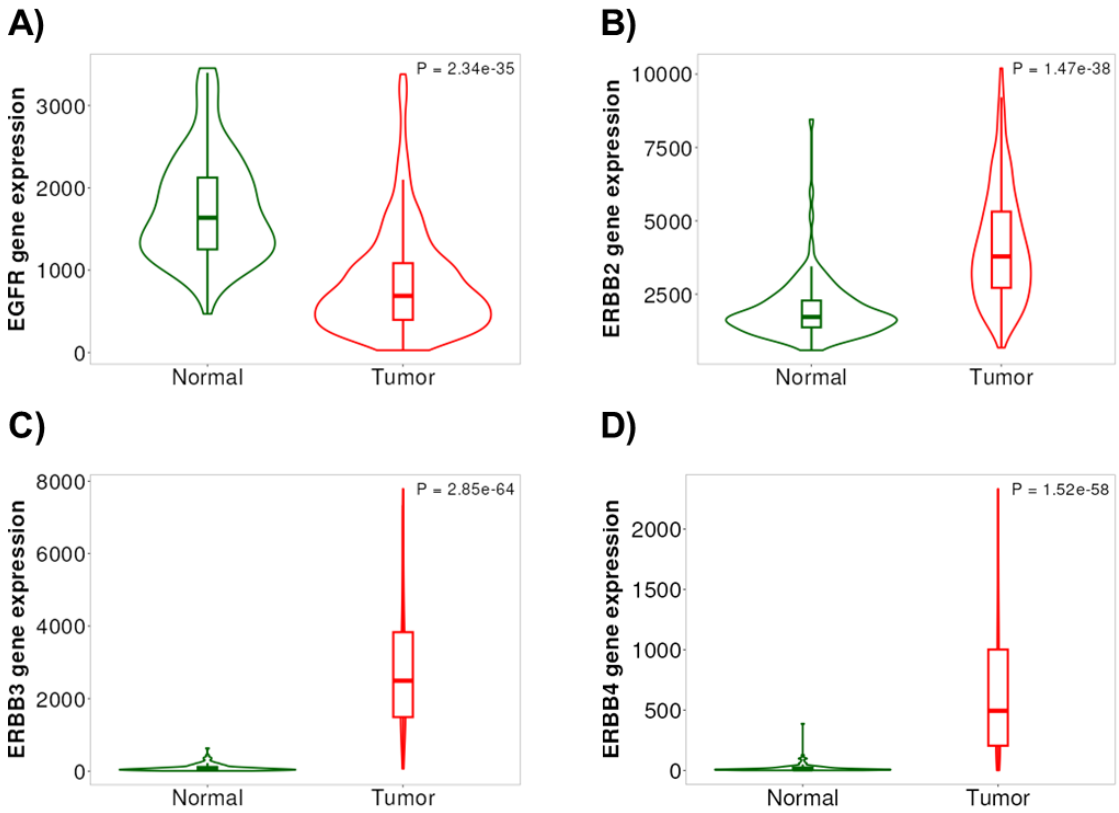

Figure 3.12.2: Gene expression levels of HER family members differ between serous OvCa samples compared to normal controls. Gene expression for **A)** EGFR, **B)**, ERBB2, **C)** ERBB3 and **D)** ERBB4 was visualised using the TNMplot database. Serous Ovarian Tumour Samples (374) show significantly increased expression in **B)** ERBB2, **C)** ERBB3, **D)** ERBB4 and significant decrease in **A)** EGFR compared to normal controls from non-cancerous patients (133).[267]

Table 3.2.2: Summary of gene expression analysis observed for IRAK1, JAK2, FLT3, EGFR, ERBB2, ERBB3 and ERBB4 using TNMplot database displayed in Figure 3.12.1 and Figure 3.12.2.[267]

Target	Mann Whitney P value	Fold Change Mean (Tumour vs Normal)	Fold Change Median (Tumour vs Normal)
IRAK1	1.81e-24	2.20	2.11
JAK2	9.47e-61	0.22	0.22
FLT3	4.64e-05	1.5	2.25
EGFR	2.34e-35	0.5	0.42
ERBB2	1.47e-38	2.97	2.29
ERBB3	2.85e-64	35.01	42.48
ERBB4	1.52e-58	35.85	47.64

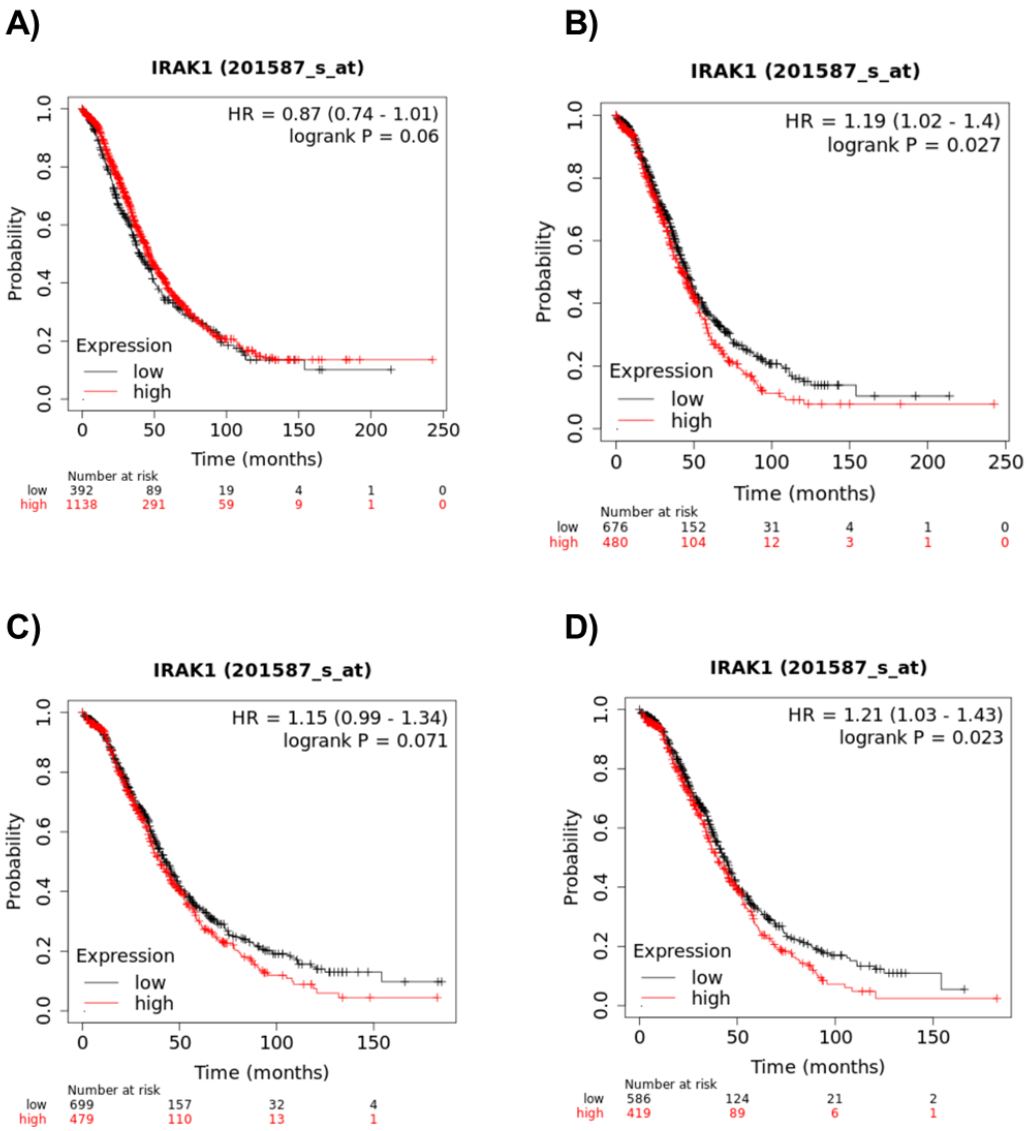

Figure 3.13.1: High IRAK1 mRNA expression correlates with reduced overall survival in serous ovarian cancer cohort. The JetSet best probe set (201587_s_at) for IRAK1 was probed for overall survival (OS) with outlier arrays excluded. IRAK1 mRNA expression was found to display no correlation with overall survival in **A)** ovarian cancer or **C)** high stage (3+4) ovarian cancer. However, the high IRAK1 mRNA expressing cohort shows significantly reduced overall survival in **B)** serous ovarian cancer and **D)** high stage (3+4) serous ovarian cancer.

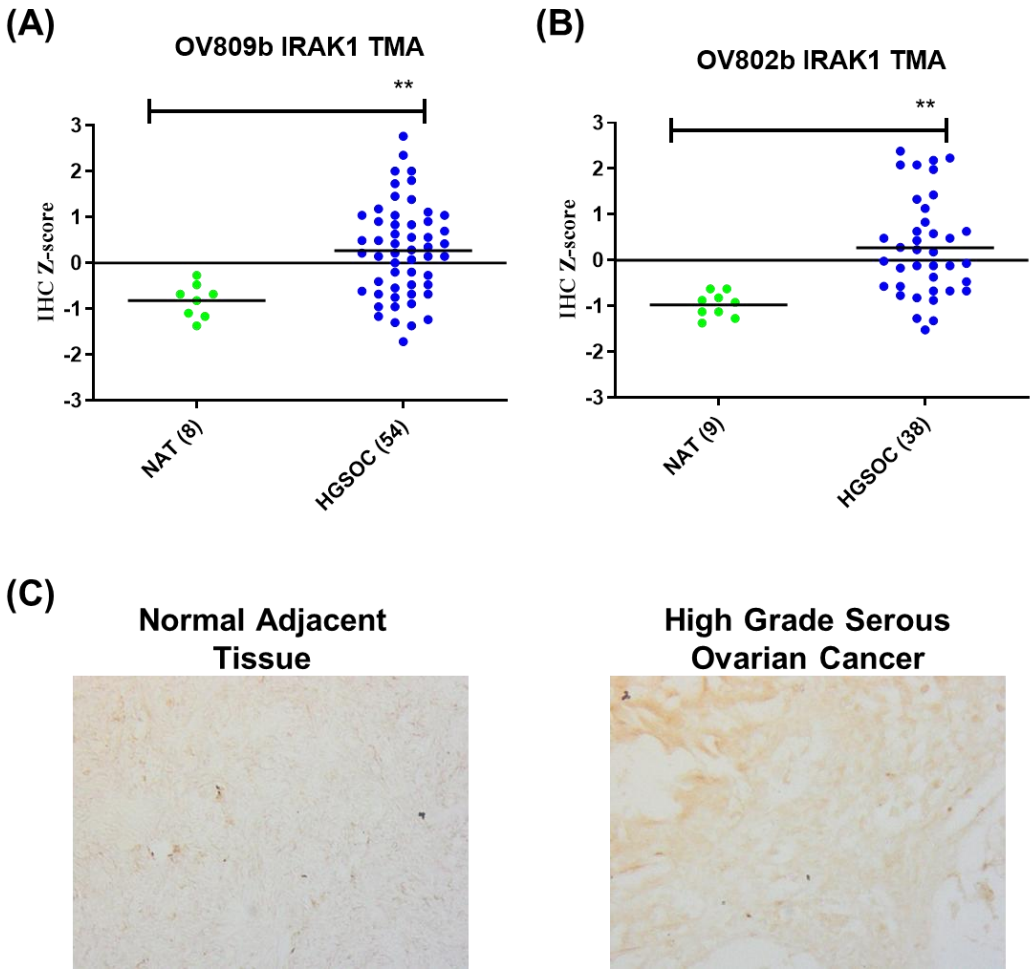

Figure 3.14.1: IRAK1 protein expression is significantly increased in High Grade Serous Ovarian Cancer (HGSOC) compared to normal adjacent tissue controls. Immunohistochemical staining for IRAK1 (SC-5288) showed increased IRAK1 protein expression in HGSOC samples compared to normal controls for tissue micro arrays **A)** OV809B and **B)** OV802B. **C)** Representative images were captured at 20X magnification and optical density was obtained using Image J. Optical density was then normalised to Z-scores. Outliers (greater than two standard deviations above the mean) were removed and statistical significance was investigated using unpaired t-tests. P-values; (*;≤0.05), (**;≤0.01). Both **A)** OV809B and **B)** OV802B show higher IRAK1 staining in HGSOC compared to NAT.

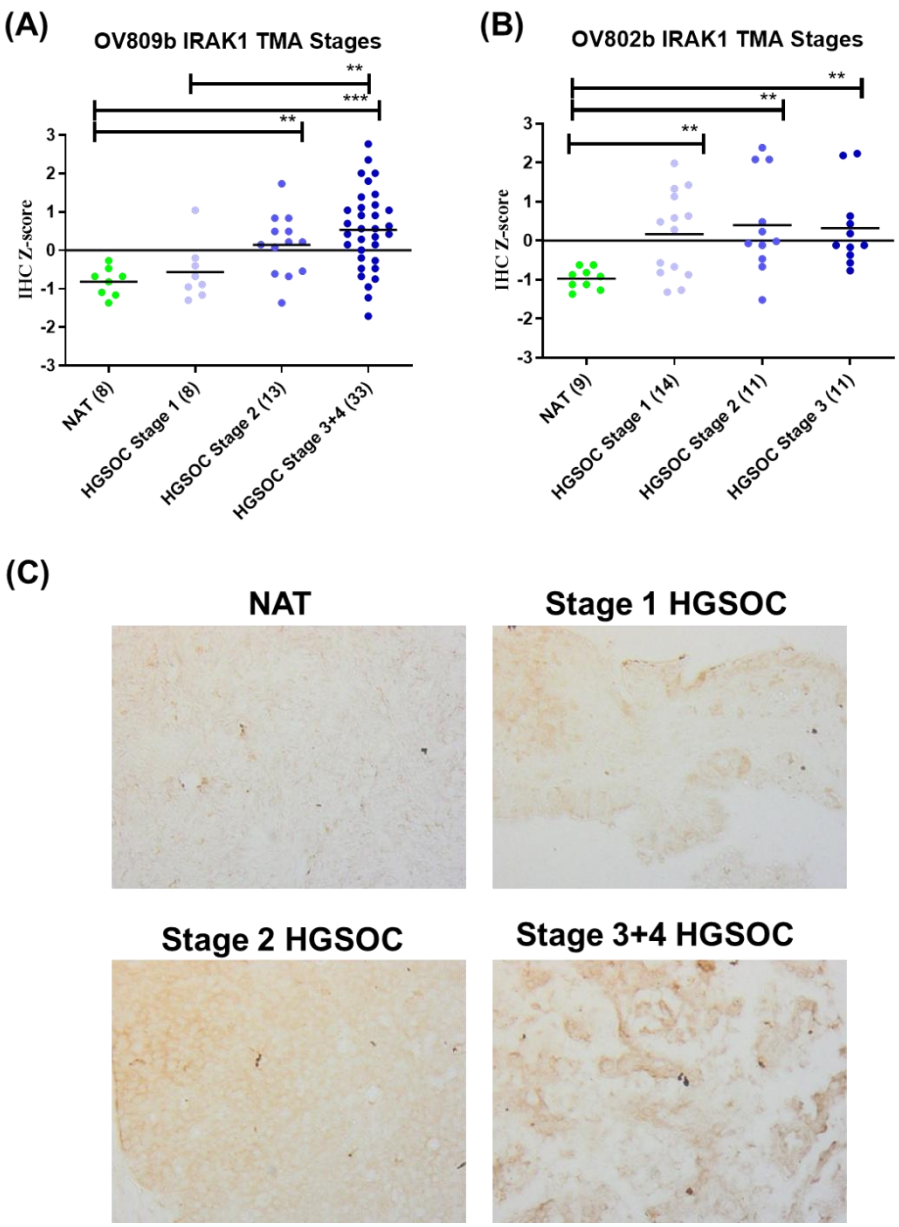

Figure 3.14.2: IRAK1 protein expression is significantly higher in high stage high grade serous carcinoma (HGSOC). Immunohistochemical staining for IRAK1 (SC-5288) showed increased IRAK1 protein expression at all stages in HGSOC samples compared to normal controls for tissue micro arrays **A)** OV809B and **B)** OV802B. **C)** Representative images were captured at 20X magnification and optical density was obtained using Image J. Optical density was then normalised to Z-scores. Outliers (greater than two standard deviations above the mean) were removed and statistical significance was investigated using unpaired t-tests. P-values; (*;≤0.05), (**;≤0.01), (***;≤0.001). **A)** OV809B shows higher IRAK1 expression in stage 3+4 HGSOC compared to both NAT and stage 1 HGSOC. **B)** OV802B shows increase IRAK1 protein expression in all HGSOC stages compared to NAT.

(3.3) Discussion

HGSC represents the most clinically relevant subtype of OvCa accounting for approximately 70% of all detections and disproportionately, between 70% and 80% of all OvCa deaths.[268] It is clear that novel therapeutic targets and strategies are required to improve outcomes for patients with HGSC. Over recent decades important roles have been observed for IRAK1, primarily through overexpression and hyperactivation, in several cancer subtypes including leukaemia's, lymphomas, pancreatic cancer and triple negative breast cancer.[65, 67, 87, 88]

Using IRAK1 knockdown models in OvCa we set out to evaluate if IRAK1 represents a novel therapeutic target in OvCa. We further evaluated if treatment with pacritinib may represent a novel therapeutic strategy in OvCa cells targeting IRAK1, JAK2 and FLT3.

(3.3.1) IRAK1 knockdown and Treatment with Pacritinib Significantly Impairs Growth of Ovarian Cancer Cell Lines.

Using an IRAK1 knockdown approach we further assessed the role that IRAK1 plays on the growth of OvCa cell lines *in vitro*. Following IRAK1 knockdown we observed significantly reduced growth in OvCa cell lines *in vitro* using several quantitative measurements of growth (Section 3.2.1). IRAK1 knockdown cell lines were shown to have reduced proliferation, colony formation, migration and invasion, 3D anchorage independent growth and spheroid formation compared to their control counterparts (Section 3.2.1). This inverse relationship between IRAK1 expression and growth indicates that IRAK1 plays a prominent positive role in promoting growth of OvCa cell lines *in vitro*. Additionally, this also indicates that the five OvCa cell lines

(PE01, PE04, OAW42, OVCAR3 and IGROV1) assessed display a dependency on IRAK1 expression for *in vitro* growth.

IRAK1 knockdown has been used to show a role for IRAK1 in the growth of several cancer types. In HCC IRAK1 knockdown led to reduced proliferation, invasion and migration.[269] In TNBC the knockdown of IRAK1 led to reduced growth using an in vivo xenograft model.[270] IRAK1 knockdown in the HGSC A1847 cell line was shown to significantly reduce colony size and number and reduced tumour forming ability in xenograft murine models.[135]

The five cell lines used for this work cover a diverse range of characteristics including histology, molecular status and prior treatment exposures. PE01, PE04 and OVCAR3 were derived from patients with HGSC while OAW42 was derived from a low-grade serous patient while IGROV1 has been used to model non-serous. PE01 is BRCA2 mutant while PE04 is BRCA2 wild type. PE01 and PE04 were derived from the same patient at different stages of treatment and can be used to model cisplatin sensitivity and resistance respectively, *in vitro.*[271] IRAK1 depletion led to the significant impairment of growth in all five of these OvCa cell lines regardless of any differences.

These findings support the hypothesis that IRAK1 is a potential therapeutic target in OvCa and plays a positive role in promoting the growth of OvCa Cells. This provides the foundation to evaluate the efficacy of therapeutic strategies targeting IRAK1 in OvCa. IRAK1 has been shown to be a promising therapeutic target in several cancers.[97,98,101,102,106,272] TCS2210, a novel IRAK1 inhibitor inhibits growth of EOC cell lines, increasing apoptosis and synergised with cisplatin.[135]

We selected the IRAK1 kinase inhibitor pacritinib due to its previous success and FDA approval for the treatment of myelofibrosis[149], promising studies showing efficacy in solid cancers including breast cancer[101], nasopharyngeal carcinoma[108] and

NSCLC.[142] Using this approach we aimed to improve our bench to bedside research and encourage the further development of pacritinib as a therapeutic strategy in OvCa.

In addition to targeting IRAK1, pacritinib also inhibits the kinase activity of both JAK2, at nano-molar concentrations. In a study of Medulloblastoma, pacritinib impaired *in vitro* and *in vivo* growth which this group attributed to inhibition of JAK2-STAT3.[117] In OvCa, the JAK2-STAT3 has been highlighted as playing a positive role in the progression[169], and JAK2-STAT3 were observed to be significantly more activated in HGSC samples compared to normal controls.[170]

These studies provide a good indication that the JAK2-STAT3 signalling pathway represents a potential therapeutic target in OvCa. These findings may further support the potential of pacritinib as a therapeutic target in OvCa which can target JAK2-STAT3 and IRAK1.

Using a series of *in vitro* growth assays we have shown that treatment with Pacritinib results in impaired growth of OvCa cell lines at low micro-molar concentrations. Following treatment with pacritinib we observed reduced colony formation, survival, 3D viability / growth, 3D spheroid formation and anchorage independent growth (Section 3.2.3). Similarly to our observations following knockdown of IRAK1, these impacts on OvCa cell line growth *in vitro* appear to be independent of any phenotypical, morphological or molecular differences between these cell lines examined. These promising findings support the potential application of using IRAK1 inhibitors in the treatment of OvCa.

These findings support the hypothesis that pacritinib is capable of significantly impairing growth of OvCa cell lines in vitro. Furthermore, these findings indicate that pacritinib may represent a novel therapeutic strategy in OvCa. Further evaluations including *in vivo* studies are required in order to further investigate this.

(3.3.2) IRAK1 Knockdown and Treatment with Pacritinib Results in Reduced Growth Factor Receptor Activity in Ovarian Cancer Cell Lines.

HER family receptors play important roles in physiology and in cancer progression where they have been observed to regulate several critical pathways and processes including activation of proliferation, differentiation, survival as well as adhesion and migration.[180] Using Western blot analysis, we profiled the expression of HER family members following IRAK1 knockdown and treatment with pacritinib (Section 3.2.2). We observed no reduction in EGFR, HER2 or HER3 following IRAK1 knockdown. PE04, OVCAR3 and OAW42 all express HER4 and following IRAK1 knockdown we observed reduced expression of total HER4 levels (Section 3.2.2). In the PE04 cell line the 80kDa fragment of HER4 was detectable in two independent experimental replicates where it was observed to be decreased following knockdown of IRAK1 (Section 3.3.2).

HER4 has been shown to play pathogenic roles in numerous cancers including breast cancer[209], colorectal cancer[208] and OvCa.[210] In OvCa HER4 has been observed to be detected in high frequency (89-95%) of serous cystadenocarcinoma.[186] It has also been shown that HER4 protein is elevated in serous OvCa compared to normal controls.[211] Finally higher HER4 expression has been associated with reduced overall survival in OvCa.[211] These findings provide a strong indication that HER4 plays an important role in the progression of OvCa.

HER4 knockdown led to inhibited proliferation and increased apoptosis in colorectal cancer cells.[208] These findings could provide an indication that reduced HER4 expression in IRAK1 knockdown cells is contributing to the reduced growth observed in OvCa cells (Section 3.2.1). This remains unclear and the role of HER4 in the growth of OvCa cell lines required further evaluation. Furthermore, the link

between HER4 and IRAK1 remains unclear to the best of my knowledge and warrants further investigation to unravel the molecular mechanisms underlying the results we observed.

One study from 2013 showed that the overexpression of HER4 CYT-1 isoform (which contains a PI3K binding domain) stimulated anchorage independent growth in the HGSC OVCAR3 cell line.[210] It was further shown that this increased anchorage independent growth could be blocked by either HER4 or PI3K inhibition.[210] These findings provide further support that reduced HER4 total protein levels following IRAK1 knockdown are contributing to the reduced growth observed in PE04, OVCAR3 and OAW42 knockdown cell lines. Currently the molecular mechanisms underlying this novel link between IRAK1 and HER4 expression remains unclear and warrants further investigation.

Future studies should investigate the potential regulation of HER4 expression by IRAK1. This could be further elaborated on by investigating if mRNA expression of HER4 is also reduced and this may give insight if IRAK1 is involved in transcriptional or post-translational regulation of HER4. It should also be considered that other pathways may mediate this association. Performing global and may provide an approach to further investigate this novel association. Finally, phospho-proteomics may allow us to understand any post-translational regulation that may link IRAK1 and HER4. These studies would allow us to potentially form a hypothesis about how IRAK1 and HER4 may be linked.

The HGSC PE01 cell line does not express HER4 at levels which are detectable by Western blot analysis with increased HER4 expression in the paired PE04 cell line first being reported in a 2001 study.[194] It is reasonable to assume that there is another molecular mechanism underlying the reduced growth observed in PE01 cells following knockdown of IRAK1. For this reason, we must remain open to

the potential that this mechanism which has yet to be found in PE01 is common among all OvCa cell lines in this study.

Treatment with pacritinib resulted in reduced colony formation, 3D viability, 3D anchorage independent growth and spheroid formation in PE01, PE04, OAW42 and OVCAR3 cell lines (Section 3.2.3). Using Western blot analysis, we observed a cell line dependent impaired activation of HER family members following treatment with pacritinib. Total EGFR, HER2, HER3 and HER4 were profiled and showed no significant decrease following treatment with pacritinib (Section 3.2.4). EGFR showed significantly reduced activation in all PE01, PE04, and OVCAR3 cell lines and numeric reduction in OAW42. HER3 activation was numerically reduced PE04 cells while HER4 activation was significantly reduced in HER4 expressing PE04 and OAW42 cell lines with numeric reduction in OVCAR3 (Section 3.2.4). While the extent to which reduced activation of each growth factor receptor plays in each cell lines remain unclear, HER family receptors have been shown to play significant roles in OvCa.

It has previously been shown that treatment with the pan-HER inhibitor Poziotinib resulted in decreased proliferation and viability, induced G1 cell cycle arrest and apoptosis while inhibiting spheroid formation and stemness of OvCa stem cells.[195] The inhibition of HER4 was observed to lead to reduced activation of STAT5, AKT and ERK in OvCa stem cells.[195] Inhibition of HER4 in CYT-1 overexpressing OVCAR3 cells has been shown to reduce anchorage independent growth.[210]

Treatment with an EGFR TKI (ZD1839) displayed efficacious reduction of tumour growth *in vivo* using a PE04 xenograft model.[196] These studies provide a strong indication of the potential therapeutic benefit which could be achieved through using pacritinib to target HER family receptor activity in OvCa. While we didn't observe any significant decrease in HER2 activation following treatment with pacritinib, HER2 (bands were too challenging for Image J) targeted inhibition using

Pertuzumab has been shown to inhibit growth in HRG1β and TGFα stimulated PE01 and PE04 cells.[202] The HER3 targeted seribantumab has previously failed to improve progression free survival in platinum-resistant or refractory OvCa during a phase two clinical trial.[205] These studies indicate that further work is required in order to evaluate the efficacy of HER family targeted therapies in OvCa.

A study from 2008 has shown HER2, HER3 and HER4 protein and median gene expression is increased in OvCa while EGFR protein expression was observed to be decreased.[189] Probing the TNMplot database we observed similar findings for serous OvCa. HER2, HER3 and HER3 gene expression were all observed to be elevated in serous OvCa compared to normal controls while EGFR gene expression was observed to be decreased. These findings indicate HER family receptors may play an important role in the growth of OvCa.

(3.3.3) The role of JAK2, STAT3 and FLT3 in the Activity of Pacritinib

Pacritinib has been used in several studies to investigate the potential of targeting the JAK2-STAT3 signalling pathway in cancer. These studies indicate that the JAK2-STAT3 signalling pathway may represent a potential therapeutic target. As such we must consider the role the inhibiting this pathway has on OvCa cells downstream of treatment with pacritinib.

Nuclear activation of JAK2 has been observed in 83% of EOC samples while nuclear activation of STAT3 was observed in 28% of EOC samples.[169] It was further observed that increased activation of STAT3 was associated with reduced OS and PFS in EOC.[169] The inhibition of the JAK2-STAT3 signalling pathway has shown considerable therapeutic value in OvCa as it induced paclitaxel sensitivity in HGSC

stem cell like cells[166] and cisplatin sensitivity in ALKBH5-HOXA10 overexpressing OvCa cell lines.[171]

We have shown that at low micromolar concentrations treatment with pacritinib results in significantly reduced activation of JAK2 in PE01, PE04 and OAW42 and with numeric reduction in OVCAR3 cells (Section 3.2.4) at similar concentrations which resulted in significant reduction in growth *in vitro* (Section 3.2.3). We further observed reduced activation of STAT3 in PE01, PE04 and OAW42 at similar micromolar concentrations which resulted in reduced growth of cells *in vitro* (Section 3.2.3).

We are not the first group to show reduced activation of STAT3 in OvCa following treatment with pacritinib. Another study looking at pacritinib in patient derived GBM brain tumour initiating cells showed reduced activation of STAT3 at similar concentrations to those used in our experiments.[119] This group further showed that at higher concentrations pacritinib impaired AKT (S473) and ERK1/2 MAPK activation. These findings may indicate that pacritinib displays dose dependent activity in cancer cell lines and may explain the lack of OVCAR3 reduced STAT3 activation which could be a result of dose dependent activity of pacritinib in different cell lines.

Interestingly a link between IRAK1 inhibition and reduced STAT3 activity has also been made.[145] Following IRAK1 knockdown in OvCa, cell line markers of stemness including STAT3 (NOTCH1, NOTCH3, p38 and p65) was observed to be reduced both in the presence and absence of hyaluronic acid stimulation.[145] It was further shown that the IRAK1 kinase inhibitor TCS2210 resulted in reduced activation of STAT3 in OvCa cells.[145]

Probing TNMplot database we observed relatively low levels of gene expression of FLT3 in both serous OvCa and normal controls (Section 3.2.5). These

findings may indicate that the reduced growth observed in OvCa cell lines following treatment with pacritinib, may not be attributed to inhibition of FLT3. The expression of FLT3 should be assessed in each cell line using Western blot analysis in order to further investigate this. In pancreatic ductal adenocarcinoma[177] and breast cancer[172] FLT3 has been observed to be a favourable prognostic indicator. The role of FLT3 may be cancer specific as it has previously been observed that FLT3, EGFR, LEPR expression and STAT3 activation are increased in HGSC patients with metastasis.[178]

(3.3.4) IRAK1 mRNA and Protein is Expressed at Higher Levels in Serous Ovarian Cancer Compared to Normal Controls.

IRAK1 has previously been identified to be one of seventeen genes differentially expressed in OvCa where it was observed to be upregulated compared to normal controls.[134] Using the publicly available database TNMplot we have confirmed and further expanded on these findings showing that IRAK1 gene expression is significantly higher in serous OvCa compared to normal controls (Section 3.2.5). Further evaluating the expression of IRAK1 we next probed the publicly available KM Plotter database. Here we observed that in serous OvCa the IRAK1 high mRNA expression cohort showed significantly reduced overall survival compared to the low IRAK1 mRNA expression cohort (Section 3.2.5). These findings provide a strong indication that IRAK1 plays a prominent role in the progression of serous OvCa and may represent a negative prognostic indicator.

Using immunohistochemistry, we evaluated the expression of IRAK1 protein levels in a tissue microarray of HGSC tissue (86) and (18) of normal adjacent ovarian tissue (Section 3.2.5). We found that IRAK1 protein levels were increased in HGSC compared to normal adjacent tissue. Given the high levels of background staining

these findings need to be validated following further optimisation of IRAK1 immunohistochemistry to confirm the observations made.

A pan-cancer analysis of IRAK1 had observed upregulation in more than twenty cancer types compared to normal tissue.[273] It was further observed that increased IRAK1 expression is associated with poor prognosis.[273] In hepatocellular carcinoma (HCC), higher IRAK1 mRNA and protein expression have been shown to correlate with advanced stages of disease and poorer patient survival.[274] In breast cancer higher expression of IRAK1 both has been associated with a shorter survival period.[275] In MDS higher IRAK1 expression has been associated with reduced overall survival.[157]

Since we have conducted this work another publication has been released investigating the role of IRAK1 in Ovarian Cancer.[145] This group observed IRAK1 mRNA expression was significantly higher in EOC compared to normal tissue (NCBI GEO Database). Using the TCGA dataset this group observed the IRAK1 high mRNA expression cohort displays significantly reduced OvCa dataset. Our findings confirm both of these findings in serous OvCa (Section 3.2.5). It was additionally shown by this group that IRAK1 mRNA was significantly upregulated in carboplatin resistant tumour tissue compared to sensitive tissue in OvCa patients. Finally, this group observed significantly increased IRAK1 protein levels in patients with high stage (3 + 4) HGSC compared to matched normal fallopian tube controls. Combined with our own observations (Section 3.2.5) these findings[145] provide a strong indication that IRAK1 plays an important role in the progression of OvCa and may represent a potential negative prognostic indicator,

(3.4) Concluding Remarks

We began by addressing objective 1 of this thesis to determine whether IRAK1 knockdown impairs the growth of OvCa cell lines *in vitro*. Using *in vitro* growth assays, we have shown that IRAK1 knockdown significantly reduced growth of OvCa cell lines. Our findings provide evidence that IRAK1 plays a role in promoting the proliferation, colony formation, migration and invasion and anchorage independent growth of OvCa cell lines *in vitro*. This study indicates an IRAK1 dependency in these cell lines.

Our findings further led to the discovery of a novel association between IRAK1 and HER4 expression. HER4 expressing cell lines were observed to have reduced levels of total HER4 following IRAK1 knockdown. The mechanisms underlying this association between IRAK1 and HER4 is novel and remain unclear. This novel association warrants further investigation.

Our second objective was to assess the efficacy of pacritinib on the growth of OvCa cell lines *in vitro*. Our research indicates IRAK1 represents a negative prognostic indicator in serous OvCa. Probing publicly available databases we have shown that IRAK1 mRNA expression is significantly increased in serous OvCa and that the IRAK1 high mRNA expression cohort displays reduced OS compared to the low expression cohort. The final objective of this chapter involved evaluating IRAK1 expression in serous OvCa. Furthermore, preliminary investigations led to the observation IRAK1 protein expression was increased in HGSC, however further optimisation and validation is required to confirm these findings.

As highlighted novel therapeutic strategies are urgently required to improve outcomes for patients with OvCa. We have shown that an IRAK1-JAK2-FLT3 inhibitor (pacritinib) displays significant efficacy in reducing growth of OvCa cell lines. Treatment with pacritinib resulted in reduced colony formation, 3D growth/viability and

anchorage independent growth of OvCa cells *in vitro*. Furthermore, we found that treatment with pacritinib resulted in reduced activation of growth factor receptor activation and JAK2/STAT3 activation in OvCa cell lines. These findings indicate that pacritinib may represent a novel therapeutic strategy in OvCa targeting IRAK1 and JAK2-STAT3.

(3.5) Future Directions

The link between IRAK1 knockdown and HER4 expression is a novel finding which has yet to be described in the literature to the best of my knowledge. Additional experiments are required to further investigate the interactions and signalling pathways mediating this novel relationship. The reduced activation of HER family members observed following treatment with pacritinib in OvCa cell lines may indicate an important link between IRAK1 kinase activity and HER family signalling, however this association remains less clear due to the fact that pacritinib additionally targets JAK2 and FLT3.

The molecular mechanisms underlying IRAK1 knockdown and HER4 expression is a novel association not yet explored in scientific literature to the best of my knowledge. It would be interesting to examine using real time PCR if this reduction in HER4 protein expression is mirrored in mRNA expression. This may allow for further conclusions to be made as to if IRAK1 is involved in the transcriptional or post translational regulation of HER4. Performing both global proteomics and phospho-proteomics would also further allow for the identification of potential pathways which may link this novel interaction.

Additionally, IRAK1 specific inhibitors should be assessed to investigate the specific role of IRAK1 kinase inhibition in impairing HER family activation *in vitro*. In a similar manner the investigation of JAK2 and FLT3 specific kinase inhibitors may lead to further clarity and better our understanding of the roles of these kinases in OvCa. Evaluating HER family activation in OvCa cell lines following treatment with JAK2 or FLT3 could also allow us to further evaluate the role of each kinase in HER family activation.

These studies should ideally use the selection of OvCa cell lines included in this body of work and evaluate efficacy using the **in vitro** growth assays we used.

This would enable comparison of efficacy with pacritinib which may give us insight into any potential additive or subtractive interaction which is happening with targeting IRAK1-JAK2-FLT3 together vs individually.

Finally, the role of each HER family member should be further profiled to evaluate what role they play in the growth of OvCa cell lines and if this is cell line specific. Several approaches could be taken to achieve this. It would first be important to evaluate role for each HER family members in the OvCa cell lines we worked with.

In vitro growth assays could be performed using knockdown or siRNA cells to assess the role of each HER family member in the *in vitro* growth of these cells. This would allow us to better understand if the reduced HER4 expression was representative of the reduced growth observed following IRAK1 knockdown or contributed to the reduced growth. In a similar manner it may allow us to draw conclusions about the impact of reduced HER family receptor activation in these OvCa cell lines following treatment with pacritinib.

Chapter 4

Assessing the Combination of Pacritinib and SHP099 in High Grade Serous Carcinoma

(4.1.1) Introduction

OvCa is most lethal gynaecological malignancy worldwide[45], which displays a high incidence (75% of patients) of advanced stage detections[9,10]. Diagnosis with advanced stage OvCa is associated with a poor prognosis and a five year survival rate of only 29%.[13] OvCa also display a high frequency of patients developing chemoresistance, with 70% of patients who initially respond to first line therapeutic interventions experiencing relapse and remission within two years of diagnosis.[26] It is clear that novel therapeutic strategies and targets are required in order to improve treatment and outcomes for these patients.

SHP2 is a protein tyrosine phosphatase which acts to positively regulate several signalling pathways including growth factors, hormone and cytokine pathways.[216] In Section 1.7.2 we have highlighted the studies which show SHP2 represents a potential therapeutic target in several cancer types including OvCa. We wanted to further investigate the role of SHP2 in the clinically relevant HGSC subtype of OvCa.

SHP099 is an allosteric inhibitor of SHP2 which has shown efficacy in reducing growth of several cancer types both *in vitro* and *in vivo* (Section 1.7.2) In addition to identifying if SHP2 represents a therapeutic target in HGSC we also wanted to investigate if SHP099 could represent a potential therapeutic strategy in this subtype.

In Chapter 3 we outlined our findings indicating that IRAK1 may represent a novel therapeutic target in OvCa. Furthermore, we showed that treatment with the IRAK1-JAK2-FLT3 inhibitor pacritinib significantly impaired *in vitro* growth of OvCa cells and may represent a novel therapeutic strategy in OvCa. In this chapter we set out to evaluate if SHP099 and pacritinib may provide a novel therapeutic strategy to target OvCa.

(4.1.4) Aims and Hypothesis

Novel therapeutic strategies are urgently required to improve treatment outcomes for patients with HGSC to improve prognosis associated with this poor outcome cancer. As shown in Chapter 3, we have found that the kinase inhibitor pacritinib displays promising efficacy in HGSC cell lines modelling both cisplatin sensitivity and cisplatin resistance. Several studies have shown considerable efficacy of both SHP099 and Pacritinib both alone and in combination. We hypothesise that SHP099 and Pacritinib in combination may target a combination of key therapeutic targets (IRAK1, JAK2 and SHP2) important for growth of OvCa cell lines *in vitro* and allow for synergistic reduction in growth.

In this work, the overall aim was to establish whether combination benefit could be observed using pacritinib and SHP099 in HGSC. To the best of our knowledge this drug combination has not been evaluated in any cancer type to date. The specific objectives of this body of work included.

Aim 2 – Investigating the role of SHP2 in OvCa

Objective 4. Examine SHP2 expression in HGSC and assess association with prognostic indicators.

Objective 5. Evaluate the efficacy of the allosteric SHP2 inhibitor SHP099 in HGSC cell lines *in vitro*.

Aim 3 – Evaluating the combination of Pacritinib and SHP099

Objective 6. Investigate the efficacy of pacritinib and SHP099 in combination on the growth of OvCa cell lines *in vitro*.

Objective 7. Examine the molecular mechanism of action following pacritinib and SHP099 in OvCa cell lines using a proteomics-based approach.

(4.2) – Results

As shown in Chapter 3, using an IRAK1 knockdown approach, we found IRAK1 plays a positive role in the growth of HGSC cell lines *in vitro* and that the IRAK1-JAK2-FLT3 kinase inhibitor pacritinib significantly impairs growth and growth factor receptor signalling in HGSC cell lines *in vitro*. We next wanted to assess the efficacy of a novel drug combination using pacritinib and SHP099 (SHP2 phosphatase inhibitor). To achieve this, we first began evaluating the role of SHP2 in HGSC by examining protein and gene expression and assessing the efficacy of the SHP2 inhibitor SHP099 using 3D *in vitro* growth assay models.

(4.2.1) SHP2 Expression is Elevated in Cisplatin-Resistant PE04 HGSC Cell Line Compared to the Paired Cisplatin Sensitive PE01 HGSC Cell Line

(4.2.1.1) SHP2 expression in PDX and parental HGSC cell lines

Whole Cell lysates were prepared from the HGSC cell lines PE01, PE04, OVCAR3, PEA1 and PEA2 and PDX whole cell lysates were provided by Dr Denis Collins (DCU). Lysates were profiled for SHP2 protein expression using Western blot analysis. Relative protein expression was normalised using β-actin as a loading control. SHP2 expression was observed in all PDX samples with the highest expression being observed in a PDX case of solid papillary carcinoma with mutant p53 (OVCA 6658) (Fig. 4.1.1). SHP2 was also detectable in all HGSC samples with SHP2 protein expression significantly increased in cisplatin-resistant PE04 cell line compared to the paired cisplatin-sensitive PE01 cell line (Fig. 4.1.1). Interestingly this

result was not mirrored in the paired PEA1 and PEA2 cells which display relatively similar levels of SHP2 by western blot analysis (Fig 4.1.1).

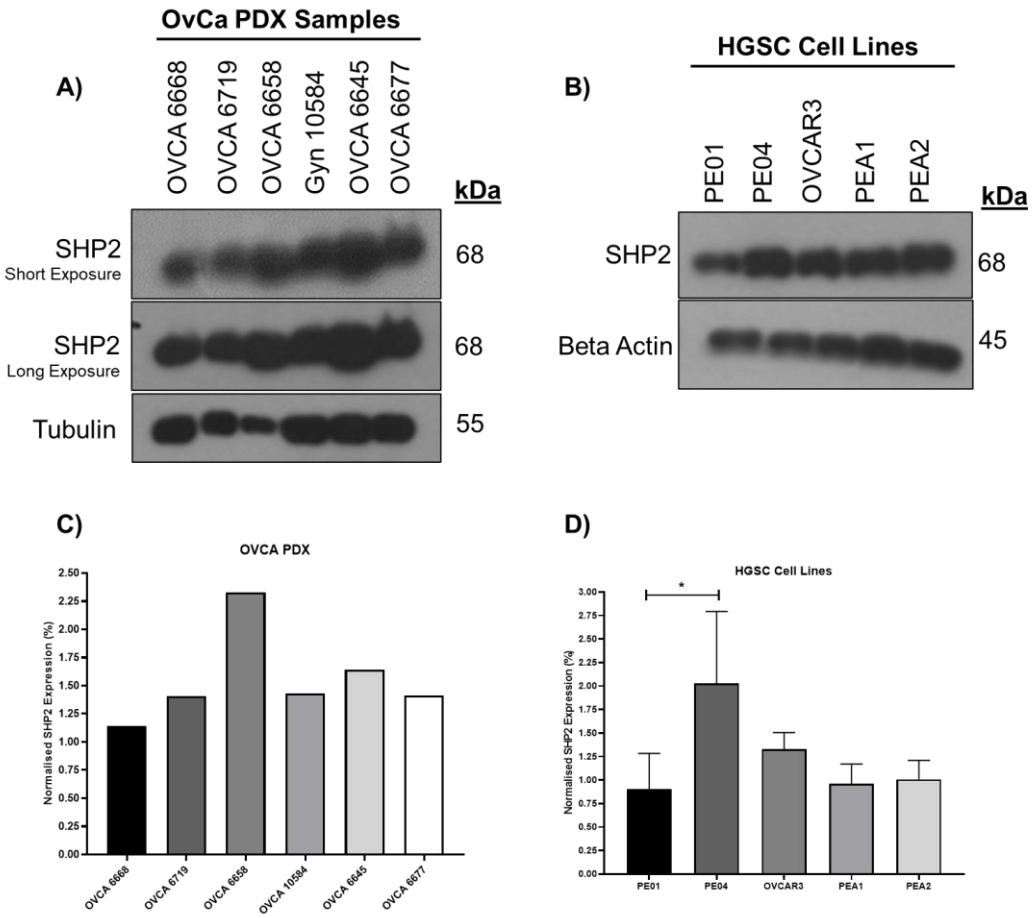

Figure 4.1.1: SHP2 protein expression is significantly increased in cisplatin resistant cell line PE04 compared to cisplatin sensitive PE01 cell line. A) A panel of six PDX samples all express SHP2. B) PE01, PE04, OVCAR3, PEA1 and PEA2 HGSC cell lines all express SHP2. PE04 expresses elevated levels of SHP2 compared to paired PE01 cell line. **C-D)** Image J densitometry was performed and SHP2 protein expression was normalised by tubulin or βeta-actin loading control. **D)** Unpaired t-test, for 4 independent experimental replicates, shows significantly increased SHP2 expression in PE04 cell line compared to PE01 cell line. , p-values; (*;≤0.05).

(4.2.2) SHP2 High Expression Cohort Display Significantly Reduced Overall Survival in Serous Ovarian Cancer

Gene expression of SHP2 (PTPN11) was examined using the publicly available database TNMplot database. PTPN11 was observed to display considerable dysregulation in cancer, with gene expression being significantly different in seventeen of the twenty-one cancers available on the platform (Fig. 4.2.1). Ten cancers show elevated gene expression of PTPN11 (AML, Colon, Oesophageal, Lung, Pancreas, Renal CH, Renal PA, Stomach, Testis and Thyroid) while seven show reduced gene expression (Bladder, Breast, Prostate, Rectum, Skin, Uterus CS and Uterus EC) compared to normal controls.

We first began by investigating the gene chip dataset available on TNMplot and our findings from this are shown in panel C of Figure 4.2.1. Probing the gene chip dataset we observed a significant decrease in PTPN11 gene expression in OvCa compared to normal controls. Given these findings we next wanted to assess if SHP2 was differentially expressed in serous OvCa compared to normal controls. To achieve this we probed the RNA sequencing dataset available on TNMplot and our findings from this are shown in panel B of Figure 4.2.1. The RNA sequencing dataset allowed us to narrow our search terms and examine only serous OvCa. Interestingly, we observed PTPN11 gene expression showed no significant difference in serous OvCa compared with normal controls.

The publicly available KM Plotter database provides a platform which allowed us to investigate the relationship between PTPN11 mRNA expression and OS. The PTPN11 high mRNA expression cohort was found to display significantly reduced OS in OvCa, serous OvCa and stage 3+4 OvCa subsets (Fig 4.3.1). We narrowed these subsets further to include only patients which had received platinum and Taxol treatment. With this refinement we again observed the PTPN11 high expression

cohort showed significantly reduced overall survival in OvCa, serous OvCa and stage 3 and 4 OvCa. These observations provide a strong indication that high SHP2 gene expression represents a negative prognostic indicator in OvCa.

These findings indicate that SHP2 expression may not be elevated in serous OvCa compared to normal controls which may lead to the conclusion that it therefore plays no role progression of serous OvCa. However, the observation that SHP2 high mRNA expression cohorts display significantly reduced OS indicate that SHP2 expression may be a negative prognostic indicator in OvCa.

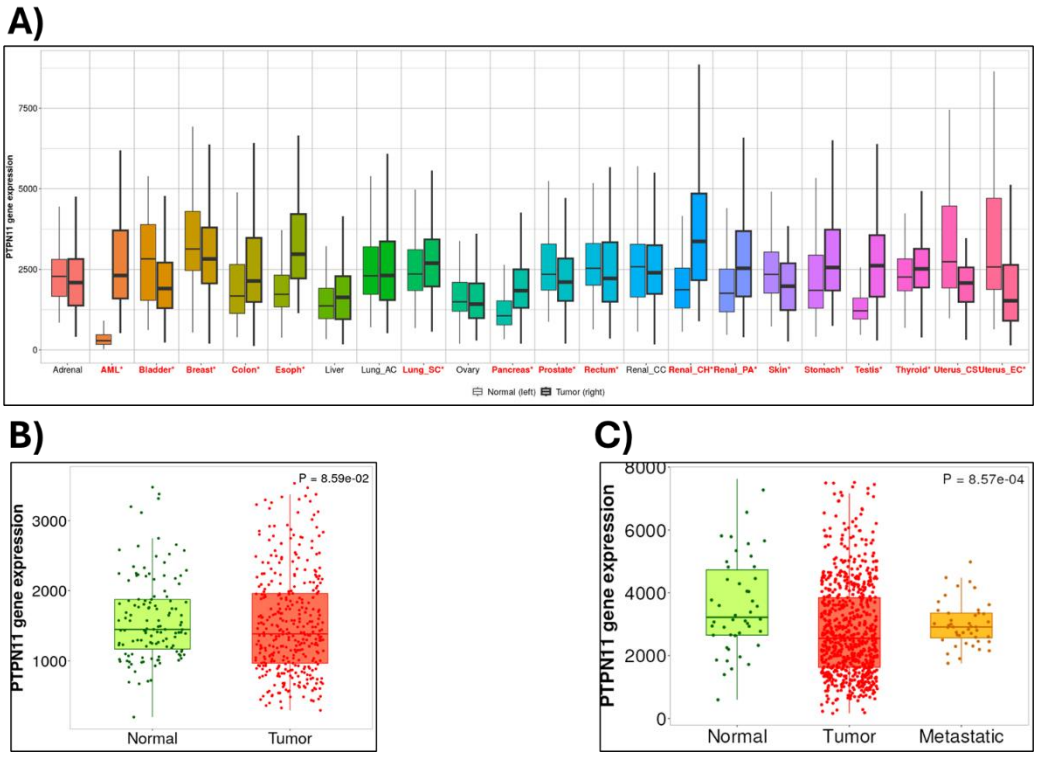

Figure 4.2.1: PTPN11 (SHP2) gene expression is not significantly different in serous ovarian cancer tumour samples compared to normal controls. PTPN11 gene expression was visualised using TNMplot. **(A)** PTPN11 gene expression was found to be significantly altered in 17 of the 21 cancers profiled. Ovarian tumour samples (n=347) showed no significant difference in PTPN11 gene expression compared to normal controls (n=133). **(B)** RNA sequencing analysis shows no significant difference in PTPN11 gene expression between serous cystadenocarcinoma ovarian cancer (n=374) compared to non-cancerous controls (n=133). **(C)** Gene chip analysis shows a significant decrease in PTPN11 gene expression levels in ovarian cancer (n=744) and no significant difference with metastatic ovarian cancer (n=44) compared to normal controls (n=46).

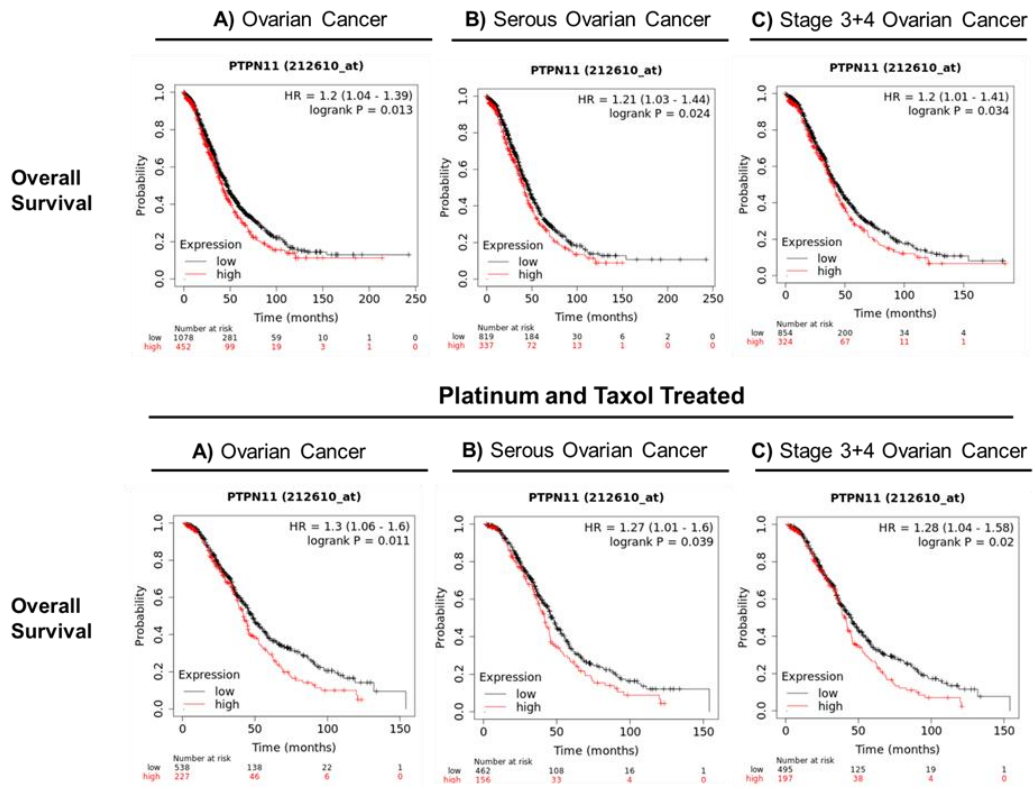

Figure 4.3.1: PTPN11 high expression cohorts show significantly reduced overall survival. Using the publicly available database KM Plotter, the JetSet best probe set (212610_at) for PTPN11 mRNA expression was probed for association with overall survival. Outlier arrays were excluded. PTPN11 high mRNA expression cohort shows significantly reduced overall survival in **A)** ovarian cancer, **B)** serous ovarian cancer and **C)** and high stage (3+4) ovarian cancer subsets. Overall survival was also significantly reduced in all three subsets when analysis refined to platinum and Taxol treated cohorts.[276, 277]

(4.2.3) SHP2 Protein Expression is Significantly Elevated in High Stage (3 + 4) HGSC Compared to Normal Controls

Having examined the publicly available mRNA databases for SHP2 expression (PTPN11) in serous OvCa, we next moved to evaluating SHP2 protein expression in HGSC tissue using immunohistochemistry (IHC). This was carried out in collaboration with Professor William Gallaghers research group in University College Dublin. SHP2 knockdown CHME3 (microglial) cell lines were previously generated by Dr Butler using a stable lentiviral-induced knockdown approach. These cell lines were used to optimise SHP2 antibody conditions for IHC work. In all corresponding figures SHP2 knockdown cell lines are denoted SHP2sh-1 and SHP2sh-2 while SHP2 expressing control cells are denoted CTsh. For the purposes of this study, CTsh and SHP2sh-1/2 cells were fixed, and cell plugs were prepared and then used to optimise the immunohistochemical staining of SHP2 (Section 2.6). These optimisation experiments are shown in Figures 4.4.1 to Figures 4.4.7.

We began by evaluating IHC staining using two SHP2 antibodies from two different suppliers Cell Signalling (cs-3397) and Santa Cruz (sc-7384). Staining with the cs-3397 antibody resulted in relatively little staining in CHME3 CTsh cells even at concentrations as high as 1:50 dilution (Fig. 4.4.1). QuPath image analysis for this experiment is displayed in Figure 4.4.2. For this reason, we decided to progress with the sc-7384 antibody which showed high levels of staining in the SHP2 expressing CTsh CHME3 cells.

SHP2 knockdown was confirmed by Western blot analysis using the sc-7384 antibody (Fig. 4.4.3). The SHP2 targeted sc-7384 antibody was observed to be capable of detecting a single band at 68kDa in control CTsh CHME3 cells which corresponds to SHP2 (Fig. 4.4.3). This band was also observed to be reduced in both SHP2 knockdown cell lines. This experiment confirmed knockdown in the SHP2

knockdown cells. These cell lines were routinely used in Dr Butlers lab for immunology-based studies.

Staining using sc-7384 was observed to result in high levels of background staining in SHP2sh-1 cells using an antibody dilution of 1:300 (Fig. 4.4.1). Due to this observation, we progressed with evaluating higher dilutions of this antibody to see if we could reduce the background and optimise staining. At a dilution of 1:1000 the sc-7384 SHP2 antibody was observed to result in a more representative staining profile with SHP2 being detected in control cells and reduced staining being observed in knockdown cells (Fig. 4.4.4). These findings indicated that higher dilutions of sc-7384 were optimal to minimise the background or non-specific staining. QuPath image analysis is displayed for this experiment in Figure 4.4.5.

Having observed higher dilutions of sc-7384 resulting in a more representative staining profile in SHP2 CTsh and SHP2sh-1/2 cells, we moved onto assessing background staining using paraffin embedded full face tissue sections (HUCAT311) of HGSC. Slides were purchased from US Biomax for these optimisation experiments. Slides were stained using 1:250 dilution of sc-7384. This dilution is at the higher end of that recommended by the manufacturer and was selected due to the higher dilutions showing more representative staining in our earlier validation experiments. Following staining, slides were scanned and analysed using QuPath image analysis software (Fig. 4.4.7). SHP2 staining was assessed by a clinician working in collaboration with Professor William Gallagher and background staining was confirmed to be optimal (Fig. 4.4.6 and Fig. 4.4.7). Interestingly, we observed reasonably high levels of nuclear staining of SHP2 in this HGSC tissue sample following QuPath analysis. This experiment marks the end of the validation experiments as we had optimised staining for this antibody in full face tissue sections.

Once SHP2 IHC staining using sc-7384 had been validated using full face tissue sections we progressed to full tissue microarrays (TMAs) to investigate SHP2

protein expression in HGSC. Two TMA slides were purchased from US Biomax OV809B and OV802B. These slides were stained at the same time using the same protocol and contain a combined 18 normal adjacent tissue (NAT) cores and 86 HGSC tissue cores. The HGSC tissue cores on these TMAs covered all four stages of cancer, stage 1 (22), stage 2 (24), stage 3 (41) and stage 4 (3). Cores were imaged using Aperio®AT2 – Leica Biosystems and DAB positive cell detection was determined for cellular, cytoplasmic and nuclear staining of SHP2, using QuPath image analysis software.

SHP2 protein expression levels at both cellular and cytoplasmic levels were observed to be significantly increased in HGSC compared to NAT (Fig. 4.5.1). These results provide an interesting finding since mRNA expression of SHP2 was observed to be unchanged in serous OvCa compared to normal controls (Section 4.2.1). QuPath image analysis is displayed in Figure 4.5.2 for this experiment.

As well as subtype the stages of disease were provided by US Biomax for each HGSC core. When divided by stages we observed a significant increase in SHP2 cellular, cytoplasmic and nuclear staining in high stage (3 + 4) HGSC compared to low stage (1) HGSC (Fig. 4.5.3). SHP2 cellular and cytoplasmic staining in high stage (3 + 4) HGSC was additionally observed to be significantly increased compared to NAT (Fig. 4.5.3). Finally, the cytoplasmic staining of SHP2 was elevated in stage 2 HGSC compared to NAT (Fig. 4.5.3). These findings are interesting as they indicate SHP2 expression is associated with higher stage HGSC which is in turn associated with poorer prognosis. These findings support the hypothesis that SHP2 represents a negative prognostic indicator in HGSC. QuPath image analysis is displayed in Figure 4.5.4 for this analysis.

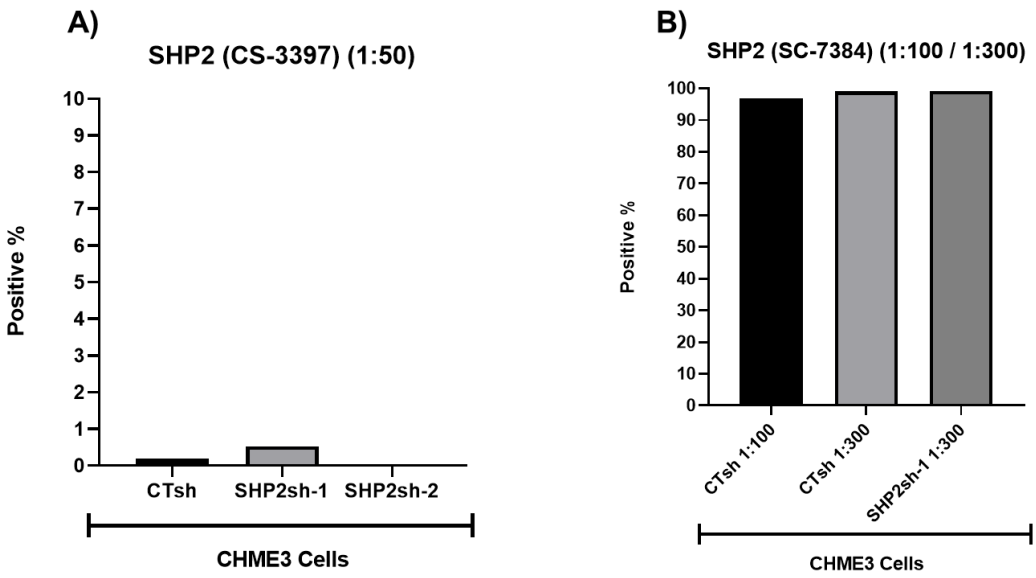

Figure 4.4.1: SHP2 primary antibody SC-7384 displays superior immunohistochemical staining profile compared to CS-3397. Paraffin embedded cell plugs were using human microglial CHME3 control (CTsh) and SHP2 knockdown (SHP2sh-1 and SHP2sh-2). Immunohistochemical staining of SHP2 with **A)** CS-3397 resulted in relatively low levels of staining while immunohistochemical staining of SHP2 with **B)** SC-7384 resulted in high levels of staining at both 1:100 and 1:300 dilutions. Percentage positive cell detection was assessed using QuPath Software.

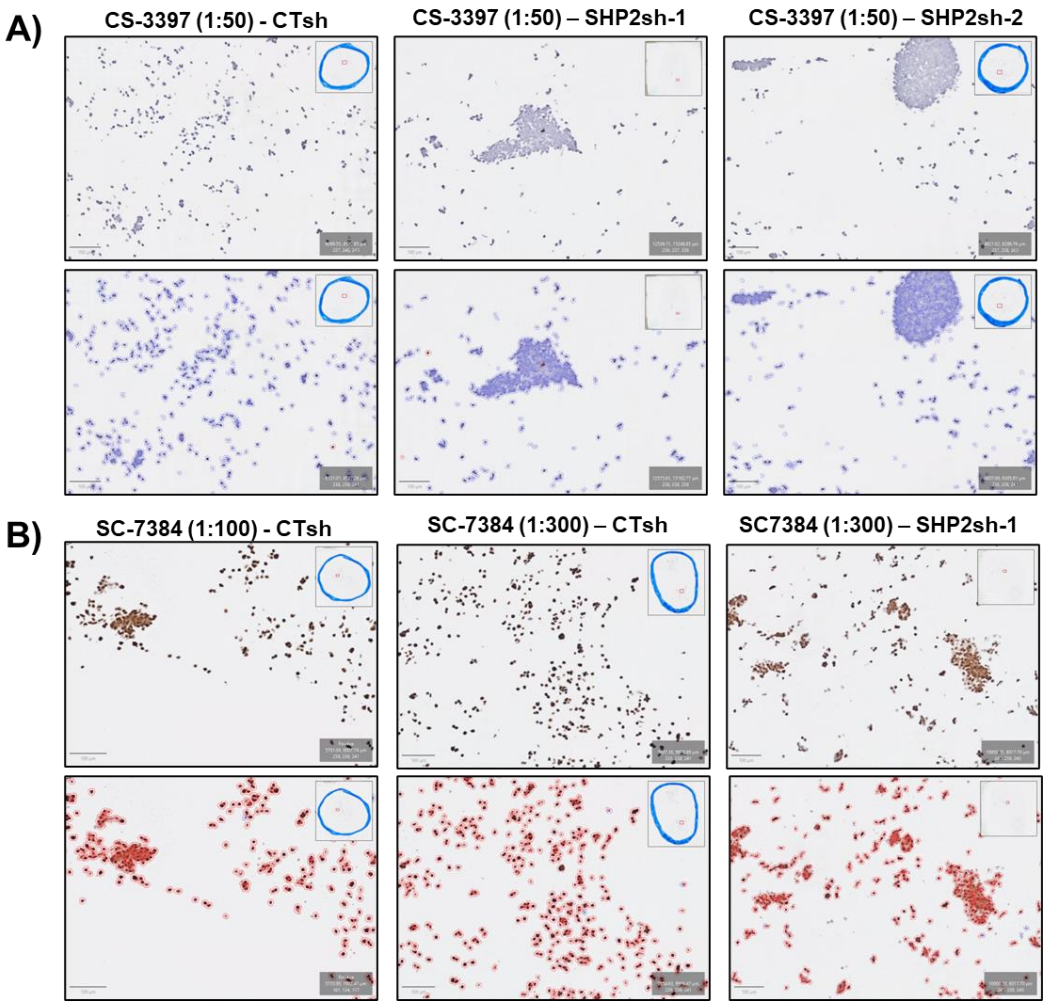

Figure 4.4.2: QuPath image analysis software shows SHP2 primary antibody SC-7384 displays superior IHC staining profile compared to CS-3397. QuPath image analysis software was used for DAB positive cell detection and quantification of SHP2 immunohistochemical staining. Images are representative of percentage positivity displayed. **A)** CS-3397 (1:50) resulted in relatively low to absent staining for SHP2. **B)** SC-7384 resulted in detectable levels of staining for SHP2 at both 1:100 and 1:300 concentrations. The upper panel of each section represents raw images while the lower panel represents QuPath markup of detections.

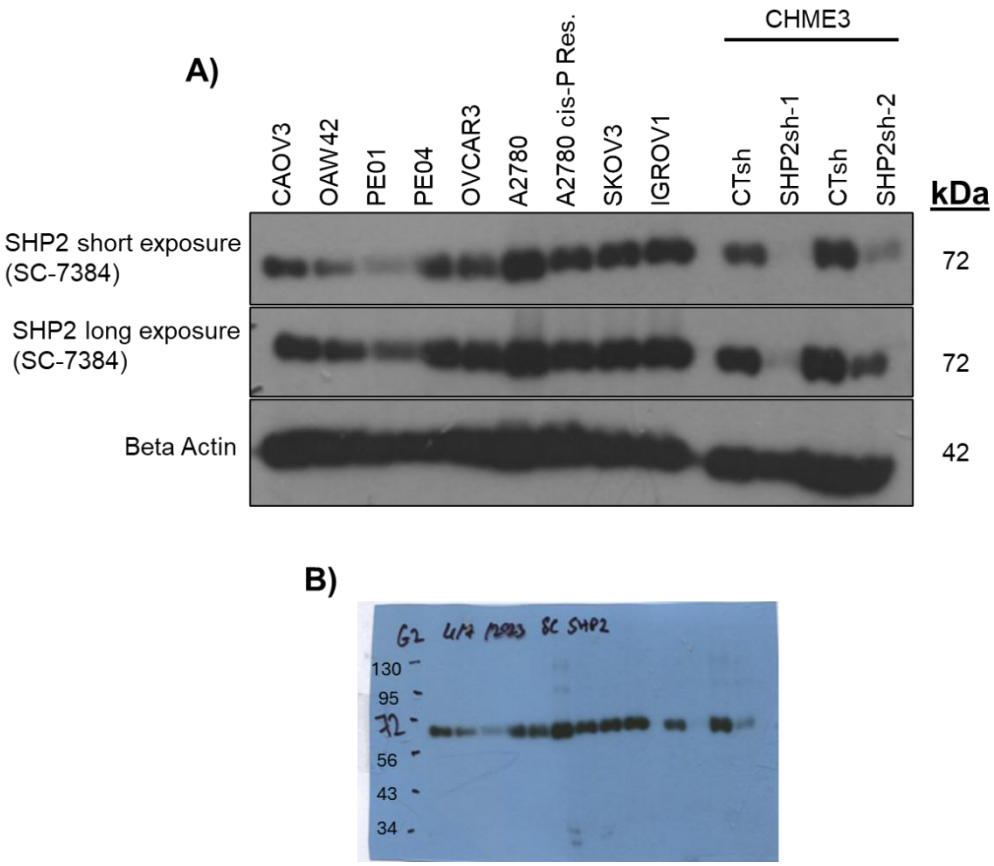

Figure 4.4.3: SHP2 primary antibody SC-7384 detects a single band by Western blot analysis showing a single band for SHP2 in control cells and reduced bands in SHP2 knockdown cells. Whole cell lysates were prepared from CHME3 control (CTsh) and CHME3 SHP2 knockdown cells (SHPsh-1 and SHPsh-2). SHP2 protein expression was determined using SC-7384. **A-B)** Staining with SC-7384 displayed higher levels of SHP2 staining in control cells compared to SHP2 knockdown cells, as expected.

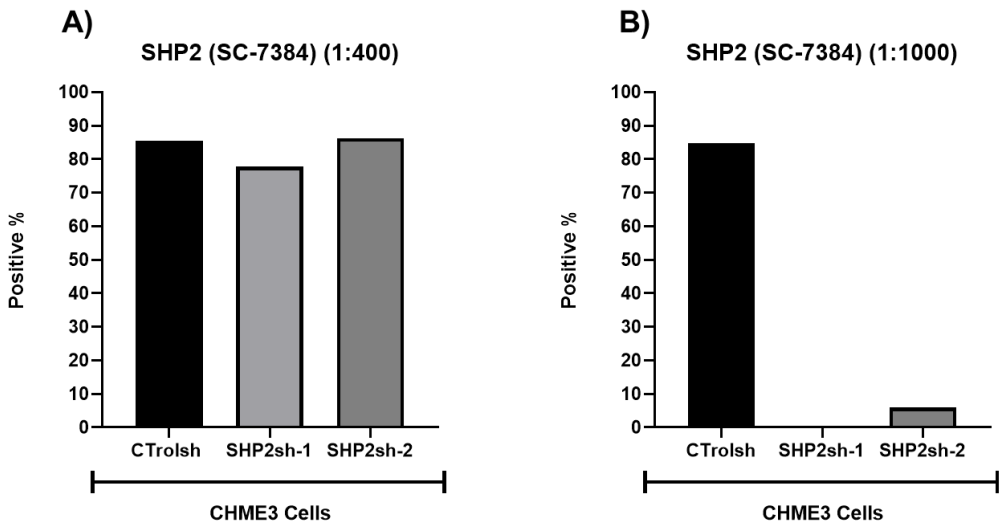

Figure 4.4.4: Higher dilutions of SHP2 primary antibody SC-7384 show more representative staining in SHP2 knockdown cell lines compared to control cells. Paraffin embedded cell plugs were generated using CHME3 control (CTsh) and SHP2 knockdown (SHP2sh-1 and SHP2sh-2). Immunohistochemical staining was carried out on the Auto stainer Link 48, Dako (UCD), and used test two further concentrations of SC-7384 **A)** 1:400 and **B)** 1:1000. The higher concentration of 1:1000 resulted in a better separation of staining between SHP2 control and knockdown cell lines. DAB positive cell detection was used to detect SHP2 positive staining and was assessed through QuPath image analysis software.

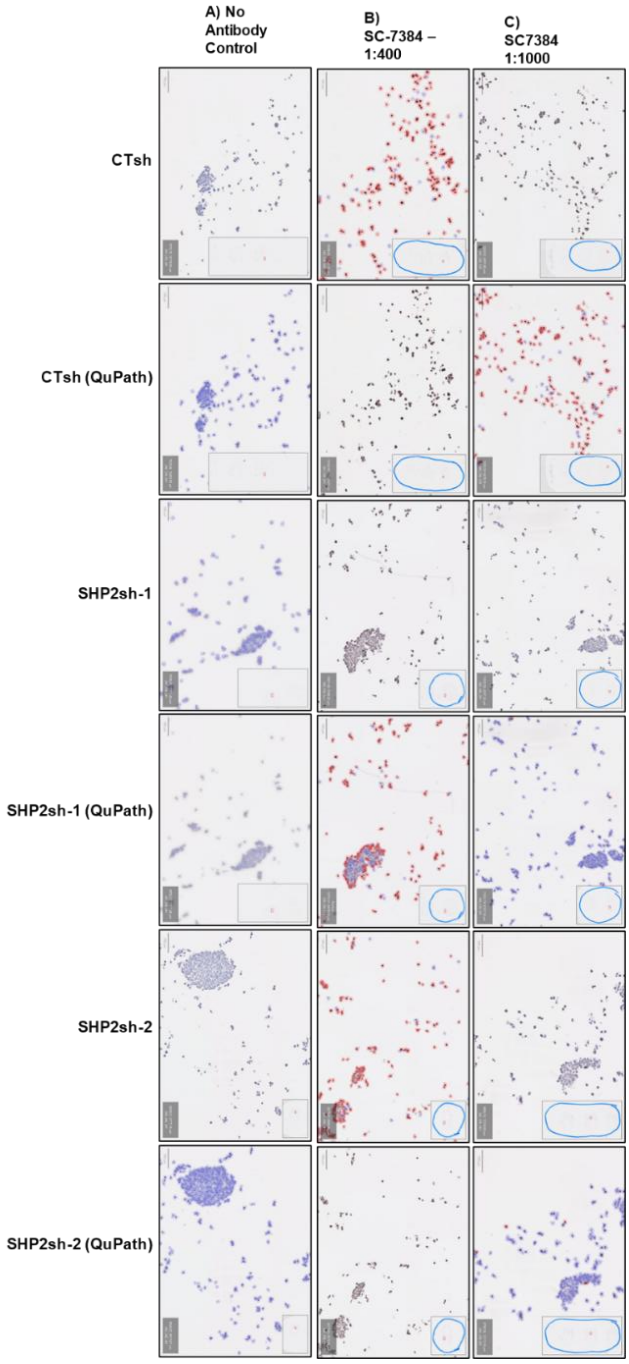

Figure 4.4.5: Higher dilutions of SC7384 show more representative staining in SHP2 knockdown cell lines compared to control cells. QuPath Image Analysis software was used for DAB positive cell detection and quantification of SHP2 staining. Images are representative of percentage positivity displayed in **Figure 4.4.4**. **(A)** No Antibody Control (NAC) was used as a negative control for staining. Decreasing dilutions of SC7384, **(B)** 1:400 dilution of primary SHP2 antibody, **(C)** 1:1000 dilution, were used to assess background staining in SHP2 knockdown cell lines compared to controls. 1:1000 concentration shows a more pronounced difference in SHP2 staining between SHP2 control and knockdown cells compared to 1:400 concentration.

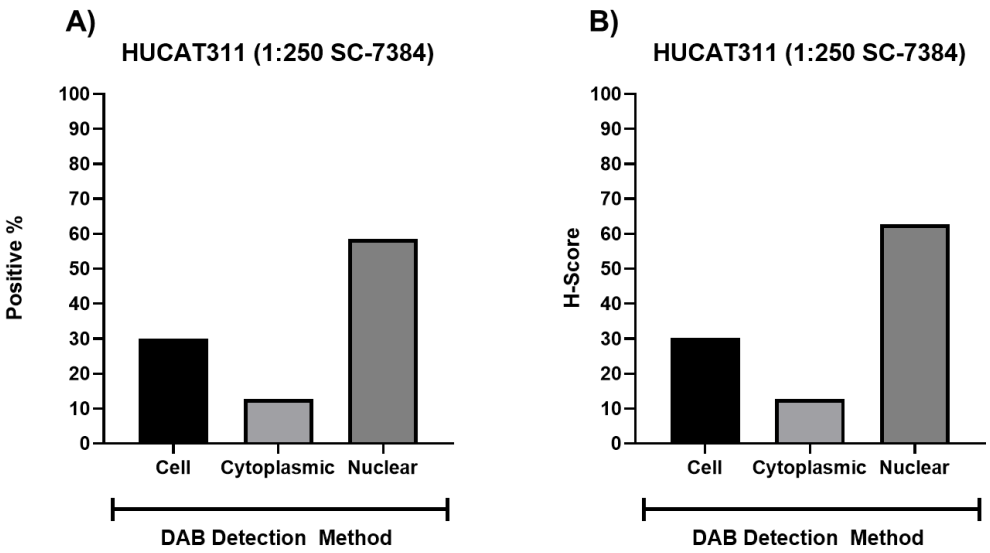

Figure 4.4.6: Optimisation of the SHP2 Primary antibody SC-7384 for IHC staining in full face tissue sections. HUCAT311 (U.S. Biomax) slides were stained for SHP2 using SC-7384 (1:250) using the Autostainer Link 48, DAKO (UCD). DAB positive cell detection, subcellular DAB positive cell detection was assessed using QuPath software. Both **A)** Percentage positivity and **B)** H-score readouts indicate strong staining of SHP2 and high levels of nuclear staining of SHP2. Background and staining were assessed by a clinician and the concentration of 1:250 was confirmed to be optimal.

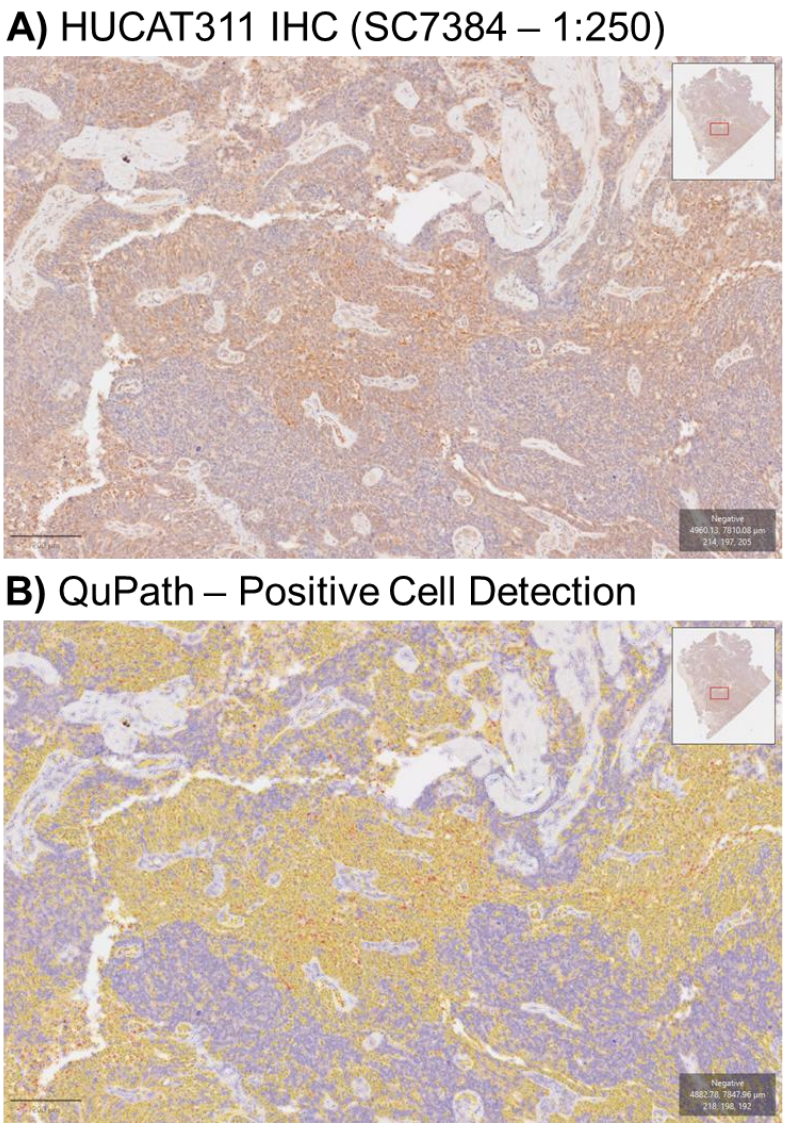

Figure 4.4.7: QuPath Image analysis software shows SHP2 primary antibody SC-7384 displayed a good staining profile with minimal background staining in full face tissue sections. A) High grade serous ovarian cancer full face tissue sections (HUCAT311) were immunohistochemically stained for SHP2 using SC-7384 primary antibody at 1:250 dilution and counterstained with haematoxylin. Stained slides were scanned using Aperio®AT2-Leica Biosystems (UCD). **B)** DAB positive cell detection was performed using QuPath Image analysis software.

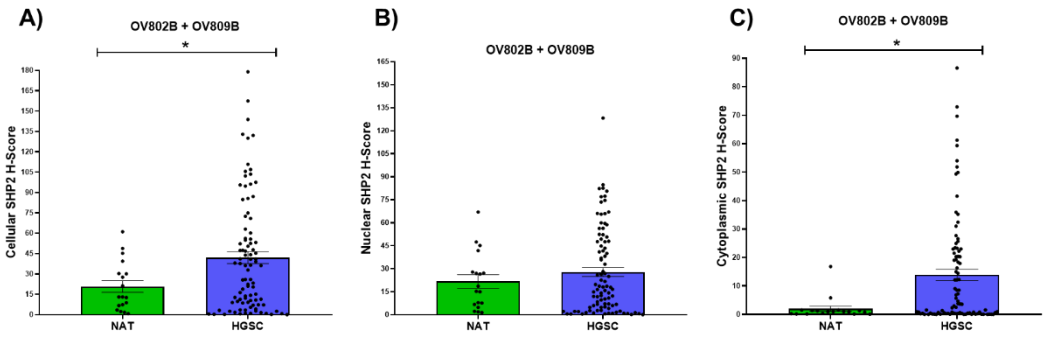

Figure 4.5.1: SHP2 protein expression is significantly higher in High Grade Serous Carcinoma (HGSC) compared to Normal Adjacent Tissue (NAT) controls: OV809B and OV802B tissue microarrays (US BIOMAX) were analysed for SHP2 expression levels. Combined, they include 18 NAT cores and 86 HGSC tissue cores. Immunohistochemical staining for SHP2 protein expression (SC-7384 at 1:250 dilution) was carried out using the Autostainer Link 48, Dako (UCD). DAB positive cell detection, H-score and subcellular staining detection were assessed using QuPath image analysis software. HGSC shows significantly higher expression of **A)** cellular and **C)** cytoplasmic SHP2 compared to normal adjacent controls. Statistical significance between groups was investigated (through PRISM) using unpaired Student t-test, p-values; (*; ≤0.05).

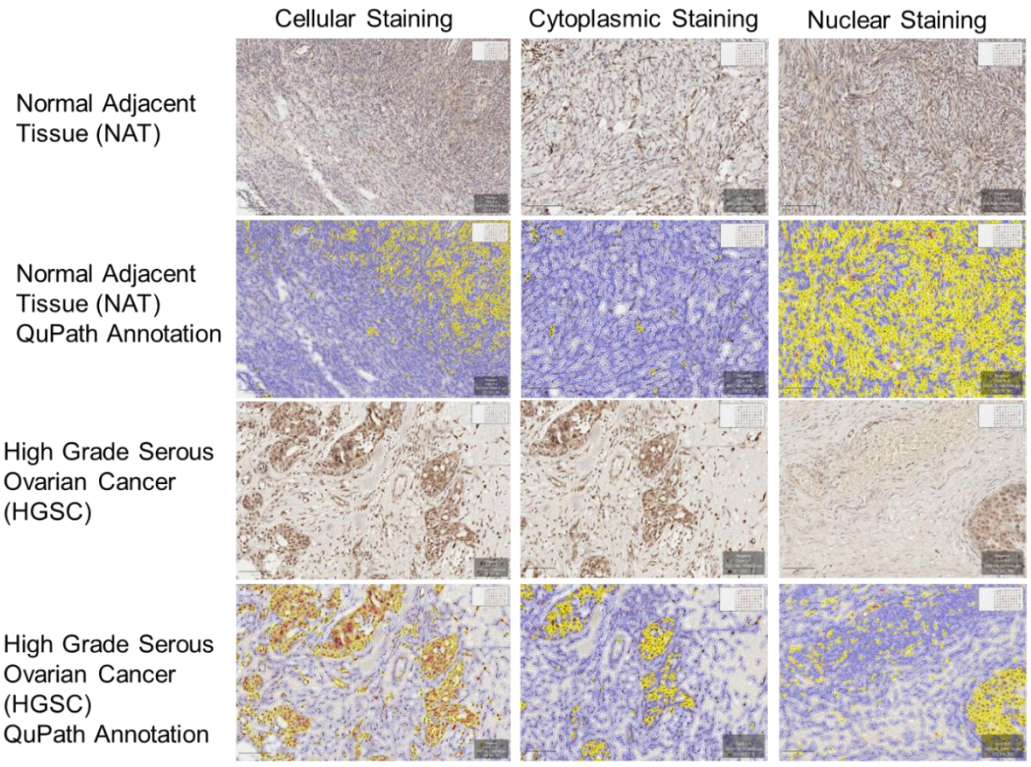

Figure 4.5.2: SHP2 protein expression is significantly higher in HGSC compared to NAT controls. Slides were scanned using Aperio®AT2 – Leica Biosystems and DAB positive cell detection and subcellular DAB detection was carried out using QuPath image analysis software. Representative images are displayed above for mean H-Scores. Blue markings indicate negative cell detection while yellow and red indicate increasing SHP2 expression level cell detections.

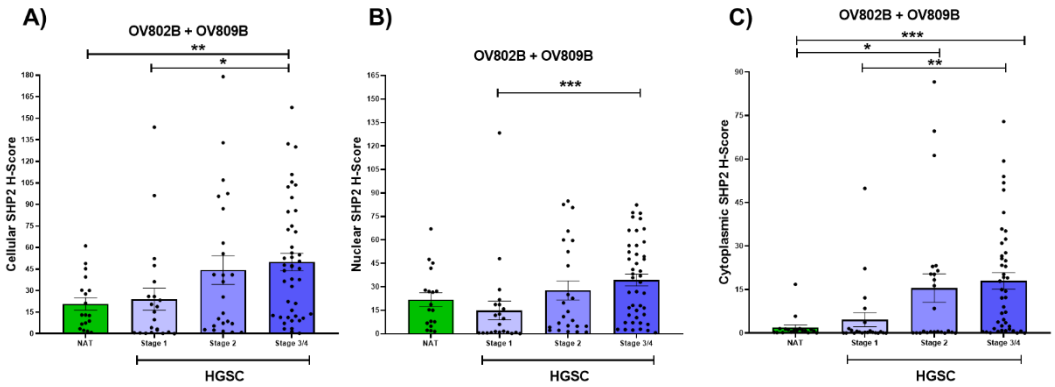

Figure 4.5.3: SHP2 protein expression is significantly increased in high stage (3+4) high grade serous carcinoma (HGSC) compared to both stage 1 and normal adjacent tissue (NAT). OV809B and OV802B tissue microarrays (US BIOMAX), contain normal adjacent tissue (18), stage 1 (22), stage 2 (24), stage 3 (41) and stage 4 (3) HGSC. Immunohistochemical staining for SHP2 protein expression (SC-7384 at 1:250 dilution) was carried out using the Autostainer Link 48, Dako (UCD). DAB positive cell detection, H-score and subcellular staining detection were assessed using QuPath Image analysis software. Stage 3/4 HGSC shows significantly higher **A)** cellular, **B)** nuclear and **C)** cytoplasmic staining for SHP2 compared to stage 1 HGSC. Statistical significance between groups was investigated (through PRISM) using unpaired Student's t-test, p-values; (*; ≤0.05), (**; ≤0.01), (**; ≤0.001).

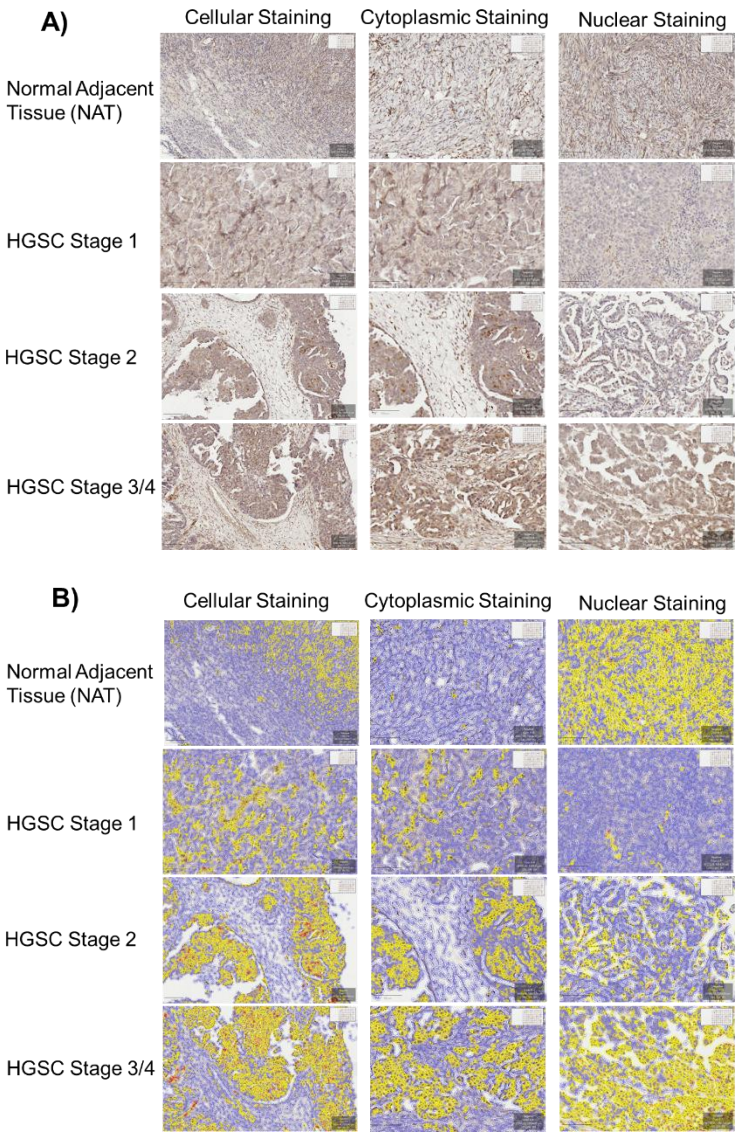

Figure 4.5.4: SHP2 protein expression is significantly increased in high stage (3+4) high grade serous carcinoma (HGSC) compared to both stage 1 and normal adjacent tissue (NAT). A) Slides were scanned using Aperio®AT2 – Leica Biosystems and DAB positive cell detection and **B)** subcellular DAB detection was carried out using QuPath image analysis software. Representative images are displayed above for mean H-Scores. Blue markings indicate negative cell detection while yellow and red indicate increasing SHP2 expression level cell detections.

(4.2.4) Treatment with SHP099 Significantly Reduces the 3D Growth and Viability of HGSC Cell Lines *In Vitro*

We next wanted to assess the efficacy of the SHP2 allosteric inhibitor SHP099 in HGSC cell lines using 3D *in vitro* growth assay models. To on achieve this, we used the paired cisplatin sensitive (PE01) and cisplatin resistant (PE04) HGSC cell lines in addition to the OVCAR3 cell line. PE01, PE04 and OVCAR3 cells were seeded in 2% Matrigel and treated with 5μM or 10μM of SHP099 or vehicle control. On day seven viability was determined using Cell Titre-Glo® reagent. We observed that treatment with SHP099 led to a significant reduction in 3D growth and viability of HGSC cells in all three cell lines tested (Fig. 4.6.1 and Fig. 4.6.2). PE01, PE04 and OVCAR3 display significantly reduced 3D growth and viability, following treatment with 5μM and 10 μM, regardless of any characteristic differences. These findings indicate that SHP099 may represent a novel therapeutic strategy to target HGSC cells.

To confirm and back up these findings we performed a second 3D *in vitro* growth assay. The paired HGSC PE01 and PE04 cell lines were seeded in low gelling agarose and treated with increasing concentrations of SHP099 (2.5μM, 5μM and 10μM) or vehicle control (Section 2.3.4). On day-21, viable colonies were stained using Neutral Red viability dye and representative counts were taken of the number of colonies formed for each treatment (Fig. 4.7.1). Treatment with SHP099 was observed to significantly inhibit colony formation and anchorage independent growth of both cisplatin sensitive and resistant HGSC cells *in vitro* (Fig 4.7.1).

Allosteric inhibition of SHP2 using SHP099 displays considerable efficacy in reducing 3D growth and viability of HGSC cells *in vitro*. These findings indicate that SHP2 represents an actionable target in HGSC and SHP099 may represent a potential therapeutic strategy through allosteric inhibition of SHP2.

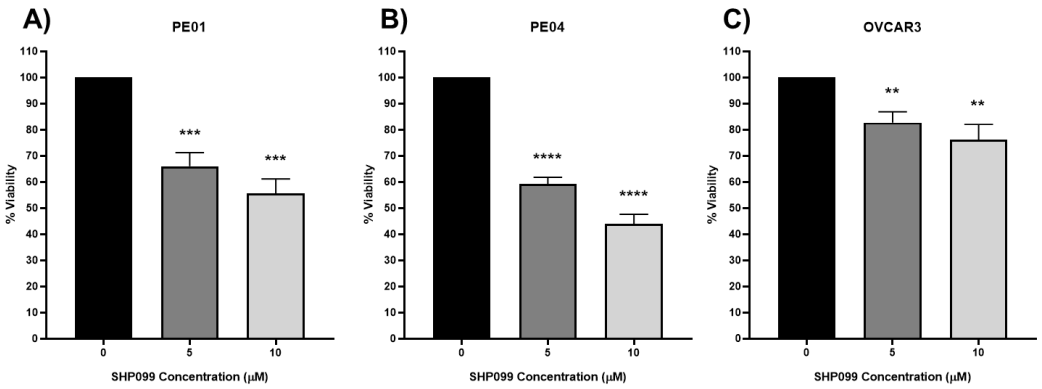

Figure 4.6.1: SHP099 Significantly reduces 3D Viability and growth of HGSC Cell lines in Vitro. A-C) Treatment with SHP099 significantly reduces 3D viability and growth of PE01, PE04 and OVCAR3 HGSC cell lines. Results are representative of greater than or equal to 4 independent replicates and statistical significance (PRISM) was assessed using a paired students t-test comparing each treatment to vehicle control. p-values; (*;≤0.05), (**;≤0.01), (***;≤0.001), (****;≤0.0001).

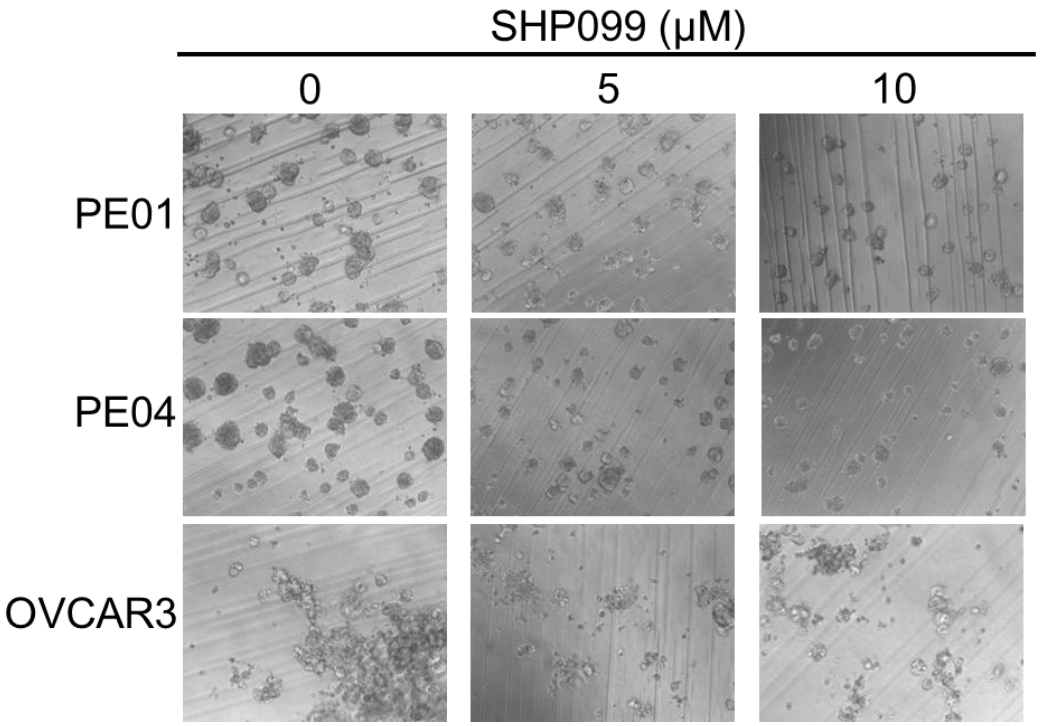

Figure 4.6.2: **Representative Images for PE01, PE04 and OVCAR3 shown in Figure 4.6.2 Show reduced 3D growth and viability following treatment with SHP099.** Representative Images were captured at 10X magnification on Olympus Microscope on Day 7.

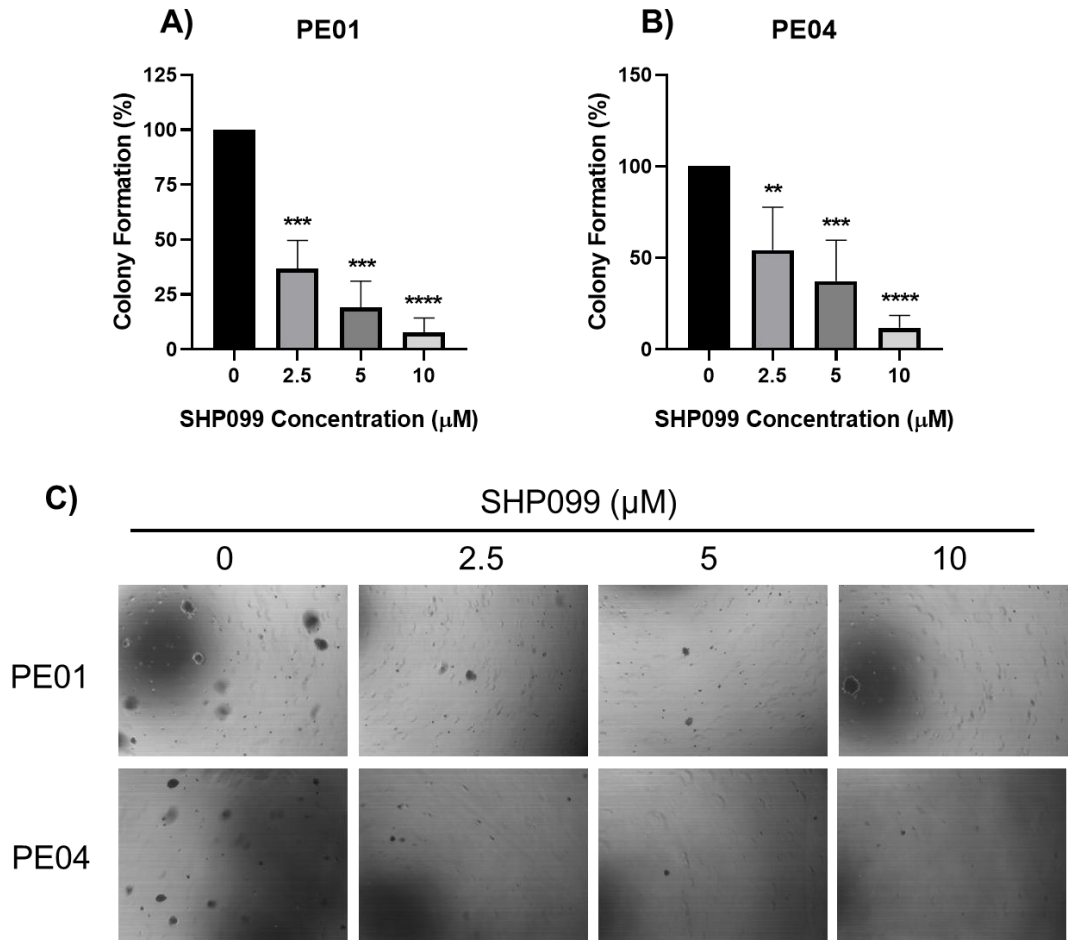

Figure 4.7.1: Treatment with SHP099 significantly reduces anchorage independent growth in high grade serous ovarian cancer (HGSC) cell lines at all concentrations tested. Treatment with SHP099 significantly reduces anchorage independent growth of **A)** PE01 and **B)** PE04 HGSC cell lines. **C)** Colonies were imaged at 4X magnification and representative counts were taken from each well and used to graph **A)** PE01 and **B)** PE04. Results are representative of greater than or equal to 4 independent replicates. Statistical significance (PRISM) was assessed using a paired students t-test comparing each treatment to the corresponding vehicle control. p-values; (*;≤0.05), (**;≤0.01), (***;≤0.001), (****;≤0.0001).

(4.2.5) The Combination of Pacritinib and SHP099 Results in Synergistic Reduction in 3D Viability and Growth of HGSC Cell Lines *in vitro*.

Given that the allosteric SHP2 inhibitor SHP099 displayed strong efficacy in HGSC cells using 3D *in vitro* growth assay models we wanted to next evaluate the potential combination with pacritinib. To do this, we used both 2D and 3D *in vitro* growth assay models and a larger panel of HGSC cell lines. These cell lines included two paired cell lines which model cisplatin sensitivity (PE01, PEA1) and cisplatin resistance (PE04, PEA2), and the OVCAR3 cell line.

(4.2.5.1) 2D *in vitro* growth assay models

We initially began these experiments by using 2D viability assays to assess the efficacy of SHP099 and pacritinib alone and determining the IC50 value for each cell line (Section 2.3.2). For the purposes of these experiments, we included the OAW42 and IGROV1 OvCa cell lines. Cells were treated with increasing concentrations of pacritinib (0.3125μM, 0.625μM, 1.25μM, 2.5μM, 5μM, 10μM, 20μM), SHP099 (0.3125μM, 0.625μM, 1.25μM, 2.5μM, 5μM, 10μM, 20μM, 40μM) or vehicle controls. After seventy-two hours viability was determined using Cell Titre-Glo® 2.0 reagent. Viability was normalised as a percentage of vehicle control. IC50 analysis was performed, using the Calcusyn program.

The efficacy of pacritinib in OvCa cell lines was assessed in Chapter 3. Treatment with pacritinib was observed to result in a dose-dependent decrease in viability and significantly reduce OvCa cell line viability at low micromolar concentrations (Fig 3.7.1). IC50 analysis revealed that pacritinib reduces viability, of all OvCa cell lines tested, at concentrations less than or equal to 2.67μM (Table 3.2.1).

Treatment with SHP099 was observed to result in limited reduction of 2D viability in OvCa cell lines evaluated (Fig 4.8.1). This reduction was observed to be significant at the higher range of concentrations assessed. With the exception of the cisplatin resistant PE04 HGSC cell line, IC50 analysis led to the finding that SHP099 did not result in a 50% reduction in OvCa cell line viability at the concentrations tested. The IC50 value determined for the PE04 cell line was 35.26μM (Table 4.2.1). It is clear that pacritinib more potently inhibits growth of OvCa cells *in vitro* with considerably lower IC50 values for each cell line.

Using western blot analysis, we have shown significantly increased SHP2 expression in PE04 cells compared to PE01 (Section 4.2.1). It is therefore interesting that SHP099 more potently inhibits 2D growth and viability of PE04 cells compared to PE01. These findings may indicate that high SHP2 expression could represent increased sensitivity to SHP099. This result is interestingly in contrast to the IC50 analysis performed for pacritinib which showed a higher IC50 value for PE04 cells compared to PE01 cells. A similar finding was observed for pacritinib in PEA1 and PEA2 paired cell lines. These findings may indicate that pacritinib is less effective in cisplatin resistant HGSC cells compared to paired sensitive cells while SHP099 is more effective.

Once we had determined effective concentration ranges for both pacritinib and SHP099 we moved onto assessing the efficacy of both drugs in combination in HGSC cell lines PE01, PE04, OVCAR3, PEA1 and PEA2. To do this, we plated cells in the same 2D format as before and treated with increasing concentrations of pacritinib (0.3125μM, 0.625μM, 1.25μM, 2.5μM and 5μM) +/- increasing concentrations of SHP099 (1.25μM, 2.5μM, 5μM and 10μM) or vehicle control in matrix assays (Section 2.3.2). The concentrations selected for these experiments covered a range of effective and subeffective concentrations for both pacritinib and SHP099. Again, after

seventy-two hours viability was determined, and synergy / antagonism analysis was performed using Combenefit software.

Following combination treatment of pacritinib and SHP099, we observed some level of antagonism in the paired PE01 and PE04 cells lines at low concentrations of pacritinib (Fig. 4.9.1). Combinations using concentrations of 2.5μM of pacritinib and 5μM/10μM of SHP099 displayed synergistic reduction in viability in OVCAR3, PEA1 and PEA2 HGSC cell lines and some limited additive benefit being observed in the PE01 and PE04 cell lines at these concentrations (Fig. 4.9.1).

(4.2.5.2) 3D *in vitro* growth assay models

Treatment with SHP099 was observed to result in significant reduction in 3D growth assay models (Fig. 4.6.1 and Fig. 4.7.1), which is in contrast to findings observed for the 2D viability assay (Fig 4.8.1). This difference between 2D and 3D efficacy of SHP099 led us to assess the efficacy of pacritinib and SHP099 in combination using 3D *in vitro* growth assay models. These 3D models allow us to more accurately represent how cancer cells grow *in vivo*.

We began by using a 3D Matrigel growth assay in which cells were plated in 2% Matrigel and treated with increasing concentrations of Pacritinib (1.25μM, 2.5μM and 5μM) +/- increasing concentrations of SHP099 (2.5μM, 5μM and 10μM) or vehicle control (Section 2.3.6). On day 7 viability was determined using Cell Titre-Glo® 3D, readouts were normalised as percentage viability and synergy / antagonism and analysis was performed using Combenefit software.

Combination of pacritinib and SHP099 was observed to result in synergistic reduction in 3D viability and growth in HGSC cell lines (Fig. 4.10.1). Interestingly, cisplatin sensitive (PE01, PEA1) HGSC cell lines were observed to display synergy

across a wider range of concentrations compared to cisplatin resistant (PE04 and PEA2) HGSC cell lines (Fig. 4.10.1). These findings provided the initial indication that SHP099 in combination with pacritinib may provide a novel therapeutic strategy to target HGSC cells.

We next sought to validate these findings using a second 3D growth assay model. Cells were seeded in Happy Cell Media (Vale Life Sciences) which facilitates the formation of spheroids (Section 2.3.8). Spheroids were then treated with increasing concentrations of pacritinib (1.25μM, 2.5μM and 5μM) +/– increasing concentrations of SHP099 (2.5μM, 5μM and 10μM). On day 7 viability was determined using Cell Titre-Glo® 3D and readouts were normalised as percentage viability. Synergy-Antagonism analysis was then performed using COMBENEFIT software (Section 2.3.8). Following combination treatment, we observed synergistic reduction in viability of PE01 and PE04 with limited synergy observed for OVCAR3 cells (Fig. 4.11.1). The combination of 2.5μM pacritinib and 10μM SHP099 was observed to result in a synergistic reduction in 3D growth and viability in all three HGSC cell lines tested.

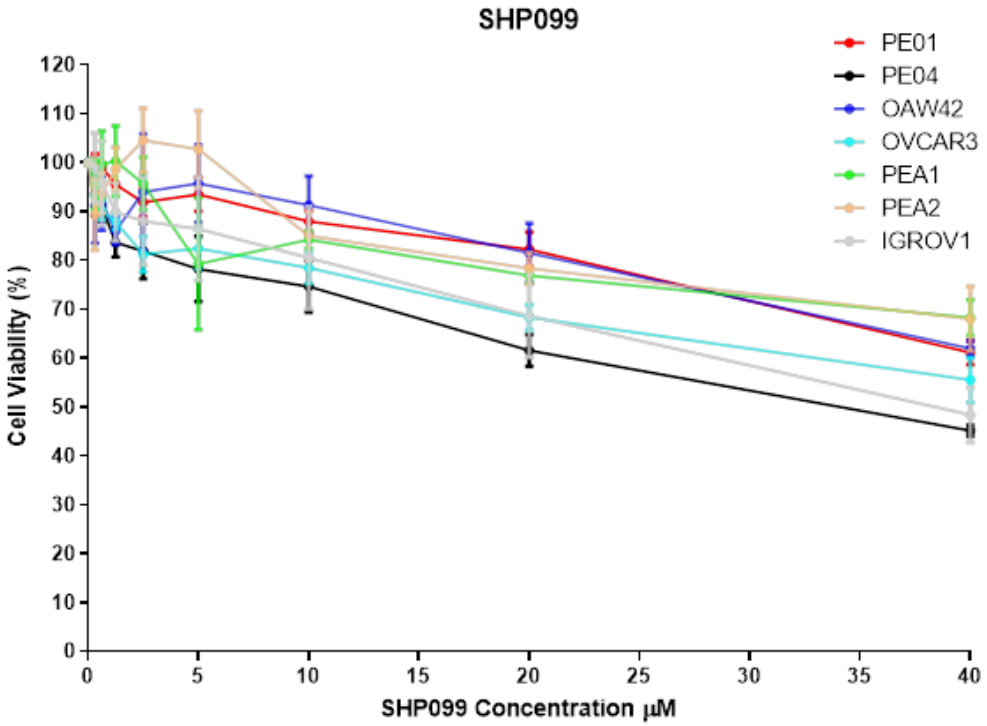

Figure 4.8.1: Treating a selection of HGSC cell lines with increasing concentrations of SHP2 inhibitor (SHP099) results in a significant decrease in cell viability at the higher range of concentrations tested. Cell viability was determined using Cell Titre-Glo® 2.0 Assay. Treatment with SHP099 resulted in a dose dependent decrease in viability in high grade serous OvCa (HGSC) cell lines PE01, PE04, OVCAR3, PEA1 and PEA2 and displayed a similar profile in the non-HGSC cell lines tested OAW42 and IGROV1. Results are representative of 3 independent experimental replicates.

Table 4.2.1: IC50 Values SHP2 inhibitor (SHP099) observed for a Selection of Ovarian Cancer Cell Lines. IC50 values were calculated using Calcusyn software.

Cell Line	Subtype	Compound	IC_{50} (μM) ± SEM
PE01	High Grade Serous Carcinoma	SHP099	>40 μM
PE04	High Grade Serous Carcinoma	SHP099	35.26 μM ± 4.94 μM
OVCAR3	High Grade Serous Carcinoma	SHP099	>40 μM
PEA1	High Grade Serous Carcinoma	SHP099	>40 μM
PEA2	High Grade Serous Carcinoma	SHP099	>40 μM
OAW42	Low Grade Serous Carcinoma	SHP099	>40 μM
ID8 Defb29 VEGF	Murine Ovarian Cancer Cell Line	SHP099	>40 μM

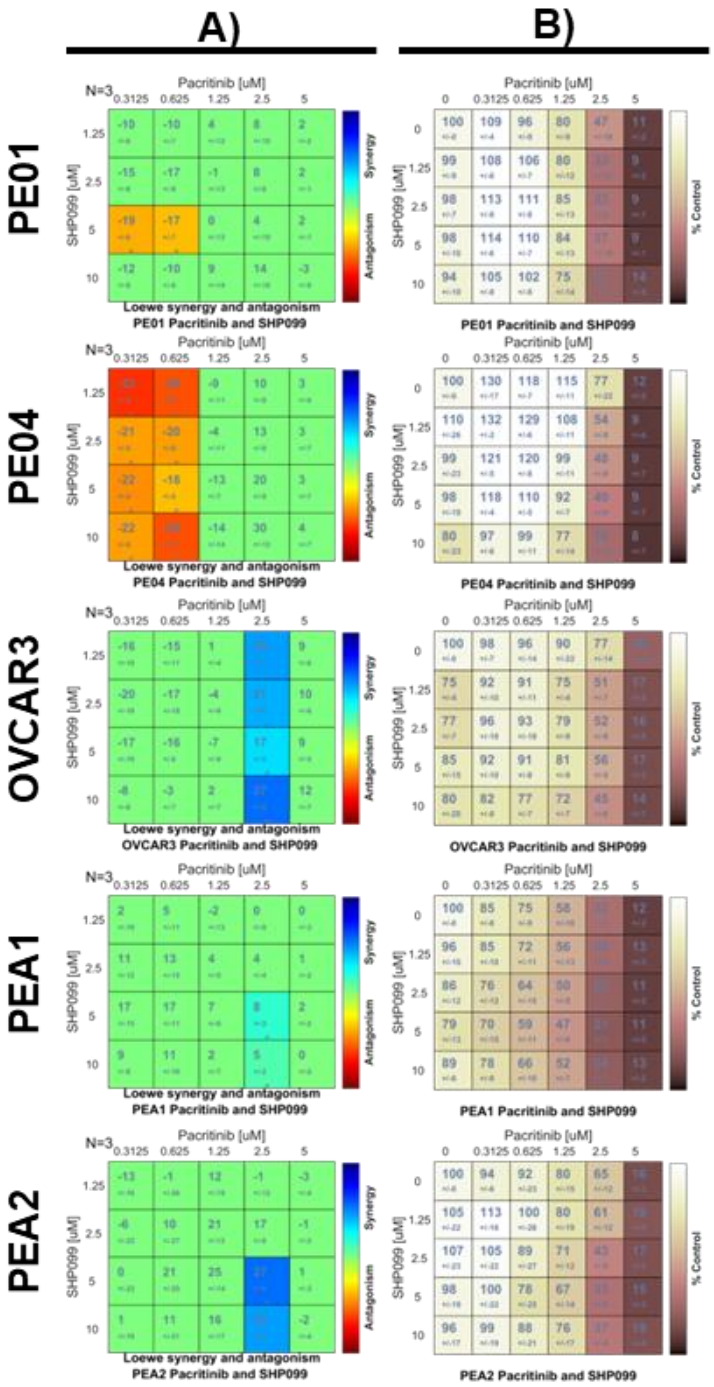

Figure 4.9.1: SHP2 inhibitor (SHP099) in combination with Pacritinib resulted in synergistic reduction in cell viability in a number of HGSC cell lines using a 2D viability assay. Cell viability was determined using Cell Titre-Glo® 2.0 Assay and relative luminescent output was measured using the Clariostar plate reader. **A)** Synergy/Antagonism analysis displays some synergistic interactions in OVCAR3, PEA1 and PEA2 cell lines and some levels of antagonism in PE01 and PE04. **B)** dose response matrices were generated using Combenefit software. Results are representative of 3 independent experiments.

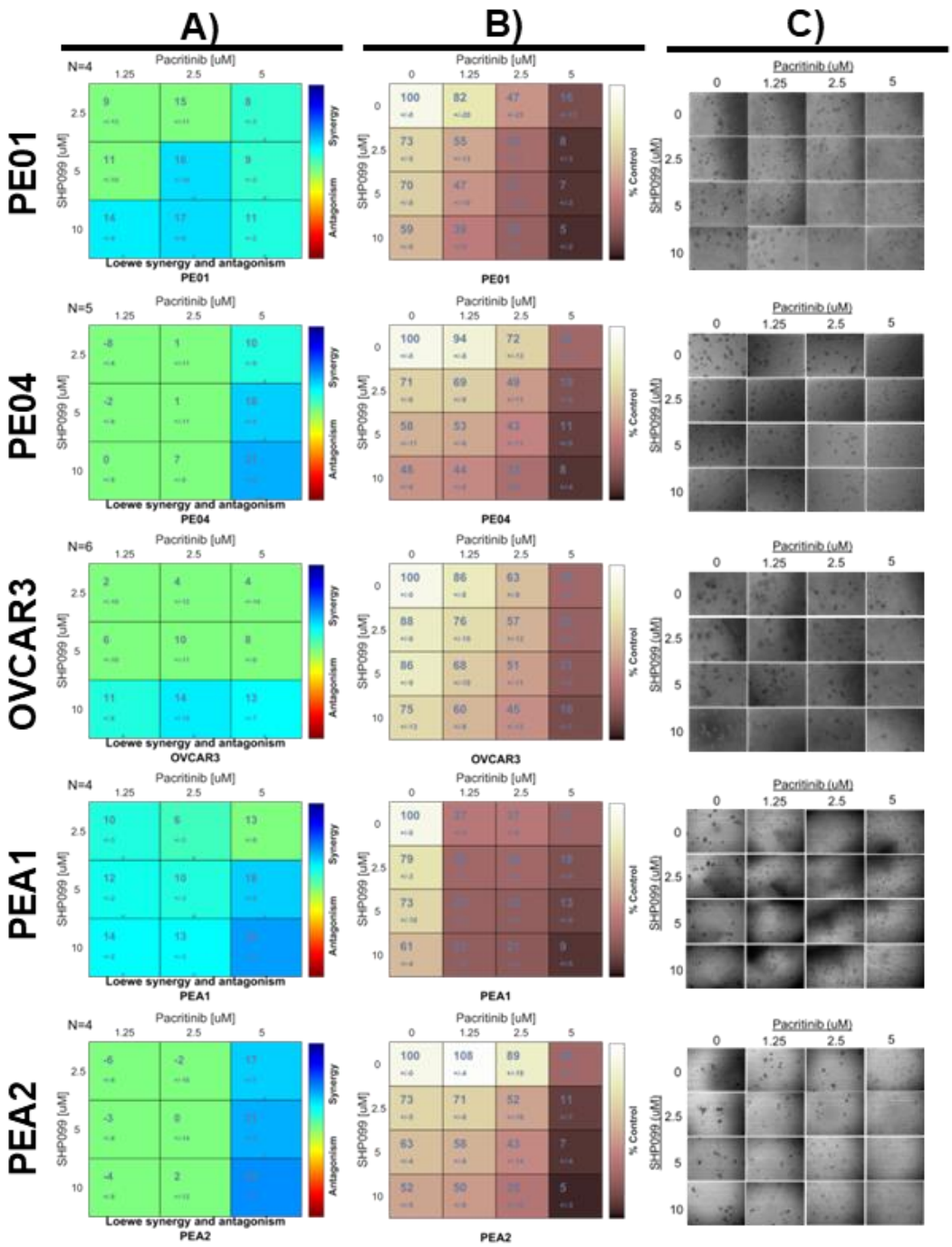

Figure 4.10.1: Pacritinib in combination with SHP099 results in synergistic reduction in 3D cell viability of HGSC cell lines. A) Treatment with pacritinib and SHP099 in combination resulted in synergistic reduction in viability in PE01, PE04, OVCAR3, PEA1 and PEA2 cells grown in 3D Matrigel matrix. **B)** dose-response matrices were generated using Combenefit software. **C)** Representative images were captured. Results are representative of greater than or equal to 4 independent replicates.

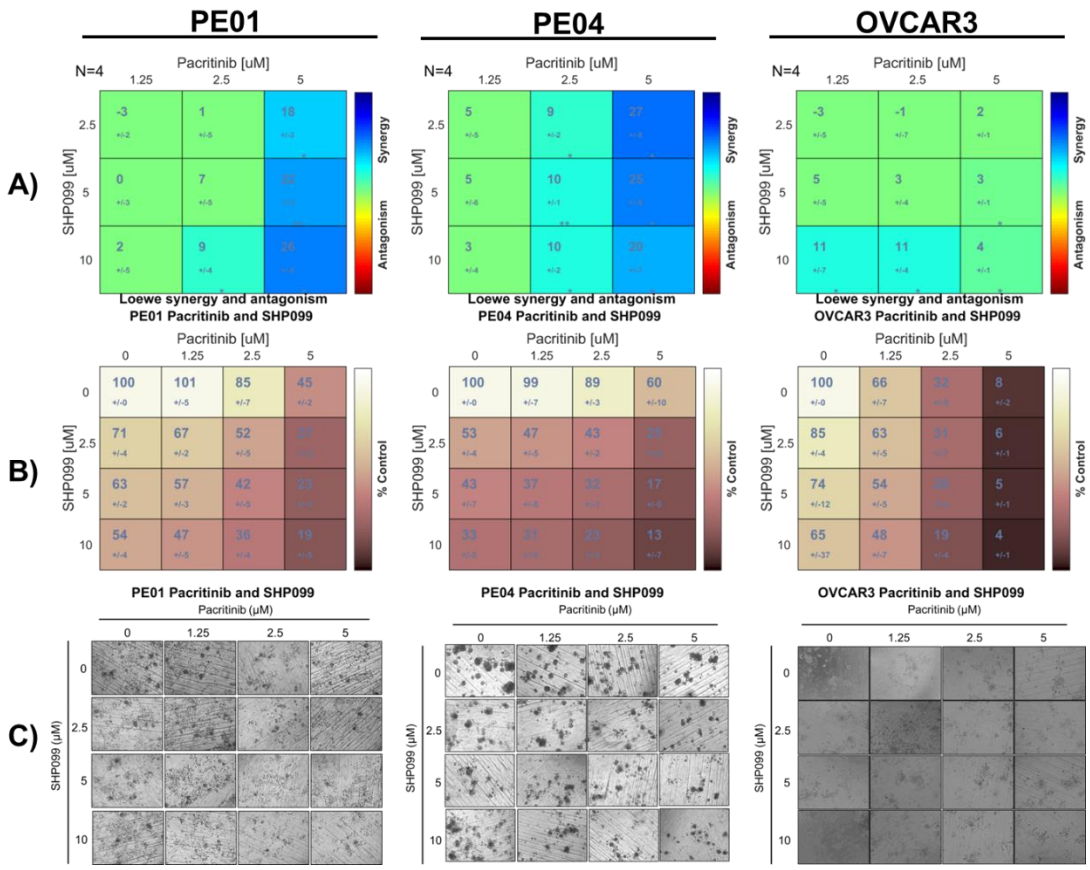

Figure 4.11.1: Pacritinib in combination with SHP099 results in synergistic reduction in viability of HGSC cells growing in 3D cultures. A) Treatment with pacritinib and SHP099 in combination resulted in synergistic reduction in viability in PE01, PE04 and OVCAR3 cells grown in 3D happy cell media matrix. **B)** dose-response matrices were generated using Combenefit software. **C)** Representative images were captured. Results are representative of greater than or equal to 4 independent replicates.

(4.2.6) Proteomics Analysis Identifies Apoptotic Pathways are Impacted Following Treatment of Cisplatin Resistant PE04 HGSC Cell Line with Pacritinib in Combination with SHP099.

Using 3D growth assays, we observed a synergistic reduction in 3D growth and viability of HGSC cell lines following treatment with pacritinib and SHP099 in combination (Section 4.2.5) (Fig. 4.10.1 and Fig 4.11.1). We next wanted to investigate the molecular mechanisms underlying this synergistic reduction in growth observed. In order achieve on this we used a multipronged approach applying proteomics analysis of protein expression, *in vitro* cell death growth assays and Western blot analysis of apoptotic markers of cell death.

The concentration of 2.5μM pacritinib and 10μM SHP099 was selected for further evaluation due to the synergistic reduction in 3D growth and viability of HGSC cell lines caused by this combination (Fig. 4.10.1 and Fig. 4.11.1).

In order to investigate the mechanisms of synergy, cisplatin-resistant PE04 cells were plated in 3D matrix using Happy Cell Media (Vale Life Sciences) and treated with 2.5μM pacritinib and 10μM SHP099 alone and in combination. These concentrations had previously been identified as synergistic in the PE04 cell line using this model (Section 4.2.5). After twenty-four hours of treatment, cells were de-suspended, whole cell lysates were prepared, and samples were processed for Mass Spectrometry using FASP methodology (Section 2.5). Raw mass spectrometry files were processed using Max Quant and proteomics analysis was carried out using PERSEUS software, Shiney Go pathway enrichment analysis and PANTHER pathway analysis.

Adjustments were made using PERSEUS to remove background and to group values based on valid values (at least three replicates in one group). Binary Comparisons were then performed and further refined to identify statistically

significant and differentially abundant targets. A total of 2644 proteins were detected for each pairwise comparison (Table 4.2.2). Once adjusted for background and detections based on valid values this reduced to 1072 detections. Non-significant (P-value greater than 0.05) and non-differentially abundant (fold change of less than 1.5) were removed from analysis.

Numerically the combination of pacritinib and SHP099 is shown to result in the largest number of statistically significant and differentially abundant proteins when compared to vehicle control or each drug alone as a control. Statistically significant and differentially abundant protein hits were visualised for each binary comparison as volcano plots (Fig. 4.12.2). This initial probing of proteomics findings indicates that the synergistic reduction in growth of HGSC cells is mirrored by a larger impact on the proteome of HGSC cells.

Principal component analysis was performed to assess clustering of individual replicates and treatments (Fig. 4.12.1). Samples which cluster together in this analysis would have similar proteomics profiles while the further away they cluster the most distinct they are from one another. Interestingly all four treatment arms (Vehicle control, SHP099 10μM, pacritinib 2.5μM and Combination) form distinct clusters, with Pacritinib and SHP099 groups showing a small level of overlap. Finally, the combination treatment showed the largest separation from the vehicle control treated cells. Two-way unsupervised hierarchical clustering was performed to generate the Heatmap displayed in this results chapter (Fig. 4.12.3). Good clustering was observed for of all four treatment groups with the combination treatment forming the most distinct group showing the largest significant difference from vehicle control. These findings taken together give us confidence that our findings are reliable and reproducible.

In Figure 4.12.4, the differences observed in significant protein abundance between binary comparisons were graphed as bar graphs in order to better convey

differences. In all binary comparisons most significantly differentially abundant proteins are decreased with a much smaller fraction being increased compared to the comparison group. Of these differentially abundant proteins the overlap between different binary comparisons were visualised in Figure 4.12.5 and this showed a high number of unique hits in the combination group compared to vehicle control or each drug alone (Fig. 4.12.5).

For the purposes of this research project we are primarily interested in the mechanism underlying the synergy observed in the 3D growth assays. This influenced the number of pathways which were followed up with due to time constraints. As such we followed up looking at the combination treatment group using vehicle control, Pacritinib alone and SHP099 alone as controls.

Pathway enrichment analysis was performed by feeding statistically significantly differentially expressed proteins into SHINEY GO and the findings from this are shown in Tables 4.2.3 to 4.2.5. Pathway enrichment analysis identifies a large number of pathways impacted following the combination treatment compared to all three controls. Interestingly, mismatch repair and DNA replication pathways were identified in the combination treated cells compared to both vehicle control and pacritinib alone. Both of these pathways were not identified while using SHP099 treatment as a control. This may indicate that SHP099 treatment alone or in combination may be contributing to the impact observed on these pathways in the combination treatment group.

Finally, Pathway analysis was performed using PANTHER for combination compared to all three comparison groups (Fig. 4.12.6, Fig. 4.12.7 and Fig.4.12.8). We observed a high number of impacted pathways being detected in the combination treatment compared to all three comparison groups. Interestingly, the apoptotic signalling pathway was identified in the combination group when compared to vehicle control, SHP099 alone and pacritinib alone. Given the synergistic reduction in viability

these findings presented a potential mechanism to explain our *in vitro* findings and warranted further evaluation of the role of cell death following treatment with pacritinib and SHP099 in combination.

Table 4.2.2: A total of 2644 proteins were detected through mass spectrometry analysis of HGSC cell line PE04 treated with Pacritinib (2.5uM), SHP099 (10uM), the combination of both or vehicle control in a 3D *in vitro* growth assay model. Adjustments were made to remove background, and groups were filtered based on valid values (at least 3 replicates in one group). Finally, proteins with a P value greater than 0.05 and a fold change of less than 1.5 were removed.

Parameters Applied	Vehicle Control vs Pacritinib 2.5µM	Vehicle Control vs SHP099 10µM	Vehicle Control vs Combination	Pacritinib 2.5µM vs Combination	SHP099 10µM vs Combination
Total Protein Detections	2644	2644	2644	2644	2644
Number of proteins following adjustment for Background	2465	2465	2465	2465	2465
Detections – based on valid values	1072	1072	1072	1072	1072
Significant ($p<0.05$) Different (1.5-fold)	52	30	192	93	86

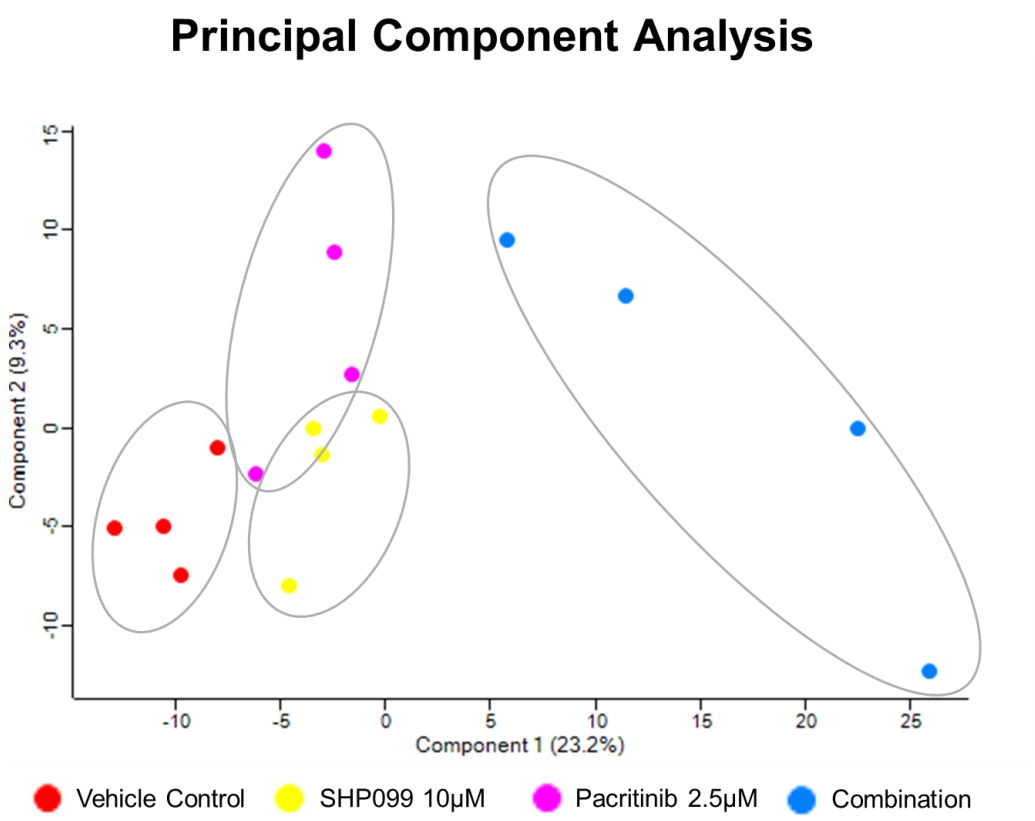

Figure 4.12.1: Principal Component Analysis shows clustering of combination technical replicates and good separation from vehicle control and single treatments pacritinib and SHP099 groups. PE04 cells cultured in 3D happy cell media matrix were treated with vehicle control, Pacritinib (2.5µM), SHP099 (10µM) or the combination of both drugs for 24hrs. Principal component analysis was performed using PERSEUS software and displays good clustering for all four treatment arms and good separation of the combination treated cluster.

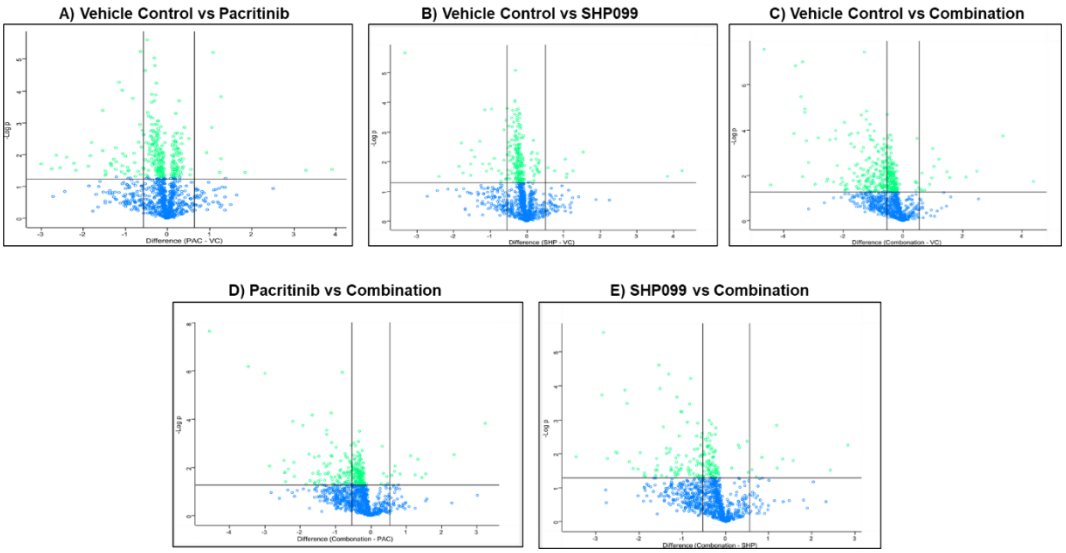

Figure 4.12.2: Volcano plots showing binary comparison of treatment arms in the PE04 cell line. Total protein detections adjusted to exclude background and filtered based on valid values (detected in at least 3 replicates in one group) were determined. Binary comparisons between vehicle control, Pacritinib and SHP099 and their combination, was performed and volcano plots were generated from these binary comparisons. Significant proteins (highlighted in green), appear above the horizontal axis included. This axis was set at $-\log_{10}(0.05) = 1.3010$ and non-significant proteins (Blue, p-value ≥ 0.05) appear below the horizontal axis. Vertical axes were included at 0.59 and -0.59, between which fold changes are less than 1.5-fold. The combination of Pacritinib and SHP099 results in the greatest number of statistically significant differentially abundant proteins compared to control or either drug alone.

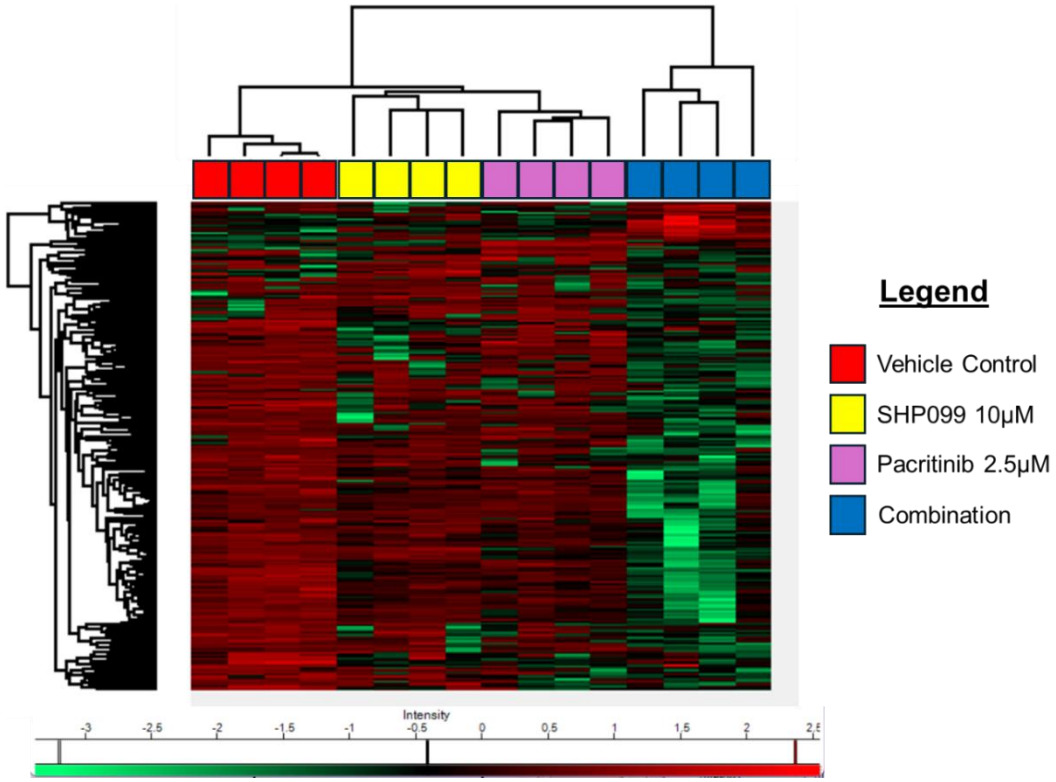

Figure 4.12.3: Heatmap clustering shows the combination of SHP099 (10μM) and Pacritinib 2.5μM displays the most distinct phenotype with the most distinct statistically significant differentially abundant protein profile in PE04 cell line. Using Perseus software protein lists were further refined to exclude non-significant protein hits (p-value ≥0.05) and proteins which displayed a fold change less than 1.5. Two-way unsupervised hierarchical clustering was then performed and the above heatmap was generated using Perseus. Green represents a decrease in abundance while red indicates an increase in abundance. All treatment arms formed individual distinct groups with the SHP099 and pacritinib combination displaying the most pronounced phenotype with many proteins decreased in abundance compared to vehicle control or either drug alone.

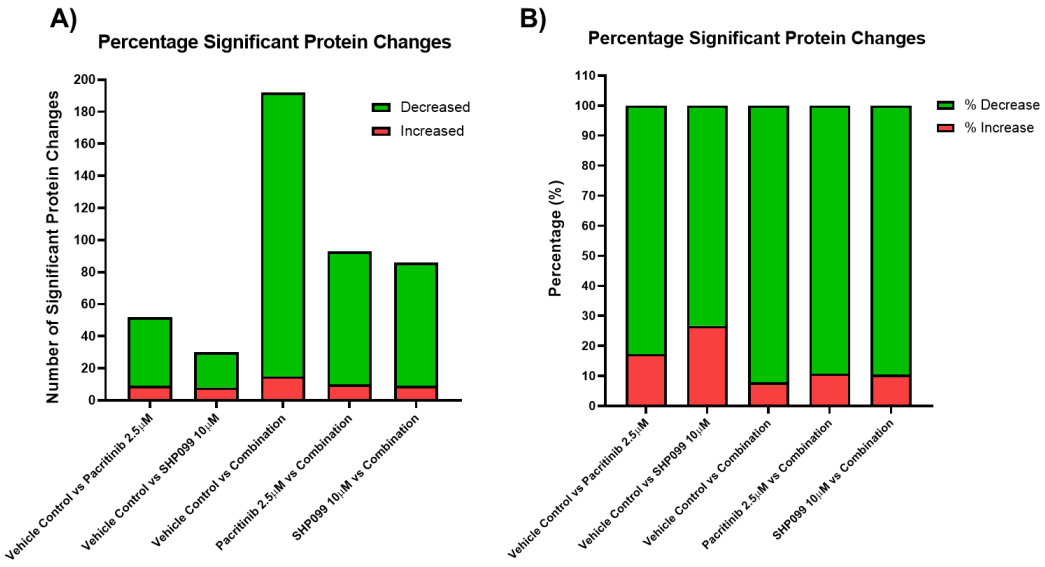

Figure 4.12.4: The combination of Pacritinib and SHP099 result in the highest number of statistically significant and differentially abundant protein in the PE04 cell line *in vitro*. The number of statistically significant (p-value<0.05) and differentially abundant (fold-change > 1.5) identified above were graphed as total and percentage changes for each treatment arm binary comparison. Following the combination of Pacritinib and SHP099 (compared to vehicle control), in HGSC PE04 cell line *in vitro*, the largest number of statistically significant and differentially abundant protein changes was observed (192), and of these over 80% were reduced compared to vehicle control. Treatment with Pacritinib and SHP099 alone similarly resulted in 52 and 30 statistically significant and differentially abundant protein hits compared to vehicle control. Of these the vast majority (<70%) were reduced compared to vehicle control.

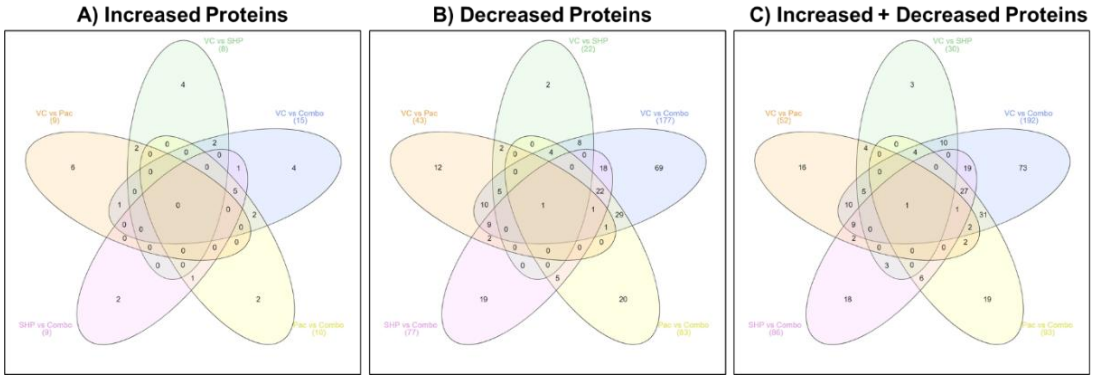

Figure 4.12.5: The combination of Pacritinib and SHP099 result in the highest number of unique statistically significant and differentially abundant proteins in the PE04 cell line in vitro. Statistically significant (p-value<0.05) and differentially abundant (fold-change > 1.5) identified above were compared and overlapping proteins between these binary comparisons were identified and visualised in the Venn diagram above. The combination of Pacritinib and SHP099 shows a high number of proteins unique to this group in binary comparisons to vehicle control (73), SHP099 10μM (18) and Pacritinib 2.5μM (19).

Table 4.2.3: Pathway enrichment analysis for vehicle control vs Pacritinib (2.5μM) and SHP099 (10μM) combination. Statistically significant and differentially expressed proteins for the binary comparison between control vs combination were input to perform pathway enrichment analysis using SHINEY GO. The three most enriched pathways included DNA replication, mismatch repair and the citrate cycle.

Pathway	Pathway Genes	nGenes	Fold Enrichment	Enrichment FDR
DNA Replication	36	5	17.5	2.4E-04
Mismatch Repair	23	3	16.4	9.3E-03
Citrate Cycle (TCA Cycle)	30	3	12.6	1.5E-03
Spliceosome	131	10	9.6	1.5E-02
Ribosome	134	10	9.4	7.1E-06
Nucleocytoplasmic Transport	108	8	9.3	8.8E-05
mRNA Surveillance Pathway	97	7	9.1	2.8E-04
RNA Degradation	79	5	8	6.7E-03
Coronavirus Disease – Covid-19	232	14	7.6	9.8E-07
Nucleotide Metabolism	85	5	7.4	7.6E-03
Protein Processing in Endoplasmic Reticulum	169	9	6.7	2.4E-4
Cell Cycle	126	6	6	7.2E-03
Influenza A	171	7	5.1	6.7E-03
Biosynthesis of Cofactors	153	6	4.9	1.4E-02
Hepatitis C	157	6	4.8	1.5E-02
Epstein-Barr Virus Infection	202	7	4.4	1.3E-02
Diabetic Cardiomyopathy	203	7	4.3	1.3E-02
Parkinson Disease	266	9	4.3	5.2E-03
Amyotrophic Lateral Sclerosis	364	12	4.1	7.4E-04
Metabolic Pathways	1538	33	2.7	7.1E-06

Table 4.2.4: Pathway enrichment analysis for Pacritinib (2.5μM) vs combination. Statistically significant and differentially expressed proteins for the binary comparison Pacritinib vs Combination were used to perform pathway enrichment analysis using SHINY GO software. The three most enriched pathways include mismatch repair, proximal tubule bicarbonate reclamation and DNA replication.

Pathway	Pathway Genes	nGenes	Fold Enrichment	Enrichment FDR
Mismatch Repair	23	2	22.9	3.9E-02
Proximal Tubule Bicarbonate Reclamation	23	2	22.9	3.9E-02
DNA Replication	36	3	21.9	9.6E-03
Cysteine and Methionine Metabolism	50	3	15.8	1.6E-02
Biosynthesis of Amino Acids	74	4	14.2	8.4E-03
Pyrimidine Metabolism	58	3	13.6	2.2E-02
MRNA Surveillance Pathway	97	4	10.8	1.0E-02
Ribosome	134	5	9.8	8.4E-03
Biosynthesis of Cofactors	153	5	8.6	9.6E-03
Protein Processing in Endoplasmic Reticulum	169	5	7.8	1.0E-02
Endocytosis	251	5	5.2	3.7E-02
Metabolic Pathways	1538	18	3.1	2.2E-03

Table 4.2.5: Pathway enrichment analysis for SHP099 (10μM) vs combination. Statistically significant and differentially expressed proteins for the binary comparison SHP099 vs Combination were used to perform pathway enrichment analysis using SHINY GO software. The three most enriched pathways including the citrate cycle, histidine metabolism and ascorbate and Aldarate metabolism.

Pathway	Pathway Genes	nGenes	Fold Enrichment	Enrichment FDR
Citrate Cycle (TCA Cycle)	4	30	35.9	1.9E-04
Histidine Metabolism	2	22	24.5	3.0E-02
Ascorbate and Aldarate Metabolism	2	30	17.9	4.5E-02
Beta-Alanine Metabolism	2	31	17.4	4.5E-02
Pyruvate Metabolism	3	47	17.2	1.1E-02
Arginine and Proline Metabolism	3	50	16.2	1.1E-02
Glycolysis / Gluconeogenesis	3	67	12.1	2.2E-02
Hepatitis C	7	157	12	1.5E-04
Spliceosome	5	131	10.3	3.2E-03
Measles	5	139	9.7	3.5E-03
Carbon Metabolism	4	115	9.4	1.1E-02
Coronavirus Disease – COVID-19	8	232	9.3	1.5E-04
AGE-RAGE Signalling Pathway in Diabetic Complications	3	100	8.1	4.5E-02
Epstein-Barr Virus Infection	6	202	8	3.2E-03
Influenza A	5	171	7.9	7.8E-03
Proteoglycans in Cancer	4	202	5.3	4.5E-02
Diabetic Cardiomyopathy	4	203	5.3	4.5E—02
Parkinson Disease	5	266	5.1	3.0E-02
Human Papillomavirus Infection	5	331	4.1	4.8E-02
Metabolic Pathways	13	1538	2.3	3.8E-02

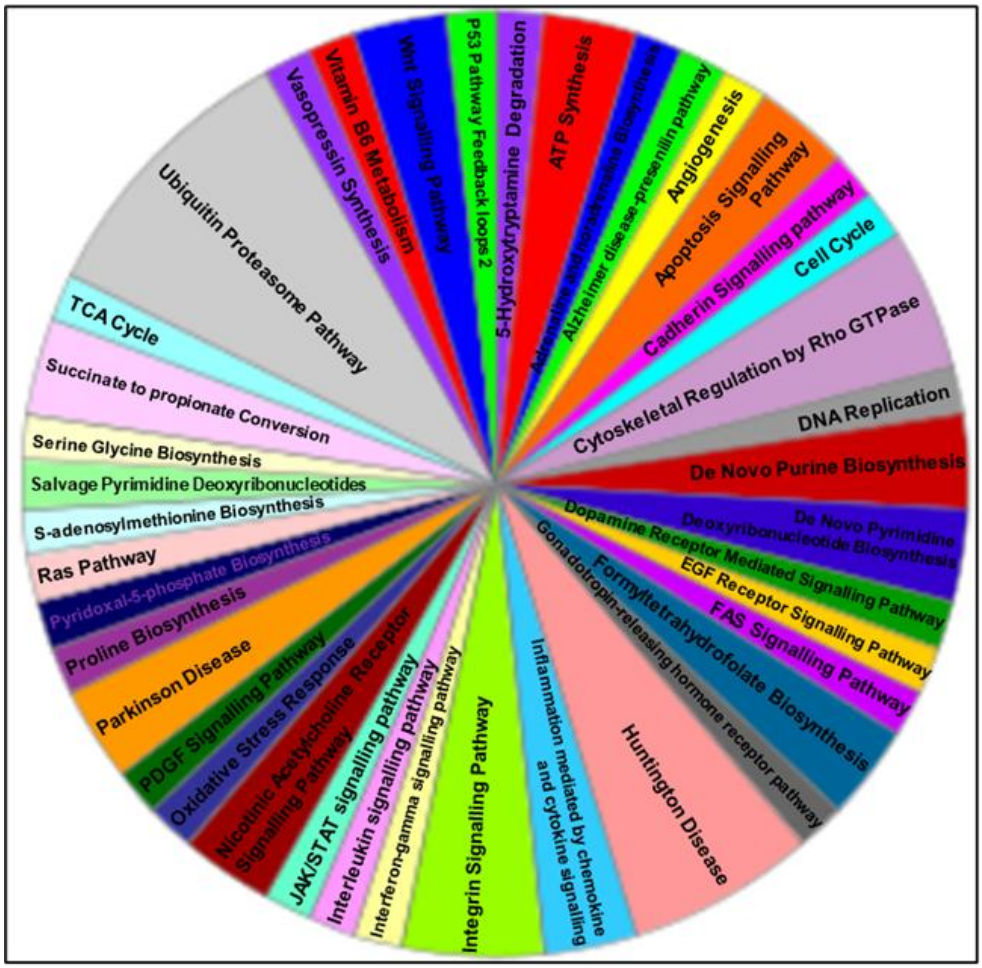

Figure 4.12.6: Panther pathway analysis identifies a range of biological processes including Apoptosis following treatment with Pacritinib (2.5μM) and SHP099 (10μM) compared to vehicle control. Statistically significant and differentially expressed proteins identified above were fed into Panther allowing for the visualisation of related biological process gene ontology terms for these proteins. The combination of Pacritinib and SHP099 in the high grade serous ovarian cancer cell line (PE04) resulted in a wide variety of impacted biological processes compared to vehicle control.

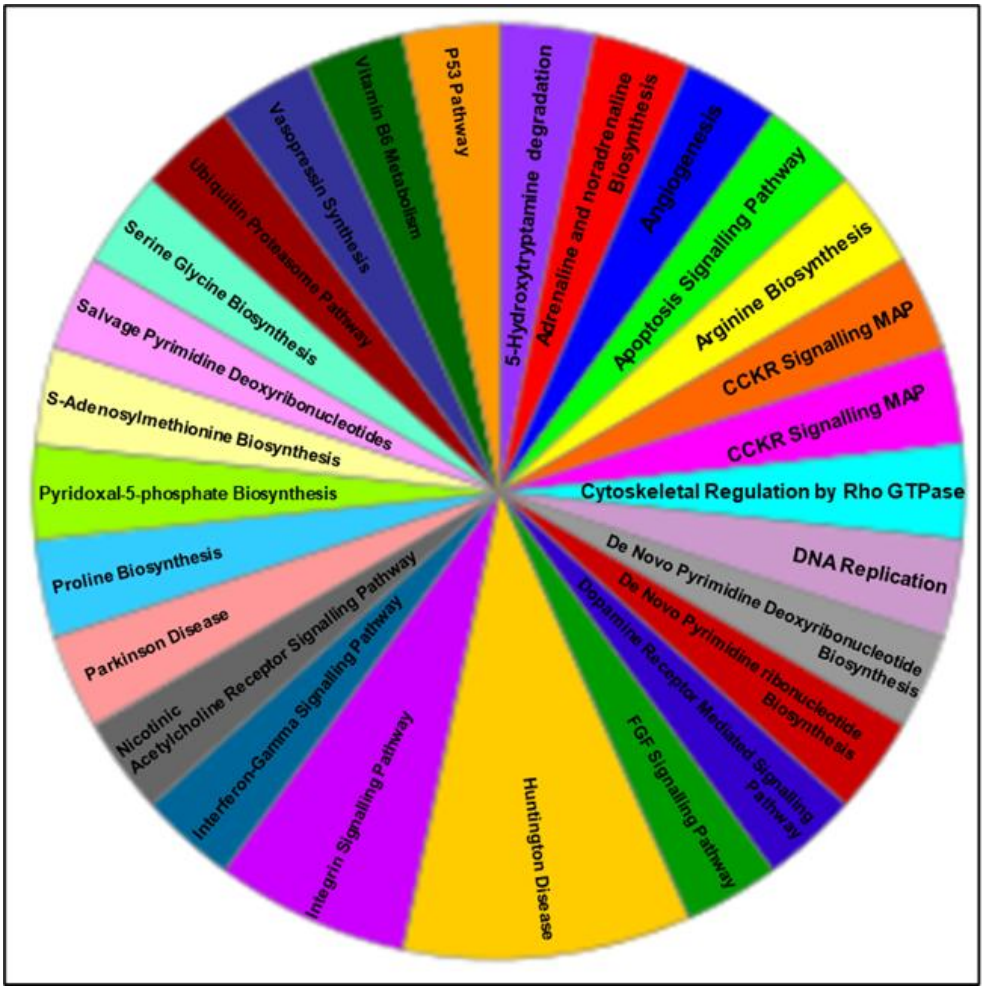

Figure 4.12.7: Panther pathway analysis identifies a several impacted pathways including Apoptosis following treatment with the combination of Pacritinib (2.5μM) and SHP099 (10μM) compared to SHP099 alone. Statistically significant and differentially expressed proteins identified above were fed into Panther allowing for the visualisation of related biological process gene ontology terms for these proteins. The combination of Pacritinib and SHP099 in the HGSC cell line PE04 resulted in a wide variety of impacted biological processes compared to SHP099 alone.

Figure 4.12.8: Panther pathway analysis highlights impacted Apoptosis following treatment with the combination of Pacritinib (2.5μM) and SHP099 (10μM) compared to Pacritinib alone. Statistically significant and differentially expressed proteins identified above were fed into Panther allowing for the visualisation of related biological process gene ontology terms for these proteins. The combination of Pacritinib and SHP099 in the HGSC cell line PE04 in vitro displayed a wide variety of impacted biological processes compared to Pacritinib alone.

(4.2.7) The Combination of Pacritinib and SHP099 Results in Elevated Levels of Cell Death in HGSC Cell Lines using 3D *In Vitro* Growth Assay Models.

Panther pathway analysis showed that apoptotic signalling pathways were impacted following treatment with pacritinib and SHP099 in combination (Section 4.2.6). We wanted to further investigate if increased levels of apoptotic cell death could explain the synergistic reduction in 3D growth and viability of HGSC cell lines which we observed (Fig. 4.10.1 and Fig. 4.11.1). To achieve this, we carried out fluorescence-based growth assays to measure cell death (Section 2.3.7).

PE01, PE04 and OVCAR3 HGSC single spheroids were treated with vehicle control or pacritinib (2.5μM) +/- SHP099 (5μM/10μM). Cells were stained with Incucyte® Cytotox Red Dye which measures loss of membrane integrity (cell death). Readings were taken every six hours for brightfield and red fluorescence. Readouts were finally normalised as a percentage of vehicle control (Fig. 4.13.1 and Fig. 4.13.2).

Treatment with pacritinib and SHP099 in combination resulted in a reduction in PE04 and OVCAR3 spheroid size compared to control treated spheroids (Fig. 4.13.1). However, there was no noticeable reduction in spheroid size observed for the PE01 cell line (Fig. 4.13.1). Interestingly both pacritinib and SHP099 led to a reduction in PE04 and OVCAR3 spheroid size as solo treatments while only SHP099 led to reduced spheroid size in PE01 cells. Treatment with pacritinib was observed to result in an increase in cell death for all three HGSC cell lines (Fig 4.13.2). Interestingly the combination of pacritinib and SHP099 led to an increase in cell death levels in the PE01 cell line, while it appears that cell death levels in PE04 and OVCAR3 were approximately equivalent to pacritinib treated cells (Fig. 4.13.2). These findings

provide an indication that cell death is occurring following treatment with SHP099 and pacritinib in combination.

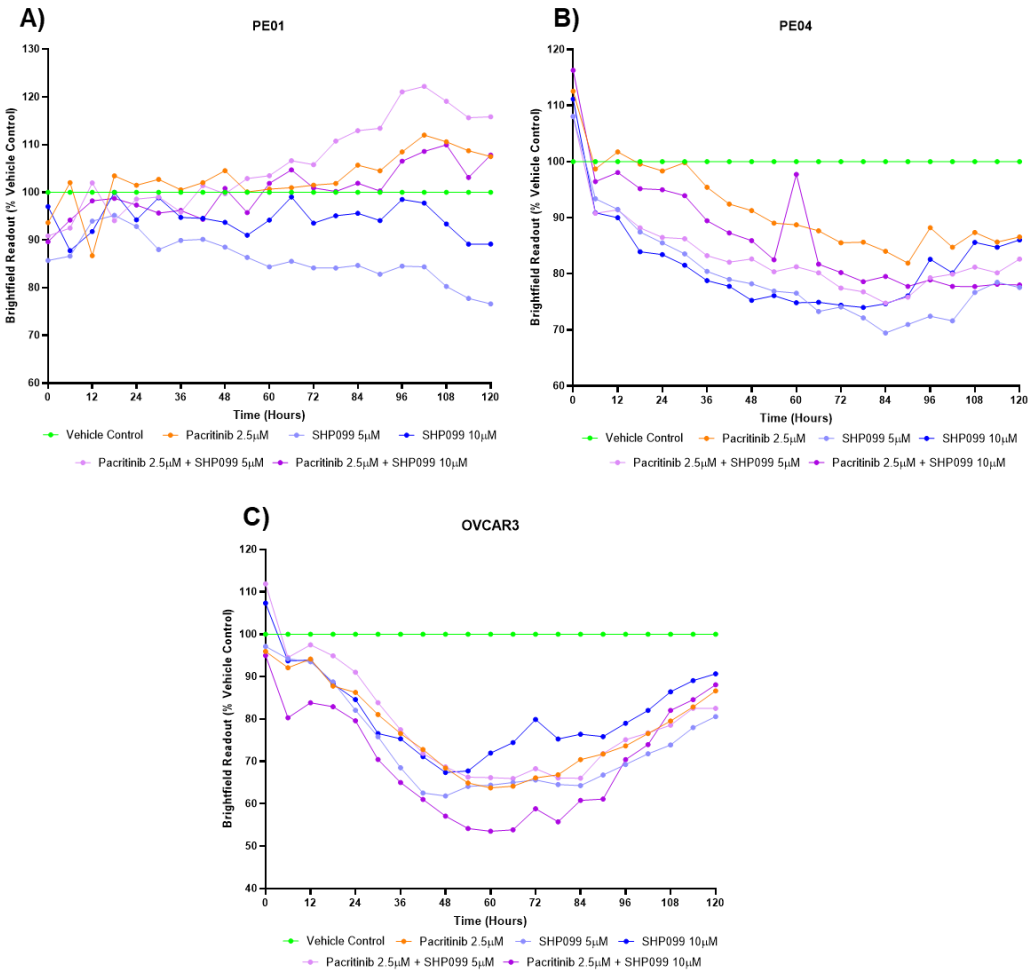

Figure 4.13.1: The combination of Pacritinib and SHP099 displays reduced 3D spheroid size in Cis-Platin resistant HGSC cell Lines PE04 and OVCAR3 in vitro. All treatments result in a reduction in spheroid size in **B)** PE04 and **C)** OVCAR3 cell lines while only 5μM SHP099 appears to reduce spheroid size in **A)** PE01. Results are representative of N=2 for each timepoint. This work was done in collaboration with Dr Neil Conlon (DCU) and Luna Stockman (DCU).

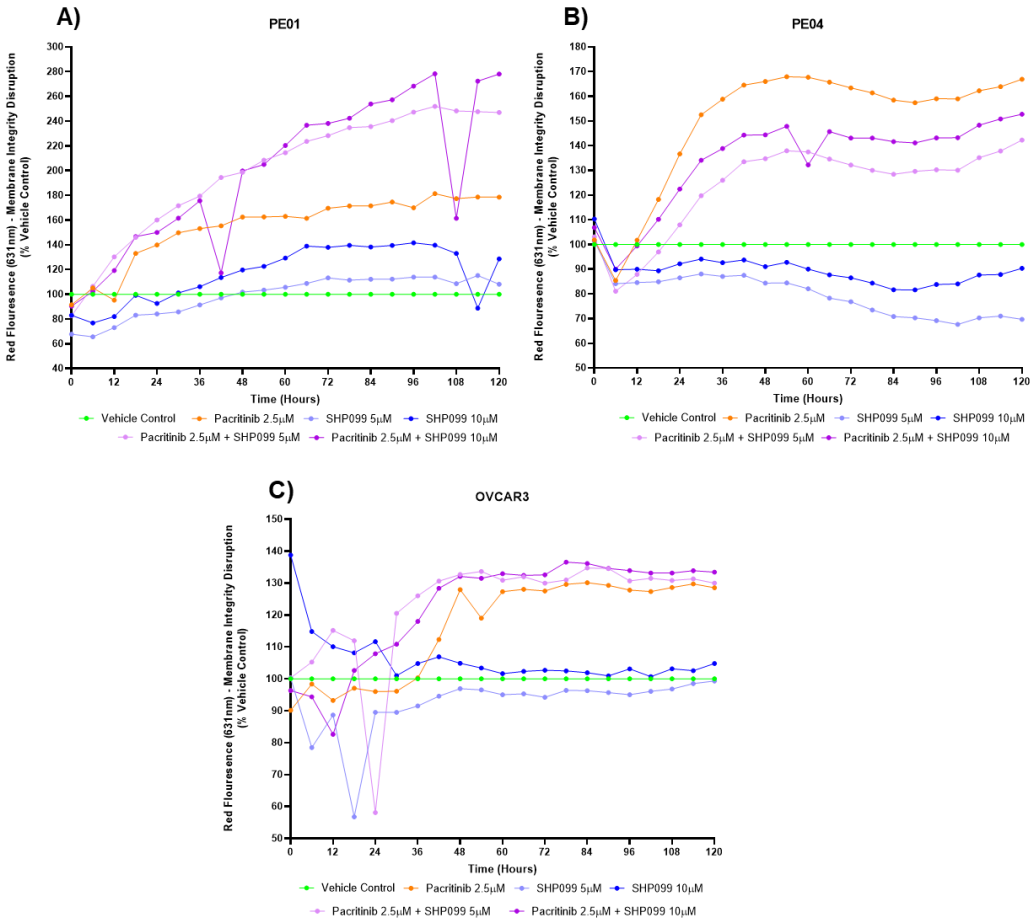

Figure 4.13.2: The combination of Pacritinib and SHP099 displays loss of membrane integrity in HGSC cell lines. Incucyte® Cytotox Red Dye (Sartorius Cat. No. 4632) was used to measures loss of membrane integrity (cell death). SHP099 appears to result in limited loss of membrane integrity in **A)** PE01 and **C)** OVCAR3 while Pacritinib results in loss of membrane integrity in all three HGSC cell lines. Combination of Pacritinib and SHP099 shows elevated loss of membrane integrity in **A)** PE01 and **B)** OVCAR3 (18-36hr) while in **C)** PE04 this appears to be slightly reduced. Results are representative of N=2 for each timepoint. This work was done in collaboration with Dr Neil Conlon (DCU) and Luna Stockman (DCU).

(4.2.8) The Combination of Pacritinib and SHP099 Results in Elevated Levels of Molecular Markers of Apoptotic Cell Death in HGSC Cell Lines.

To further investigate the role of cell death in the synergistic reduction of HSGC 3D growth and viability following combination of pacritinib and SHP099 (Section 4.2.7), we progressed to investigating molecular markers of apoptotic cell death using Western blot analysis. Cisplatin resistant HGSC PE04 cells were treated with vehicle control, 2.5μM Pacritinib, 10μM SHP099, the combination of both inhibitors and as a control high dose (25μM) of cisplatin. After twenty-four hours of treatment whole cell lysates were collected and profiled for markers of apoptosis.

Following combination of pacritinib and SHP099 we observed cleavage of caspase 3 (marker of apoptotic cell death) in PE04 cells (Fig. 4.14.1). Cleaved caspase 3 was also detectable in the positive control (cisplatin treatment) but was undetectable by Western blot in vehicle control, pacritinib alone or SHP099 alone treated spheroids (Fig. 4.14.1). These findings indicate that increased levels of apoptotic cell death are occurring in the cisplatin resistant PE04 HGSC cell line following combination treatment with pacritinib and SHP099 in 2D. These results support our proteomics findings (SECTION 4.2.6).

We additionally profiled the levels of PARP cleavage in PE01, PE04 and OVCAR3 cell lines treated with vehicle control, pacritinib (2.5μM), SHP099 (10μM) or the combination. Interestingly we observed significantly increased levels of cleaved PARP following treatment with pacritinib alone and the combination of pacritinib and SHP099 in all three cell lines assessed (Fig. 4.15.1 and Fig. 4.15.2). In the combination treated PE01 cell line PARP cleavage is significantly increased compared to pacritinib alone, while for PE04 an increase is observed although this was not observed to be significant. While in the OVCAR3 cell line PARP cleavage

appears to be relatively equal for both the Pacritinib treated and combination treated cells. Full length PARP was observed to be significantly decreased in combination treated PE01 cells while for PE04 cells full length PARP was significantly decreased in both pacritinib and combination treated cells. These findings also agree with the proteomics findings we observed (Section 4.2.6) and indicate that treatment with pacritinib and SHP099 may be inhibiting growth and viability of HGSC cells through stimulating cell death.

Interestingly treatment with SHP099 and pacritinib in combination resulted in reduced SHP2 expression in PE01 cells (Fig. 4.16.1 and Fig 4.16.2). This result was not mirrored in the paired PE04 cells. SHP099 is known to inhibit ERK activation and at the concentrations evaluated SHP099 both alone and in combination with pacritinib led to a reduction in ERK activation in PE04 and OVCAR3 cell lines (Fig. 4.16.1 and Fig 4.16.3).

It is clear that our western blot findings displaying cleaved PARP indicates that apoptotic cell death is occurring in all three cell lines in pacritinib treated and combination treated HGSC cells. This does not fully align with our Incucyte findings which only detected cell death in PE01 cells. This may be due to the difference in sensitivity of these two experiments as they are measuring different outputs. Potentially in vitro growth assays measuring different markers of apoptosis, such as caspase 3 or 7 cleavage, could be used to assess apoptosis in these cell lines.

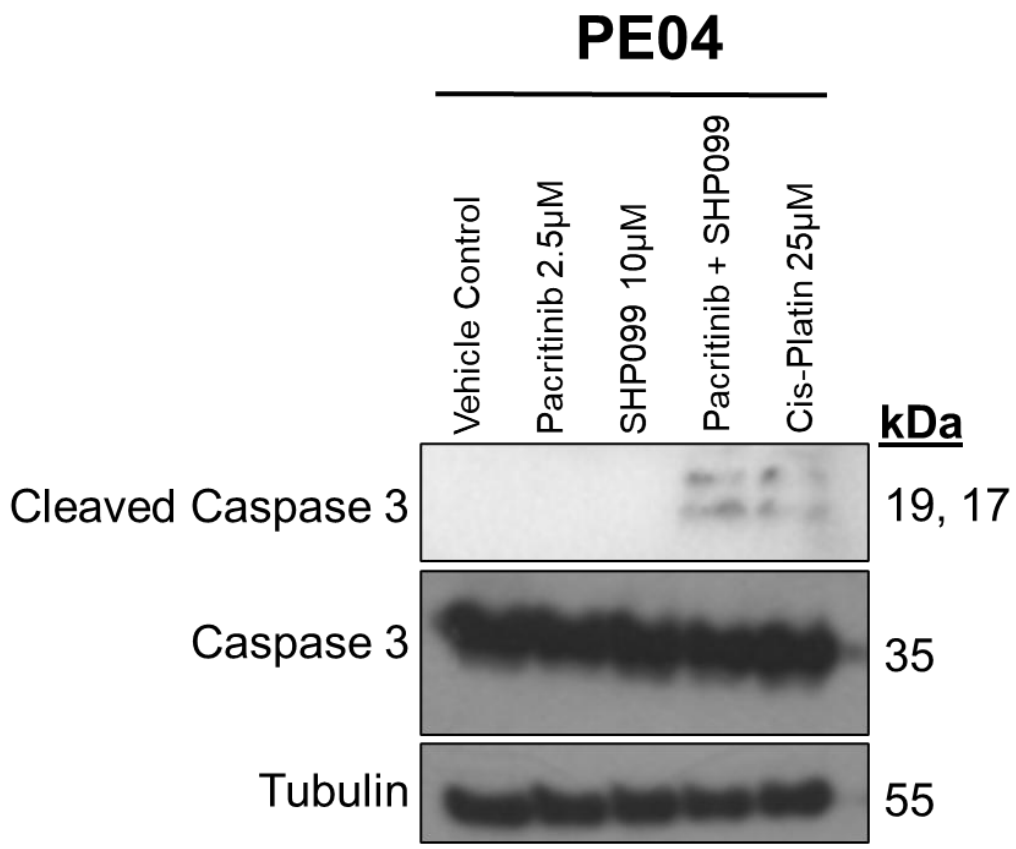

Figure 4.14.1: Pacritinib in combination with SHP099 results in increased cleavage of Caspase 3 in the HGSC PE04 cell line. Treatment with SHP099 and pacritinib in combination resulted in increased cleavage of Caspase 3 detected by western blot analysis. Results are representative of n=2.

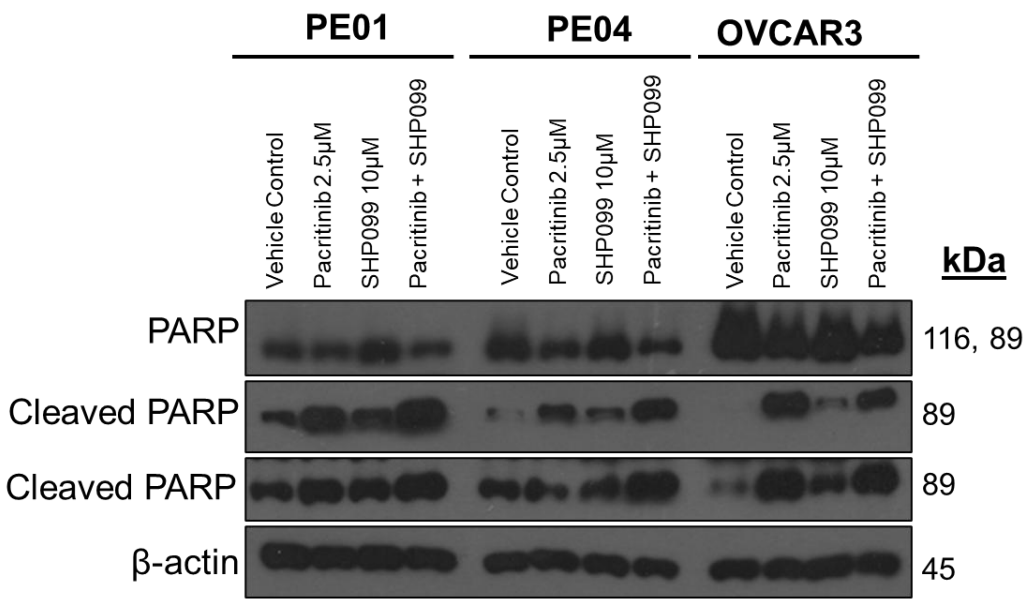

Figure 4.15.1: The combination of Pacritinib and SHP099 results in increased levels of cleaved PARP in HGSC cell lines. Treatment with pacritinib both alone and in combination with SHP099 resulted in an increase in PARP cleavage (detected by western blot analysis) in PE01, PE04 and OVCAR3 cells. PARP cleavage in combination treated cells appears to be elevated compared to pacritinib treated cells in PE01 and PE04 cells. Results shown for PARP + Cleaved PARP are representative of n=5.

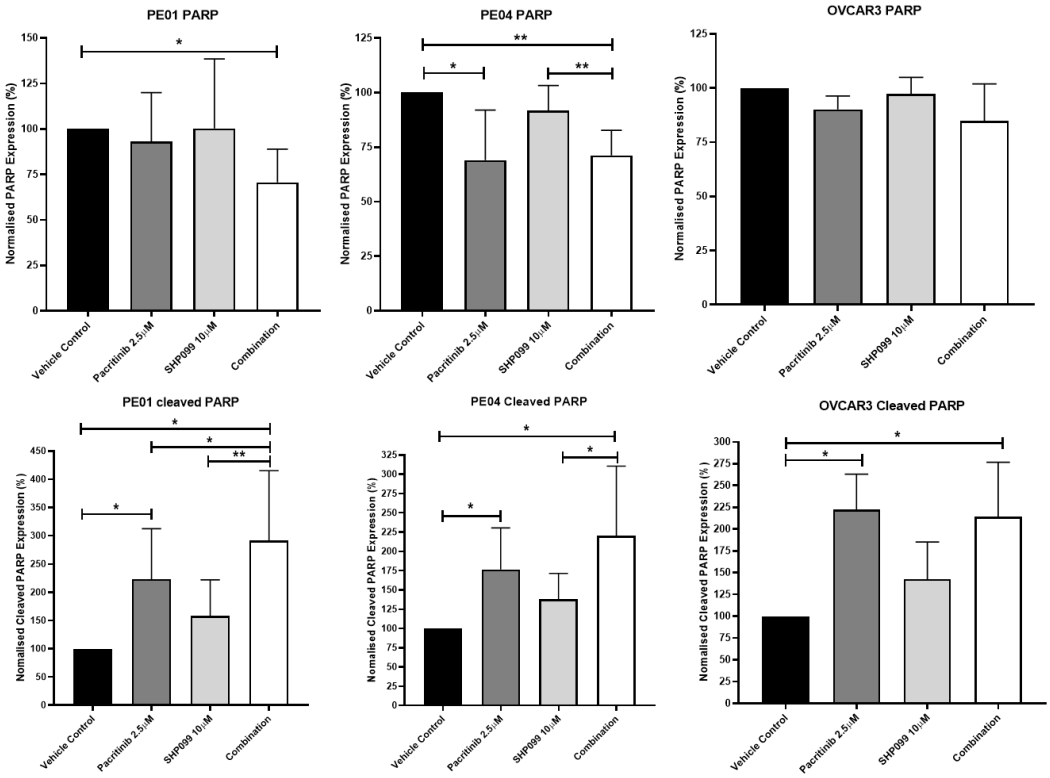

Figure 4.15.2: Densitometry analysis shows PARP cleavage following combination of pacritinib (2.5μM) and SHP099 (10μM) in PE01, PE04 and OVCAR3 cell lines. Treatment with pacritinib both alone and in combination with SHP099 resulted in an increase in PARP cleavage (detected by western blot analysis) in PE01, PE04 and OVCAR3 cells. PARP cleavage in combination treated cells appears to be elevated compared to pacritinib treated cells in PE01 and PE04 cells. Full length and cleaved PARP fragments were detected by Western blot and band intensity was measured using Image J densitometry. PARP and cleaved PARP expression was normalised using β-actin loading control and presented as a percentage of vehicle control expression. Statistical significance was assessed (PRISM) through paired students t-test comparisons. , p-values; (*;≤0.05), (**;≤0.01). Results are representative of five independent replicates.

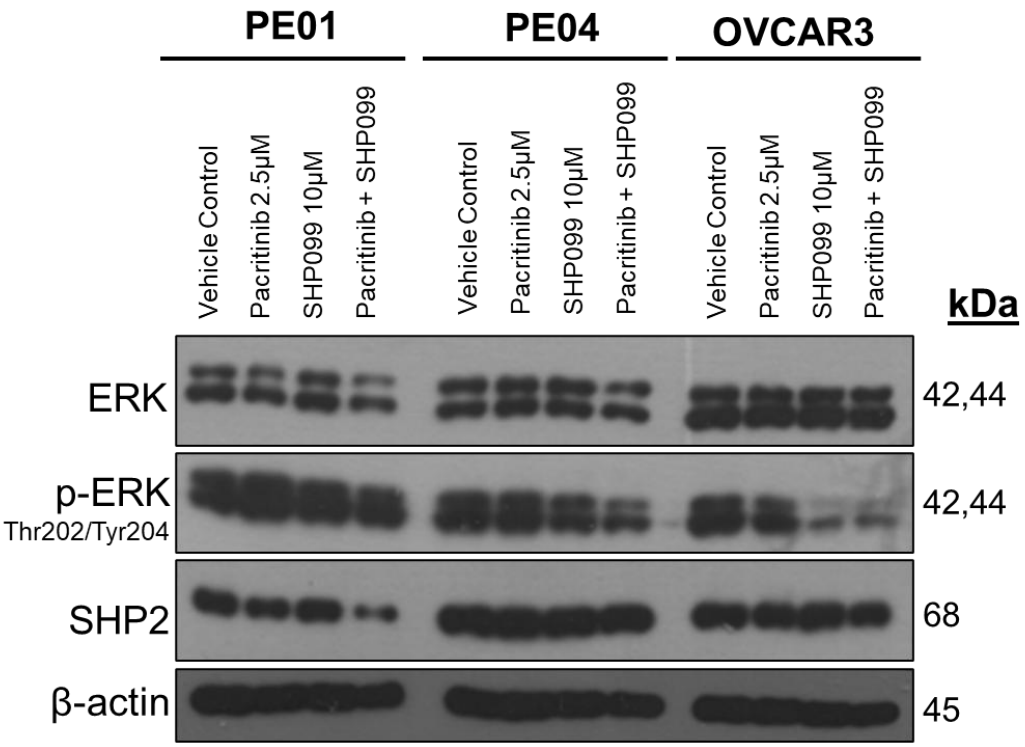

Figure 4.16.1: The combination of Pacritinib and SHP099 results in reduced ERK activation and SHP2 expression in HGSC cell line. SHP2 protein expression was observed to be decreased in combination treated PE01 cells. SHP099 and combination treated cells display a reduction in the activation of ERK. ERK, p-ERK, SHP2 western blots are representative of n=4.

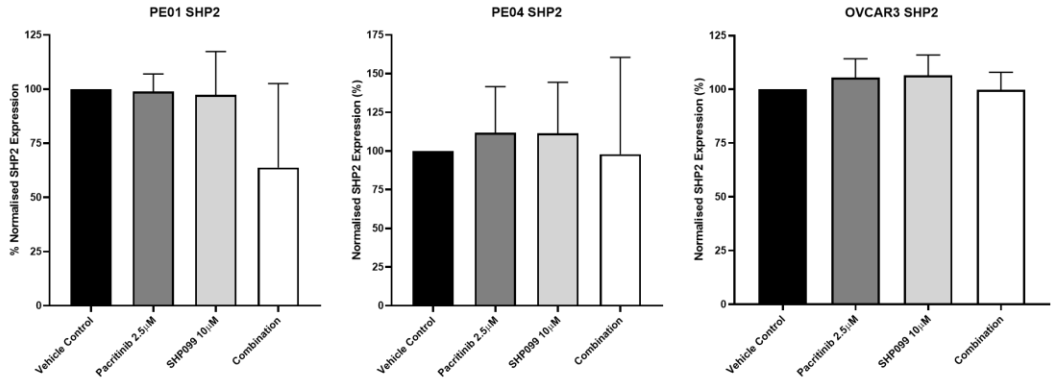

Figure 4.16.2: Densitometry analysis shows decreased SHP2 levels in the PE01 cell line following the combination treatment of Pacritinib (2.5μM) and SHP099 (10μM). SHP2 protein expression was observed to be decreased in combination treated PE01 cells. SHP2 protein expression was detected using western blot and band intensity was measured using Image J densitometry. SHP2 expression was normalised using β-actin loading control and presented as a percentage expression of vehicle control. Statistical significance was assessed (PRISM) through paired students t-test comparisons.

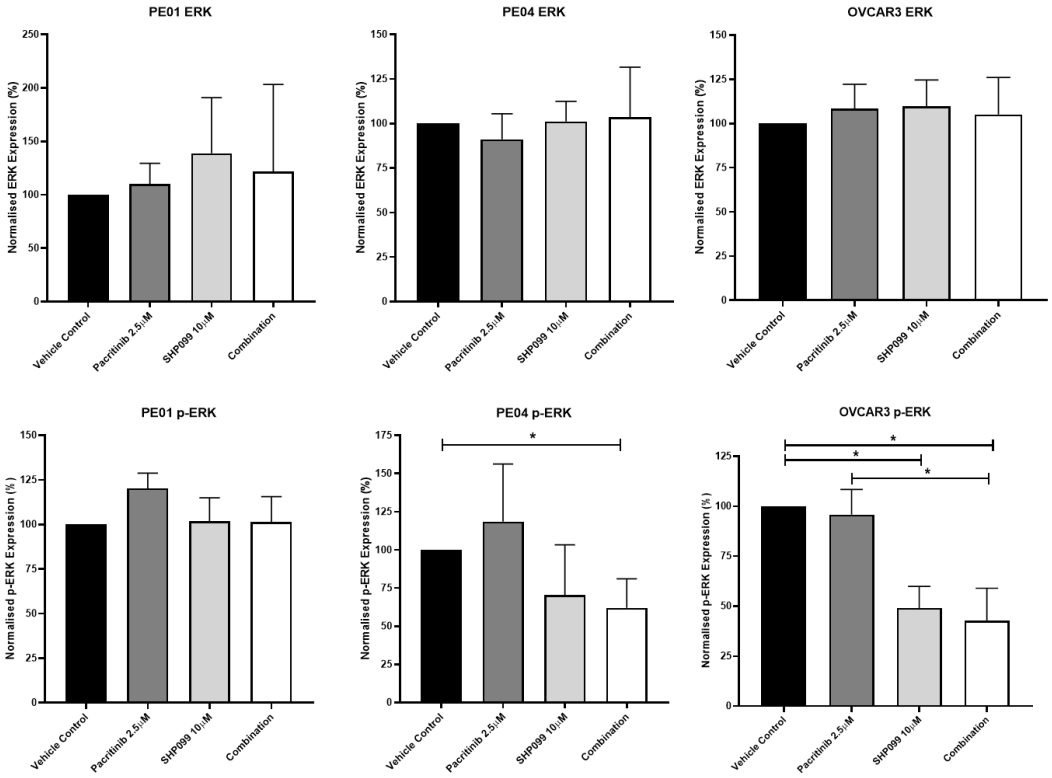

Figure 4.16.3: Densitometry analysis shows significantly reduced levels of ERK activation following combination of pacritinib and SHP099 in PE04 and OVCAR3 cell line. SHP099 and combination treated cells display a reduction in the activation of ERK. ERK and p-ERK protein expression was detected using western blot and band intensity was measured using Image J densitometry. ERK and p-ERK expression was normalised using β-actin loading control and presented as a percentage expression of vehicle control. Statistical significance was assessed (PRISM) through paired students t-test comparisons. , p-values; (*;≤0.05), (**;≤0.01), (***;≤0.001), (****;≤0.0001).

(4.2.9) Treatment of Cisplatin Resistant HGSC PE04 Cell Line with SHP099 Results in the Statistically Significant Differential Abundance of 30 Proteins in 3D *In Vitro* Models.

We have shown that treatment with SHP099 reduces 3D growth and viability of HGSC cell lines *in vitro* (Section 4.2.4) (Fig. 4.6.1 and Fig. 4.7.1). For this reason, we sought to gain further mechanistic understanding into the action of SHP099 in HGSC cells. Further analysis was performed on the proteomics dataset (section 4.2.6) generated above in order to investigate the binary comparison of SHP099 treated vs vehicle control treated cisplatin resistant PE04 HGSC cells.

A total of thirty statistically significant and differentially abundant proteins were identified to be differentially abundant in SHP099 treated PE04 cells compared to vehicle control treated cells (Table 4.2.7) and it is these proteins which we focus on in this section. Of these targets, eight were observed to be increased in SHP099 treated cells while twenty-two were observed to be decreased (Fig. 4.18.1).

These proteins were fed into SHINEY Go in order to perform pathway enrichment analysis (Table 4.2.6). A total of six pathways were identified using this analysis. These pathways include **i)** Glutathione Metabolism, **ii)** Pyrimidine Metabolism, **iii)** Spliceosome, **iv)** Drug metabolism-other enzymes, **v)** Nucleotide Metabolism and **vi)** Metabolic Pathways.

Panther pathway analysis was performed on these thirty proteins and identified six pathways (Fig. 4.17.1). The pathways identified including **i)** De Novo Purine Biosynthesis, **ii)** De Novo Pyrimidine Deoxyribonucleotide Biosynthesis, **iii)** Formyltetrahydrofolate Biosynthesis, **iv)** S-Adenosylmethionine Biosynthesis, **v)** Salvage Pyrimidine Deoxyribonucleotides and **v)** P53 pathway.

Finally, String analysis was performed to identify any potential functional connections between the identified targets (Fig. 4.17.2). Interestingly one functional node can be identified from this analysis which centres around DDX3X. This DDX3X node includes EIF3C, SRSF5 and GEMIN5 (Fig. 4.17.2). This functional node may represent a novel cluster of therapeutic targets in HGSC which could be targeted using SHP099.

In order to further evaluate the importance of these targets and to investigate if they may play a role in OvCa, we examined gene expression profiles using TNMplot database. Three genes were observed to be decreased and eighteen elevated in OvCa compared to normal controls (Fig. 4.19.1). A total of eight genes were observed to be elevated and ten decreased in metastatic OvCa compared to OvCa tumours (Fig.4.19.1). Significance and fold change are summarised for each of these genes in Table 4.2.8.

Using the RNA sequencing dataset, we were able to refine our analysis to serous OvCa. Interestingly these targets identified show considerable levels of dysregulation in serous OvCa. Nineteen genes were observed to be elevated and nine decreased in serous OvCa compared to normal controls (Fig. 4.19.2). As one target (ACACA) was not available for analysis on the platform this leaves one target (STAM) which did not display dysregulated gene expression in serous OvCa. Significance and fold change are summarised in Table 4.2.8.

Using KM plotter database, we next investigated the relationship between gene expression and OS / (PFS) in serous OvCa, and platinum + Taxol treated serous OvCa. The findings from this analysis are summarised in Table 4.2.9 and Table 4.2.10. Interestingly for twenty-two of these genes the high expression cohort (HEC) were observed to display significantly different OS or PFS in serous OvCa compared to the low expression cohorts. Additionally, twenty-three of these targets were observed to

display significantly different OS or PFS in serous OvCa patients treated with platinum and Taxol compared to low expression cohorts.

SHP099 led to the reduced abundance of 22 proteins (Section 4.2.6). Of these the HEC of DDX3X, MAT2A, SRPRB or ACACA all display reduced PFS in serous OvCa while HEC of MLRP15, ACACA or NUTF2 all display reduced OS in serous OvCa. When further refined to platin and Taxol treated serous OvCa the HEC of MAT2A, SRPRB or NUTF2 were associated with reduced PFS while MRPL15, ACACA or NUTF2 HEC was associated with reduced OS.

A total of eight proteins displayed increased abundance in cisplatin resistant PE04 cells following treatment with SHP099. Of these the HEC of GPX1 and PFDN5 were associated with increased progression free survival with the HEC of PFDN5 being further associated with increased OS. When further refined to serous OvCa treated with platinum and Taxol H2AFV, GPX1, PFDN5 or SF3B4 HEC were all associated with improved PFS. The HEC of GPX1 or PFDN5 were further associated with improved overall survival in this cohort.

These gene expression analysis studies display considerable dysregulation for the thirty significantly differentially abundant proteins identified following treatment of cisplatin resistant PE04 cells with SHP099. A large number of these proteins display differential gene expression in serous OvCa with high expression correlating to overall survival or progression free survival in a majority of targets. It is clear that these targets identified following SHP099 play important roles in OvCa, however the exact roles and inter-relationships between these targets require further evaluation to fully understand if these targets represent novel targets in OvCa which could be targeted using SHP099.

Table 4.2.6: Pathway enrichment analysis for vehicle control vs SHP099 (10μM). Statistically significant and differentially abundant proteins, for the binary comparison vehicle control vs SHP099 (10μM) was used to perform pathway enrichment analysis using SHINY GO. The three most enriched pathways included glutathione metabolism, pyrimidine metabolism and spliceosome.

Pathway	Pathway Genes	nGenes	Fold Enrichment	Enrichment FDR	Genes
Glutathione Metabolism	57	2	26.8	2.8E-02	GPX1 RRM2
Pyrimidine Metabolism	58	2	26.3	2.8E-02	RRM2 TK1
Spliceosome	131	4	23.3	8.8E-04	SF3B4 LSM8 PRPF40A SRSF5
Drug Metabolism – Other Enzymes	79	2	29.3	3.2E-02	RRM2 TK1
Nucleotide Metabolism	85	2	17.9	3.2E-02	RRM2 TK1
Metabolic Pathways	1538	7	3.5	2.8E-02	MTHFD2 DAD1 FAH GPX1 MAT2A RRM2 TK1

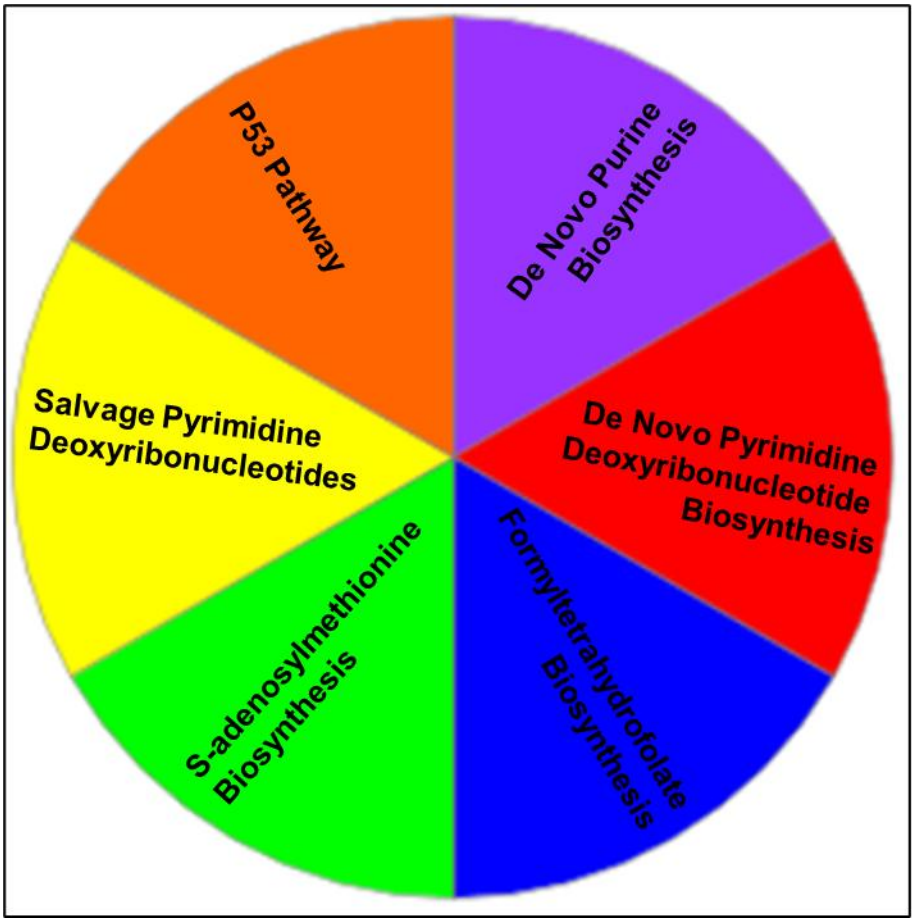

Figure 4.17.1: Panther pathway analysis identifies several impacted pathways in high grade serous ovarian cancer cell line PE04 following treatment with SHP099 (10μM) in a 3D in vitro model. Statistically significant and differentially expressed proteins identified above were fed into Panther allowing for the visualisation of related biological process gene ontology terms for these proteins. Treatment with SHP099 in vitro resulted in changes in protein abundance of proteins involved in 6 biological processes.

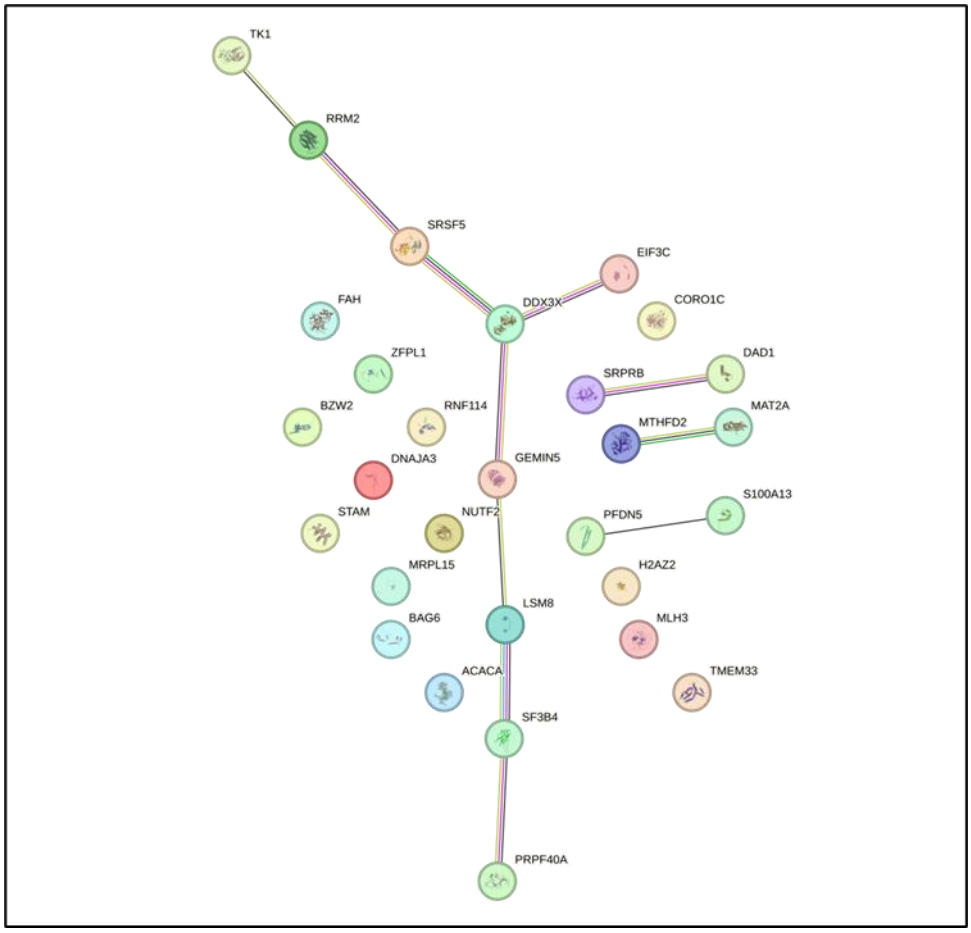

Figure 4.17.2: STRING analysis identifies several functional connections between statistically significant and differentially abundant proteins identified following treatment of PE04 with SHP099 (10μM). Statistically significant and differentially expressed proteins identified above were fed into STRING allowing for the visualisation of functional interconnections between these proteins. 14 proteins identified showed no functional connections to any other protein. 6 proteins formed dimeric functional connections. Finally, 9 proteins formed a one string of connections centred around DDX3X.

Table 4.2.7: Thirty proteins were found to be significantly and differentially abundant in PE04 cells treated with SHP099 compared to control treated PE04 cells. Increased abundance is indicated by green font while decreased abundance is indicated by the red font in the fold change column.

Protein ID	Gene Names	Full Name	Fold Change
Q71UI9	H2AZ2 H2AFV H2AV	Histone H2A Variant	18.86538278
Q92783	STAM STAM1	Signal Transducing Adaptor Molecule 1	14.27831115
P07203	GPX1	Glutathione Peroxidase 1	2.897890707
Q9ULV4	CORO1C CRN2 CRNN4	Coronin 1C	2.384381987
O95159	ZFPL1	Zinc Finger protein-like 1	2.129031895
Q15427	SF3B4 SAP49	Splicing factor 3B subunit 4	2.113573462
Q99471	PFDN5 MM1 PFD5	Prefoldin subunit 5	2.065601163
Q9Y508	RNF114 ZNF228 ZNF313	Ring finger protein 114	1.683153022
O00571	DDX3X DBX DDX3	DEAD-box helicase 3, X-linked	1.552798392
P31153	MAT2A AMS2 MATA2	Methionine Adenosyl transferase II, Alpha	1.555870018
Q9Y6E2	BZW2 5MP1 HSPC028 MSTP017	Basic Leucine Zipper and W2 domain containing protein 2	1.61566403
Q96EY1	DNAJA3 HCA57 TID1	DNAJ heat shock protein family (Hsp40) member A3	1.629849886
Q9Y5M8	SRPRB PSEC0230	Signal Recognition particle receptor subunit beta	1.70978245
P57088	TMEM33 DB83	Transmembrane protein 33	1.858420308
Q9P015	MRPL15 HSPC145	Mitochondrial ribosomal protein L15	1.957579517
P31350	RRM2 RR2	Ribonucleotide reductase regulatory subunit M2	1.964708347
P46379	BAG6 BAT3 G3	BAG cochaperone 6	2.049629574
Q99613	EIF3C EIF3S8	Eukaryotic translational initiation factor 3 subunit C	2.143288203
O75400	PRPF40A FBP11 FLAF1 FNBP3 HIP10 HYPA HSPC225	Pre-mRNA processing factor 40 homolog A	2.221831076
P04183	TK1	Thymidine Kinase 1	2.327628194
Q13085	ACACA ACAC ACC1 ACCA	Acetyl-Co-A Carboxylase Alpha	2.448610966
Q8TEQ6	GEMIN5	Gem (nuclear organelle) associated protein 5	2.678163696
P13995	MTHFD2 NMDMC	Methylenetetrahydrofolate dehydrogenase (NADP+ dependent) 2	2.879128902
O95777	LSM8	LSM8 homolog, U6 small nuclear RNA associated	2.897445362
P61803	DAD1	Defender against cell death 1	2.906398912
Q13243	SRSF5 HRS SFRS5 SRP40	Serine and arginine rich splicing factor 5	3.36831716
Q9UHC1	MLH3	MutL homolog 3	3.470872997
P16930	FAH	Fumarylacetoacetate Hydrolase	3.614607307
P61970	NUTF2 NTF2	Nuclear Transport Factor 2	5.307847168
Q99584	S100A13	S100 calcium binding protein A13	10.10825422

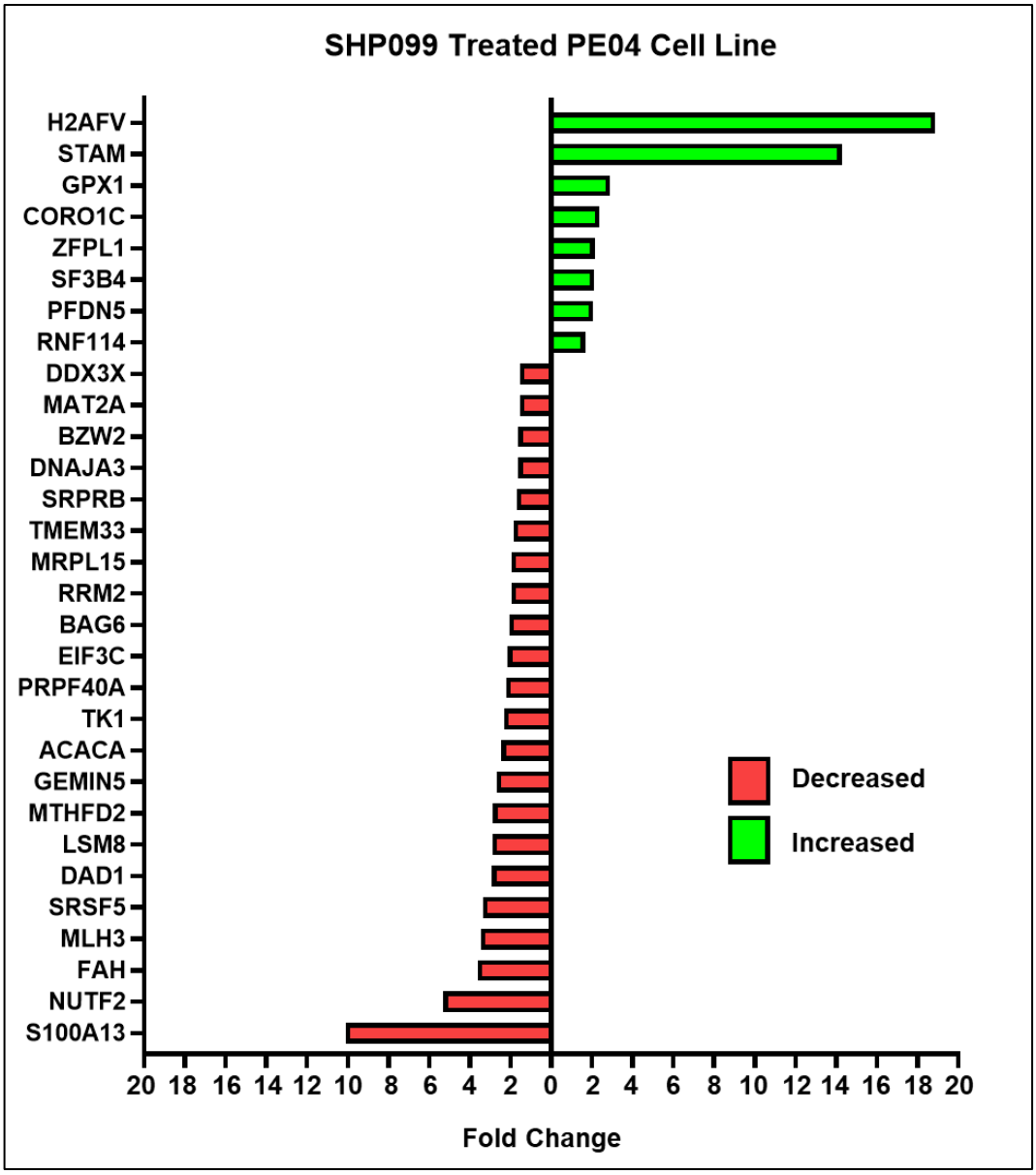

Figure 4.18.1: Treatment of high grade serous ovarian cancer cell line PE04 with SHP099 resulted in the detection of 30 statistically significant and differentially abundant proteins being identified using Mass Spectrometry. Statistically significant (p-value<0.05) and differentially abundant (fold-change > 1.5) proteins were identified in SHP099 (10μM) treated PE04 HGSC cells and presented as significantly decreased (red) or significantly increased (green). A total of 8 proteins were detected as significantly increased (Green) in SHP099 (10μM) treated PE04 cells compared to vehicle control. A total of 22 proteins were detected as significantly decreased (Red) in SHP099 (10μM) treated PE04 cells compared to vehicle control.

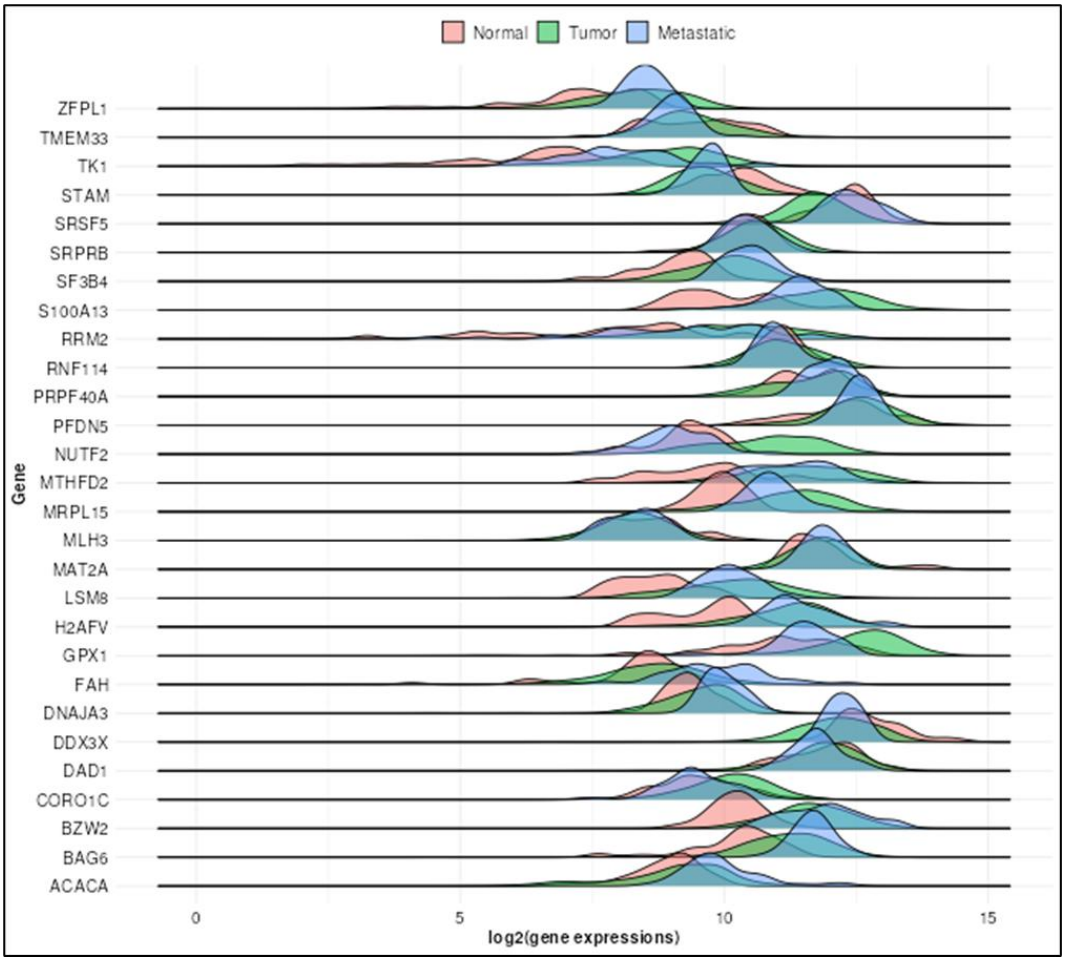

Figure 4.19.1: Gene Chip data was probed for gene expression of targets identified in SHP099 (10μM) treated PE04 high grade serous ovarian cancer cell line. TNM Plotter database was probed, using gene chip dataset, for targets identified following SHP099 (10μM) treated PE04 high grade serous ovarian cancer cell line and gene expression was graphed for Ovarian Tumours (744), Metastatic (44) and Normal controls (46). Three genes were observed to be significantly decreased, and eighteen genes were observed to be significantly increased in ovarian cancer tumours compared to normal controls. Furthermore, eight genes were increased and 9 decreased in metastatic samples compared to ovarian tumours. [267].

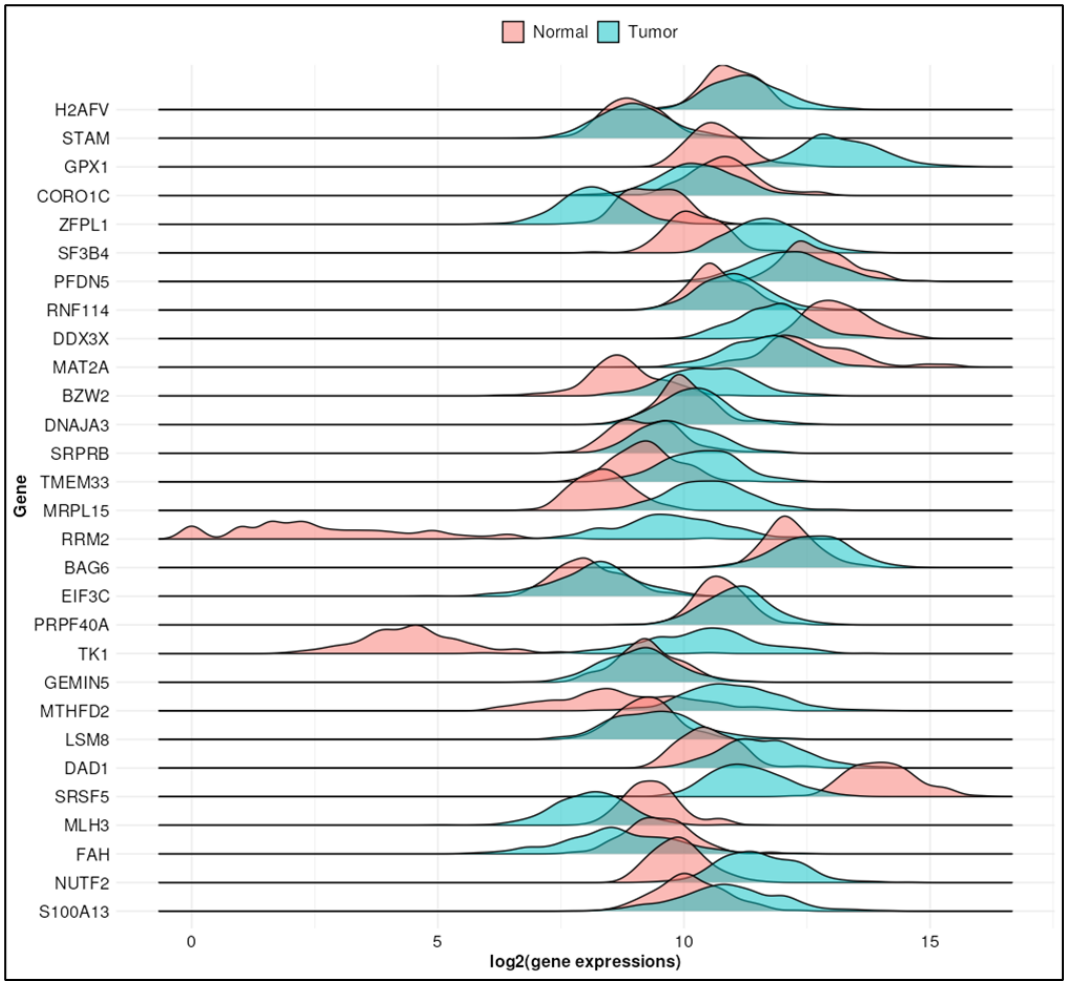

Figure 4.19.2: RNA-sequencing dataset was probed for gene expression of targets identified in SHP099 (10μM) treated PE04 high grade serous ovarian cancer cell line. TNM Plotter database was probed, using the RNA sequencing dataset, for targets identified following SHP099 (10μM) treatment of PE04 high grade serous ovarian cancer cell line. Gene expression was graphed for serous ovarian tumours (374) and Normal controls (133). Nineteen genes were observed to be increased, and nine genes were observed to be decreased in serous ovarian tumours compared to normal controls. [267].

Table 4.2.8: Gene Chip (ovarian cancer) and RNA sequencing (Serous ovarian cancer) datasets were probed for gene expression of 30 proteins identified following SHP099 treatment in high grade serous ovarian cancer cell line PE04. Fold change and p-values are annotated below for each of these genes. [267]. Targets increased in SHP099 treated PE04 indicated in green font, while those decreased are indicated in red font.

	RNA-Sequencing - Serous Ovarian Cancer Normal vs Tumour		Gene Chip – Ovarian Cancer Ovarian tissue vs tumour and metastatic				
Target	Fold Change (Mean)	Mann Whitney P value	Fold Change Normal vs Tumour	Fold Change Tumour vs Metastatic	Dunn test P value		
					Normal vs Tumour	Normal vs Metastatic	Tumour vs Metastatic
H2AFV	1.3	1.85E-04	3.13	1.14	4.48E-21	1.96E-14	1.30E-01
STAM	1.06	8.99E-01	0.68	0.96	6.23E-08	1.60E-03	1.21E-01
GPX1	5.99	2.11E-63	2.52	0.44	8.85E-17	4.02E-01	5.37E-15
CORO1C	0.71	3.43E-11	1.44	0.63	6.54E-07	3.09E-01	3.04E-08
ZFPL1	0.44	3.29E-46	1.91	0.97	6.47E-09	7.80E-07	1.61E-01
SF3B4	2.82	1.95E-53	1.95	1.29	6.11E-13	5.78E-17	8.22E-06
PFDN5	0.73	1.36E-11	1.2	0.92	5.93E-03	4.79E-02	4.21E-01
RNF114	1.28	1.44E-05	1.12	0.87	2.51E-01	3.11E-01	9.23E-02
DDX3X	0.41	5.90E-47	0.65	0.99	1.53E-08	6.22E-04	1.50E-01
MAT2A	0.46	3.19E-20	0.92	0.99	1.47E-01	8.60E-02	2.30E-01
BZW2	3.43	2.56E-51	2.85	1.2	1.19E-23	5.93E-18	3.02E-02
DNAJA3	1.2	2.20E-03	1.26	1.22	4.56E-04	3.80E-08	2.46E-05
SRPRB	1.51	5.19E-14	1.22	0.86	3.86E-03	3.26E-01	2.30E-02
TMEM33	2.19	5.51E-36	0.95	0.68	3.69E-01	1.81E-03	1.44E-04
MRPL15	4.82	4.21E-62	2.95	0.68	1.04E-20	1.28E-05	4.14E-04
RRM2	41.23	2.99E-63	4.64	0.63	3.33E-17	1.31E-04	7.68E-04
BAG6	1.44	1.39E-11	1.98	1.26	1.21E-13	3.31E-18	2.74E-06
EIF3C	1.13	4.80E-02	NA	NA	NA	NA	NA
PRPF40A	1.3	9.91E-08	1.05	1.16	2.69E-01	8.51E-03	4.13E-03
TK1	44.4	1.07E-64	4.77	0.61	1.62E-21	2.48E-04	3.03E-06
ACACA	NA	NA	1.27	1.75	1.62E-02	1.61E-08	2.99E-08
GEMIN5	0.94	2.48E-02	NA	NA	NA	NA	NA
MTHFD2	3.8	6.48E-45	2.97	0.79	5.07E-17	4.38E-07	7.39E-02
LSM8	1.24	4.74E-02	3.26	0.8	2.21E-19	3.13E-09	1.99E-01
DAD1	2.32	3.57E-35	0.99	0.88	4.05E-01	7.80E-02	4.52E-02
SRSF5	0.15	3.34E-65	0.65	1.64	1.79E-12	3.26E-01	5.87E-14
MLH3	0.46	6.26E-46	0.84	0.97	8.05E-02	1.87E-01	4.48E-01
FAH	0.68	2.45E-16	1.23	2.35	8.92E-02	2.34E-10	4.37E-13
NUTF2	3.35	1.15E-55	3.27	0.27	2.95E-18	2.56E-01	4.59E-21
S100A13	1.97	3.85E-16	3.18	0.65	2.43E-19	4.78E-05	3.04E-04

Table 4.2.9: KM Plotter database was probed to assess correlation between gene expression and prognostic indicators (overall survival and progression free survival) of 8 proteins increased in abundance in PE04 following SHP099 treatment. JetSet best probe set was, auto select best cut off and exclude outlier array parameters were included.

Target	Serous Ovarian Cancer	Platinum + Taxol Treated Serous Ovarian Cancer
H2AFV	No Significance	**HEC displays increased Progression Free Survival** (Median Survival: 17.68 vs 15 months) - (log rank P = 0.01)
STAM	**HEC displays decreased Overall Survival** (Median Survival: 38.77 vs 45.77 months) - (log rank P = 0.0121) **HEC displays decreased Progression Free Survival** (Median Survival: 16 vs 18 months) - (log rank P = 0.0095)	**HEC displays decreased Overall Survival** (Median Survival: 40.07 vs 45.77 months)- (log rank P = 0.027) **HEC displays decreased Progression Free Survival** (Median Survival: 15.87 vs 16.83 months) - (log rank P = 0.038)
GPX1	**HEC displays increased Progression Free Survival** (Median Survival: 18.43 vs 15 months) - (log rank P = 0.048)	**HEC displays increased Overall Survival** (Median Survival: 48.73 vs 40.43 months) - (log rank P = 0.049) **HEC displays increased Progression Free Survival** (Median Survival: 18 vs 14.9 months) - (log rank P = 0.0065)
CORO1C	**HEC displays decreased Overall Survival** (Median Survival: 38.93 vs 46.52 months) - (log rank P = 0.012) **HEC displays decreased Progression Free Survival** (Median Survival: 13 vs 20 months) - (log rank P = 3E-07)	**HEC displays decreased Overall Survival** (Median Survival: 44 vs 47.8 months) - (log rank P = 0.049) **HEC displays decreased Progression Free Survival** (Median Survival: 13 vs 19 months) - (log rank P = 0.0029)
ZFPL1	No Significance	**HEC displays decreased Overall Survival** (Median Survival: 40.07 vs 48 months) - (log rank P = 0.023) **HEC displays increased Progression Free Survival** (Median Survival: 16.93 vs 15.13 months) - (log rank P = 0.023)
SF3B4	No Significance	**HEC displays increased Progression Free Survival** (Median Survival: 17.38 vs 15 months) - (log rank P = 0.0043)
PFDN5	**HEC displays increased Overall Survival** (Median Survival: 47.8 vs 39.87 months) - (log rank P = 0.02) **HEC displays increased Progression Free Survival** (Median Survival: 18.3 vs 15.27 months) - (log rank P = 0.0081)	**HEC displays increased Overall Survival** (Median Survival: 46.13 vs 30.4 months) - (log rank P = 0.048) **HEC displays increased Progression Free Survival** (Median Survival: 17.77 vs 15.01 months) - (log rank P = 0.019)
RNF114	No Significance	**HEC displays decreased Overall Survival** (Median Survival: 41.83 vs 49.97 months) - (log rank P = 0.033)

Abbreviations: HEC = High Expression Cohort.

Table 4.2.10 (A): KM Plotter database was probed to assess correlation between gene expression and prognostic indicators (overall survival and progression free survival) of 22 proteins decreased in abundance in PE04 following SHP099 treatment. JetSet best probe set was, auto select best cut off and exclude outlier array parameters were included.

Target	Serous Ovarian Cancer	Platinum + Taxol Treated Serous Ovarian Cancer
DDX3X	**HEC displays decreased Progression Free Survival** (Median Survival: 15.13 vs 18.3 months) - (log rank P = 0.0078)	**No Significance**
MAT2A	**HEC displays decreased Progression Free Survival** (Median Survival: 15.93 vs 18.93 months) - (log rank P = 0.0018)	**HEC displays decreased Progression Free Survival** (Median Survival: 15.33 vs 18.1 months) - (log rank P = 0.032)
BZW2	**HEC displays increased Progression Free Survival** (Median Survival: 18.79 vs 15.01 months) - (log rank P = 0.016)	**HEC displays increased Progression Free Survival** (Median Survival: 18.1 vs 14.03 months) - (log rank P = 0.0025)
DNAJA3	**HEC displays increased Overall Survival** (Median Survival: 45.53 vs 43.97 months) - (log rank P = 0.035)	**No Significance**
SRPRB	**HEC displays decreased Progression Free Survival** (Median Survival: 14 vs 19 months) - (log rank P = 0.0034)	**HEC displays decreased Progression Free Survival** (Median Survival: 14 vs 18 months) - (log rank P = 0.046)
TMEM33	**HEC displays increased Overall Survival** (Median Survival: 45.77vs 36.83 months) - (log rank P = 0.021) **HEC displays increased Progression Free Survival** (Median Survival: 17.68 vs 13 months) - (log rank P = 0.00021)	**HEC displays increased Overall Survival** (Median Survival: 55.46 vs 38.93 months) - (log rank P = 0.0033) **HEC displays increased Progression Free Survival** (Median Survival: 19 vs 14 months) - (log rank P = 0.0013)
MRPL15	**HEC displays decreased Overall Survival** (Median Survival: 41.6 vs 45.63 months) - (log rank P = 0.045)	**HEC displays decreased Overall Survival** (Median Survival: 44 vs 49 months) - (log rank P = 0.048)
RRM2	**No Significance**	**HEC displays increased Progression Free Survival** (Median Survival: 17.53 vs 14.93 months) - (log rank P = 0.036)
BAG6	**HEC displays increased Overall Survival** (Median Survival: 46.52 vs 43 months) - (log rank P = 0.021) **HEC displays increased Progression Free Survival** (Median Survival: 19.02 vs 16.83 months) - (log rank P = 0.023)	**HEC displays increased Overall Survival** (Median Survival: 48.07 vs 44.03 months) - (log rank P = 0.016) **HEC displays increased Progression Free Survival** (Median Survival: 19.37 vs 15 months) - (log rank P = 0.00018)
EIF3C	**No Data**	**No Data**
PRPF40A	**HEC displays increased Progression Free Survival** (Median Survival: 17.68 vs 15 months) - (log rank P = 0.018)	**No Significance**

Abbreviations: HEC = High Expression Cohort.

Table 4.2.10 (B): KM Plotter database was probed to assess correlation between gene expression and prognostic indicators (overall survival and progression free survival) of 22 proteins decreased in abundance in PE04 following SHP099 treatment. JetSet best probe set was, auto select best cut off and exclude outlier array parameters were included.

Target	Serous Ovarian Cancer	Platinum + Taxol Treated Serous Ovarian Cancer
TK1	**HEC displays increased Overall Survival** (Median Survival: 46.6 vs 41.63 months) - (log rank P = 0.027)	**HEC displays increased Overall Survival** (Median Survival: 49.47 vs 43 months) - (log rank P = 0.022)
ACACA	**HEC displays decreased Overall Survival** (Median Survival: 40.97 vs 49.47 months) - (log rank P = 0.00044) **HEC displays decreased Progression Free Survival** (Median Survival: 16.03 vs 18.4 months) – (log rank P = 0.012)	**HEC displays decreased Overall Survival** (Median Survival: 41.83 vs 48.37 months) - (log rank P = 0.014)
GEMIN5	**No Significance**	**No Significance**
MTHFD2	**HEC displays increased Progression Free Survival** (Median Survival: 18.23 vs 17.03 months) - (log rank P = 0.017)	**HEC displays increased Progression Free Survival** (Median Survival: 17.53 vs 14.43 months) - (log rank P = 0.013)
LSM8	**HEC displays increased Overall Survival** (Median Survival: 50.69 vs 38.4 months) - (log rank P = 0.028) **HEC displays increased Progression Free Survival** (Median Survival: 17 vs 14 months) - (log rank P = 0.012)	**No Significance**
DAD1	**HEC displays increased Progression Free Survival** (Median Survival: 20.57 vs 16.13 months) - (log rank P = 0.017)	**HEC displays increased Progression Free Survival** (Median Survival: 18.23 vs 15 months) - (log rank P =0.023)
SRSF5	**No Data**	**No Data**
MLH3	**HEC displays increased Overall Survival** (Median Survival: 49 vs 44 months) - (log rank P = 0.037)	**HEC displays increased Overall Survival** (Median Survival: 46.13 vs 45 months) - (log rank P = 0.04)
FAH	**HEC displays increased Overall Survival** (Median Survival: 52.77 vs 41.63 months) - (log rank P = 0.00067) **HEC displays increased Progression Free Survival** (Median Survival: 18.43 vs 15.87 months) - (log rank P = 0.00064)	**HEC displays increased Overall Survival** (Median Survival: 47.8 vs 40 months) - (log rank P = 0.0078) **HEC displays increased Progression Free Survival** (Median Survival: 17.43 vs 15.13 months) - (log rank P = 0.0019)
NUTF2	**HEC displays decreased Overall Survival** (Median Survival: 40.4 vs 48 months) - (log rank P = 0.045)	**HEC displays decreased Overall Survival** (Median Survival: 36.4 vs 50 months) - (log rank P = 0.0026) **HEC displays decreased Progression Free Survival** (Median Survival: 13.6 vs 18.2 months) - (log rank P = 0.018)
S100A13	**HEC displays increased Overall Survival** (Median Survival: 48.2 vs 40.07 months) - (log rank P = 0.0067)	**HEC displays increased Overall Survival** (Median Survival: 46.13 vs 42.6 months) - (log rank P = 0.04)

Abbreviations: HEC = High Expression Cohort.

(4.2.10) Treatment with Pacritinib and SHP099 in Combination Results in Synergistic Reduction of 3D Growth and Viability of Murine ID8 OvCa Cell Line *In Vitro*.

The synergistic reduction in growth and viability of HGSC cell lines following treatment with pacritinib in combination with SHP099 provides a strong rationale for the progression of this work to *in vivo* studies. In preparation for this the efficacy of pacritinib and SHP099 in combination was evaluated *in vitro* using the murine OvCa cell line ID8. The ID8 Defb29 VEGF cell line was provided by Dr Niamh Buckley (Queens University Belfast) for the purposes of this work. This modified cell line is capable of subcutaneous growth in immunocompetent C57BL6 mice, allowing for investigation of efficacy in the presence of a functioning immune system to facilitate a more representative study.

Using 2D methodologies, we observed similar findings for pacritinib and SHP099 treated ID8 Defb29 VEGF cells when compared to HGSC cell lines. Pacritinib was observed to reduce the 2D viability from 1.25μM in ID8 Defb29 VEGF cells (Fig. 4.20.1). Treatment with SHP099 concentrations between 0.3125μM and 40μM result in limited viability inhibition using this methodology (Fig. 4.20.1). When applied in combination there was no synergy or antagonism observed using 2D *in vitro* growth assay models (Fig. 4.21.1).

We progressed to evaluating the efficacy of Pacritinib and SHP099 in combination using the same 3D methodologies applied in HGSC cell line experiments above. Combination of pacritinib and SHP099 resulted in considerable levels of synergistic reduction in 3D growth and viability of ID8 cells *in vitro* (Fig. 4.22.1).

Additionally, we observed that treatment with pacritinib and SHP099 potently inhibit anchorage independent growth and colony formation in ID8 Defb29 VEGF cells (Fig. 4.23.1). We did not observe any synergistic reduction in spheroid formation or

anchorage independent growth likely due to the potent activity of each drug alone (Fig. 4.23.1). As each drug potently inhibits anchorage independent growth in this cell line it was not possible to observe any synergistic or antagonistic interaction at the concentrations evaluated. It may be beneficial to repeat these assays at a lower concentration of one or both inhibitors.

The observations made from these 3D growth assay models using the OvCa murine ID8 cell line strongly support the progression of this novel drug combination to *in vivo* mouse. This would allow for the further assessment of efficacy in a more clinically relevant model.

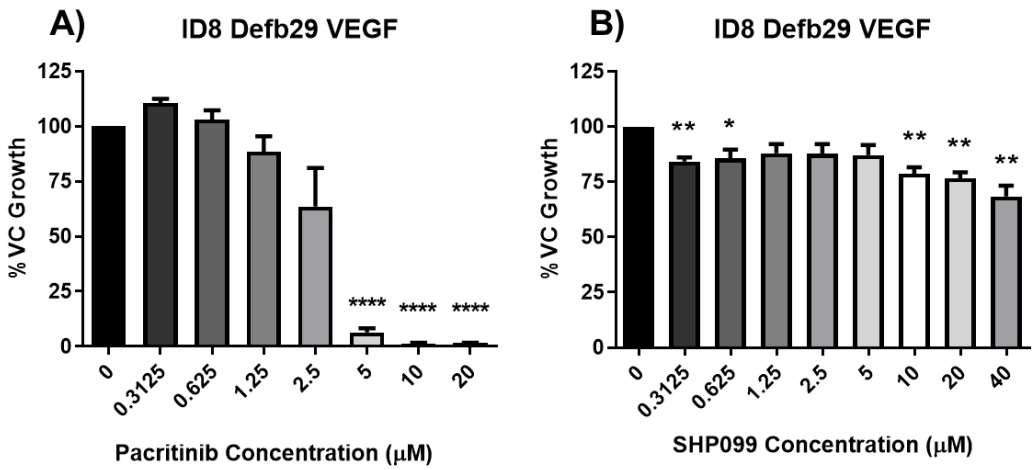

Figure 4.20.1: Pacritinib and SHP099 significantly impair 2D viability of Murine OvCa ID8 cell line. A) Treatment with pacritinib resulted in a significant reduction in 2D viability of ID8 Defb29 VEGF cells at concentrations greater than 5μM. **B)** Treatment with SHP099 resulted in a limited significant reduction in 2D viability of ID8 Defb29 VEGF cells. Statistical significance for Dose Curves **A)** and **B)** was assessed (PRISM) through paired student t-test comparing vehicle control to each concentration of Pacritinib, p-values; (*;≤0.05), (**;≤0.01), (***;≤0.001), (****;≤0.0001) using four independent experimental replicates.

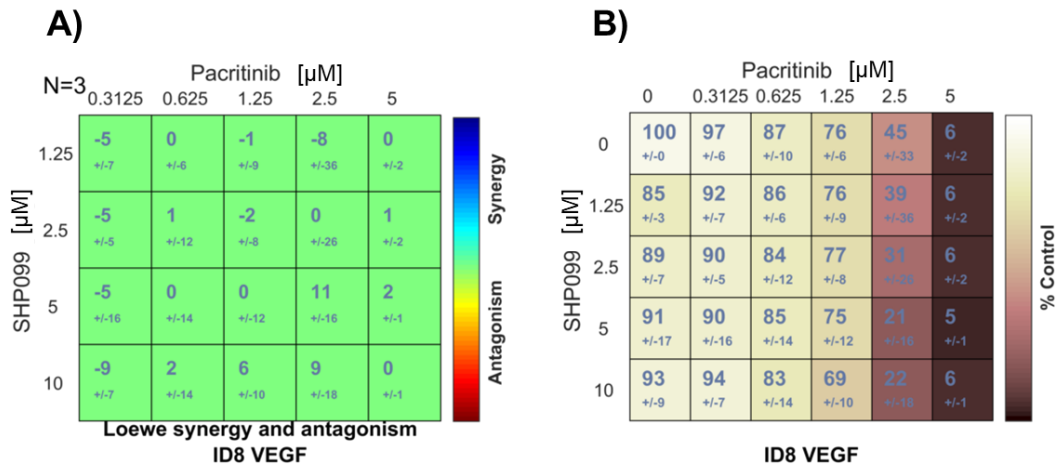

Figure 4.21.1: Pacritinib and SHP099 display no significant synergistic or antagonistic impact on 2D viability in combination. A) Treatment with pacritinib and SHP099 in combination resulted in no observable synergistic or antagonistic difference in 2D viability of ID8 cells. **B)** dose response matrices were generated using Combenefit software for three independent experimental replicates.

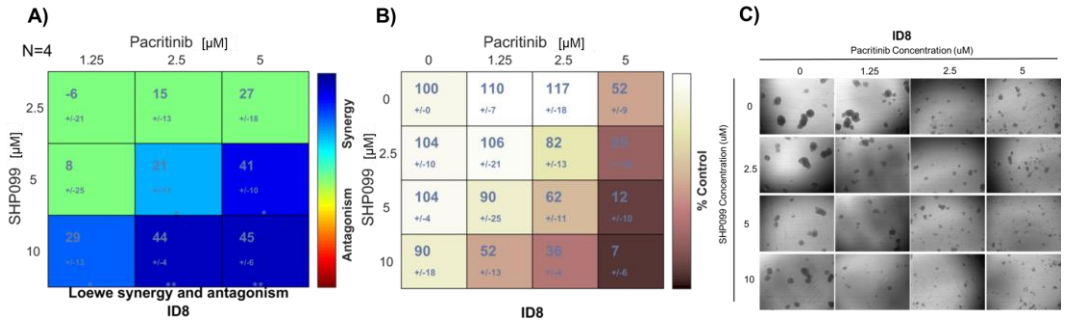

Figure 4.22.1: Pacritinib and SHP099 combination shows significant synergistic reduction in 3D viability and growth of Murine OvCa ID8 cell line in vitro: **A)** Treatment with pacritinib and SHP099 in combination resulted in synergistic reduction in 3D viability of ID8 cell line grown in Matrigel matrix. **B)** dose response matrices were performed and generated using COMBENEFIT software. **C)** Representative images were captured. Results are representative of four independent experimental replicates.

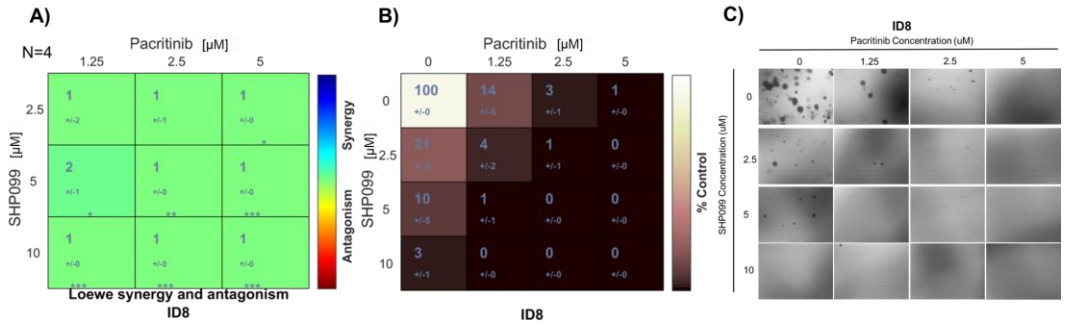

Figure 4.23.1: Pacritinib and SHP099 potently inhibit anchorage independent growth of ID8 Cells: **A)** Treatment with pacritinib and SHP099 in combination resulted in minor synergy at low concentrations. **B)** dose response matrices were performed and generated using COMBENEFIT software and shows pacritinib and SHP099 potently inhibit anchorage independent growth of ID8 cells. **C)** Representative images were captured post staining with neutral red viable cell dye. Results are representative of four independent experimental replicates.

(4.3) Discussion

Due to high incidence of advanced stage detection and high frequency of chemo-resistant disease HGSC represents the most lethal gynaecological malignancy worldwide. It is clear that novel therapeutic targets and treatment strategies are urgently required to provide more options to patients with HGSC. In this package of work, we have investigated if the phosphatase SHP2 could represent a novel therapeutic target in HGSC. In addition to this we evaluated the efficacy of the SHP2 allosteric inhibitor SHP099 both alone and in combination with the IRAK1-JAK2-FLT3 inhibitor pacritinib.

(4.3.1) SHP2 Represents a Potential Therapeutic Target in High-Grade Serous Carcinoma.

Western blot profiling of SHP2 expression in HGSC cell lines led to the observation that SHP2 was significantly increased in cisplatin resistant cells compared to the paired cisplatin sensitive cell line (Section 4.2.1). This finding may indicate an important role for SHP2 in the development of chemoresistance in HGSC. Interestingly SHP2 has been shown to be upregulated in oxaliplatin-resistant colon cancer cells where it contributed to increased proliferation and oxaliplatin resistance through the activation of ERK and AKT.[278] Similar findings were observed in lung cancer where SHP2 was observed to mediate cisplatin resistance and inhibit apoptosis through the activation of RAS-PI3K-AKT1-Survivin signalling pathway.[279]

We assessed the gene expression of SHP2 (PTPN11) in OvCa using the publicly available TNMplot database (Section 4.2.2). This led to the finding that PTPN11 gene expression was widely dysregulated in various cancers compared to normal controls. PTPN11 was observed to be significantly increased in ten cancer

types and significantly decreased in seven cancer types compared to normal controls (Section 4.2.2). Probing the gene chip dataset we assessed PTPN11 expression and observed a significant decrease in PTPN11 gene expression in OvCa compared to normal control. Using the RNA sequencing dataset, we were able to refine our analysis to serous OvCa where we found no significant difference in PTPN11 gene expression compared to normal controls (Section 4.2.2).

Probing the KM Plotter database, we evaluated correlation between PTPN11 mRNA expression levels and (Section 4.2.2). We observed that the PTPN11 high mRNA expression cohort (HEC) displays significantly reduced OS for OvCa, serous OvCa and high stage (3+4) OvCa compared to the low expression cohorts (Section 4.2.2). We next further refined our analysis to only serous OvCa patients treated with platinum and Taxol (Section 4.2.2). Here we observed a significant reduction in OS of PTPN11 HEC for OvCa, serous OvCa and high stage (3+4) OvCa (Section 4.2.2). These findings indicate that higher SHP2 mRNA expression represents a negative prognostic indicator in OvCa, serous OvCa and high stage OvCa.

Using immunohistochemical staining of SHP2 we observed significantly increased cellular protein expression in HGSC compared to normal controls. SHP2 protein expression has previously been observed to be increased in EOC (60 cases) compared to normal ovarian tissue (60 cases).[243] This study did not investigate SHP2 protein expression in the different subtypes of EOC, stage of disease or subcellular staining and did not focus on HGSC. As such our findings provide a novel insight into the SHP2 expression levels in HGSC.

Subcellular analysis of SHP2 protein expression shows nuclear staining was relatively similar in both HGSC and normal adjacent tissue (Section 4.2.3). Interestingly, the cytoplasmic SHP2 levels in normal adjacent tissue were relatively low compared to HGSC. However, our findings do show nuclear staining of SHP2 are elevated in stage 3/4 HGSC compared to stage 1 (Section 4.2.3).

SHP2 subcellular localisation has previously been investigated in NSCLC. IHC analysis of 102 NSCLC samples has previously shown that nuclear SHP2 expression was correlated to YAP1 expression with high nuclear expression of SHP2 and YAP1 being shown to correlate with reduced OS.[280] It was observed that the overall survival was shorter for patients with cytoplasmic, nuclear or cytoplasmic and nuclear staining of SHP2 in NSCLC.[280] The same observations were then made for YAP1.[280]

To date no study has shown nuclear localisation of SHP2 is associated with reduced OS in OvCa. However, the fact that this association has been made in NSCLC we must consider that the same could be true in OvCa. As previously highlighted high stage HGSC display reduced OS compared to low stage HGSC. It is therefore interesting that we observed elevated nuclear staining of HGSC in high stage HGSC compared to low stage. This warrants future investigation into the association between nuclear localisation of SHP2 and OS in OvCa.

When we further divided HGSC based on stage of disease we observed high stage (3 and 4) HGSC showed elevated levels of SHP2 protein expression compared to low stage (1) HGSC samples (Section 4.2.3). SHP2 protein expression showed a significant increase in high stage HGSC in both nuclear and cytoplasmic fractions compared to low stage (1) HGSC. These findings are interesting given that PTPN11 high mRNA expression cohort was observed to display reduced OS in serous OvCa (Section 4.2.2). These findings support the hypothesis that SHP2 represents a negative prognostic indicator in serous OvCa and HGSC.

In other cancer types, elevated SHP2 protein expression has been associated with worse prognosis. Over recent years SHP2 expression has been shown to be a negative prognostic indicator in breast cancer[240], laryngeal cancer[242] and gallbladder cancer.[243] In pancreatic ductal adenocarcinoma (PDAC) SHP2 protein expression was observed to be significantly increased in cancerous tissue compared to normal

adjacent controls.[281] Interestingly in PDAC, SHP2 expression was not observed to correlate with T classification or TNM stage.[281] Using TNM classification SHP2 protein expression has been observed to be significantly elevated in T3+T4 gastric cancer compared to T1+T2 group.[282]

In summary SHP2 protein expression was observed to be increased in HGSC compared to NAT, with high stage (3+4) HGSC displaying higher levels of SHP2 protein expression (Section 4.2.3). Furthermore, SHP2 high mRNA expression cohort were observed to display reduced OS in serous OvCa and serous OvCa treated with platinum and Taxol (Section 4.2.2). Finally, SHP2 protein expression was observed to be elevated in cisplatin resistant HGSC cells compared to cisplatin sensitive HGCS cells. These findings provide a strong indication that SHP2 plays a negative role in OvCa and may represent a potential therapeutic target in HGSC.

Next, we assessed the potential of using a SHP2 inhibitor in OvCa cells using *in vitro* growth assays. SHP2 allosteric inhibitors prevent the conformational activation of SHP2 and effectively prevent its phosphatase activity as a result. We selected the SHP099 inhibitor for the purposes of this study to investigate the efficacy of SHP2 inhibition in HGSC. This inhibitor has shown considerable efficacy in *in vivo* models of oesophageal squamous cell carcinoma[239], KRAS mutant NSCLC[251] and OvCa.[56]

2D viability assays performed using SHP099 display a limited but significant reduction in viability of HGSC cells *in vitro* (Section 4.2.4). For this study we also utilised 3D *in vitro* growth assay models. In these assays cells are allowed to grow in spheroids using 3D matrices or low gelling agarose which allowed us to more accurately model how cancer cells grow *in vivo*. Following treatment with SHP099 we observed significantly reduced anchorage independent growth and 3D spheroid formation in the paired PE01 and PE04 HGSC cell lines (Section 4.2.4). In addition to this we observed significantly reduced 3D growth and viability, using a Matrigel growth assay, in all HGSC cell lines examined following treatment with SHP099.

These findings display a strong efficacy of SHP099 to impair 3D growth and viability of HGSC cell lines in vitro at low micromolar concentrations.

Following stimulation SHP2 is activated on residue Y542 through phosphorylation.[222] This post-translational modification is required to release the intramolecular interaction keeping SHP2 in an enzymatically inactive state. [217] Interestingly previous studies have shown that phosphorylation of SHP2 at Y542 is elevated in 3D cell cultures compared to 2D, which is believed to be attributed to ECM signalling activation.[222] These findings may explain why our 3D *in vitro* growth assays display a more considerable reduction in growth following treatment with SHP099 compared to our 2D *in vitro* growth assays.

These findings provide a strong indication that SHP2 represents a potential therapeutic target in HGSC and that the small molecule inhibitor SHP099 may provide an effective therapeutic strategy targeting SHP2.

(4.3.2) The Combination of SHP099 and Pacritinib Results in a Synergistic Reduction of 3D Growth and Viability of HGSC Cell Lines *In Vitro*.

In chapter 3 we have shown the IRAK1-JAK2-FLT3 inhibitor pacritinib displays considerable efficacy in reducing growth and viability of HGSC cell lines *in vitro*. Other groups have shown that pacritinib displays considerable efficacy when applied in combination with other inhibitors including selumetinib (medulloblastoma)[117], temozolomide (glioblastoma)[119] and erlotinib (NSCLC)[142]. In a very recent publication, the combination of JAK2 (Ruxolitinib) and SHP2 (RMC-4550) inhibitors has been shown to result in the enhanced inhibition of *in vitro* growth in myeloproliferative neoplasms.[215] We wanted to evaluate if there was synergistic potential in the novel

combination of SHP099 and pacritinib which have independently shown efficacy in HGSC *in vitro*.

Using 2D cell viability assays we determined the effective concentration range for both pacritinib and SHP099 and performed IC50 analysis for a panel of OvCa cell lines including five HGSC cell lines (Section 4.2.4 and Section 3.2.3). Interestingly, pacritinib results in significantly reduced 2D growth and viability at micromolar concentrations five HGSC cell lines including paired cisplatin sensitive and resistant lines (Section 3.2.3). SHP099 was observed to result in limited but still significant reduction in 2D growth and viability of PE01, PE04, OVCAR3 and PEA1 HGSC cell. While Pacritinib shows considerable efficacy at low micromolar concentrations the IC50 value for SHP099 was not obtainable for PE01, OVCAR3, PEA1 and PEA2 cell lines as it exceeded the SHP2 specificity range.

To assess potential combination synergy, we selected both effective and sub effective concentrations of pacritinib and SHP099. 2D viability assays were initially employed to assess the synergistic-antagonistic potential of this novel drug combination. Following the combination of pacritinib and SHP099 we observed limited synergy at higher concentrations in three of the five HGSC cell lines tested (Section 4.2.4).

3D growth assay models allow us to more accurately model how cancer cells grow *in vivo* and provide a more appropriate model to assess efficacy of inhibitors *in vitro*. Using a Matrigel growth assay we cultured five HGSC cell lines in a matrix and assessed 3D growth and viability using ATP levels as a readout (Section 4.2.5). Following combination of pacritinib and SHP099 we observed considerable levels of synergistic reduction in 3D growth and viability in all five HGSC cell lines (Section 4.2.5). Interestingly this included two sets of paired cell lines covering cisplatin sensitive and cisplatin resistant HGSC.

To confirm this observation, we employed an additional 3D methodology. We used the Happy Cell Media reagent to form 3D spheroids from PE01, PE04 and OVCAR3 HGSC cell lines. This allowed us to assess efficacy of inhibitors on spheroid growth and viability. This methodology was used to prepare lysates for the proteomic analysis. These spheroids were then treated with pacritinib and SHP099 both alone and in combination to assess the potential synergistic benefit (Section 4.2.5). We again observed synergistic reduction in 3D growth and viability in PE01, PE04 and OVCAR3 HGSC cell lines using this model (Section 4.2.5). The concentration of 2.5μM pacritinib was shown to be synergistic with 10μM SHP099 in all three HGSC cell lines assessed (Section 4.2.5).

The cell lines used for this work (PE01, PE04, OVCAR3, PEA1 and PEA2) were all derived from patients with HGSC. However, they all show differences. For example, PE04 and PEA2 were isolated from the same patients as PE01 and PEA1 (respectively), at later stages of treatment and are typically used to model cisplatin resistance *in vitro*. The combination of pacritinib and SHP099 was observed to result in a synergistic reduction in 3D viability and growth in all HGSC cell lines assessed irrespective of whether the cell line was isolated from cisplatin sensitive or resistant patients.

We observed higher levels of synergistic reduction in viability using 3D growth assay models compared to the 2D *in vitro* growth assay models evaluated. These increased levels of synergy may directly relate to increased activity or potency of the SHP099 inhibitor in 3D models compared to 2D models. It has previously been shown that SHP2 activation (increased phosphorylation at Y542) is increased in 3D cell culture conditions.[222] Interestingly it was further shown that SHP099 displays increased efficacy in 3D growth environments compared to 2D cell culture models.[222] This may explain why we observed limited reduction in 2D viability in HGSC cell lines

and more pronounced reduction in 3D viability and anchorage independent growth in the same cell lines.

(4.3.3) The Combination of Pacritinib and SHP099 Results in Elevated Markers of Apoptotic Cell Death in Cisplatin Resistant PE04 HGSC Cell Line *In Vitro*.

Having observed higher synergistic reduction in 3D viability and growth following the combination of pacritinib and SHP099 (Section 4.2.5), we wanted to evaluate the molecular mechanisms underlying this. To achieve this, we employed a global proteomics approach. Spheroids were formed in 3D matrix, from cisplatin resistant HGSC PE04 cell line, and treated with concentrations of pacritinib (2.5μM) and SHP099 (μM) observed to be synergistic.

Proteomic analysis revealed considerable impact on the proteome of cisplatin resistant HGSC cells following combination of pacritinib and SHP099 compared to vehicle control or single treatments with SHP099 or pacritinib (Section 4.2.6). Following adjustments to remove background and filter based on valid values (present in at least three replicates in one treatment group) statistically significant (p-value ≤0.05) and differentially abundant (fold change ≥ 1.5) proteins were identified for each relevant pairwise comparison.

Principal component analysis indicates good clustering of each treatment arm and good separation of combination treatment replicates compared to any control treated replicates. Hierarchical clustering analysis was performed and confirms good clustering of replicates and separation of treatment arms. These findings provide an indication that our findings are treatments are resulting in unique and reproducible proteomes.

A total of 192 significantly differently abundant proteins were identified in combination treated cells while 30 were identified in SHP099 treated cells and 52 in pacritinib treated cells (Section 4.2.6). Further analysis led to the observation that the majority of targets identified were decreased in combination treated cells compared to all three controls, with only a small fraction of targets being increased by comparison. Interestingly combination treated cells display the highest number of unique targets (73) which were not observed to be increased or decreased following treatment with SHP099 or pacritinib alone (Section 4.2.6).

These proteomics findings show combination treated HGSC cells display considerable proteome difference compared to all three controls. These findings indicate that the synergistic reduction observed in growth and viability of HGSC cells following treatment with pacritinib and SHP099 in combination aligns with a more pronounced impact in the proteome.

Using vehicle control, pacritinib and SHP099 treated cells as controls we investigated the pathways which were impacted in the combination treatment in a cisplatin resistant HGSC cell line. Statistically significant and differentially abundant proteins identified for each pairwise comparison were input into SHINEY GO to assess pathway enrichment analysis and into PANTHER to assess pathway analysis (Section 4.2.6). For both of these analyses we detected quite a large number of pathways in the combination treated cells compared to the single drug treatment condition or vehicle control group. Again, this indicates that the synergistic reduction in growth observed following SHP099 and pacritinib treatment aligns with a more pronounced impact on the proteome of HGSC cells.

PANTHER analysis identified the apoptotic signalling pathway in combination treated cells compared to vehicle or single treatment control groups. Increased levels of apoptosis provide a likely explanation for the higher extent of growth reduction observed in 3D growth assays following treatment with SHP099 and pacritinib in

combination (Section 4.2.5). We wanted to further investigate if increased levels of apoptotic death could be detected in combination cells using *in vitro* growth assays and profiling molecular markers of cell death.

In collaboration with Dr Neil Conlon (DCU) we performed 3D cell death *in vitro* assays (Section 4.2.7). Following treatment with pacritinib and SHP099 alone and in combination, we used the Incucyte to capture readouts of spheroid size and cell death levels every six hours. Fluorescent labels were added which allowed us to measure cell membrane integrity as a readout of cell death.

Following treatment with pacritinib and SHP099 in combination we observed reduction in spheroid size for PE04 and OVCAR3 HGSC cell lines (Section 4.2.7). The cisplatin sensitive PE01 cell line displayed elevated levels of cell death following combination treatment. However, this did not exactly align with PE04 and OVCAR3 which showed similar levels of cell death in combination and pacritinib treated cells (Section 4.2.7). These findings provide an indication that increased cell death may be contributing to the synergistic reduction in growth observed following combination treatment. Following on from these findings we decided to investigate molecular markers of apoptosis using Western blot analysis to gain a clearer understanding of the role of cell death in this novel drug combination.

With a good understanding of the molecular processes of Apoptosis, we can profile molecular markers of apoptosis using western blot analysis. Apoptosis represents a highly regulated process in which programmed, and tightly controlled cell death occurs. Apoptosis plays critical roles in homeostasis through the elimination of unwanted or damaged cells. Apoptotic cell death is characterised by a series of cellular phenotypes and molecular biochemical features. These include cell shrinkage, nucleosome fragmentation, chromatin condensation and plasma membrane blebbing, protein cleavage, DNA fragmentation, increased mitochondrial membrane permeability and increased expression of phosphatidylserine on the cell

plasma membrane.[283] Apoptotic cell death can be induced by a number of extracellular and intracellular stimuli including hypoxia, heat, radiation and cytotoxic chemicals.[284]

Apoptosis can be divided into six key stages including **i)** apoptosis triggering **ii)** activation or pro-apoptotic proteins **iii)** activation of caspase cascade **iv)** degradation of intracellular organelles **v)** Formation of apoptotic bodies **vi)** phagocytosis.[285] Three key pathways exist for apoptosis, divided based on the original stimulating signals, these include the intrinsic pathway, extrinsic pathway and the granzyme / perforin pathway.

The perforin / granzyme apoptotic pathway is induced by the release of proteases from granules present in the cytoplasm of cytotoxic T cells and Natural Killer cells.[284] The extrinsic pathway occurs following ligation, and activation, of death receptors with their respective ligands expressed on activated immune cells[286] while the intrinsic pathway of apoptosis, following mitochondrial outer membrane permeabilization (MOMP), there is formation of the apoptosome complex (cytochrome c / Apaf-1 / Caspase 9), which promotes the activation of the initiator caspase 9 and following this the cleavage and activation of the effector caspase-3.[286]

P53 is mutated in the vast majority of HGSC cell lines. It is important to note that P53 acts a tumour suppressor gene through several mechanisms, key to this role is regulating apoptosis. P53 transcriptionally upregulates the expression of pro-apoptotic proteins such as PUMA, BID and BAX while physically interacting with and blocking the actions of the anti-apoptotic proteins BCL-2 and BCL-XL.[287]

Caspases, synthesised as inactive enzymes, contain a pro-domain, a large p20 and small p10 subunit and upon activation the pro-domain is removed and the large and small subunits are cleaved and assemble into active caspases.[288] Eleven human caspases have been described and can be divided into inflammatory (1, 4 and

5), initiator (2, 8 and 9) or executioner (3, 6 and 7) caspases.[285] As key mediators of apoptosis it is possible to use caspase cleavage as an indicator of apoptosis occurrence in response to treatments.

Using Western blot analysis, we assessed cleavage of the effector caspase 3 in PE04 whole cell lysates treated with pacritinib and SHP099 both alone and in combination (Section 4.2.8). We included a high dose of cisplatin treatment as a positive control. Our findings show elevated levels of caspase 3 cleavage in cisplatin and combination treated HGSC cells (Section 4.2.8). In contrast caspase 3 cleavage was undetectable, by Western blot analysis, following treatment with either pacritinib or SHP099 alone. These findings provide a molecular indication of apoptosis occurring in combination treated cells. We next set about confirming this by assessing another molecular marker of apoptosis PARP-1 cleavage.

PARP-1 is cleaved by activated caspases to an 89kDa fragment and a 24kDa fragment. The 89kDa fragment displays significantly reduced DNA binding capacity while the 24kDa fragment irreversibly binds to nicked DNA acting as a trans dominant inhibitor of active PARPs.[289] This contributes to inhibition of DNA repair enzymes and attenuation of DNA repair.[286] During necrosis PARP-1 has been observed to be cleaved into a 50kDa fragment.[290] PARP1 is involved in DNA repair, including the repair of single strand breaks and double strand breaks, and inhibitors of PARP have been shown to kill cancer cells with BRCA mutations.[291] BRCA2 and PARP have been shown to independently protect stalled replication forks.[292]

In BRCA mutated cells, PARP inhibitors display synthetic lethality due to impaired single strand and double strand break repair which ultimately lead to replication fork collapse, cell cycle arrest and apoptosis.[293] PARP inhibitors have shown considerable efficacy, with Olaparib being the first PARP inhibitor to receive approval for use in advanced stage BRCA mutated OvCa as a maintenance therapy.[294] Since then, Niraparib and Rucaparib also received approval for use in

treatment of recurrent EOC.[295] Results generated from PRIMA, SOLO1 and PAOLA-1 phase III clinical trials has contributed to approval for the use of PARP inhibitors in the first line setting.[294]

As PARP is characteristically cleaved by effector caspase, during apoptosis, we can use PARP cleavage as a marker of apoptosis. Having observed elevated levels of caspase 3 cleavage in combination treated cisplatin resistant HGSC cells we treated we wanted to assess PARP cleavage in HGSC cells (Section 4.2.8). Using Western blot analysis, we observed elevate levels of PARP cleavage following treatment with pacritinib in all HGSC cell lines tested. Interestingly PARP cleavage was observed to be further elevated in combination treated cisplatin resistant and sensitive HGSC cell lines compared to pacritinib treatment.

These findings provide further validation of our proteomics analysis. Furthermore, it provides evidence that elevated levels of apoptosis align with synergistic reduction in growth and viability of HGSC cells *in vitro*. Finally, these findings support the hypothesis that treatment with SHP099 and pacritinib in combination represents a novel therapeutic strategy in HGSC cells.

(4.3.4) Treatment with SHP099 Leads to Impacted Nucleotide Metabolism Pathways in Cisplatin Resistant PE04 HGSC Cell Line *In Vitro*.

Proteomic analysis of cisplatin resistant PE04 HGSC cells treated with SHP099 led to the observation that thirty proteins were statistically significantly and differentially abundant in SHP099 treated cells compared to those treated with vehicle control (Section 4.2.9). These thirty proteins were fed into SHINEY GO and PANTHER to assess the pathways which these proteins are involved in. This led to

the observation that nucleotide metabolism pathways are impacted in cisplatin resistant HGSC cells following treatment with SHP099 (Section 4.2.9). Rapidly dividing cells are reliant on a steady supply of nucleotides in order to replicate their genome with each division. As these results may provide an interesting insight into the mechanisms underlying SHP099 activity in HGSC these findings warranted further investigation to understand the molecular mechanisms underlying reduced 3D growth observed in SHP099 treated HGSC cells.

Pathway enrichment analysis identified two pathways involved in nucleotide synthesis and DNA replication including **i)** pyrimidine metabolism and **ii)** nucleotide metabolism (Section 4.2.9). While Panther pathway analysis identified **i)** *De novo* purine biosynthesis, **ii)** *de novo* pyrimidine deoxyribonucleotide biosynthesis, **iii)** formyltetrahydrofolate biosynthesis, **iv)** salvage pyrimidine deoxyribonucleotides and **v)** p53 pathway. Reviewing the literature led to the conclusion that these pathways are implicated in cancer growth and progression.

Nucleotide metabolism is a critical pathway which mediates the availability of purine and pyrimidine molecules used as building blocks for DNA and RNA synthesis. *De novo* pathways refer to the generation of nucleotides from amino acid precursors while salvage pathways mediate the recycling of pre-existing nucleic acid components to generate nucleotides.[296] Cancer cells rely on nucleotide metabolism pathways to ensure a consistent supply of deoxyribonucleotides to support uncontrolled proliferation and growth.[297, 298] Pyrimidine metabolism has been shown to be dysregulated in gastric cancer[299] and observed to play a critical role in prostate cancer progression and drug sensitivity.[300]

The tumour suppressor protein p53 is mutated in approximately 90% of all HGSC cases and interestingly panther pathway analysis identified the p53 pathway following treatment with SHP099. Previous studies have shown that p53 promotes nucleotide metabolism as the knockdown of mutant p53 was observed to reduce the

expression of nucleotide metabolism genes and in turn result in the depletion of nucleotide pools required for proliferation.[301] These observations led to the conclusion that mutant p53 harbouring cells have an acquired synthetic lethality with the nucleotide salvage pathway.

Finally, Formyltetrahydrofolate was the last pathway identified which plays roles in nucleotide biosynthesis. One carbon metabolism (also known as the folate cycle) is an important cellular pathway which through enzymatic reactions provides the metabolites necessary for the synthesis of nucleotides.[302] In this pathway folic acid is converted to tetrahydrofolate which is in turn is used in nucleotide synthesis in addition to s-adenosylmethionine and glutathione synthesis.[303]

Each of the pathways mentioned above play significant roles in the biosynthesis of nucleotides for DNA and RNA synthesis. Interestingly three targets are regularly identified in these pathways from the targets which were statistically significantly differentially abundant following treatment with SHP099. Panther analysis identified the Ribonucleotide Reductase Regulatory Subunit M2 (RRM2) in *de novo* purine biosynthesis, *de novo* pyrimidine deoxyribonucleotide Biosynthesis and the p53 pathway. Methylenetetrahydrofolate dehydrogenase (NADP+ dependent) 2 (MTHFD2) was identified in the Formyltetrahydrofolate biosynthesis pathway while Thymidine Kinase 1 (TK1) was identified in the salvage pyrimidine deoxyribonucleotides pathway by panther analysis. SHINEY GO pathway enrichment analysis identified RRM2 and TK1 in both pyrimidine metabolism pathway and nucleotide metabolism pathway.

It is clear from these findings that RRM2, TK1 and MTHFD2 are involved in a number of the pathways identified in our proteomics analysis and warrant further investigation. From our proteomics analysis we observed that all three of these proteins were significantly reduced in SHP099 treated HGSC cells compared to vehicle control (Section 4.2.9). Probing mRNA expression of these targets (TNMplot)

we observed RRM2 (41.23-fold), TK1 (44.4-fold) and MTHFD2 (3.8-fold) showed significantly higher expression in serous OvCa compared to normal controls. This provided an indication that these targets themselves represent negative prognostic indicators in OvCa.

While each of these targets show a high increase in gene expression in serous OvCa we did not find any negative association with OS or PFS using KM plotter database. However, we observed that RRM2 HEC display increased PFS in platinum and Taxol treated serous OvCa. TK1 HEC was additionally observed to display increased overall survival in serous OvCa and platinum/Taxol treated serous OvCa. Finally, MTHFD2 HEC were observed to display increased PFS in serous OvCa and platinum/Taxol treated serous OvCa.

Finally, it is clear that nucleotide biosynthesis pathways are impacted in cisplatin resistant PE04 cells following treatment with SHP099. In the sections below I will outline the published literature on three key targets involved in nucleotide biosynthesis which have been shown to play a role in OvCa. These proteins include RRM2 (Section 4.3.4.1), TK1 (Section 4.3.4.2) and MTHFD2 (Section 4.3.4.3). These studies in the context of our findings may indicate that these proteins contribute to the growth of HGSC cells and that treatment with SHP099 may provide a novel therapeutic strategy to target all of these proteins in HGSC at once.

(4.3.4.1) Ribonucleotide reductase M2 (RRM2)

Ribonucleotide reductase (RNR) is a critical enzyme which mediates the reduction of ribonucleotides to deoxyribonucleotides while Ribonucleotide Reductase M2 (RRM2) tightly regulates the activity of RNR with RRM2 expression being a rate limiting factor for RNR activity.[304,305] RRM2 is necessary for the synthesis of

deoxyribonucleotides during the S phase of cell cycle when DNA replication occurs.[306] As mentioned above mutant p53 plays an important role in the expression of nucleotide metabolism proteins. Interestingly this same study observed that mutant p53 promotes the expression of both RRM2 and TK1[301] which we observed to be reduced following treatment with SHP099.

RRM2 has been identified as a potential driver in prostate cancer progression[300] and in lung adenocarcinoma where RRM2 has been observed to be upregulated with high expression being found to be associated with poor survival.[307] RRM2 has been found to be expressed at higher levels in EOC compared to both surface ovarian epithelium and fallopian tube epithelium controls.[306] Additionally, RRM2 expression was observed to be correlated with Ki67 expression, tumour grade and tumour stage with high RRM2 expression being found to be an independent predictor of shorter overall survival in EOC patients.[306]

In EOC cell lines the knockdown of RRM2 has been observed to inhibit growth and trigger cellular senescence and DNA damage response.[306] One study investigating the role of RRM2 in cervical, endometrial and OvCa observed RRM2 promotes proliferation, migration and DNA synthesis *in vitro.*[308] This study further observed that RRM2 inhibits cisplatin drug sensitivity. RRM2 has been observed to promote resistance to both cisplatin and 5-fluorouracil while the knockdown of RRM2 in chronic myeloid leukaemia cell lines included cell death through the activation of Bcl-2 / caspase pathway.[290] Interestingly trans-4,4'-dihydroxystilbene (DHS), by inhibiting RRM2, has been shown to be a potent inhibitor of DNA replication and has shown considerably efficacy in vitro with a relatively low IC50 value in OVCAR3 cell line.[305]

We are not the first group to show SHP099 inhibits ERK activation, but we have confirmed this finding in the HGSC PE04 and OVCAR3 cell lines using Western blotting analysis. Interestingly the reduction in RRM2 expression following treatment

with SHP099 in PE04 cells may be directly related to reduced activation of ERK as one study in Renal cell carcinoma observed ERK inhibitors reduce expression of RRM2.[309]

All these studies show that RRM2 represents a potential therapeutic target in OvCa. Our findings indicate that SHP2 inhibition using SHP099 may be used to target RRM2 in HGSC cells (Section 4.2.9). This may provide a novel mechanism to therapeutically target RRM2 in HGSC. It is clear that further analysis is required but our research in the context of published literature supports the potential that RRM2 may represent a therapeutic target in HGSC which can be targeted downstream of SHP2 inhibition using SHP099.

(4.3.4.2) Thymidine Kinase 1 (TK1)

Thymidine Kinase 1 (TK1) is an important protein involved in *de novo* and salvage nucleotide synthesis through catalysing the synthesis of deoxythymidine monophosphate from thymidine.[310] TK1 has been shown to play significant roles in cancer. In hepatocellular carcinoma cell lines, the overexpression of TK1 enhanced proliferative capacity while knockdown of TK1 significantly reduced proliferation and included G0/G1 cell cycle arrest.[311]

TK1 has previously been highlighted as a biomarker in ovarian cancer as expression was observed to be elevated in malignant ovarian tumours compared to normal benign controls.[312] This study further showed TK1 expression correlated with stage, intrapelvic, lymphatic and distant metastasis. An immunohistochemical study of TK1 protein expression in 109 serous ovarian adenocarcinoma samples observed TK1 expression was an independent prognostic factor for relapse but not survival.[313]

These studies indicate that TK1 represents a negative prognostic indicator in OvCa. However, to the best of my knowledge no studies have been done showing a link between TK1 and growth of HGSC cells. Our findings indicate that following SHP099 treatment TK1 is significantly reduced in HGSC (Section 4.2.9). As we have shown SHP099 significantly reduced growth and viability of HGSC cells (Section 4.2.4) it may be that reduced TK1 expression contributes to this. It is clear that further experiments are required to investigate the role of TK1 in HGCS cell growth *in vitro*. It is clear that SHP099 can be used to target TK1 in HGSC cells and may represent a novel therapeutic strategy to target TK1, should TK1 be shown to positively regulate HGSC growth .

(4.3.4.3) Methylenetetrahydrofolate Dehydrogenase (NADP+ Dependent) 2 (MTHFD2)

Methylenetetrahydrofolate Dehydrogenase (NADP+ Dependent) 2 (MTHFD2) plays a key role in the formyltetrahydrofolate biosynthesis which provides crucial precursors required for the synthesis of nucleic acids. Interestingly in nasopharyngeal carcinoma MTHFD2 has been observed to be upregulated and associated with poor prognosis while the knockdown of MTHFD2 supressed proliferation, migration and ERK signalling.[314]

In OvCa MTHFD2 has been observed to be highly expressed while siRNA silencing of MTHFD2 impaired ERK activation and induced ferroptosis in ovarian cancer cells.[315] Another study observed MTHFD2 was highly expressed in ovarian cancer tissue and knockdown induced apoptosis, reduced STAT3 activation and G2/M cell cycle arrest.[316] Similar findings were observed where MTHFD2 expression was observed to be upregulated in OvCa compared to normal samples with the high expression cohorts showing reduced survival rates.[317] This group additionally

observed that MTHFD2 knockdown inhibited proliferation, migration and invasion in vitro.[317]

These studies show that MTHFD2 represents a therapeutic target in OvCa. It is also clear from these published works that MTHFD2 plays an important role in the survival and growth of OvCa cells. Our findings show that MTHFD2 is significantly decreased in HGSC cells following treatment with SHP099 (Section 4.2.9). Treatment with SHP099 may represent a novel therapeutic strategy to target MTHFD2 in OvCa.

(4.3.4.4) DEAD-Box Helicase 3, X-Linked (DDX3X)

DEAD-Box Helicase 3, X-Linked (DDX3X) was observed to be decreased in cisplatin resistant HGSC cells following treatment with SHP099. TNMplot analysis led to the observation that DDX3X is significantly decreased in serous OvCa compared to normal controls (Section 4.2.9). Further analysis using KM plotter led to the observation that the DDX3X high mRNA expression cohort displays significantly reduced progression free survival in serous OvCa (Section 4.2.9).

String analysis identified a cluster of targets which appears to be centred around DDX3X. DDX3X has been characterised to be a multifunctional protein involved in a range of biological processes and pathways including RNA transcription, translation, micro-RNA expression and metabolic / cellular stress responses.[318] Considering that DDX3X was not identified in the pathway enrichment analysis these interactions may lie outside the scope of the pathways identified and investigated.

Three targets directly connect to DDX3X in the string analysis. These include Serine / Arginine-Rich Splicing Factor 5 (SRSF5), Eukaryotic Translation Initiation Factor 3 Subunit C (EIF3C) and Gem Nuclear Organelle Associated Protein 5 (GEMIN5). Of these three targets EIF3C may hold the most interest in connection to

DDX3X. DDX3X has previously been shown to interact with eIF3.[319] This interaction may represent an interesting finding in HGSC. DDX3X has previously been shown to promote metastasis of head and neck squamous cell carcinoma (HNSCC) where higher protein expression of DDX3X was also observed to correlate with poor prognosis.[320] DDX3X was observed to achieve this through activation of cap-binding complex (CBC) – eIF3 mediated translation of uORF containing oncogenic mRNA's.[320]

Our findings indicate that DDX3X may represent a negative prognostic indicator in OvCa (Section 4.2.9) and that targeting DDX3X using SHP099 may provide a novel therapeutic strategy in OvCa. It is clear that not enough published literature exists to confirm if DDX3X plays a negative or positive role in growth of OvCa. Further studies are required to confirm this.

(4.3.5) Treatment with Pacritinib and SHP099 Synergistically Reduces 3D Growth and Viability of Murine OvCa ID8 Cell Line *In Vitro*

We have shown considerable synergistic reduction in 3D growth and viability of HGSC cell lines treated with pacritinib and SHP099 *in vitro* (Section 4.2.9). The logical progression of this work would involve using an animal model to assess efficacy of pacritinib and SHP099 both alone and in combination using *in vivo* models (xenograft and syngeneic). SHP099 has shown considerable efficacy in murine models of oesophageal squamous cell carcinoma[239], KRAS mutant non-small cell lung cancer[251] and OvCa xenograft models.[56]

Pacritinib has displayed considerable efficacy in murine models of several cancer types which have been highlighted in (Table 1.5.1 and Table 1.5.2). Pacritinib

has shown considerable efficacy in murine models including medulloblastoma[107], acute myeloid leukaemia[92] and non-small cell lung cancer[131].To the best of our knowledge pacritinib has not been evaluated alone or in combination with SHP099 in murine models of ovarian cancer to date.

In preparation for future *in vivo* studies, we assessed the efficacy of this novel drug combination in the OvCa murine ID8 VEGF Defb29f cell line. Interestingly we observed quite similar results compared to the human HGSC cell line *in vitro* growth assays. In 3D growth models the combination of pacritinib and SHP099 result in considerable levels of synergistic reduction in ID8 growth and viability. In addition to this we observed that SHP099 and pacritinib both potently inhibit 3D anchorage independent growth and spheroid formation of the ID8 cell line independently. These findings strongly support investigation of this novel drug combination in murine models of ovarian cancer.

(4.4) Concluding Remarks

HGSC represents the most clinically relevant subtype of ovarian cancer. It is clear that novel therapeutic strategies are required to combat the high frequency of chemo-resistant disease observed in this poor outcome cancer. Our research aimed to show that SHP2 represents a therapeutic target in HGSC using SHP099 both alone and in combination with pacritinib.

The first objective of this chapter was to examine SHP2 expression in HGSC and assess association with prognostic indicators. Probing the KM plotter database we have shown that the SHP2 high expression cohort displays significantly reduced overall survival in all OvCa, serous OvCa and high stage (3+4) OvCa, both refined for platinum and Taxol treatment and unrefined. Using immunohistochemical staining we observed SHP2 protein expression was significantly increased in HGSC compared to normal adjacent tissue and in high stage (3+4) HGSC compared to low stage (1) HGSC. These findings indicate that SHP2 represents a negative prognostic indicator in HGSC.

We have observed increased SHP2 expression in the cisplatin resistant PE04 cell line compared to the paired PE01 cell line which could provide an indication that SHP2 plays a role in the development of cisplatin resistance in HGSC.

Our second objective of this chapter was to evaluate the efficacy of the allosteric SHP2 inhibitor SHP099 in HGSC cell lines *in vitro*. Using 3D in vitro growth assay models we have shown that SHP2 represents a potential therapeutic target in HGSC. Treatment with SHP099 led to a significant reduction in 3D growth and viability of HGSC cells *in vitro*.

The third objective of this chapter was to investigate the efficacy of pacritinib and SHP099 in combination on the growth of OvCa cell lines *in vitro*. Our findings using in vitro growth assays indicate that the combination of pacritinib and SHP099

may represent a novel therapeutic strategy in HGSC. Following treatment with pacritinib and SHP099 in combination we observed synergistic reduction in 3D growth and viability of HGSC cell lines *in vitro*.

The fourth and final objective of this chapter was to examine the molecular mechanism of action following treatment with pacritinib and SHP099 in OvCa cell lines using a proteomics-based approach. Our proteomics and western blot analysis indicates that apoptotic cell death is contributing to the reduced growth and viability observed.

The synergistic reduction in growth of HGSC observed following treatment with pacritinib and SHP099 in combination provides evidence that this novel therapeutic strategy may hold potential in the treatment of HGSC. It is clear that further in vivo studies are required in order to further investigate this. Using OvCa murine ID8 cells we have shown synergistic reduction in 3D growth and viability of following treatment with pacritinib and SHP099 in combination. These observations strongly support the progression of this work to xenograft and syngeneic animal models to further investigate the efficacy of this novel drug combination.

Nucleotide metabolism pathways are impacted following treatment with SHP099 in cisplatin resistant HGSC cells and may contribute to the reduced growth and viability observed in the *in vitro* growth assays. Further analysis of SHP099 treated PE04 cells led to the observation that proteins implicated in nucleotide metabolism were statistically significant and differentially reduced compared to vehicle control treated cells.

Three proteins identified from this proteomics analysis have been shown to represent potential therapeutic targets in OvCa. These include RRM2, TK1 and MTHFD2. Our findings may support the use of SHP099 as a novel therapeutic strategy targeting TK1, RRM2 and MTHFD2 in OvCa. It is clear that further analysis

is required to further evaluate the efficacy of this approach and the role of each of these targets in HGCS.

Furthermore, gene expression of both RRM2 and TK1 are considerably higher in serous OvCa compared to normal controls. HGSC subtype shows a high frequency of p53 mutation and previous studies have shown mutant p53 increases the expression of RRM2 and TK1. These targets may provide a novel therapeutic strategy to target p53 mutant HGSC using SHP099

In conclusion it is clear that SHP2 represents a negative prognostic indicator in HGSC and that treatment with SHP099 may provide a therapeutic strategy in HGSC both alone and in combination with pacritinib.

(4.5) Future Directions

To date no study has shown nuclear localisation of SHP2 is associated with reduced OS in OvCa. However, the fact that this association has been made in NSCLC we must consider that the same could be true in OvCa. As previously highlighted high stage HGSC display reduced OS compared to low stage HGSC. It is therefore interesting that we observed elevated nuclear staining of HGSC in high stage HGSC compared to low stage. This warrants future investigation into the association between nuclear localisation of SHP2 and OS in OvCa.

In this study we have shown nuclear staining of SHP2 protein is elevated in stage 3/4 HGSC compared to stage 1 HGSC. As HGSC diagnosed in the advanced stage is associated with lower OS this opens an important follow up set of experiments. Further SHP2 IHC should be performed (with ethical approval) using patients' samples to investigate the association between OS and nuclear staining. This is analysis which was not possible from the results we have as we did not have access to OS.

Potential therapeutic strategies involving the combination of pacritinib and SHP099 represent a novel therapeutic approach for the treatment of the clinically relevant HGSC OvCa subtype. Our findings have shown promising synergistic reduction of 3D growth and viability of HGSC cell lines *in vitro* following treatment with pacritinib and SHP099 in combination. This opens several research pathways up for further investigation.

It is important to better understand the cause and mechanism of the synergy we observed in our growth assays. In order to do this, we need to evaluate a number of other potential drug combinations including SHP099 with IRAK1, JAK2, STAT3 and FLT3 specific inhibitors. This would allow us to further focus in on novel synergistic

interactions and potentially further dissect the mechanisms of action following SHP099 and pacritinib combination.

In this study we identified apoptotic cell death was occurring downstream of both pacritinib treated HGSC and combination treated HGSC cell lines *in vitro*. Proteomics analysis of pacritinib and SHP099 combination also highlighted proteins involved in DNA replication, mismatch repair and cell cycle were differentially abundant in PE04 cells following treatment. As each of these pathways are important during cell division which is commonly dysregulated in cancer it may be valuable to perform flow cytometry-based cell cycle analysis in order to preliminarily investigate if combination treatment is resulting in cell cycle arrest in addition to cell death.

Proteomics analysis and investigation of the targets identified following treatment of PE04 cells with SHP099 has provided a number of interesting targets for further evaluation. A number of these have been highlighted by our research including RRM2 and TK1. It is clear that further evaluation of these targets is needed in the context of HGSC. In order to achieve this in vitro growth assays could be performed using targeted inhibitors, siRNA or lentiviral knockdown to assess the role these targets play in the growth of the HGSC cell lines we evaluated.

Our proteomics studies in this chapter provided some nice insights into the mechanisms of SHP099 both alone and in combination with pacritinib. For these studies we have used the cisplatin resistant PE04 HGSC cell line. Further studies including the paired cisplatin sensitive PE01 cell line could allow for the comparison of these therapeutic strategies in both cisplatin sensitive and resistant HGSC. As outlined cisplatin resistance represents a major barrier to effective treatment of patients diagnosed with advanced stage HGSC and this proteomics analysis may prove considerably valuable in this context.

Our findings strongly have shown pacritinib and SHP099 synergistically reduce growth and viability of HGSC human cell lines and ID8 murine cell lines *in vitro*. These studies provide the groundwork for and support the progression to murine studies to investigate the efficacy of pacritinib and SHP099 using an *in vivo* model. During the course of my PhD, I prepared a draft application which could be used to support an application to the HPRA to conduct these studies.

The ID8 cell line we have used in these studies could be used for these in vivo studies and would allow for the use of a syngeneic murine model to further assess the efficacy of this novel drug combination in an immunocompetent model. This would be very valuable to this project as it would allow us to progress from bench to bedside research and take a step closer to the clinic. It is with this goal in mind that it is important to evaluate the impact using a syngeneic animal model as in the clinic our treatment would be applied in the presence of an immune system.

Section 5

Concluding Remarks

(5) Concluding Remarks

HGSC represents the most clinically relevant subtype of EOC and accounts for the majority of cases (~70%) and deaths (~70%). HGSC is characterised by a high frequency of advanced stage detections. While HGSC patients initially respond quite well (70%) to first line therapeutic interventions the majority (70%-80% of initial responders) of patients will eventually relapse and be challenged with chemoresistance disease. Both of these factors pose considerable challenges in the treatment of patients with HGSC and contribute heavily to the poor prognosis associated with HGSC patients diagnosed with advanced stage disease. It is clear that novel therapeutic strategies are urgently required in order improve outcomes for HGSC patients.

The first aim of our research was to investigate the role of IRAK1 in OvCa. In chapter 3 we showed that IRAK1 represents a negative prognostic indicator in in OvCa. Probing publicly available databases we have shown that IRAK1 mRNA expression is significantly increased in serous OvCa and that IRAK1 high mRNA expression cohort display significantly reduced OS in comparison to the IRAK1 low mRNA expression cohort.

We further showed that IRAK1 plays a positive role in promoting the growth of OvCa cells. IRAK1 knockdown led to a significant reduction in colony formation, proliferation, migration/invasion and anchorage independent growth of OvCa cell lines *in vitro*. Our analysis of IRAK1 knockdown cells further uncovered a novel association between IRAK1 and HER4 expression. HER4 expression was observed to be significantly reduced in HER4 expressing OvCa cells following IRAK1 knockdown. Reduced HER4 may be contributing to the reduced growth in this model however the mechanism underlying the association between IRAK1 and HER4 remain unclear and warrant further investigation.

Our research indicates that pacritinib may provide an effective therapeutic strategy to target IRAK1 in OvCa. Following treatment with Pacritinib we observed significant reduction in both 2D and 3D growth of OvCa cell lines *in vitro*. Furthermore, we have shown that OvCa cells treated with pacritinib display impaired activation of growth factor receptors and JAK2/STAT3 activation which may be contributing to the reduced growth observed in this model.

The second aim of our research was to investigate the role of SHP2 in OvCa. In chapter 4 we evaluated our second target, the protein tyrosine phosphatase SHP2. Our findings show that SHP2 may represent a negative prognostic indicator in in OvCa. In OvCa the SHP2 high mRNA expression cohort displayed significantly reduced OS compared to the SHP2 low mRNA expression cohort. Using IHC we further showed that SHP2 protein expression is significantly elevated in HGSC compared to normal adjacent tissue. SHP2 protein expression was also shown to be elevated in high stage (3+4) HGSC compared to stage 1 HGSC. These findings indicate SHP2 may play a role in the progression of HGSC.

Our expression analysis showed significantly elevated SHP2 expression in the cisplatin resistant PE04 cell line compared to the cisplatin sensitive paired PE01 cell line. This finding may indicate that SHP2 plays a role in the development of cisplatin resistance in OvCa.

Furthermore, we have shown that pharmacological inhibition of SHP2 may hold therapeutic efficacy in HGSC. Treatment with the allosteric SHP2 inhibitor SHP099 resulted in significantly impaired 2D and 3D growth/viability and reduced anchorage independent growth of HGSC cells.

Proteomics analysis of SHP099 treated HGSC cells showed impacted nucleotide metabolism pathways. These findings led to the observation that treatment with SHP099 results in a significant reduction in RRM2 and TK1 in HGSC cells. Both

of these proteins have been identified as potential therapeutic targets in p53 mutant OvCa. Our findings may support treatment with SHP099 as a novel therapeutic strategy to target RRM2 and TK1 in HGSC.

The final aim of our research was to evaluate the combination of SHP099 and Pacritinib *in vitro*. SHP099 and pacritinib in combination may provide a novel therapeutic strategy to target HGSC. Treatment with SHP099 and pacritinib in combination resulted in synergistic reduction in 3D growth and viability of HGSC cells including cell lines isolated from both cisplatin sensitive and cisplatin resistant patients.

Our findings further indicate this synergistic reduction in growth and viability may be occurring due to increased cell death. Proteomics and western blot analysis led to the observation that markers of apoptosis, including cleaved caspase 3 and cleaved PARP, were elevated following the combination of pacritinib and SHP099 in HGSC cells.

Our *in vitro* growth assays strongly support the further evaluation of this novel drug combination using *in vivo* murine models. In preparation for the progression to *in vivo* studies, we performed *in vitro* growth assays using murine OvCa cell lines to assess this novel drug combination. Following treatment with SHP099 and pacritinib in combination we observed synergistically reduced 3D growth and viability of murine OvCa cells *in vitro*.

Section 6

Posters and Presentations

Over the course of my PhD, I was fortunate to present my research findings from work included on both of my research chapters. These have included national and international conferences which focused on cutting edge-cancer research and internal research days in Maynooth University (Table 6.1).

These experiences have been a highlight of my PhD journey and contributed significantly to my personal and professional development. These conferences allowed me to engage with a diverse scientific community, receive valuable feedback and insights on my work while refining my scientific communications skills.

Table 6.1: List of research posters and oral presentations presented on during my PhD.

Conference name	Location	Date(s)	Title of presentation or poster
Biology Department Research Day	Maynooth University	11/05/2022	Investigating IRAK1 Knockdown in Ovarian Cancer.
Immunology Society Ireland (ISI)	Maynooth University	01/09/2022	Investigating the Role of IRAK1 in Ovarian Cancer
The Irish Society of Gynaecological Oncology (ISGO)	Dean Hotel Galway, 80 Prospect Hill, Centre, Galway	18/11/2022	Investigating the role of IRAK1 in Ovarian Cancer
The Irish Association for Cancer Research (IACR)	Radisson Hotel Northgate Street, Athlone	22/02/2023	Investigating IRAK1 in Ovarian Cancer (Shortlisted for best poster presentation)
Biology Department Research Day	Maynooth University	11/05/2023	The Role of IRAK1 in Ovarian Cancer
The European Association for Cancer Research (EACR)	Turino Italy	12th-15th of June 2023	Investigating the role of IRAK1 in Ovarian Cancer.
Biology Department Research Day	Maynooth University	14/05/2024	Investigating the potential of IRAK1 and SHP2 inhibitors in Ovarian Cancer
The Irish Association for Cancer Research (IACR)	Europa Hotel Belfast	5th-7th of March 2025	Investigating the Role of SHP2 in High Grade Serous Carcinoma

Section 7

Bibliography

(7.1) Bibliography

1. Hanahan, D. & Weinberg, R. A. Hallmarks of cancer: The next generation. *Cell* **144**, 646–674 (2011).
2. Hanahan, D. Hallmarks of Cancer: New Dimensions. *Cancer Discov.* **12**, 31–46 (2022).
3. Cancer. https://www.who.int/health-topics/cancer#tab=tab_1.
4. Ovarian Cancer Key Stats* – World Ovarian Cancer Coalition. https://worldovariancancercoalition.org/about-ovarian-cancer/key-stats/.
5. Ovary. https://gco.iarc.fr/today (2020).
6. Zhu, X., Cai, H., Zhao, L., Ning, L. & Lang, J. CAR-T cell therapy in ovarian cancer: from the bench to the bedside. *Oncotarget* **8**, 64607 (2017).
7. Lisio, M. A., Fu, L., Goyeneche, A., Gao, Z. H. & Telleria, C. High-grade serous ovarian cancer: Basic sciences, clinical and therapeutic standpoints. *Int. J. Mol. Sci.* **20**, (2019).
8. Lheureux, S., Gourley, C., Vergote, I. & Oza, A. M. Epithelial ovarian cancer. *The Lancet* **393**, 1240–1253 (2019).
9. Milanesio, M. C., Giordano, S. & Valabrega, G. Clinical implications of DNA repair defects in high-grade serous ovarian carcinomas. *Cancers (Basel).* **12**, 1–20 (2020).
10. Cortez, A. J., Tudrej, P., Kujawa, K. A. & Lisowska, K. M. Advances in ovarian cancer therapy. *Cancer Chemotherapy and Pharmacology 2017 81:1* **81**, 17–38 (2017).
11. Lheureux, S., Gourley, C., Vergote, I. & Oza, A. M. Epithelial ovarian cancer. *The Lancet* **393**, 1240–1253 (2019).
12. Lisio, M. A., Fu, L., Goyeneche, A., Gao, Z. H. & Telleria, C. High-grade serous ovarian cancer: Basic sciences, clinical and therapeutic standpoints. *Int. J. Mol. Sci.* **20**, (2019).
13. Borella, F. *et al.* Immune Checkpoint Inhibitors in Epithelial Ovarian Cancer: An Overview on Efficacy and Future Perspectives. *Diagnostics* **10**, 146 (2020).
14. Hallas-Potts, A., Dawson, J. C. & Herrington, C. S. Ovarian cancer cell lines derived from non-serous carcinomas migrate and invade more aggressively than those derived from high-grade serous carcinomas. *Scientific Reports 2019 9:1* **9**, 1–10 (2019).
15. Kim, J. *et al.* Cell Origins of High-Grade Serous Ovarian Cancer. *Cancers 2018, Vol. 10, Page 433* **10**, 433 (2018).
16. Moffitt, L., Karimnia, N., Stephens, A. & Bilandzic, M. Therapeutic Targeting of Collective Invasion in Ovarian Cancer. *Int. J. Mol. Sci.* **20**, (2019).

17. Kurman, R. J. Origin and molecular pathogenesis of ovarian high-grade serous carcinoma. *Annals of Oncology* **24**, x16–x21 (2013).

18. Della Pepa, C. *et al.* Low Grade Serous Ovarian Carcinoma: From the molecular characterization to the best therapeutic strategy. *Cancer Treat. Rev.* **41**, 136–143 (2015).

19. Gadducci, A. *et al.* Current strategies for the targeted treatment of high-grade serous epithelial ovarian cancer and relevance of BRCA mutational status. *J. Ovarian Res.* **12**, 1–8 (2019).

20. Yeung, T. L. *et al.* Cellular and molecular processes in ovarian cancer metastasis. A review in the theme: Cell and molecular processes in cancer metastasis. *Am. J. Physiol. Cell Physiol.* **309**, C444–C456 (2015).

21. Petousis, S. *et al.* PARP Inhibitor Maintenance After First-Line Chemotherapy in Advanced-Stage Epithelial Ovarian Cancer. *JAMA Netw. Open* **8**, e2541648 (2025).

22. Ngoi, N. Y. L. *et al.* Weekly versus tri-weekly paclitaxel with carboplatin for first-line treatment in women with epithelial ovarian cancer. *Cochrane Database of Systematic Reviews* vol. 2022 Preprint at https://doi.org/10.1002/14651858.CD012007.pub2 (2022).

23. Tucker, S. L. *et al.* Molecular biomarkers of residual disease after surgical debulking of high-grade serous ovarian cancer. *Clinical Cancer Research* **20**, 3280–3288 (2014).

24. Lengyel, E. Ovarian Cancer Development and Metastasis. *Am. J. Pathol.* **177**, 1053 (2010).

25. Haslehurst, A. M. *et al.* EMT transcription factors snail and slug directly contribute to cisplatin resistance in ovarian cancer. *BMC Cancer* **12**, 1–10 (2012).

26. Zhao, Y. *et al.* Chemotherapy exacerbates ovarian cancer cell migration and cancer stem cell-like characteristics through GLI1. *British Journal of Cancer 2020 122:11* **122**, 1638–1648 (2020).

27. Liu, W. *et al.* Cisplatin-stimulated macrophages promote ovarian cancer migration via the CCL20-CCR6 axis. *Cancer Lett.* **472**, 59–69 (2020).

28. Dasari, S. & Bernard Tchounwou, P. Cisplatin in cancer therapy: Molecular mechanisms of action. *European Journal of Pharmacology* vol. 740 364–378 Preprint at https://doi.org/10.1016/j.ejphar.2014.07.025 (2014).

29. Mai, J. *et al.* Molecular mechanisms of platinum-based chemotherapy resistance in ovarian cancer (Review). *Oncology Reports* vol. 47 Preprint at https://doi.org/10.3892/or.2022.8293 (2022).

30. Nunes, M. *et al.* Deciphering the Molecular Mechanisms behind Drug Resistance in Ovarian Cancer to Unlock Efficient Treatment Options. *Cells* vol. 13 Preprint at https://doi.org/10.3390/cells13090786 (2024).

31. McMullen, M., Karakasis, K., Madariaga, A. & Oza, A. M. Overcoming platinum and parp-inhibitor resistance in ovarian cancer. *Cancers* vol. 12 1–18 Preprint at https://doi.org/10.3390/cancers12061607 (2020).

32. Nag, S., Aggarwal, S., Rauthan, A. & Warrier, N. Maintenance therapy for newly diagnosed epithelial ovarian cancer– a review. *Journal of Ovarian Research* vol. 15 Preprint at https://doi.org/10.1186/s13048-022-01020-1 (2022).

33. Leong, H. S. *et al.* Efficient molecular subtype classification of high-grade serous ovarian cancer. *J. Pathol.* **236**, 272–277 (2015).

34. Hu, J. *et al.* Development of survival predictors for high-grade serous ovarian cancer based on stable radiomic features from computed tomography images. *iScience* **25**, 104628 (2022).

35. Bowtell, D. D. *et al.* Rethinking ovarian cancer II: reducing mortality from high-grade serous ovarian cancer. *Nature Reviews Cancer 2015 15:11* **15**, 668–679 (2015).

36. Hoppenot, C., Eckert, M. A., Tienda, S. M. & Lengyel, E. Who are the long-term survivors of high grade serous ovarian cancer? *Gynecol. Oncol.* **148**, 204–212 (2018).

37. Takaya, H., Nakai, H., Takamatsu, S., Mandai, M. & Matsumura, N. Homologous recombination deficiency status-based classification of high-grade serous ovarian carcinoma. *Scientific Reports 2020 10:1* **10**, 1–8 (2020).

38. Clarke, C. L. *et al.* Predictors of long-term survival among high-grade serous ovarian cancer patients. *Cancer Epidemiology Biomarkers and Prevention* **28**, 996–999 (2019).

39. Dao, F. *et al.* Characteristics of 10-year survivors of high-grade serous ovarian carcinoma. *Gynecol. Oncol.* **141**, 260–263 (2016).

40. Yang, S. Y. C. *et al.* Landscape of genomic alterations in high-grade serous ovarian cancer from exceptional long- and short-term survivors. *Genome Med.* **10**, 1–17 (2018).

41. Zhang, S. *et al.* Both fallopian tube and ovarian surface epithelium are cells-of-origin for high-grade serous ovarian carcinoma. *Nature Communications 2019 10:1* **10**, 1–16 (2019).

42. Chui, M. H., Momeni Boroujeni, A., Mandelker, D., Ladanyi, M. & Soslow, R. A. Characterization of TP53-wildtype tubo-ovarian high-grade serous carcinomas: rare exceptions to the binary classification of ovarian serous carcinoma. *Modern Pathology 2020 34:2* **34**, 490–501 (2020).

43. Cole, A. J. *et al.* Assessing mutant p53 in primary high-grade serous ovarian cancer using immunohistochemistry and massively parallel sequencing. *Scientific Reports 2016 6:1* **6**, 1–12 (2016).

44. Takaya, H. *et al.* Intratumor heterogeneity and homologous recombination deficiency of high-grade serous ovarian cancer are associated with prognosis

and molecular subtype and change in treatment course. *Gynecol. Oncol.* **156**, 415–422 (2020).

45. Himoto, Y. *et al.* Does the method of primary treatment affect the pattern of first recurrence in high-grade serous ovarian cancer? *Gynecol. Oncol.* **155**, 192–200 (2019).

46. Mahmood, R. D., Morgan, R. D., Edmondson, R. J., Clamp, A. R. & Jayson, G. C. First-Line Management of Advanced High-Grade Serous Ovarian Cancer. *Curr. Oncol. Rep.* **22**, 1–14 (2020).

47. Friedlander, M. *et al.* Long-term efficacy, tolerability and overall survival in patients with platinum-sensitive, recurrent high-grade serous ovarian cancer treated with maintenance olaparib capsules following response to chemotherapy. *British Journal of Cancer 2018 119:9* **119**, 1075–1085 (2018).

48. Gralewska, P., Gajek, A., Rybaczek, D., Marczak, A. & Rogalska, A. The Influence of PARP, ATR, CHK1 Inhibitors on Premature Mitotic Entry and Genomic Instability in High-Grade Serous BRCAMUT and BRCAWT Ovarian Cancer Cells. *Cells* **11**, 1889 (2022).

49. Sun, J. *et al.* Immuno-genomic characterisation of high-grade serous ovarian cancer reveals immune evasion mechanisms and identifies an immunological subtype with a favourable prognosis and improved therapeutic efficacy. *British Journal of Cancer 2022 126:11* **126**, 1570–1580 (2022).

50. Drakes, M. L. *et al.* Stratification of ovarian tumor pathology by expression of programmed cell death-1 (PD-1) and PD-ligand- 1 (PD-L1) in ovarian cancer. *J. Ovarian Res.* **11**, 1–11 (2018).

51. Hu, Y. *et al.* Integrated Proteomic and Glycoproteomic Characterization of Human High-Grade Serous Ovarian Carcinoma. *Cell Rep.* **33**, 108276 (2020).

52. Bicaku, E. *et al.* In vitro analysis of ovarian cancer response to cisplatin, carboplatin, and paclitaxel identifies common pathways that are also associated with overall patient survival. *British Journal of Cancer 2012 106:12* **106**, 1967–1975 (2012).

53. Helm, C. W. & States, J. C. Enhancing the efficacy of cisplatin in ovarian cancer treatment – could arsenic have a role. *J. Ovarian Res.* **2**, 2 (2009).

54. Wang, J. & Wu, G. S. Role of Autophagy in Cisplatin Resistance in Ovarian Cancer Cells *. *Journal of Biological Chemistry* **289**, 17163–17173 (2014).

55. Patel, J. N. *et al.* Characterisation of homologous recombination deficiency in paired primary and recurrent high-grade serous ovarian cancer. *British Journal of Cancer 2018 119:9* **119**, 1060–1066 (2018).

56. Sun, B. *et al.* Synergistic effects of SHP2 and PI3K pathway inhibitors in GAB2-overexpressing ovarian cancer. *Am. J. Cancer Res.* **9**, 145 (2019).

57. Bahar, E., Kim, J. Y., Kim, H. S. & Yoon, H. Establishment of Acquired Cisplatin Resistance in Ovarian Cancer Cell Lines Characterized by Enriched Metastatic Properties with Increased Twist Expression. *Int. J. Mol. Sci.* **21**, 1–27 (2020).

58. Bubici, C. & Papa, S. JNK signalling in cancer: In need of new, smarter therapeutic targets. *British Journal of Pharmacology* vol. 171 24–37 Preprint at https://doi.org/10.1111/bph.12432 (2014).

59. Weber, A., Wasiliew, P. & Kracht, M. Interleukin-1 (IL-1) pathway. *Sci. Signal.* **3**, 1–6 (2010).

60. Cohen, P. The TLR and IL-1 signalling network at a glance. *J. Cell Sci.* **127**, 2383–2390 (2014).

61. Gottipati, S., Rao, N. L. & Fung-Leung, W. P. IRAK1: a critical signaling mediator of innate immunity. *Cell. Signal.* **20**, 269–276 (2008).

62. Rhyasen, G. W. & Starczynowski, D. T. IRAK signalling in cancer. *British Journal of Cancer 2015 112:2* **112**, 232–237 (2014).

63. Gosu, V., Basith, S., Durai, P. & Choi, S. Molecular Evolution and Structural Features of IRAK Family Members. *PLoS One* **7**, e49771 (2012).

64. Gan, L. & Li, L. Regulations and roles of the interleukin-1 receptor associated kinases (IRAKs) in innate and adaptive immunity. *Immunol. Res.* **35**, 295–302 (2006).

65. Wang, L. *et al.* Crystal structure of human IRAK1. *Proc. Natl. Acad. Sci. U. S. A.* **114**, 13507–13512 (2017).

66. Liu, P. H. & Sidi, S. Targeting the Innate Immune Kinase IRAK1 in Radioresistant Cancer: Double-Edged Sword or One-Two Punch? *Front. Oncol.* **9**, 1–7 (2019).

67. Kawagoe, T. *et al.* Sequential control of Toll-like receptor–dependent responses by IRAK1 and IRAK2. *Nature Immunology 2008 9:6* **9**, 684–691 (2008).

68. Yadav, H. & Shirumalla, R. K. Emerging trends in IRAK-4 kinase research. *Mol. Biol. Rep.* **50**, 7825–7837 (2023).

69. Freihat, L. A. *et al.* IRAK3 modulates downstream innate immune signalling through its guanylate cyclase activity. *Scientific Reports 2019 9:1* **9**, 1–12 (2019).

70. Zhou, H. *et al.* IRAK-M mediates Toll-like receptor/IL-1R-induced NFκB activation and cytokine production. *EMBO Journal* **32**, 583–596 (2013).

71. Jain, A., Kaczanowska, S. & Davila, E. IL-1 receptor-associated kinase signaling and its role in inflammation, cancer progression, and therapy resistance. *Front. Immunol.* **5**, 1–8 (2014).

72. Conze, D. B., Wu, C.-J., Thomas, J. A., Landstrom, A. & Ashwell, J. D. Lys63-Linked Polyubiquitination of IRAK-1 Is Required for Interleukin-1 Receptor- and Toll-Like Receptor-Mediated NF-κB Activation. *Mol. Cell. Biol.* **28**, 3538–3547 (2008).

73. Li, Y. *et al.* miR-146a suppresses invasion of pancreatic cancer cells. *Cancer Res.* **70**, 1486–1495 (2010).

74. Boraschi, D., Italiani, P., Weil, S. & Martin, M. U. The family of the interleukin-1 receptors. *Immunol. Rev.* **281**, 197–232 (2018).

75. Moresco, E. M. Y., LaVine, D. & Beutler, B. Toll-like receptors. *Current Biology* **21**, R488–R493 (2011).

76. Sasai, M. & Yamamoto, M. Pathogen recognition receptors: Ligands and signaling pathways by toll-like receptors. *Int. Rev. Immunol.* **32**, 116–133 (2013).

77. Motshwene, P. G. *et al.* An Oligomeric Signaling Platform formed by the toll-like receptor signal transducers MyD88 and IRAK-4. *Journal of Biological Chemistry* **284**, 25404–25411 (2009).

78. Casadio, R. *et al.* Model of interaction of the IL-1 receptor accessory protein IL-1RAcP with the IL-1L/IL-1R I complex. *FEBS Lett.* **499**, 65–68 (2001).

79. Vollmer, S. *et al.* The mechanism of activation of IRAK1 and IRAK4 by interleukin-1 and Toll-like receptor agonists. *Biochemical Journal* **474**, 2027–2038 (2017).

80. Janssens, S. & Beyaert, R. Functional diversity and regulation of different interleukin-1 receptor-associated kinase (IRAK) family members. *Mol. Cell* **11**, 293–302 (2003).

81. Srivastava, R. *et al.* Augmentation of therapeutic responses in melanoma by inhibition of IRAK-1,-4. *Cancer Res.* **72**, 6209–6216 (2012).

82. Arend, W. P., Palmer, L., Gaby, GABAY & Cem. IL-1, IL-18, and IL-33 families of cytokines. *Immunol. Rev.* **223**, 20–38 (2008).

83. Takatsuna, H. *et al.* Identification of TIFA as an adapter protein that links tumor necrosis factor receptor-associated factor 6 (TRAF6) to interleukin-1 (IL-1) receptor-associated kinase-1 (IRAK-1) in IL-1 receptor signaling. *Journal of Biological Chemistry* **278**, 12144–12150 (2003).

84. Liu, G., Park, Y.-J. & Abraham, E. Interleukin-1 receptor-associated kinase (IRAK) -1- mediated NF-κ activation requires cytosolic and nuclear activity. *The FASEB Journal* **22**, 2285–2296 (2008).

85. Fernandes-Alnemri, T. *et al.* Cutting Edge: TLR Signaling Licenses IRAK1 for Rapid Activation of the NLRP3 Inflammasome. *The Journal of Immunology* **191**, 3995–3999 (2013).

86. Uematsu, S. *et al.* Interleukin-1 receptor-associated kinase-1 plays an essential role for Toll-like receptor (TLR)7- and TLR9-mediated interferon-α induction. *Journal of Experimental Medicine* **201**, 915–923 (2005).

87. Jain, V. G. *et al.* IRAK1 Is a Critical Mediator of Inflammation-Induced Preterm Birth. *The Journal of Immunology* **204**, 2651–2660 (2020).

88. Hosseini, N. *et al.* IRAK1 Gene Polymorphism in Rheumatoid Arthritis. *Immunol. Invest.* **50**, 304–321 (2021).

89. Shi, Z. *et al.* IRAK1 polymorphisms are associated with susceptibility to neuromyelitis optica spectrum disorder. *Mult. Scler. Relat. Disord.* **37**, (2020).

90. Wu, M. & Mayes, M. Insights into the genetic basis of systemic sclerosis: immunity in human disease and in mouse models. *Adv. Genomics Genet.* 143 (2014) doi:10.2147/agg.s46813.

91. Huang, H. C. *et al.* Inhibition of IRAK1 Is an Effective Therapy for Autoimmune Hypophysitis in Mice. *Int. J. Mol. Sci.* **23**, (2022).

92. Jacob, C. O. *et al.* Identification of IRAK1 as a risk gene with critical role in the pathogenesis of systemic lupus erythematosus. *Proc. Natl. Acad. Sci. U. S. A.* **106**, 6256–6261 (2009).

93. Zhou, Z. *et al.* Upregulated IL-1 Receptor-associated Kinase 1 (IRAK1) in Systemic Lupus Erythematosus: IRAK1 Inhibition Represses Th17 Differentiation with Therapeutic Potential. *Immunol. Invest.* **47**, 468–483 (2018).

94. Ji, L. *et al.* Paeoniflorin inhibits activation of the IRAK1-NF-κB signaling pathway in peritoneal macrophages from lupus-prone MRL/lpr mice. *Microb. Pathog.* **124**, 223–229 (2018).

95. Li, J. *et al.* Comprehensive Pan-Cancer Analysis of IRAK Family Genes Identifies IRAK1 as a Novel Oncogene in Low-Grade Glioma. *J. Oncol.* **2022**, (2022).

96. Liu, M. *et al.* A Pan-Cancer Analysis of IRAK1 Expression and Their Association With Immunotherapy Response. *Front. Mol. Biosci.* **9**, 507 (2022).

97. Rhyasen, G. W. *et al.* Targeting IRAK1 as a Therapeutic Approach for Myelodysplastic Syndrome. *Cancer Cell* **24**, 90–104 (2013).

98. Wee, Z. N. *et al.* IRAK1 is a therapeutic target that drives breast cancer metastasis and resistance to paclitaxel. *Nature Communications 2015 6:1* **6**, 1–16 (2015).

99. Yang, M., Qin, X., Qin, G. & Zheng, X. The role of IRAK1 in breast cancer patients treated with neoadjuvant chemotherapy. *Onco. Targets. Ther.* **12**, 2171 (2019).

100. Li, Y., Li, W., Lin, J., Lv, C. & Qiao, G. miR-146a Enhances the Sensitivity of Breast Cancer Cells to Paclitaxel by Downregulating IRAK1. *Cancer Biother. Radiopharm.* **37**, 624–635 (2022).

101. Goh, J. Y. *et al.* Chromosome 1q21.3 amplification is a trackable biomarker and actionable target for breast cancer recurrence. *Nat. Med.* **23**, 1319–1330 (2017).

102. Hosseini, M. M. *et al.* Inhibition of interleukin-1 receptor-associated kinase-1 is a therapeutic strategy for acute myeloid leukemia subtypes. *Leukemia* **32**, 2374–2387 (2018).

103. Ngo, V. N. *et al.* Oncogenically active MYD88 mutations in human lymphoma. *Nature* **470**, 115–121 (2011).

104. Kogo, R., Mimori, K., Tanaka, F., Komune, S. & Mori, M. Clinical significance of miR-146a in gastric cancer cases. *Clinical Cancer Research* **17**, 4277–4284 (2011).

105. Chen, W., Wei, T., Chen, Y., Yang, L. & Wu, X. Downregulation of irak1 prevents the malignant behavior of hepatocellular carcinoma cells by blocking activation of the mapks/nlrp3/il-1β pathway. *Onco. Targets. Ther.* **13**, 12787–12796 (2020).

106. Cheng, B. Y. *et al.* Irak1 augments cancer stemness and drug resistance via the ap-1/akr1b10 signaling cascade in hepatocellular carcinoma. *Cancer Res.* **78**, 2332–2342 (2018).

107. Schagdarsurengin, U., Breiding, V., Loose, M., Wagenlehner, F. & Dansranjav, T. Interleukin-1 receptor associated kinase 1 (IRAK1) is epigenetically activated in luminal epithelial cells in prostate cancer. *Front. Oncol.* **12**, 991368 (2022).

108. Liu, L. *et al.* Targeting the IRAK1-S100A9 Axis Overcomes Resistance to Paclitaxel in Nasopharyngeal Carcinoma. https://doi.org/10.1158/0008-5472.CAN-20-2125 doi:10.1158/0008-5472.CAN-20-2125.

109. miR-146a promotes cervical cancer cell viability via targeting IRAK1 and TRAF6. https://www.spandidos-publications.com/or/39/6/3015.

110. Zhang, X., Dang, Y., Li, P., Rong, M. & Chen, G. Expression of IRAK1 in lung cancer tissues and its clinicopathological significance: a microarray study. *Int. J. Clin. Exp. Pathol.* **7**, 8096 (2014).

111. Liu, Y. N. *et al.* miR-146b-5p Enhances the Sensitivity of NSCLC to EGFR Tyrosine Kinase Inhibitors by Regulating the IRAK1/NF-κB Pathway. *Mol. Ther. Nucleic Acids* **22**, 471–483 (2020).

112. Toh, M. R. *et al.* Global Epidemiology and Genetics of Hepatocellular Carcinoma. *Gastroenterology* **164**, 766–782 (2023).

113. Conforti, C. & Zalaudek, I. Epidemiology and Risk Factors of Melanoma: A Review. *Dermatol. Pract. Concept.* **11**, e2021161S (2021).

114. Saginala, K., Barsouk, A., Aluru, J. S., Rawla, P. & Barsouk, A. Epidemiology of Melanoma. *Medical Sciences 2021, Vol. 9, Page 63* **9**, 63 (2021).

115. Choi, J. Y. Medulloblastoma: Current Perspectives and Recent Advances. *Brain Tumor Res. Treat.* **11**, 28–38 (2023).

116. Liu, Y., Xiao, B., Li, S. & Liu, J. Risk Factors for Survival in Patients With Medulloblastoma: A Systematic Review and Meta-Analysis. *Front. Oncol.* **12**, 827054 (2022).

117. Zagozewski, J. *et al.* Combined MEK and JAK/STAT3 pathway inhibition effectively decreases SHH medulloblastoma tumor progression. *Communications Biology 2022 5:1* **5**, 1–17 (2022).

118. Grochans, S. *et al.* Epidemiology of Glioblastoma Multiforme–Literature Review. *Cancers 2022, Vol. 14, Page 2412* **14**, 2412 (2022).

119. Jensen, K. V., Cseh, O., Aman, A., Weiss, S. & Luchman, H. A. The JAK2/STAT3 inhibitor pacritinib effectively inhibits patient-derived GBM brain tumor initiating cells in vitro and when used in combination with temozolomide increases survival in an orthotopic xenograft model. *PLoS One* **12**, 1–18 (2017).

120. Jensen, K. V., Hao, X., Aman, A., Luchman, H. A. & Weiss, S. EGFR blockade in GBM brain tumor stem cells synergizes with JAK2/STAT3 pathway inhibition to abrogate compensatory mechanisms in vitro and in vivo. *Neurooncol. Adv.* **2**, 1–13 (2020).

121. Sukswai, N., Lyapichev, K., Khoury, J. D. & Medeiros, L. J. Diffuse large B-cell lymphoma variants: an update. *Pathology* **52**, 53–67 (2020).

122. Susanibar-Adaniya, S. & Barta, S. K. 2021 Update on Diffuse large B cell lymphoma: A review of current data and potential applications on risk stratification and management. *Am. J. Hematol.* **96**, 617–629 (2021).

123. De Kouchkovsky, I. & Abdul-Hay, M. 'Acute myeloid leukemia: A comprehensive review and 2016 update'. *Blood Cancer J.* **6**, e441–e441 (2016).

124. Kantarjian, H. *et al.* Acute myeloid leukemia: current progress and future directions. *Blood Cancer Journal 2021 11:2* **11**, 1–25 (2021).

125. Hong, R. & Xu, B. Breast cancer: an up-to-date review and future perspectives. *Cancer Commun.* **42**, 913–936 (2022).

126. Katsura, C., Ogunmwonyi, I., Kankam, H. K. N. & Saha, S. Breast cancer: Presentation, investigation and management. *Br. J. Hosp. Med.* **83**, (2022).

127. Medina, M. A. *et al.* Triple-Negative Breast Cancer: A Review of Conventional and Advanced Therapeutic Strategies. *International Journal of Environmental Research and Public Health 2020, Vol. 17, Page 2078* **17**, 2078 (2020).

128. Derakhshan, F. & Reis-Filho, J. S. Pathogenesis of Triple-Negative Breast Cancer. *Annual Review of Pathology: Mechanisms of Disease* **17**, 181–204 (2021).

129. Liu, S. *et al.* HER2 overexpression triggers an IL1a proinflammatory circuit to drive tumorigenesis and promote chemotherapy resistance. *Cancer Res.* **78**, 2040–2051 (2018).

130. Beverly, L. J. & Starczynowski, D. T. IRAK1: oncotarget in MDS and AML. *Oncotarget* **5**, 1699 (2014).

131. Rawla, P. Epidemiology of Prostate Cancer. *World J. Oncol.* **10**, 63 (2019).

132. Sekhoacha, M. *et al.* Prostate Cancer Review: Genetics, Diagnosis, Treatment Options, and Alternative Approaches. *Molecules 2022, Vol. 27, Page 5730* **27**, 5730 (2022).

133. Chen, Y. P. *et al.* Nasopharyngeal carcinoma. *The Lancet* **394**, 64–80 (2019).

134. Wu, L., Li, C. & Pan, L. Nasopharyngeal carcinoma: A review of current updates. *Exp. Ther. Med.* **15**, 3687–3692 (2018).

135. Zhao, Z. Y. & Liu, W. Pancreatic Cancer: A Review of Risk Factors, Diagnosis, and Treatment. *Technol. Cancer Res. Treat.* **19**, (2020).

136. Hu, J. X. *et al.* Pancreatic cancer: A review of epidemiology, trend, and risk factors. *World J. Gastroenterol.* **27**, 4298 (2021).

137. Cohen, P. A., Jhingran, A., Oaknin, A. & Denny, L. Cervical cancer. *The Lancet* **393**, 169–182 (2019).

138. Smyth, E. C., Nilsson, M., Grabsch, H. I., van Grieken, N. C. & Lordick, F. Gastric cancer. *The Lancet* **396**, 635–648 (2020).

139. Sexton, R. E., Al Hallak, M. N., Diab, M. & Azmi, A. S. Gastric cancer: a comprehensive review of current and future treatment strategies. *Cancer and Metastasis Reviews 2020 39:4* **39**, 1179–1203 (2020).

140. Barta, J. A., Powell, C. A. & Wisnivesky, J. P. Global Epidemiology of Lung Cancer. *Ann. Glob. Health* **85**, 8 (2019).

141. Schabath, M. B. & Cote, M. L. Cancer Progress and Priorities: Lung Cancer. *Cancer Epidemiology, Biomarkers & Prevention* **28**, 1563–1579 (2019).

142. Ochi, N. *et al.* Synergistic effect of pacritinib with erlotinib on JAK2-mediated resistance in epidermal gowth factor receptor mutation-positive non-small cell lung Cancer. https://doi.org/10.1016/j.yexcr.2016.05.008 (2016) doi:10.1016/j.yexcr.2016.05.008.

143. Chen, D. W., Lang, B. H. H., McLeod, D. S. A., Newbold, K. & Haymart, M. R. Thyroid cancer. *The Lancet* **401**, 1531–1544 (2023).

144. Kawamura, Y., Saijo, K., Imai, H. & Ishioka, C. Inhibition of IRAK1/4 enhances the antitumor effect of lenvatinib in anaplastic thyroid cancer cells. *Cancer Sci.* **112**, 4711–4721 (2021).

145. Standing, D. *et al.* Selective targeting of IRAK1 attenuates low molecular weight hyaluronic acid-induced stemness and non-canonical STAT3 activation in epithelial ovarian cancer. *Cell Death & Disease 2024 15:5* **15**, 1–16 (2024).

146. Zhu, X., Cai, H., Zhao, L., Ning, L. & Lang, J. CAR-T cell therapy in ovarian cancer: From the bench to the bedside. *Oncotarget* vol. 8 64607–64621 Preprint at https://doi.org/10.18632/oncotarget.19929 (2017).

147. Lheureux, S., Gourley, C., Vergote, I. & Oza, A. M. Epithelial ovarian cancer. *The Lancet* **393**, 1240–1253 (2019).

148. Singer, J. W. *et al.* Comprehensive kinase profile of pacritinib, a nonmyelosuppressive Janus kinase 2 inhibitor. *J. Exp. Pharmacol.* **8**, 11 (2016).

149. Lamb, Y. N. Pacritinib: First Approval. *Drugs* **82**, 831–838 (2022).

150. Zagozewski, J. *et al.* Combined MEK and JAK/STAT3 pathway inhibition effectively decreases SHH medulloblastoma tumor progression. *Communications Biology 2022 5:1* **5**, 1–17 (2022).

151. Jensen, K. V., Hao, X., Aman, A., Luchman, H. A. & Weiss, S. EGFR blockade in GBM brain tumor stem cells synergizes with JAK2/STAT3 pathway inhibition to abrogate compensatory mechanisms in vitro and in vivo. *Neurooncol. Adv.* **2**, 1–13 (2020).

152. Jensen, K. V., Cseh, O., Aman, A., Weiss, S. & Luchman, H. A. The JAK2/STAT3 inhibitor pacritinib effectively inhibits patient-derived GBM brain tumor initiating cells in vitro and when used in combination with temozolomide increases survival in an orthotopic xenograft model. *PLoS One* **12**, 1–18 (2017).

153. Goh, J. Y. *et al.* Chromosome 1q21.3 amplification is a trackable biomarker and actionable target for breast cancer recurrence. *Nat. Med.* **23**, 1319–1330 (2017).

154. Cheng, B. Y. *et al.* Irak1 augments cancer stemness and drug resistance via the ap-1/akr1b10 signaling cascade in hepatocellular carcinoma. *Cancer Res.* **78**, 2332–2342 (2018).

155. Srivastava, R. *et al.* Augmentation of therapeutic responses in melanoma by inhibition of IRAK-1,-4. *Cancer Res.* **72**, 6209–6216 (2012).

156. Liu, L. *et al.* Targeting the IRAK1-S100A9 Axis Overcomes Resistance to Paclitaxel in Nasopharyngeal Carcinoma. https://doi.org/10.1158/0008-5472.CAN-20-2125 doi:10.1158/0008-5472.CAN-20-2125.

157. Rhyasen, G. W. *et al.* Targeting IRAK1 as a Therapeutic Approach for Myelodysplastic Syndrome. *Cancer Cell* **24**, 90–104 (2013).

158. Hosseini, M. M. *et al.* Inhibition of interleukin-1 receptor-associated kinase-1 is a therapeutic strategy for acute myeloid leukemia subtypes. *Leukemia* **32**, 2374–2387 (2018).

159. Kawamura, Y., Saijo, K., Imai, H. & Ishioka, C. Inhibition of IRAK1/4 enhances the antitumor effect of lenvatinib in anaplastic thyroid cancer cells. *Cancer Sci.* **112**, 4711–4721 (2021).

160. Hart, S. *et al.* Pacritinib (SB1518), a JAK2/FLT3 inhibitor for the treatment of acute myeloid leukemia. *Blood Cancer J.* **1**, e44 (2011).

161. Brooks, A. J. & Putoczki, T. JAK-STAT Signalling Pathway in Cancer. *Cancers 2020, Vol. 12, Page 1971* **12**, 1971 (2020).

162. Huang, B., Lang, X. & Li, X. The role of IL-6/JAK2/STAT3 signaling pathway in cancers. *Front. Oncol.* **12**, 1023177 (2022).

163. Du, W. *et al.* Inhibition of JAK2/STAT3 signalling induces colorectal cancer cell apoptosis via mitochondrial pathway. *J. Cell. Mol. Med.* **16**, 1878–1888 (2012).

164. Judd, L. M. *et al.* Inhibition of the JAK2/STAT3 Pathway Reduces Gastric Cancer Growth In Vitro and In Vivo. *PLoS One* **9**, e95993 (2014).

165. Kim, M. S., Lee, W. S., Jeong, J., Kim, S. J. & Jin, W. Induction of metastatic potential by TrkB via activation of IL6/JAK2/STAT3 and PI3K/AKT signaling in breast cancer. *Oncotarget* **6**, 40158 (2015).

166. Abubaker, K. *et al.* Inhibition of the JAK2/STAT3 pathway in ovarian cancer results in the loss of cancer stem cell-like characteristics and a reduced tumor burden. *BMC Cancer* **14**, 1–22 (2014).

167. Park, S. Y. *et al*. The JAK2/STAT3/CCND2 Axis promotes colorectal Cancer stem cell persistence and radioresistance. *Journal of Experimental and Clinical Cancer Research* **38**, 1–18 (2019).

168. Zhang, X. *et al*. Human colorectal cancer-derived mesenchymal stem cells promote colorectal cancer progression through IL-6/JAK2/STAT3 signaling. *Cell Death & Disease 2018 9:2* **9**, 1–13 (2018).

169. JAK2/STAT3 pathway as a therapeutic target in ovarian cancers. https://www.spandidos-publications.com/ol/15/4/5772.

170. Colomiere, M. *et al*. Cross talk of signals between EGFR and IL-6R through JAK2/STAT3 mediate epithelial–mesenchymal transition in ovarian carcinomas. *British Journal of Cancer 2009 100:1* **100**, 134–144 (2008).

171. Nie, S. *et al*. ALKBH5-HOXA10 loop-mediated JAK2 m6A demethylation and cisplatin resistance in epithelial ovarian cancer. *Journal of Experimental and Clinical Cancer Research* **40**, 1–18 (2021).

172. Cueto, F. J. & Sancho, D. The Flt3L/Flt3 Axis in Dendritic Cell Biology and Cancer Immunotherapy. *Cancers 2021, Vol. 13, Page 1525* **13**, 1525 (2021).

173. Grafone, T., Palmisano, M., Nicci, C. & Storti, S. An overview on the role of FLT3-tyrosine kinase receptor in acute myeloid leukemia: biology and treatment. *Oncol. Rev.* **6**, e8 (2012).

174. Somers, K. D. *et al*. Orthotopic treatment model of prostate cancer and metastasis in the immunocompetent mouse: Efficacy of flt3 ligand immunotherapy. *Int. J. Cancer* **107**, 773–780 (2003).

175. Goh, K. C. *et al*. TG02, a novel oral multi-kinase inhibitor of CDKs, JAK2 and FLT3 with potent anti-leukemic properties. *Leukemia 2012 26:2* **26**, 236–243 (2011).

176. Hsiao, S. H. *et al*. The FLT3 inhibitor midostaurin selectively resensitizes ABCB1-overexpressing multidrug-resistant cancer cells to conventional chemotherapeutic agents. *Cancer Lett.* **445**, 34–44 (2019).

177. Ger, M. *et al*. Proteomic Identification of FLT3 and PCBP3 as Potential Prognostic Biomarkers for Pancreatic Cancer. *Anticancer Res.* **38**, 5759–5765 (2018).

178. Fogg, K. C. *et al*. Alternatively activated macrophage-derived secretome stimulates ovarian cancer spheroid spreading through a JAK2/STAT3 pathway. *Cancer Lett.* **458**, 92–101 (2019).

179. Yamaguchi, H., Chang, S. S., Hsu, J. L. & Hung, M. C. Signaling cross-talk in the resistance to HER family receptor targeted therapy. *Oncogene 2014 33:9* **33**, 1073–1081 (2013).

180. Barros, F. F. T., Powe, D. G., Ellis, I. O. & Green, A. R. Understanding the HER family in breast cancer: interaction with ligands, dimerization and treatments. *Histopathology* **56**, 560–572 (2010).

181. Lynch, T. J. *et al.* Activating Mutations in the Epidermal Growth Factor Receptor Underlying Responsiveness of Non–Small-Cell Lung Cancer to Gefitinib. *New England Journal of Medicine* **350**, 2129–2139 (2004).

182. Cheng, X. A Comprehensive Review of HER2 in Cancer Biology and Therapeutics. *Genes* vol. 15 Preprint at https://doi.org/10.3390/genes15070903 (2024).

183. Uribe, M. L., Marrocco, I. & Yarden, Y. EGFR in Cancer: Signaling Mechanisms, Drugs, and Acquired Resistance. *Cancers 2021, Vol. 13, Page 2748* **13**, 2748 (2021).

184. Kumar, R. *et al.* HER family in cancer progression: From discovery to 2020 and beyond. *Adv. Cancer Res.* **147**, 109–160 (2020).

185. Olayioye, M. A. Intracellular signaling pathways of ErbB2/HER-2 and family members. *Breast Cancer Research* **3**, 385–389 (2001).

186. Mota, J. M. *et al.* A comprehensive review of heregulins, HER3, and HER4 as potential therapeutic targets in cancer. *Oncotarget* **8**, 89284 (2017).

187. Mujoo, K., Choi, B. K., Huang, Z., Zhang, N. & An, Z. Regulation of ERBB3/HER3 signaling in cancer. *Oncotarget* **5**, 10222 (2014).

188. Mishra, R., Patel, H., Alanazi, S., Yuan, L. & Garrett, J. T. HER3 signaling and targeted therapy in cancer. *Oncol. Rev.* **12**, 45–62 (2018).

189. Dahl Steffensen, K. *et al.* Protein levels and gene expressions of the epidermal growth factor receptors, HER1,H ER2, HER3 and HER4 in benign and malignant ovarian tumors. *Int. J. Oncol.* **33**, 195–204 (2008).

190. Braicu, C. *et al.* A Comprehensive Review on MAPK: A Promising Therapeutic Target in Cancer. *Cancers 2019, Vol. 11, Page 1618* **11**, 1618 (2019).

191. Burotto, M., Chiou, V. L., Lee, J. M. & Kohn, E. C. The MAPK pathway across different malignancies: A new perspective. *Cancer* **120**, 3446–3456 (2014).

192. Yang, J. *et al.* Targeting PI3K in cancer: mechanisms and advances in clinical trials. *Molecular Cancer 2019 18:1* **18**, 1–28 (2019).

193. Martini, M., De Santis, M. C., Braccini, L., Gulluni, F. & Hirsch, E. PI3K/AKT signaling pathway and cancer: An updated review. *Ann. Med.* **46**, 372–383 (2014).

194. Gilmour, L. M. R. *et al.* Expression of erbB-4/HER-4 growth factor receptor isoforms in ovarian cancer. *Cancer Res.* **61**, 2169–2176 (2001).

195. Lee, H. *et al.* Poziotinib suppresses ovarian cancer stem cell growth via inhibition of HER4-mediated STAT5 pathway. *Biochem. Biophys. Res. Commun.* **526**, 158–164 (2020).

196. Sewell, J. M., Macleod, K. G., Ritchie, A., Smyth, J. F. & Langdon, S. P. Targeting the EGF receptor in ovarian cancer with the tyrosine kinase inhibitor ZD 1839 (‘Iressa’). *Br. J. Cancer* **86**, 456 (2002).

197. Bull Phelps, S. L. *et al.* Implications of EGFR inhibition in ovarian cancer cell proliferation. *Gynecol. Oncol.* **109**, 411–417 (2008).

198. Russo, A. *et al.* A decade of EGFR inhibition in EGFR-mutated non small cell lung cancer (NSCLC): Old successes and future perspectives. *Oncotarget* **6**, 26814 (2015).

199. Oh, D. Y. & Bang, Y. J. HER2-targeted therapies — a role beyond breast cancer. *Nature Reviews Clinical Oncology 2019 17:1* **17**, 33–48 (2019).

200. Ménard, S., Pupa, S. M., Campiglio, M. & Tagliabue, E. Biologic and therapeutic role of HER2 in cancer. *Oncogene 2003 22:42* **22**, 6570–6578 (2003).

201. Dean-Colomb, W. & Esteva, F. J. Her2-positive breast cancer: Herceptin and beyond. *Eur. J. Cancer* **44**, 2806–2812 (2008).

202. Mullen, P., Cameron, D. A., Hasmann, M., Smyth, J. F. & Langdon, S. P. Sensitivity to pertuzumab (2C4) in ovarian cancer models: cross-talk with estrogen receptor signaling. *Mol. Cancer Ther.* **6**, 93–100 (2007).

203. The Outcome of Heregulin-induced Activation of Ovarian Cancer Cells Depends on the Relative Levels of HER-2 and HER-3 Expression1 | Clinical Cancer Research | American Association for Cancer Research. https://aacrjournals.org/clincancerres/article/5/11/3653/286172/The-Outcome-of-Heregulin-induced-Activation-of.

204. Davies, S. *et al.* High incidence of ErbB3, ErbB4 and MET expression In ovarian cancer. https://doi.org/10.1097/PGP.0000000000000081 doi:10.1097/PGP.0000000000000081.

205. Isabelle, R. C. *et al.* Randomized phase II trial of seribantumab in combination with paclitaxel in patientswith advanced platinum-resistant or -refractory ovarian cancer. *Journal of Clinical Oncology* **34**, 4345–4353 (2016).

206. Odintsov, I. *et al.* The anti-HER3 mAb seribantumab effectively inhibits growth of patient-derived and isogenic cell line and xenograft models with oncogenic NRG1 fusions. *Clinical Cancer Research* **27**, 3154–3166 (2021).

207. Yarden, Y. & Sliwkowski, M. X. Untangling the ErbB signalling network. *Nat. Rev. Mol. Cell Biol.* **2**, 127–137 (2001).

208. Jia, X. *et al.* HER4 promotes the progression of colorectal cancer by promoting epithelial-mesenchymal transition. *Mol. Med. Rep.* **21**, 1779 (2020).

209. Thor, A. D., Edgerton, S. M. & Jones, F. E. Subcellular Localization of the HER4 Intracellular Domain, 4ICD, Identifies Distinct Prognostic Outcomes for Breast Cancer Patients. *Am. J. Pathol.* **175**, 1802–1809 (2009).

210. Paatero, I. *et al.* CYT-1 isoform of ErbB4 is an independent prognostic factor in serous ovarian cancer and selectively promotes ovarian cancer cell growth in vitro. *Gynecol. Oncol.* **129**, 179–187 (2013).

211. Saglam, O. *et al.* ERBB4 expression in ovarian serous carcinoma resistant to platinum-based therapy. *Cancer Control* **24**, 89–95 (2017).

212. Jones, F. E. HER4 Intracellular Domain (4ICD) Activity in the Developing Mammary Gland and Breast Cancer. https://doi.org/10.1007/s10911-008-9076-6 doi:10.1007/s10911-008-9076-6.

213. Calzetta, L. & Koziol-White, C. Pharmacological interactions: Synergism, or not synergism, that is the question. *Current Research in Pharmacology and Drug Discovery* vol. 2 Preprint at https://doi.org/10.1016/j.crphar.2021.100046 (2021).

214. Oh, Y. *et al.* Co-treatment of Low Dose Pacritinib, a Phase III Jak2 Inhibitor, Greatly Increases Apoptosis of P-gp Over-expressing Cancer Cells With Multidrug Resistance. *Anticancer Res.* **42**, 2433–2442 (2022).

215. Pandey, G. *et al.* SHP2 inhibition displays efficacy as a monotherapy and in combination with JAK2 inhibition in preclinical models of myeloproliferative neoplasms. *Am. J. Hematol.* **99**, 1040–1055 (2024).

216. Liu, Q., Qu, J., Zhao, M., Xu, Q. & Sun, Y. Targeting SHP2 as a promising strategy for cancer immunotherapy. *Pharmacol. Res.* **152**, 104595 (2020).

217. Grossmann, K. S., Rosário, M., Birchmeier, C. & Birchmeier, W. The Tyrosine Phosphatase Shp2 in Development and Cancer. *Adv. Cancer Res.* **106**, 53–89 (2010).

218. Dong, L. *et al.* Activating Mutation of SHP2 Establishes a Tumorigenic Phonotype Through Cell-Autonomous and Non-Cell-Autonomous Mechanisms. *Front. Cell Dev. Biol.* **9**, 3 (2021).

219. Chan, G. & Neel, B. G. Role of <Emphasis Type="Italic">PTPN11</Emphasis> (SHP2) in Cancer. *Protein Tyrosine Phosphatases in Cancer* 115–143 (2016) doi:10.1007/978-1-4939-3649-6_4.

220. Zhou, X.-D. & Agazie, Y. M. Inhibition of SHP2 leads to mesenchymal to epithelial transition in breast cancer cells. *Cell Death & Differentiation 2008 15:6* **15**, 988–996 (2008).

221. Zhang, J., Zhang, F. & Niu, R. Functions of Shp2 in cancer. *J. Cell. Mol. Med.* **19**, 2075–2083 (2015).

222. Chen, H. *et al.* SHP2 is a multifunctional therapeutic target in drug resistant metastatic breast cancer. *Oncogene 2020 39:49* **39**, 7166–7180 (2020).

223. Chen, X. *et al.* Tyrosine phosphatase PTPN11/SHP2 in solid tumors - bull's eye for targeted therapy? *Frontiers in Immunology* vol. 15 Preprint at https://doi.org/10.3389/fimmu.2024.1340726 (2024).

224. Garcia Fortanet, J. *et al.* Allosteric Inhibition of SHP2: Identification of a Potent, Selective, and Orally Efficacious Phosphatase Inhibitor. *J. Med. Chem.* **59**, 7773–7782 (2016).

225. LaMarche, M. J. *et al.* Identification of TNO155, an Allosteric SHP2 Inhibitor for the Treatment of Cancer. *J. Med. Chem.* **63**, 13578–13594 (2020).

226. Fu, N. jie *et al.* Hexachlorophene, a selective SHP2 inhibitor, suppresses proliferation and metastasis of KRAS-mutant NSCLC cells by inhibiting

RAS/MEK/ERK and PI3K/AKT signaling pathways. *Toxicol. Appl. Pharmacol.* **441**, 115988 (2022).

227. Zhu, D. *et al.* Osteosarcoma cell proliferation suppression via SHP-2-mediated inactivation of the JAK/STAT3 pathway by tubocapsenolide A. *J. Adv. Res.* **34**, 79–91 (2021).

228. Dillon, M. *et al.* Progress on Ras/MAPK Signaling Research and Targeting in Blood and Solid Cancers. *Cancers 2021, Vol. 13, Page 5059* **13**, 5059 (2021).

229. Matozaki, T., Murata, Y., Saito, Y., Okazawa, H. & Ohnishi, H. Protein tyrosine phosphatase SHP-2: A proto-oncogene product that promotes Ras activation. *Cancer Sci.* **100**, 1786–1793 (2009).

230. Dance, M., Montagner, A., Salles, J. P., Yart, A. & Raynal, P. The molecular functions of Shp2 in the Ras/Mitogen-activated protein kinase (ERK1/2) pathway. *Cell. Signal.* **20**, 453–459 (2008).

231. Bunda, S. *et al.* Inhibition of SHP2-mediated dephosphorylation of Ras suppresses oncogenesis. *Nature Communications 2015 6:1* **6**, 1–12 (2015).

232. He, Y. *et al.* Targeting PI3K/Akt signal transduction for cancer therapy. *Signal Transduction and Targeted Therapy 2021 6:1* **6**, 1–17 (2021).

233. Uddin, S. *et al.* Role of RAS signaling in ovarian cancer. *F1000Res.* **11**, 1253 (2022).

234. Wu, C. J. *et al.* The tyrosine phosphatase SHP-2 is required for mediating phosphatidylinositol 3-Kinase/Akt activation by growth factors. *Oncogene* **20**, 6018–6025 (2001).

235. Zito, C. I., Kontaridis, M. I., Fornaro, M., Feng, G. S. & Bennett, A. M. SHP-2 regulates the phosphatidylinositide 3'-kinase/Akt pathway and suppresses caspase 3-mediated apoptosis. *J. Cell. Physiol.* **199**, 227–236 (2004).

236. Yuan, Y. *et al.* SHP2 promotes proliferation of breast cancer cells through regulating Cyclin D1 stability via the PI3K/AKT/GSK3β signaling pathway. *Cancer Biol. Med.* **17**, 707–725 (2020).

237. Hu, X., li, J., Fu, M., Zhao, X. & Wang, W. The JAK/STAT signaling pathway: from bench to clinic. *Signal Transduction and Targeted Therapy 2021 6:1* **6**, 1–33 (2021).

238. Fiebelkow, J. *et al.* The tyrosine phosphatase SHP2 increases robustness and information transfer within IL-6-induced JAK/STAT signalling. *Cell Communication and Signaling* **19**, 1–19 (2021).

239. Chen, Y. N. P. *et al.* Allosteric inhibition of SHP2 phosphatase inhibits cancers driven by receptor tyrosine kinases. *Nature 2016 535:7610* **535**, 148–152 (2016).

240. Muenst, S. *et al.* Src homology phosphotyrosyl phosphatase-2 expression is an independent negative prognostic factor in human breast cancer. https://doi.org/10.1111/his.12140 (2013) doi:10.1111/his.12140.

241. Hu, Z., Li, J., Gao, Q., Wei, S. & Yang, B. SHP2 overexpression enhances the invasion and metastasis of ovarian cancer in vitro and in vivo. *Onco. Targets. Ther.* **10**, 3881 (2017).

242. Gu, J. *et al.* SHP2 promotes laryngeal cancer growth through the Ras/Raf/Mek/Erk pathway and serves as a prognostic indicator for laryngeal cancer. *Int. J. Oncol.* **44**, 481–490 (2014).

243. Wang, Q. *et al.* Cancer Investigation SHP2 and UGP2 are Biomarkers for Progression and Poor Prognosis of Gallbladder Cancer SHP and UGP are Biomarkers for Progression and Poor Prognosis of Gallbladder Cancer. *CANCER INVESTIGATION* https://doi.org/10.1080/07357907.2016.1193745 (2016) doi:10.1080/07357907.2016.1193745.

244. Bai, S. *et al.* EGFL6 Regulates the Asymmetric Division, Maintenance, and Metastasis of ALDH+ Ovarian Cancer Cells. *Cancer Res.* **76**, 6396–6409 (2016).

245. Wang, Y. *et al.* SHP2 blockade enhances anti-tumor immunity via tumor cell intrinsic and extrinsic mechanisms. *Scientific Reports 2021 11:1* **11**, 1–23 (2021).

246. Takehara, T. *et al.* PD-L2 suppresses T cell signaling via coinhibitory microcluster formation and SHP2 phosphatase recruitment. *Communications Biology 2021 4:1* **4**, 1–12 (2021).

247. Liu, C. *et al.* Combinations with Allosteric SHP2 Inhibitor TNO155 to Block Receptor Tyrosine Kinase Signaling. *Clinical Cancer Research* **27**, 342–354 (2021).

248. Brightwell, R. M. *et al.* The CD47 "don't eat me signal" is highly expressed in human ovarian cancer. *Gynecol. Oncol.* **143**, 393–397 (2016).

249. Song, Y., Zhao, M., Zhang, H. & Yu, B. Double-edged roles of protein tyrosine phosphatase SHP2 in cancer and its inhibitors in clinical trials. *Pharmacol. Ther.* 107966 (2021) doi:10.1016/J.PHARMTHERA.2021.107966.

250. Chen, Y. N. P. *et al.* Allosteric inhibition of SHP2 phosphatase inhibits cancers driven by receptor tyrosine kinases. *Nature* **535**, 148–152 (2016).

251. Mainardi, S. *et al.* SHP2 is required for growth of KRAS-mutant non-small-cell lung cancer in vivo. *Nature Medicine 2018 24:7* **24**, 961–967 (2018).

252. Fedele, C. *et al.* SHP2 Inhibition Prevents Adaptive Resistance to MEK Inhibitors in Multiple Cancer Models. *Cancer Discov.* **8**, 1237–1249 (2018).

253. Ma, W. *et al.* Early Combined SHP2 Targeting Reverses the Therapeutic Resistance of Vemurafenib in Thyroid Cancer. *J. Cancer* **14**, 1592 (2023).

254. Valencia-Sama, I. *et al.* NRAS status determines sensitivity to SHP2 inhibitor combination therapies targeting the RAS-MAPK pathway in neuroblastoma. *Cancer Res.* **80**, 3413–3423 (2020).

255. Zhao, M. *et al.* SHP2 inhibition triggers anti-tumor immunity and synergizes with PD-1 blockade. *Acta Pharm. Sin. B* **9**, 304–315 (2019).

256. Langdon, S. P. *et al.* Characterization and Properties of Nine Human Ovarian Adenocarcinoma Cell Lines. *Cancer Res.* **48**, 6166–6172 (1988).

257. Andersen, C. L. *et al.* Active estrogen receptor-alpha signaling in ovarian cancer models and clinical specimens. *Clinical Cancer Research* **23**, 3802–3812 (2017).

258. Bradbury, A., O'donnell, R., Drew, Y., Curtin, N. J. & Saha, S. S. Characterisation of Ovarian Cancer Cell Line NIH-OVCAR3 and Implications of Genomic, Transcriptomic, Proteomic and Functional DNA Damage Response Biomarkers for Therapeutic Targeting. *Cancers 2020, Vol. 12, Page 1939* **12**, 1939 (2020).

259. *Characterization of a Human Ovarian Carcinoma Cell Line (NIH:OVCAR-3)1 with Androgen and Estrogen Receptors*. *CANCER RESEARCH* vol. 43 http://aacrjournals.org/cancerres/article-pdf/43/11/5379/2415897/cr0430115379.pdf (1983).

260. Cooke, S. L. *et al.* Genomic analysis of genetic heterogeneity and evolution in high-grade serous ovarian carcinoma. *Oncogene* **29**, 4905 (2010).

261. Hawkins, R. A. *et al.* Oestrogen receptor expression and the effects of oestrogen and tamoxifen on the growth of human ovarian carcinoma cell lines. *Br. J. Cancer* **62**, 213–216 (1990).

262. Hallas-Potts, A., Dawson, J. C. & Herrington, C. S. Ovarian cancer cell lines derived from non-serous carcinomas migrate and invade more aggressively than those derived from high-grade serous carcinomas. *Scientific Reports 2019 9:1* **9**, 1–10 (2019).

263. Domcke, S., Sinha, R., Levine, D. A., Sander, C. & Schultz, N. Evaluating cell lines as tumour models by comparison of genomic profiles. *Nature Communications 2013 4:1* **4**, 1–10 (2013).

264. Foss, C. A. *et al.* Imaging tumor and ascites-associated macrophages in a mouse model of metastatic ovarian cancer. *EJNMMI Res.* **14**, 1–11 (2024).

265. Wang, S. *et al. Tumor-Associated Macrophages (TAMs) Depend on Shp2 for Their Anti-Tumor Roles in Colorectal Cancer*. *Am J Cancer Res* vol. 9 www.ajcr.us/ (2019).

266. Kumar, G., Breen, E. J. & Ranganathan, S. Identification of ovarian cancer associated genes using an integrated approach in a Boolean framework. *BMC Syst. Biol.* **7**, 12 (2013).

267. Bartha, Á. & Győrffy, B. Tnmplot.Com: A web tool for the comparison of gene expression in normal, tumor and metastatic tissues. *Int. J. Mol. Sci.* **22**, 1–12 (2021).

268. Ignacio, R. M. C. *et al.* Chemokine Network and Overall Survival in TP53 Wild-Type and Mutant Ovarian Cancer. *Immune Netw.* **18**, (2018).

269. Chen, W., Wei, T., Chen, Y., Yang, L. & Wu, X. Downregulation of irak1 prevents the malignant behavior of hepatocellular carcinoma cells by blocking activation of the mapks/nlrp3/il-1β pathway. *Onco. Targets. Ther.* **13**, 12787–12796 (2020).

270. Wee, Z. N. *et al*. IRAK1 is a therapeutic target that drives breast cancer metastasis and resistance to paclitaxel. *Nature Communications 2015 6:1* **6**, 1–16 (2015).

271. Valdivia, A. *et al*. E2F1 mediates competition, proliferation and response to cisplatin in cohabitating resistant and sensitive ovarian cancer cells. *Front. Oncol.* **14**, 1304691 (2024).

272. Rhyasen, G. W. & Starczynowski, D. T. IRAK signalling in cancer. *Br. J. Cancer* **112**, 232–237 (2015).

273. Liu, M. *et al*. A Pan-Cancer Analysis of IRAK1 Expression and Their Association With Immunotherapy Response. *Front. Mol. Biosci.* **9**, 507 (2022).

274. Cheng, B. Y. *et al*. Irak1 augments cancer stemness and drug resistance via the ap-1/akr1b10 signaling cascade in hepatocellular carcinoma. *Cancer Res.* **78**, 2332–2342 (2018).

275. Yang, M., Qin, X., Qin, G. & Zheng, X. The role of IRAK1 in breast cancer patients treated with neoadjuvant chemotherapy. *Onco. Targets. Ther.* **12**, 2171 (2019).

276. Győrffy, B. Integrated analysis of public datasets for the discovery and validation of survival-associated genes in solid tumors. *Innovation* **5**, (2024).

277. Győrffy, B. Transcriptome-level discovery of survival-associated biomarkers and therapy targets in non-small-cell lung cancer. *Br. J. Pharmacol.* **181**, 362–374 (2024).

278. Yu, M. *et al*. The tyrosine phosphatase SHP2 promotes proliferation and oxaliplatin resistance of colon cancer cells through AKT and ERK. *Biochem. Biophys. Res. Commun.* **563**, 1–7 (2021).

279. Src homology phosphotyrosyl phosphatase 2 mediates cisplatin-related drug resistance by inhibiting apoptosis and activating the Ras/PI3K/Akt1/survivin pathway in lung cancer cells. https://www.spandidos-publications.com/10.3892/or.2017.6109?text=fulltext.

280. Chen, M. J., Wang, Y. C., Wu, D. W., Chen, C. Y. & Lee, H. Association of nuclear localization of SHP2 and YAP1 with unfavorable prognosis in non-small cell lung cancer. *Pathol. Res. Pract.* **215**, 801–806 (2019).

281. Zheng, J. *et al*. Expression and prognosis value of SHP2 in patients with pancreatic ductal adenocarcinoma. *Tumor Biology* **37**, 7853–7859 (2016).

282. Dong, S. *et al*. Expression and clinical significance of SHP2 in gastric cancer. *Journal of International Medical Research* **40**, 2083–2089 (2012).

283. O'Brien, M. A. & Kirby, R. Apoptosis: A review of pro-apoptotic and anti-apoptotic pathways and dysregulation in disease. *Journal of Veterinary Emergency and Critical Care* **18**, 572–585 (2008).

284. Kashyap, D., Garg, V. K. & Goel, N. Intrinsic and extrinsic pathways of apoptosis: Role in cancer development and prognosis. *Adv. Protein Chem. Struct. Biol.* **125**, 73–120 (2021).

285. Savitskaya, M. A. & Onishchenko, G. E. Mechanisms of apoptosis. *Biochemistry (Moscow)* **80**, 1393–1405 (2015).

286. Fulda, S. & Debatin, K. M. Extrinsic versus intrinsic apoptosis pathways in anticancer chemotherapy. *Oncogene 2006 25:34* **25**, 4798–4811 (2006).

287. Neophytou, C. M., Trougakos, I. P., Erin, N. & Papageorgis, P. Apoptosis Deregulation and the Development of Cancer Multi-Drug Resistance. *Cancers 2021, Vol. 13, Page 4363* **13**, 4363 (2021).

288. Li, J. & Yuan, J. Caspases in apoptosis and beyond. *Oncogene 2008 27:48* **27**, 6194–6206 (2008).

289. Chaitanya, G. V., Alexander, J. S. & Babu, P. P. PARP-1 cleavage fragments: Signatures of cell-death proteases in neurodegeneration. *Cell Communication and Signaling* **8**, 1–11 (2010).

290. Gobeil, S., Boucher, C. C., Nadeau, D. & Poirier, G. G. Characterization of the necrotic cleavage of poly(ADP-ribose) polymerase (PARP-1): implication of lysosomal proteases. *Cell Death & Differentiation 2001 8:6* **8**, 588–594 (2001).

291. Singh, D. D., Parveen, A. & Yadav, D. K. Role of PARP in TNBC: Mechanism of Inhibition, Clinical Applications, and Resistance. *Biomedicines 2021, Vol. 9, Page 1512* **9**, 1512 (2021).

292. Haynes, B., Murai, J. & Lee, J. M. Restored replication fork stabilization, a mechanism of PARP inhibitor resistance, can be overcome by cell cycle checkpoint inhibition. *Cancer Treat. Rev.* **71**, 1–7 (2018).

293. Franzese, E. *et al.* PARP inhibitors in ovarian cancer. *Cancer Treat. Rev.* **73**, 1–9 (2019).

294. Foo, T., George, A. & Banerjee, S. PARP inhibitors in ovarian cancer: An overview of the practice-changing trials. *Genes Chromosomes Cancer* **60**, 385–397 (2021).

295. Mittica, G. *et al.* PARP Inhibitors in Ovarian Cancer. *Recent Pat. Anticancer Drug Discov.* **13**, 392–410 (2018).

296. Wang, W., Cui, J., Ma, H., Lu, W. & Huang, J. Targeting Pyrimidine Metabolism in the Era of Precision Cancer Medicine. *Front. Oncol.* **11**, 684961 (2021).

297. Siddiqui, A. & Ceppi, P. A non-proliferative role of pyrimidine metabolism in cancer. *Mol. Metab.* **35**, 100962 (2020).

298. Mullen, N. J. & Singh, P. K. Nucleotide metabolism: a pan-cancer metabolic dependency. *Nature Reviews Cancer 2023 23:5* **23**, 275–294 (2023).

299. Wu, Z. *et al.* Identification of crucial genes of pyrimidine metabolism as biomarkers for gastric cancer prognosis. *Cancer Cell Int.* **21**, 1–13 (2021).

300. Huang, L. *et al.* Elucidating the role of pyrimidine metabolism in prostate cancer and its therapeutic implications. *Sci. Rep.* **15**, 2003 (2025).

301. Kollareddy, M. *et al.* Regulation of nucleotide metabolism by mutant p53 contributes to its gain-of-function activities. *Nature Communications 2015 6:1* **6**, 1–13 (2015).

302. Quevedo-Ocampo, J. *et al.* Folate Metabolism in Hepatocellular Carcinoma. What Do We Know So Far? *Technol. Cancer Res. Treat.* **21**, (2022).

303. Yang, C. *et al.* Folate-mediated one-carbon metabolism: a targeting strategy in cancer therapy. *Drug Discov. Today* **26**, 817–825 (2021).

304. Aird, K. M. & Zhang, R. Nucleotide metabolism, oncogene-induced senescence and cancer. *Cancer Lett.* **356**, 204–210 (2015).

305. Chen, C. W. *et al.* DHS (trans−4,4'-dihydroxystilbene) suppresses DNA replication and tumor growth by inhibiting RRM2 (ribonucleotide reductase regulatory subunit M2). *Oncogene 2018 38:13* **38**, 2364–2379 (2018).

306. Aird, K. M., Li, H., Xin, F., Konstantinopoulos, P. A. & Zhang, R. Identification of ribonucleotide reductase M2 as a potential target for pro-senescence therapy in epithelial ovarian cancer. *Cell Cycle* **13**, 199–207 (2014).

307. Ma, C. *et al.* Independent prognostic implications of RRM2 in lung adenocarcinoma. *J. Cancer* **11**, 7009 (2020).

308. Yang, L. *et al.* Study on the effects and mechanism of RRM2 on three gynecological malignancies. *Cell. Signal.* **129**, 111674 (2025).

309. Zou, Y. *et al.* ERK Inhibitor Enhances Everolimus Efficacy through the Attenuation of dNTP Pools in Renal Cell Carcinoma. *Mol. Ther. Nucleic Acids* **14**, 550–561 (2019).

310. Fujiwaki, R. *et al.* Thymidine kinase in epithelial ovarian cancer: Relationship with the other pyrimidine pathway enzymes. *Int. J. Cancer* **99**, 328–335 (2002).

311. Li, Z., Wu, Z., You, X. & Tang, N. Pan-cancer analysis reveals that TK1 promotes tumor progression by mediating cell proliferation and Th2 cell polarization. *Cancer Cell International* **24**, 1–14 (2024).

312. Zhu, C. *et al.* A combined strategy of TK1, HE4 and CA125 shows better diagnostic performance than risk of ovarian malignancy algorithm (ROMA) in ovarian carcinoma. *Clinica Chimica Acta* **524**, 43–50 (2022).

313. Wang, J. *et al.* Thymidine kinase 1 expression in ovarian serous adenocarcinoma is superior to Ki-67: A new prognostic biomarker. *Tumor Biology* **39**, (2017).

314. Wu, S. *et al.* Knockdown of MTHFD2 inhibits proliferation and migration of nasopharyngeal carcinoma cells through the ERK signaling pathway. *Biochem. Biophys. Res. Commun.* **614**, 47–55 (2022).

315. Mo, X., Liu, Q., Liang, K. & Song, Y. Interference with MTHFD2 induces ferroptosis in ovarian cancer cells through ERK signaling to suppress tumor malignant progression. *J. Bioenerg. Biomembr.* **56**, 333–345 (2024).

316. Li, Q. *et al*. MTHFD2 promotes ovarian cancer growth and metastasis via activation of the STAT3 signaling pathway. *FEBS Open Bio* **11**, 2845–2857 (2021).

317. Cui, X. *et al*. Up-regulation of MTHFD2 is associated with clinicopathological characteristics and poor survival in ovarian cancer, possibly by regulating MOB1A signaling. *J. Ovarian Res.* **15**, 1–14 (2022).

318. Mo, J. *et al*. DDX3X: structure, physiologic functions and cancer. *Molecular Cancer 2021 20:1* **20**, 1–20 (2021).

319. Lee, C. S. *et al*. Human DDX3 functions in translation and interacts with the translation initiation factor eIF3. *Nucleic Acids Res.* **36**, 4708–4718 (2008).

320. Chen, H. H., Yu, H. I., Yang, M. H. & Tarn, W. Y. DDX3 Activates CBC-eIF3–Mediated translation of uORF-containing oncogenic mRNAs to promote metastasis in HNSCC. *Cancer Res.* **78**, 4512–4523 (2018).

Section 8

Supplementary Material

(8) Supplementary Figures

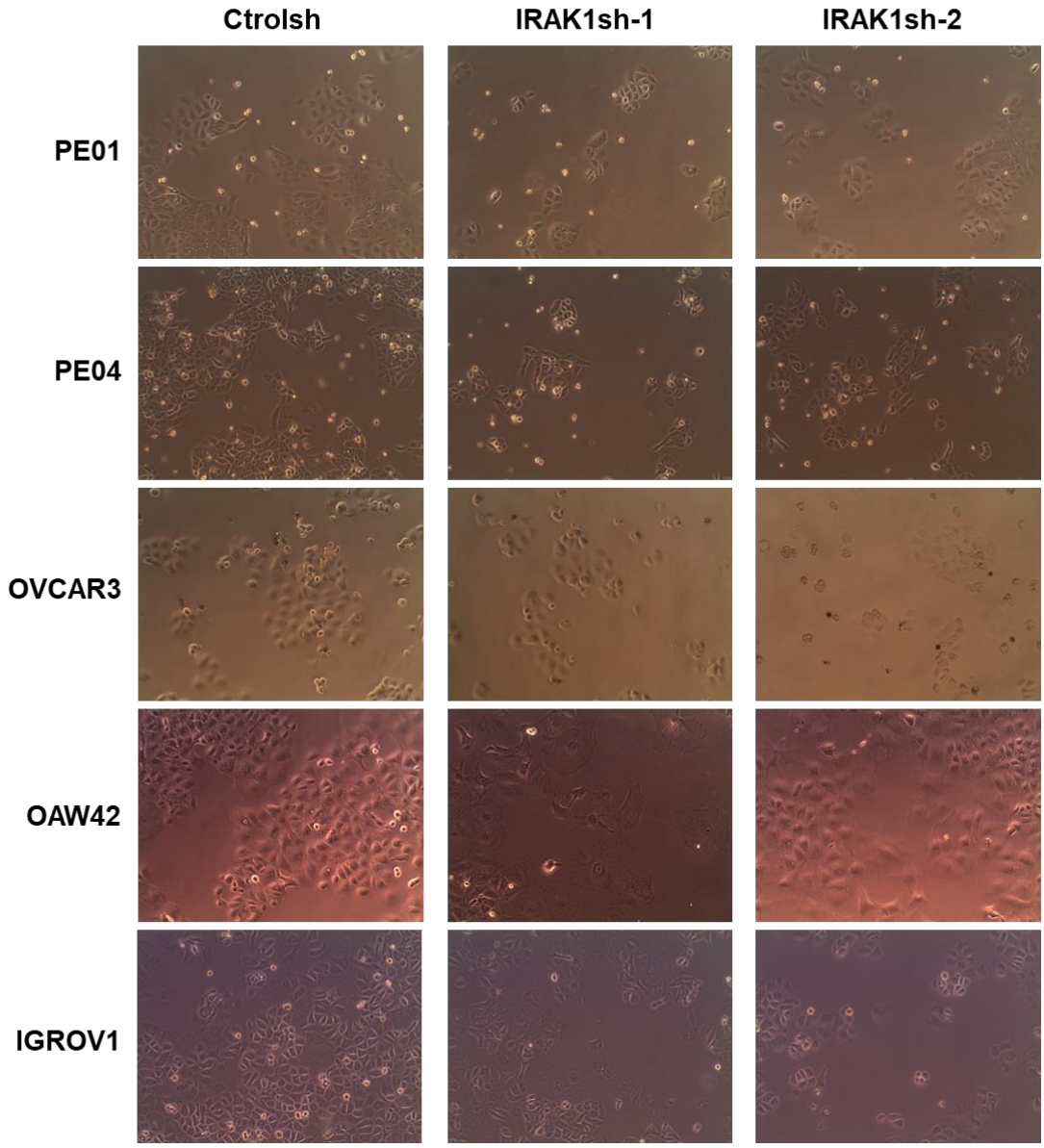

Supplementary Figure 3.1.1: IRAK1 knockdown reduces the proliferation of Ovarian Cancer cell lines at 4-day timepoint. Representative images were taken for control (Ctrolsh) and IRAK1 knockdown (IRAK1sh-1/2) cell lines at 4X magnification.

Representative Images captured (4X): Day 7

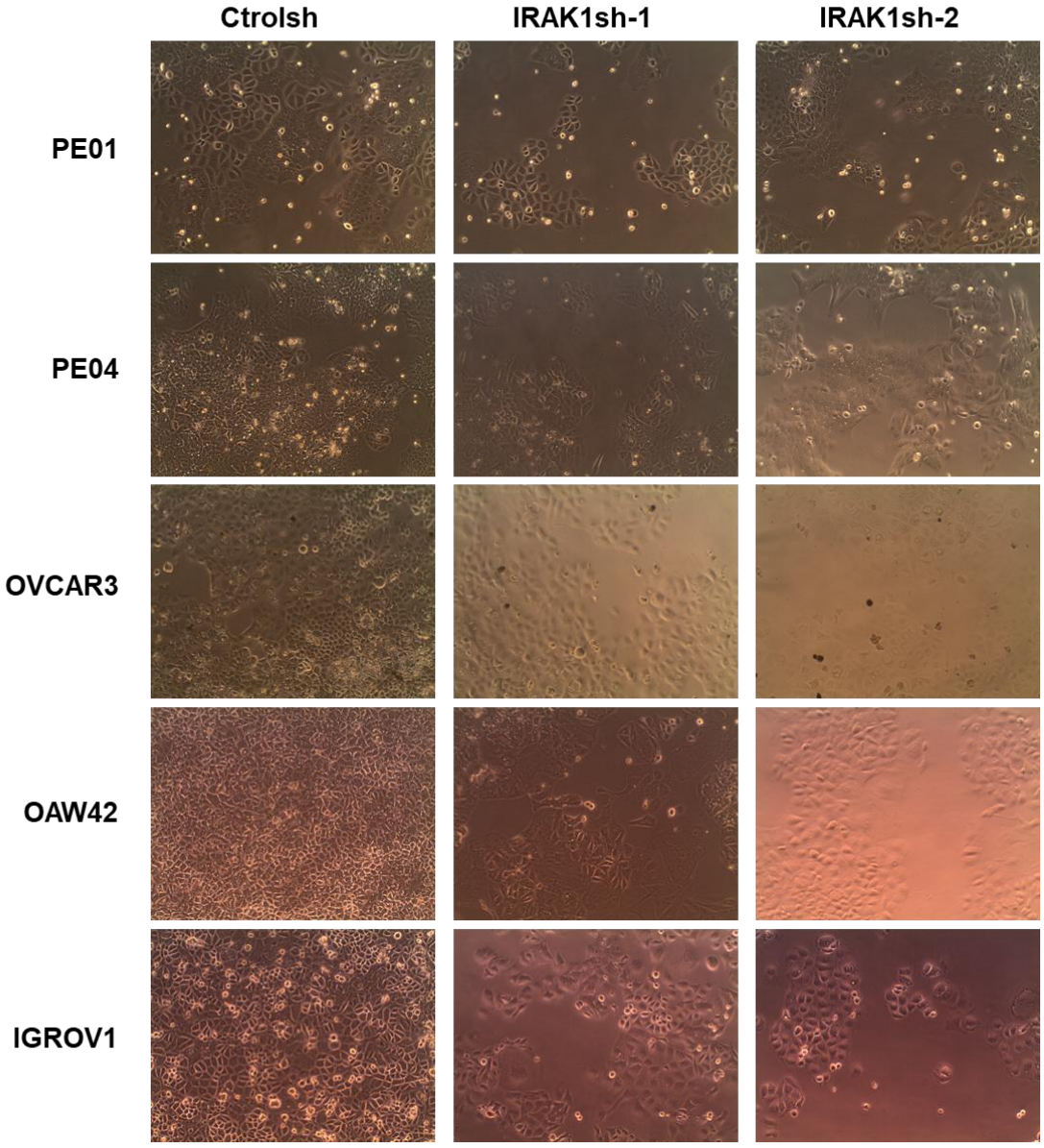

Supplementary Figure 3.1.2: IRAK1 knockdown reduces the proliferation of Ovarian Cancer cell lines at 7-day timepoint. Representative images were taken for control (Ctrolsh) and IRAK1 knockdown (IRAK1sh-1/2) cell lines at 4X magnification.

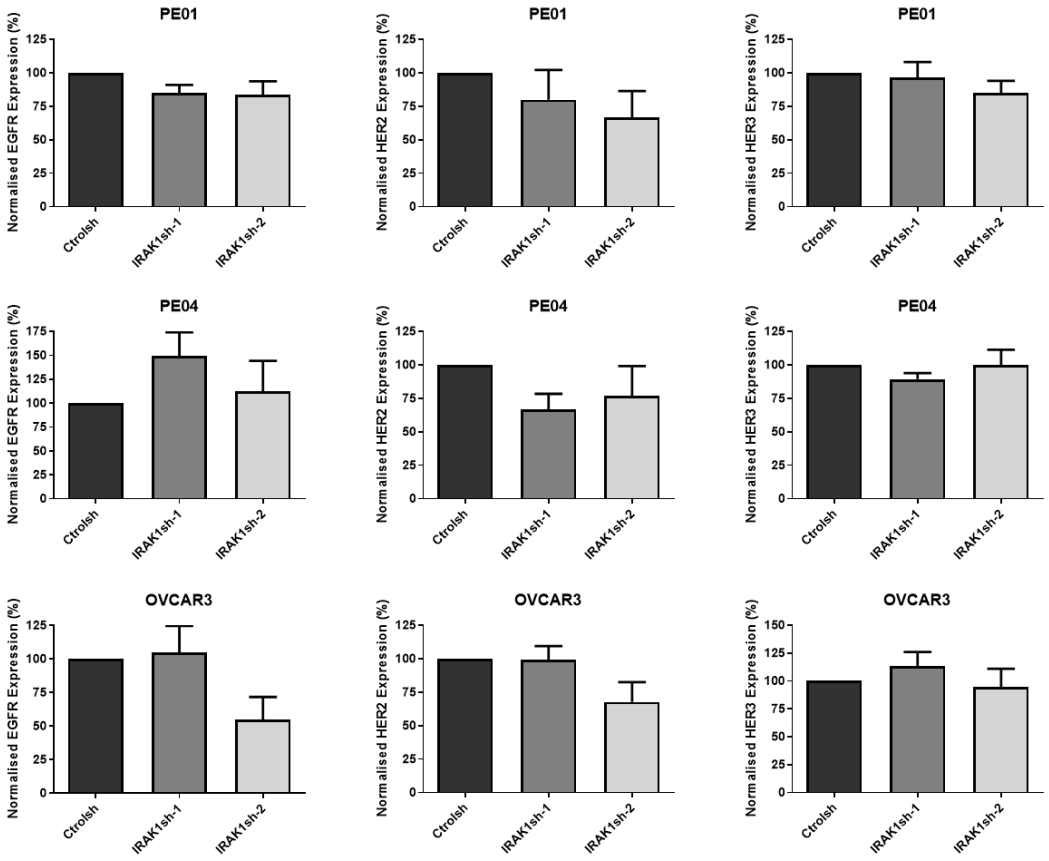

Supplementary Figure 3.2.1: HER2 shows slightly reduced levels in IRAK1 knockdown PE01 and PE04 cells. Optical density was determined using Image J and expression was normalised using Tubulin as a loading control and provided as a percentage of Ctrolsh cell lines. Statistical significance was investigated using an unpaired students t-test. PE01 and PE04 results are representative of n=4 while OVCAR3 EGFR and HER2 are representative of n=3 and HER3 n=2 respectively.

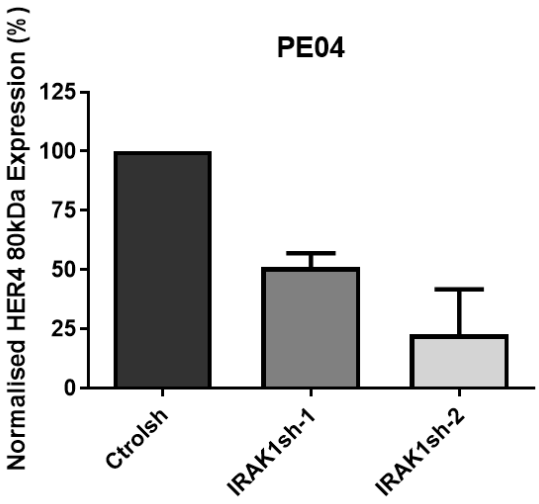

Supplementary Figure 3.3.1: HER4 80kDa ICD shows slightly reduced levels in IRAK1 knockdown PE04 cells. Optical density was determined using Image J and expression was normalised using tubulin as a loading control and provided as a percentage of Ctrolsh cell lines. Statistical significance was investigated using a unpaired students t-test. Results are representative of n=2.

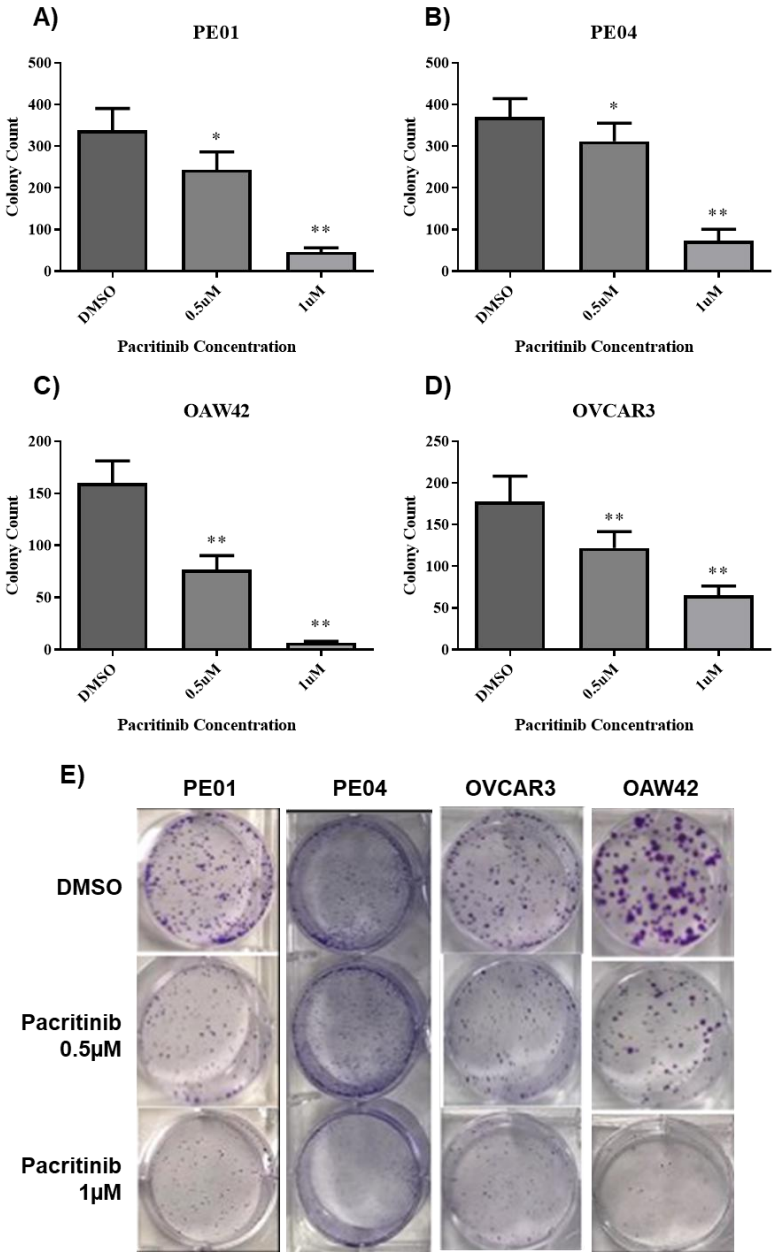

Supplementary Figure 3.4.1: Pacritinib significantly reduces colony formation and survival of ovarian cancer cell lines. **A)** PE01, **B)** PE04 and **D)** OVCAR3 seeded at 3000 cells per well and **C)** OAW42 were seeded at 1000 cells per well. All cells were seeded in six-well plates. Twenty-four hours later cells were treated with Pacritinib (0.5μM, 1μM) or vehicle control (DMSO). Colonies were allowed to grow for 10-21 days, then colonies were fixed in methanol and stained with 0.5% crystal violet. **E)** Representative images were captured, and visible colonies were counted using OpenCFU software tool. Statistical significance was investigated using a paired student's t-test. P-values; (*;≤0.05), (**;≤0.01). Results are representative of greater than or equal to three independent experimental replicates. Data shown in this figure was contributed by Dr Marion Butler and Dr Devlin Wall Coughlan.

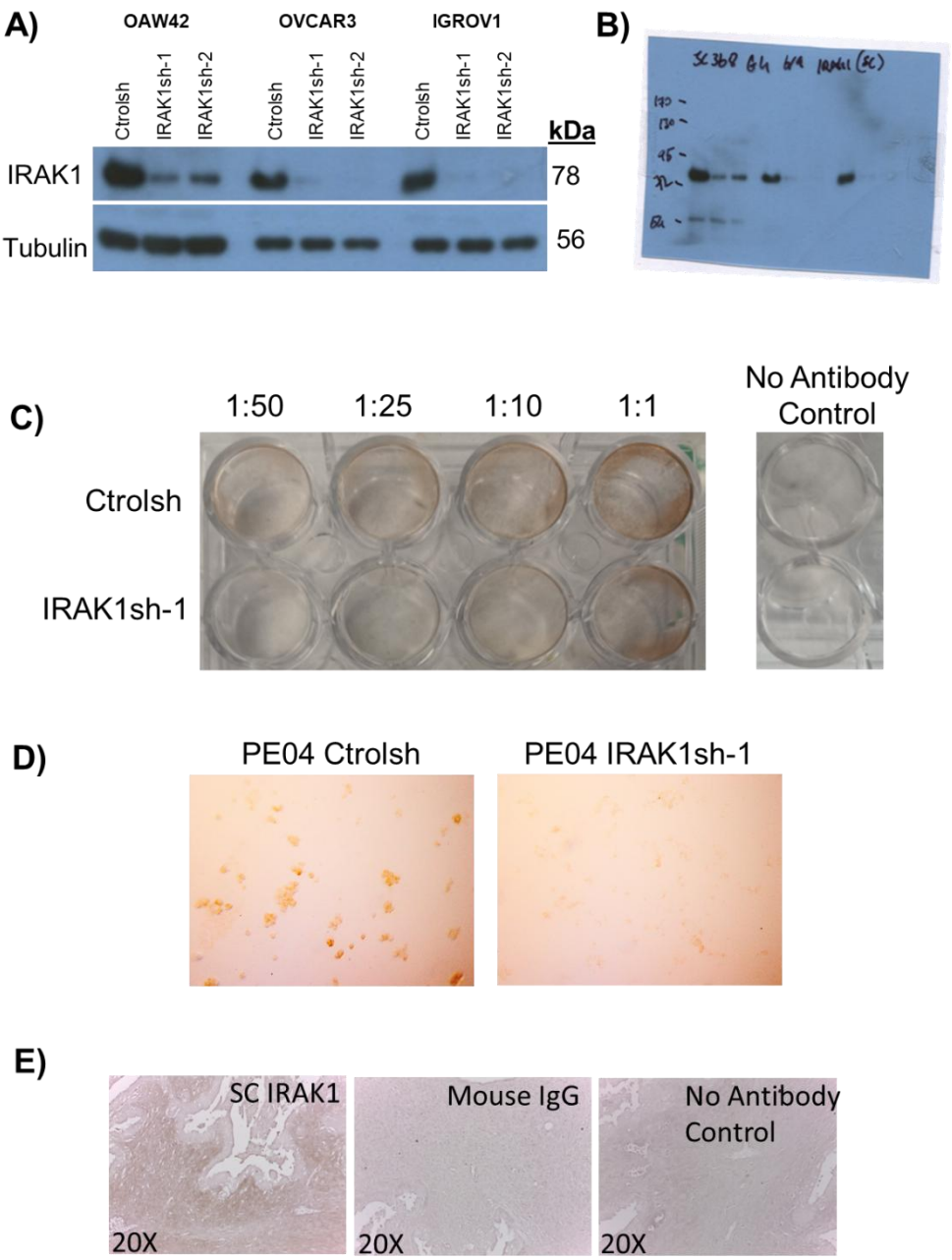

Supplementary Figure 3.5.1: Santa Cruz IRAK1 (SC-5288) antibody validation experiments: A-B) SC-5288 specificity and background staining was assessed using western blot analysis of OAW42, OVCAR3 and IGROV1 Ctrolsh and IRAK1sh-1/2 cells. **C)** Background staining was assessed for background staining using methanol fixed PE04 cells. **D)** PE04 Ctrolsh and IRAK1sh-1 cell plugs were used to evaluate immunohistochemistry protocol using 1:50 dilution of SC-5228. **E)** 1:50 dilution of SC-5288 was assessed using Immunohistochemical staining of HUCAT311 full face tissue section.

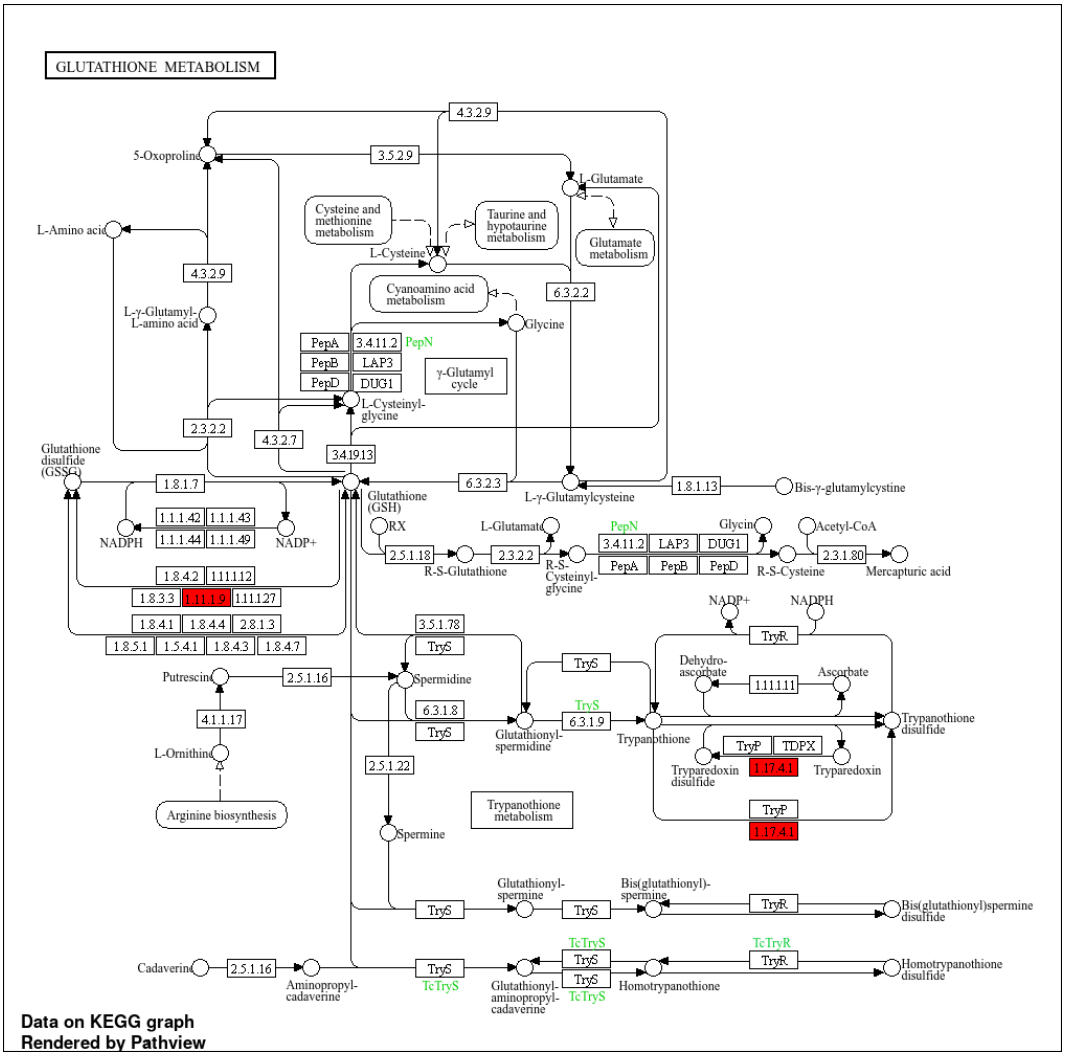

Supplementary Figure 4.1.1: Statistically significant and differentially abundant proteins identified from the SHP099 10μM vs Vehicle control binary comparison were entered into SHINEY GO and used to generate the KEGG Map for the Glutathione metabolism pathway identified.

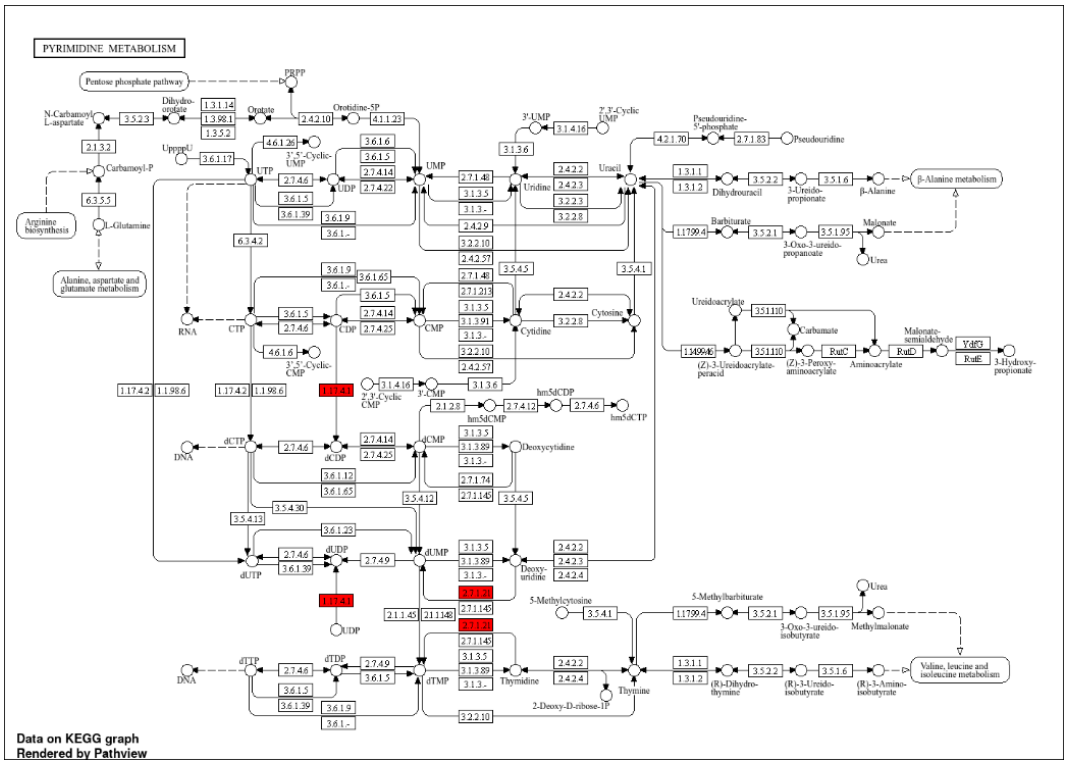

Supplementary Figure 4.1.2: Statistically significant and differentially abundant proteins identified from the SHP099 10μM vs Vehicle control binary comparison were entered into SHINEY GO and used to generate the KEGG Map for the Pyrimidine metabolism pathway identified.

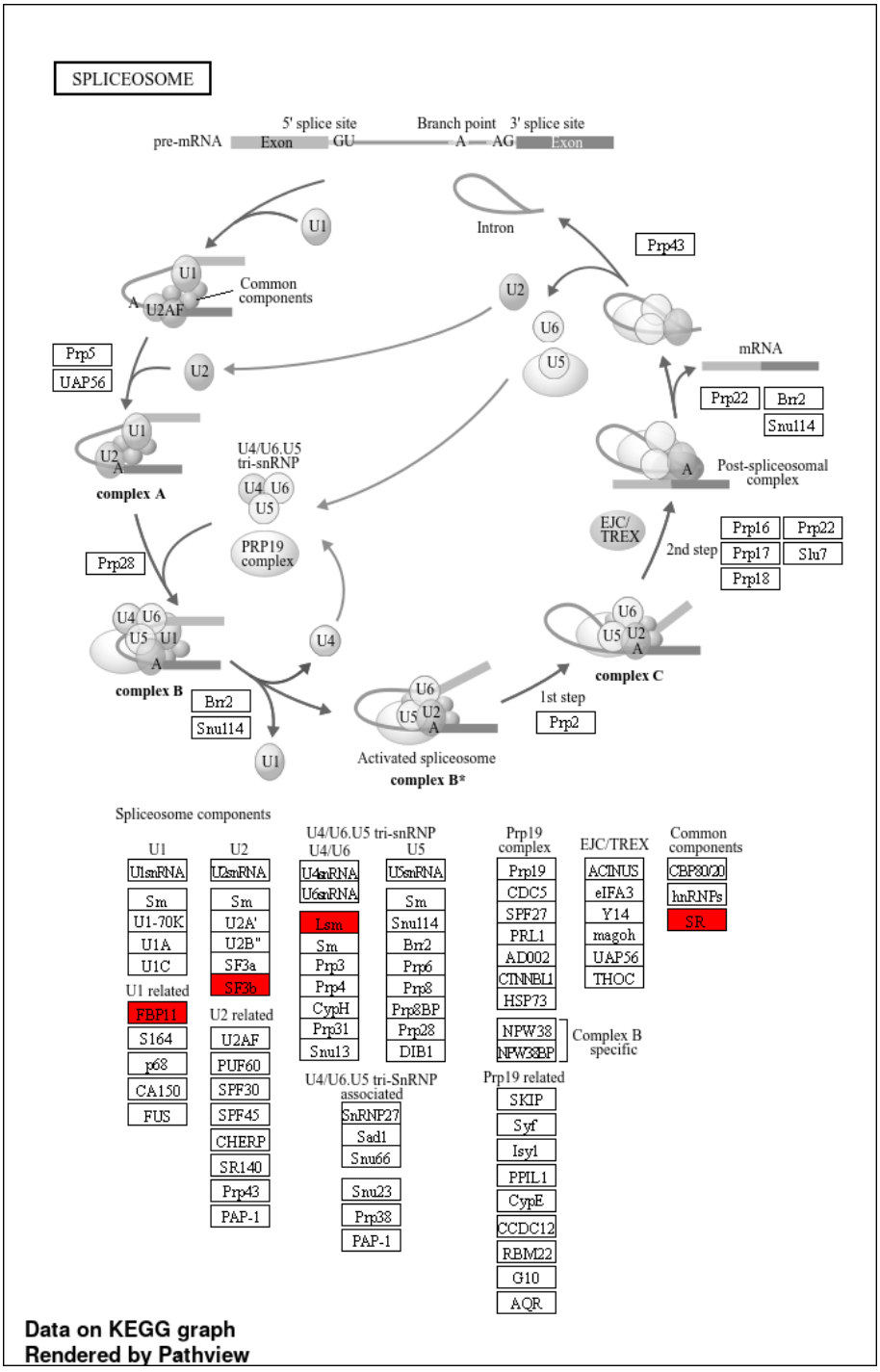

Supplementary Figure 4.1.3: Statistically significant and differentially abundant proteins identified from the SHP099 10μM vs Vehicle control binary comparison were entered into SHINEY GO and used to generate the KEGG Map for the Spliceosome pathway identified.

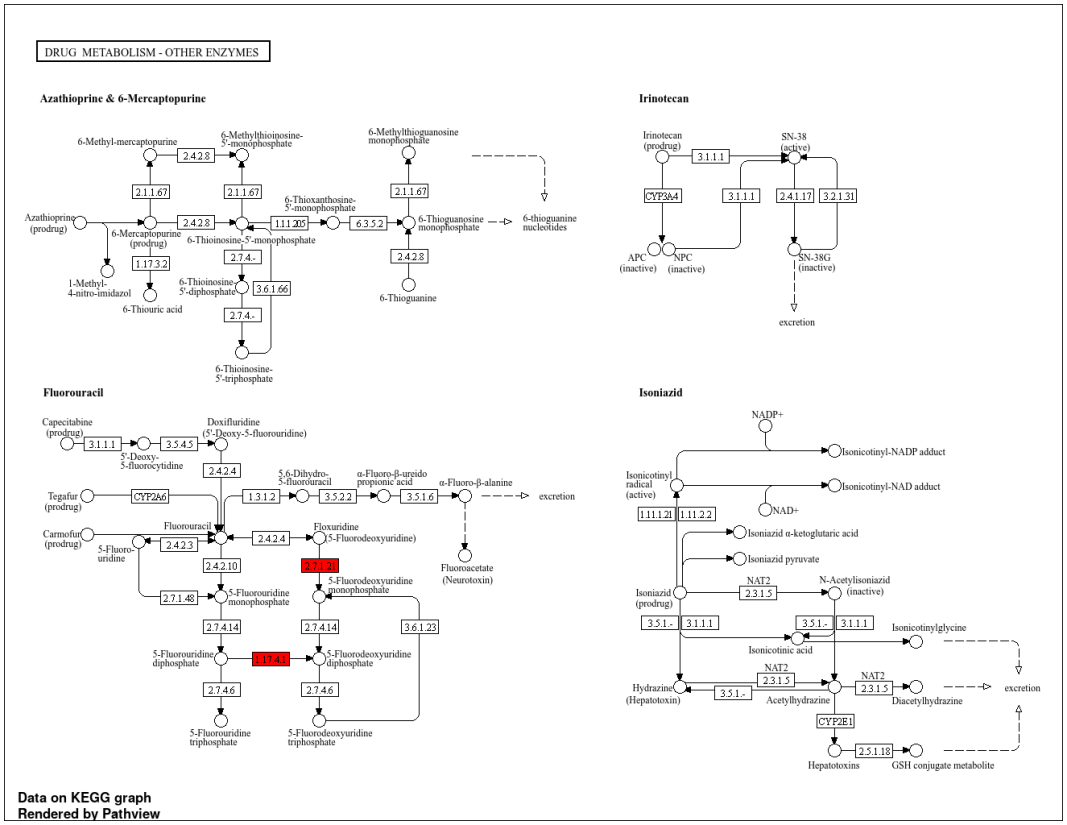

Supplementary Figure 4.1.4: Statistically significant and differentially abundant proteins identified from the SHP099 10μM vs Vehicle control binary comparison were entered into SHINEY GO and used to generate the KEGG Map for the Drug Metabolism – Other Enzymes pathway identified.